Ionic Mechanisms of Murine Urethral Smooth Muscle Contractility

A thesis submitted to the

School of Health and Science,

Dundalk Institute of Technology

For the degree of **Doctor of Philosophy**

By

Neha Gupta, M.sc

March 2026

Supervised by **Dr. Bernard T. Drumm** &

Co. Supervised by **Prof. Gerard P. Sergeant**

Smooth Muscle Research Centre,

Dundalk Institute of Technology, Ireland

Declaration

I hereby certify that this material, which I now submit for assessment on the programme of study leading to the award of Doctor of Philosophy is entirely my own work, and that I have exercised reasonable care to ensure that the work is original and have conformed to the regulations on the use of and declaration of Generative AI, and does not to the best of my knowledge breach any law of copyright, and has not been taken from the work of others save and to the extent that such work has been cited and acknowledged within the text of my work.

Signed: Neha Gupta

(Candidate) ID No.: d00262092

Date: 30th March 2026

Acknowledgement

In loving memory of my father, Rajnath Gupta (1966-2024), whose strength, love, and quiet faith continue to guide me every day.

I wish to express my sincere gratitude to my supervisor, Dr Bernard Drumm, for his guidance and support throughout my PhD, which were central to the completion of this research. I am also deeply thankful to my co-supervisor, Prof Gerard Sergeant, for his valuable advice and guidance during the course of this work. I am grateful to Prof Keith Thornbury, Prof Mark Hollywood, and Dr Caoimhin Griffin, for their insightful suggestions throughout the project. I would like to thank Billie McIlveen for her support and encouragement during my time in SMRC.

I am grateful to Prof Kenton M. Sanders for providing the opportunity to undertake research at the Department of Physiology and Cell Biology, University of Nevada, Reno (UNR), and to Prof Salah Baker for allowing me to work in his laboratory and for providing access to laboratory resources. I am sincerely grateful to Prof Sean Wards, Prof Scott Earley, Prof Brian Perrino, Dr Peter Blair, Dr Alison Bartlett, Dr Emer Ni Bhraonain, Dr Evan Yamasaki, Jenna Strahan, Nancy and Victoria for their generous help during my time at UNR.

I am thankful to Dr Ritu Dwivedi for sharing crucial information at the start, which greatly facilitated my joining. My appreciation also goes to Dr Kaneez Rabab, Dr Tuleen Alkawadri, Dr Caoimhin Griffin, and Dr Pei Yee Wong (Alina) for taking the time to explain the required lab experimental protocols. I am grateful to Yaly and Anshika for bringing warmth and joy to my initial few months in the lab; their presence made those days lighter. My sincere thanks go to Zainab and Rabab for their encouragement and for being available whenever I needed support. I also wish all the very best to my fellow PhD colleagues- Mitchell, Srijit, Zainab, Neeraj, and Alex, and to our junior PhD students, Denzel and Shubhendu in their future endeavours.

I owe a special debt of gratitude to my husband, Kabi, whose patience, encouragement and quiet strength carried me through every high and low of this journey. His love and steadiness made the most difficult moments bearable.

I am profoundly thankful to my mother, Anita, whose constant love and support kept me grounded during the most difficult times. I remember my father, Rajnath, with deep gratitude; his memory continues to inspire me, and this work reflects the values and strength he instilled in me. I also wish to thank my in-laws, Prabash and Kabita, for their encouragement and kindness throughout these years.

Abstract

"Ionic Mechanisms of Murine Urethral Smooth Muscle Contractility"

Neha Gupta

Urethral smooth muscle (USM) contraction is essential for continence, and dynamic spontaneous calcium (Ca^{2+}) activity in interstitial cells of Cajal-like cells (ICC-LC) is thought to influence USM cells (USMC) by generating Ca^{2+} signals that help regulate USMC excitability and basal tone. We studied ICC-LC in the murine urethra using a transgenic Kit-GCaMP6f mouse model, which expresses the GCaMP Ca^{2+} sensor in kit^{+} cells through kit-promoter-driven iCre. This approach allowed us to visualise ICC-LC in intact tissue, whereas earlier studies depended mainly on isolated cells and identified ICC-LC by morphology rather than definitive cellular markers. ICC-LC in USM were spindle-shaped, sparsely distributed, and exhibited asynchronous Ca^{2+} activity. ICC-LC lacked functional innervation, as they showed no response to endogenous excitatory or inhibitory neurotransmitter release evoked by neural stimulation. However, they responded to the exogenous α1-adrenergic receptor (α1-AR) agonist phenylephrine (PE), but not to a nitric oxide (NO) donor, indicating that they possess α1-AR. ICC-LC Ca^{2+} activity was primarily sustained by store-operated Ca^{2+} entry (SOCE). ANO1 (anoctamin-1, Ca^{2+}-activated-chloride channel) was expressed in USMC but not in ICC-LC; however, modulating ANO1 did not alter murine urethral contractility under the conditions tested. In addition, L-type Ca^{2+} channels (LTCC) or T-type Ca^{2+} channels (TTCC) inhibition had no effect, whereas Orai channel (Ca^{2+}-release activated Ca^{2+} channel) inhibition reduced agonist- or EFS-induced contractions in both male and female USM. In contrast, inhibition of Kv7 and BK_{Ca} channels enhanced nifedipine-sensitive phasic contractions during agonist and EFS stimulation in male USM, indicating their role in limiting LTCC activity, a mechanism largely absent in female USM, most likely due to lower functional LTCC. Overall, our findings show that Orai-mediated SOCE and SR Ca^{2+} release generate and maintain tonic contractions in murine USM, while BK_{Ca} and Kv7 limit LTCC-dependent phasic contractions in male USM. These findings enhance understanding of the cellular and ionic mechanisms controlling USM contractility and provide a foundation for future studies aimed at developing strategies to treat UI.

Findings generated throughout this thesis have been disseminated through peer-reviewed publications and presentations at national and international scientific conferences, as detailed below.

Peer- reviewed publications:

- **Gupta, N**., Baker, S. A., Sanders, K. M., Rabab, K., Thean, D., Alkawadri, T., Griffin, C. S., Sergeant, G. P., Hollywood, M. A., Thornbury, K. D., & Drumm, B. T. (2025). ANO1 channels are expressed in mouse urethral smooth muscle but do not contribute to agonist or neurally-evoked contractions. *Scientific Reports*, 15, 17365 (2025).
- **Gupta, N**., Baker, S. A., Sanders, K. M., Griffin, C. S., Sergeant, G. P., Hollywood, M. A., Thornbury, K. D., & Drumm, B. T. (2024). Interstitial cell of Cajal-like cells (ICC-LC) exhibit dynamic spontaneous activity but are not functionally innervated in mouse urethra. *Cell calcium*, 123, 102931.

Oral communications:

- **Gupta N,** Baker SA, Sanders KM, Griffin CS, Hollywood MA, Thornbury KD, Sergeant GP & Drumm BT (2024). Interstitial cell of Cajal-like cells (ICC-LC) exhibit dynamic spontaneous activity but are not functionally innervated in mouse urethra. *Oral presentation, Physiology in focus 2024, The Physiological society, Northumbria University, Newcastle, UK.*
- **Gupta N**, Baker SA, Sanders KM, Griffin CS, Hollywood MA, Thornbury KD, Sergeant GP & Drumm BT (2024). Interstitial cell of Cajal-like cells (ICC-LC) exhibit dynamic spontaneous activity but are not functionally innervated in mouse urethra. *Oral presentation, Command and Control: Unveiling the Regulation of Smooth Muscle Function, The Physiological society, Dundalk Institute of Technology, Ireland.*

Poster communications:

- **Gupta N**, Griffin CS, Hollywood MA, Thornbury KD, Sergeant GP & Drumm BT (2025). Basal opening of Kv7 and BK_{Ca} channels provide a hyperpolarizing brake

to activation of L-type Ca^{2+} channels in male mouse urethral smooth muscle. IUPS 2025, Europhysiology, KAP Europa, Frankfurt, Germany.

- **Gupta N**, Griffin CS, Hollywood MA, Thornbury KD, Sergeant GP & Drumm BT (2024). Basal opening of Kv7 and BK_{Ca} channels provide a hyperpolarizing brake to activation of L-type Ca^{2+} channels in male mouse urethral smooth muscle. ECS 2024, European Calcium Society, Homerton College, University of Cambridge, UK.

- **Gupta N**, Baker SA, Sanders KM, Griffin CS, Hollywood MA, Thornbury KD, Sergeant GP & Drumm BT (2024). Interstitial cell of Cajal-like cells (ICC-LC) exhibit dynamic spontaneous activity but are not functionally innervated in mouse urethra. *Command and Control: Unveiling the Regulation of Smooth Muscle Function, The Physiological society, Dundalk Institute of Technology, Ireland.*

- **Gupta N**, Baker SA, Sanders KM, Griffin CS, Hollywood MA, Thornbury KD, Sergeant GP & Drumm BT (2024). Interstitial cell of Cajal-like cells (ICC-LC) exhibit dynamic spontaneous activity but are not functionally innervated in mouse urethra. *DKIT School of Health & Science Research Day, Ireland.*

- **Gupta N,** Griffin CS, Hollywood MA, Thornbury KD, Sergeant GP & Drumm BT (2023). Orai Ca^{2+} channels but not ANO1 or L-type Ca^{2+} channels contribute to adrenergic contractions of male mouse urethral smooth muscle. *Poster Presentation, Physiology 2023, The Physiological society, Harrogate, UK.*

- **Gupta N**, Griffin CS, Hollywood MA, Thornbury KD, Sergeant GP & Drumm BT (2023). The role of Ca^{2+} ion channels in regulation of contractility in mouse urethral smooth muscle. *DKIT School of Health & Science Research Day, Ireland.*

Table of Contents

Glossary 9
1. Review of literature 12
1.1 Introduction 13
1.2. Anatomy and physiology of the lower urinary tract 14
1.3 Role of USM in maintaining continence 23
1.4 Intracellular Ca^{2+} signalling 25
1.5 Spontaneous activity in urethral smooth muscle 26
1.6 Interstitial cells of Cajal (ICC) 28
1.7 Role of chloride conductances in ICC 31
1.8 Interstitial cells of Cajal- like cells (ICC-LC) 33
1.9 Anoctamin 1 (ANO1) channels 37
1.10 Voltage-gated Ca^{2+} channels (VGCC) 42
1.11 Kv7 channels (Voltage gated potassium channels) 46
1.12 BK channels (Ca^{2+} activated K^+ channels) 48
1.13 K_{ATP} channels (ATP-sensitive potassium channels) 49
1.14 CRAC (Ca^{2+} release-activated Ca^{2+} channel) 50
1.15 Current gaps in literature in urethral physiology 55
1.16 Aims 57
2. Materials & Methods 58
2.1 Ethical approval 59
2.2 Tissue preparation 59
2.3 Isometric tension recording 61
2.4 Tissue Ca^{2+} Imaging 63
2.5 Total RNA isolation 64
2.6 cDNA synthesis 65
2.7 Real-time quantitative PCR 66
2.8 Immunohistochemistry 68
2.9 Isolation of mouse smooth muscle cells 69
2.10 Immunocytochemistry 69
2.11 Solutions 70

2.12 Drugs 71
2.13 Statistical analysis 72

3. Identification and classification of interstitial cell of Cajal like cells (ICC-LC) in murine urethra 73

3.1 Introduction 74
3.2 Results 76

3.2.1 Urethral ICC-LC imaged using Kit-GCaMP6f mice 76
3.2.2 Extracellular and intracellular Ca^{2+} sources for ICC-LC Ca^{2+} activity 83
3.2.3 Neuronal control of ICC-LC Ca^{2+} activity 88
3.2.4 ANO1 Expression in ICC-LC 94

3.3 Discussion 96

4. Do ANO1 channels contribute to murine urethral smooth muscle contractility? 102

4.1 Introduction 103
4.2 Results 107

4.2.1 ANO1 expression in urethral tissues 107
4.2.2 Effects of ANO1 inhibition on agonist evoked urethral contractions 110
4.2.3 Effects of ANO1 inhibition on EFS evoked urethral contractions 113
4.2.4 Effects of ANO1 inhibition on USM Ca^{2+} signals 113
4.2.5 Effects of ANO1 inhibition on colonic contractions & Ca^{2+} signals 116
4.2.6 PE & EFS-evoked contractions are abolished by IP_3R antagonist 118
4.2.7 Arginine vasopressin but not phenylephrine contracts female urethra ... 118
4.2.8 Investigating effects of other CaCC inhibitors on urethral contractions .. 122

4.3 Discussion 126

5. Role of VGCC and Orai channels in murine urethral smooth muscle contractility 130

5.1 Introduction 131
5.2 Results 133

5.2.1 Expression of LTCC and Orai in murine USM 133
5.2.2 Effects of LTCC inhibition in murine USM 133
5.2.3 Effects of LTCC activation in murine urethra 143

5.2.4 Effect of T-type Ca^{2+} channel (TTCC) inhibition in murine USM 147
5.2.5 Role of SOCE in murine urethra..... 149
5.3 Discussion..... 163
6. Kv7 and BK_{Ca} channels opening limits L-type Ca^{2+} channels activity during Gq-coupled GPCR activation in male mouse USM..... 169
6.1 Introduction 170
6.2 Results 173
6.2.1 Effect of Kv7 and BK_{Ca} inhibition in male mouse USM..... 173
6.2.2 Effects of Orai and Kv7 channel inhibition in precontracted male USM . 180
6.2.3 Effects of RyR and Kv7 inhibition on precontracted male urethra 198
6.2.4 Effects of ANO1 inhibition on phasic contractions in male USM 200
6.2.5 Effects of Kv7 and BK_{Ca} blockade on precontracted female USM..... 200
6.2.6 Role of K_{ATP} channels in male and female USM 203
6.2.7 Expression of Kv7 and BK_{Ca} in male USM 203
6.3 Discussion..... 209
7.1 General Discussion 217
Future prospects 221
8. Bibliography..... 223

Glossary

Abbreviations

9-AC - anthracene chloride

AC - adenylate cyclase

ANO1 - anoctamin1

2-APB - 2-aminoethoxydiphenyl borate

AR - adrenergic receptors

ATP - adenosine triphosphate

AUC - area under curve

AVP - arginine vasopressin

BSA - bovine serum albumin

CaCC - Ca^{2+}-activated chloride channels

cAMP - 3'-5'-cyclic adenosine monophosphate

cGMP - cyclic guanosine monophosphate

CICR - Ca^{2+}-induced- Ca^{2+} release

CPA - cyclopiazonic acid

cPEGFP – circularly permuted enhanced green fluorescent protein

CRAC - Ca^{2+} release-activated Ca^{2+} channel

DAG - 1,2-diacylglycerol

DIDS - 4,4’-diisothiocyanstilbene-2,2’-disulphonic acid

DTE - dithioerythritol

DSM - detrusor smooth muscle

DSMC - detrusor smooth muscle cells

ER - endoplasmic reticulum

EUS - external urethral sphincter

EFS - electrical field stimulation

EJP - excitatory junction potential

FOV - field of view

FDHM - full duration half maximal

GFP - green fluorescent protein

GI - gastrointestinal

HPRA - Health Products Regulatory Authority

IAS - internal anal sphincter

I_{CRAC} - Ca^{2+} release-activated current

ICC - interstitial cells of Cajal

ICC-LC - interstitial cell of Cajal like cells

IJP - inhibitory junction potential

IP_3 - inositol-1, 4, 5- triphosphate

IP_3R - inositol-1, 4, 5-triphosphate receptor

IPHFO - intraluminal pressure high-frequency oscillations

IUS - internal urethral sphincter

K_v - voltage-gated potassium channels

LES - lower esophageal sphincter

L-NNA - NG-nitro-L-arginine

LTCC - L-type Ca^{2+} channels

LUT - lower urinary tract

MLCK - myosin light chain kinase

MLC - myosin light chain

NA - noradrenaline

NANC - non-adrenergic-non-cholinergic

NPPB - 5-nitro-2-(3-phenylpropylamino)-benzoic acid

NO - nitric oxide

No-RT - no-Reverse Transcriptase

NOS - nitric oxide synthase

NTC - non-template control

PBS - phosphate saline buffer

PE - phenylephrine

PFA - paraformaldehyde

PKC - protein kinase C

PKG - protein kinase G

PLC - phospholipase C

PM - plasma membrane

PDGFR - platelet derived growth factor receptor

ROI - region of interest

RMP - resting membrane potential

RT - room temperature

SD - spontaneous depolarisation

SERCA - sarcoplasmic reticulum calcium ATPase

sGC - soluble guanylate cyclase

SITS - 4-acetoamido-4-isothiocyanatostilbene-2,2'-disulfonic acid

SK channel - small conductance Ca^{2+} activated potassium channel

SM - smooth muscle

SMC - smooth muscle cell

SOAR - STIM Orai-activating region

SOCE - store-operated calcium entry

SOCC - store-operated calcium channel

SR - sarcoplasmic reticulum

STD - spontaneous transient depolarisations

STH - spontaneous transient hyperpolarisations

STIC - spontaneous transient inward current

STIM - stromal interaction molecule

SW - slow waves

TMD - transmembrane domains

TTCC - T-type Ca^{2+} channels

RyR - ryanodine receptor

UI - urethral incontinence

USM - urethral smooth muscle

USMC - urethral smooth muscle cells

VAChT - anti-vesicular acetylcholine transporter

$V1_AR$ - vasopressin 1_A receptor

VGCC - voltage-gated calcium channels

WT - wild type

1. Review of literature

1.1 Introduction

Storage and elimination of urine is well coordinated between upper and lower urinary tract (LUT) organs (De Groat, 2006). The kidneys filter blood and produce urine, which is pumped into the ureter by peristaltic contractions of the renal pelvis where it travels to the urinary bladder for storage (Baker and Silverton, 1976). The urinary bladder and urethra constitute the LUT (Fig 1.1), and have a reciprocal contractile relationship (Fowler *et al.,* 2008). The bladder expands significantly as it fills without a corresponding increase in intravesical pressure (Pan, 2018). Meanwhile, the urethra remains contracted during bladder filling to prevent urine leakage (Rembetski *et al.,* 2018). At a threshold volume, i.e. 400-500 ml in humans, 0.15 ml in mice (Andersson & Arner, 2004), 1 ml in rats (Reis *et al.,* 2011), 500-550 ml in pigs (Chen *et al.,* 2015), elimination (micturition) occurs through coordinated contractions of the bladder wall (Fry *et al.,* 2010) and urethral relaxation to form a passage for release of urine outside the body (Andersson & Arner, 2004).

When this coordinated process is disrupted due to malfunction of either bladder or urethra, it results in urinary incontinence (UI). UI is characterized by involuntary passing of urine, increased sensation to urinate, and inability to urinate or completely empty the bladder (Jung *et al.,* 2012). UI can present as continuous dribbling or as sporadic voiding, either with or without the individual's awareness of a need to urinate. UI is a broad term encompassing numerous conditions such as overactive bladder, an increase in bladder smooth muscle (detrusor, DSM) activity leading to urgency (Franken *et al.,* 2014). Conversely, underactive bladder, results in sensations of incomplete emptying or prolonged voiding (Suskind, 2017).

Benign prostatic hyperplasia causes the prostate gland to enlarge, partially occluding the urethra, leading to urine retention (Roehrborn, 2005). This condition affects a substantial proportion of men, with prevalence rates ranging from 10% of males > 30, 20% of males > 40 and increases more in higher age groups (Roehrborn, 2005; Bardsley, 2016). Stress incontinence is associated with increased bladder and mid-urethral mobility, which affects women more than men, especially after childbirth or as a result of aging (Sangsawang & Sangsawang, 2013; Zimmern *et al.,* 2014). This condition is due to a malfunction in bladder, urethra, or pelvic muscles, which results

in impaired pressure transmission, where urethral pressure becomes weaker than intravesical pressure (Pirpiris *et al.,* 2010), resulting in urine leakage.

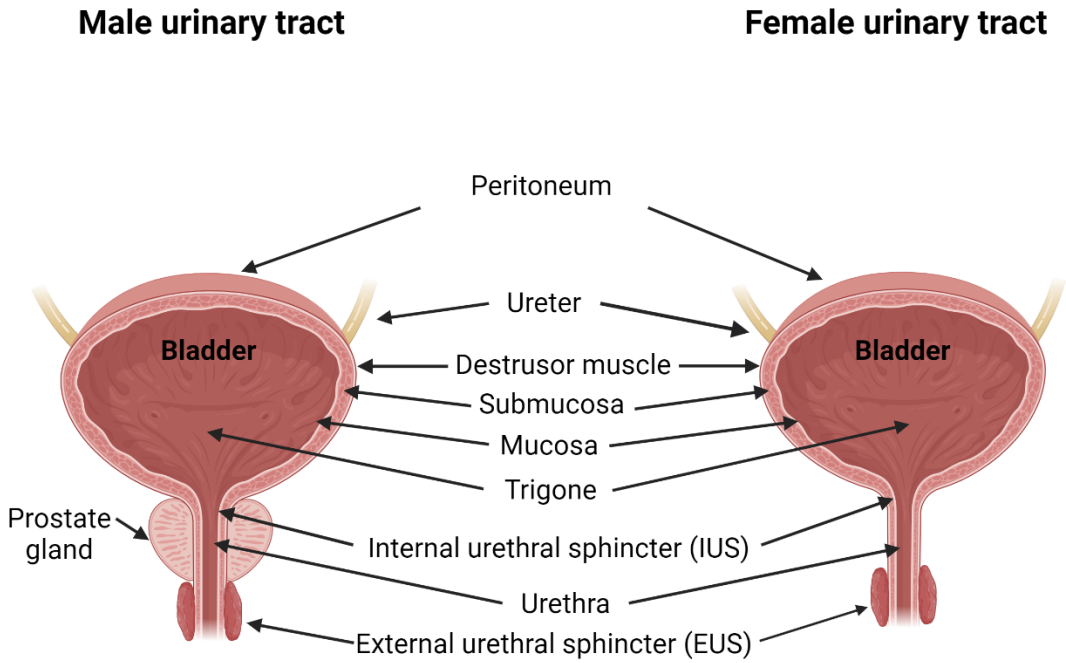

Fig 1.1: Diagrammatic representation of anatomy of lower urinary tract of adult male and female. Urethra connects bladder to the external urinary meatus. Internal urethral sphincter (IUS) and external urethral sphincter (EUS) are common in both male and female. The prostate gland is a unique male structure surrounding the proximal urethra.

1.2. Anatomy and physiology of the lower urinary tract

1. Urinary bladder:

The urinary bladder is a hollow organ and is a storage reservoir for urine until an appropriate time for micturition occurs (Groat, 2006). The bladder is located in the pelvis, posterior to the pubic symphysis, anterior to the rectum in males and anterior to the vagina and uterus in females (Kuntz, 1965). A cross section of bladder reveals the following layers arranged from outermost to innermost:

1. Outer serosa and adventitia: bladder dome is enveloped by a thin layer of connective tissue (serosa), which maintains continuity with the peritoneal layer

of the abdominal wall (Liebhold *et al.,* 1995). In regions of bladder where the serosa is absent, the outer layer is referred to as the adventitia, characterized by its loose arrangement of connective tissue (Bolla *et al.,* 2023).

2. Detrusor (muscularis propria): composed of smooth muscle (SM), within three sub-layers: inner longitudinal, middle circular, and outer longitudinal (Andersson & Arner, 2004). Detrusor smooth muscle (DSM) bundles are organized in an irregular, crisscross pattern, resembling a basket weave (Mangera *et al.,* 2010; Bolla *et al.,* 2023). The basket-weave arrangement facilitates coordinated DSM contraction during urination. The multiple directional orientations of muscle fibres enable the bladder to contract evenly and efficiently to expel urine, and retain its structural integrity when stretched during storage (Borsdorf *et al.,* 2019). The ureter takes a diagonal path through DSM, preventing urine reflux into the kidney during filling (Sam *et al.,* 2022).

3. Submucosa (lamina propria): connects outer and internal muscular layers. Lamina propria contains heterogenous proteins and cells such as immune cells, fibroblasts, nerve endings and adipocytes (Andersson & McCloskey, 2014).

4. Mucosa: continuous with internal renal, ureteric and proximal urethral lining. Predominantly composed of urothelium, a transitional cell epithelium forming a superficial layer of polyhedral flattened cells (Keyser *et al.,* 1992).

The bottom of the bladder (bladder neck) has a triangular structure called the trigone, a transitional area between the main detrusor and urethra (Dixon & Gosling, 1987). Two ureteral openings are located at the trigone base, through which urine enters the bladder from the upper urinary tract (Young & Macht, 1923; Mahadevan, 2016).

Neural pathways involved in bladder control

The proper functioning of the bladder relies on its intricate network of nerves. This neural circuit regulates storage and release of urine, and involves complex communication among the brain, spinal cord and bladder itself (Agarwal *et al.,* 2019). Neural innervation of the bladder encompasses three key components:

parasympathetic excitatory innervation, sympathetic inhibitory innervation, and sensory innervation (see Fig 1.2) (De Groat *et al.,* 2015; Fowler *et al.,* 2008).

Parasympathetic innervation arising from sacral nerves S2-S4, plays a pivotal role in exciting DSM, while simultaneously inhibiting urethral smooth muscle (USM) (Jung *et al.,* 2012). This dual action allows contraction of the bladder and subsequent voiding of urine (Jung *et al.,* 2012). In contrast, sympathetic innervation originating from thoracolumbar nerves T10-L2, excites USM while inhibiting DSM (Clemens, 2010). This aids in bladder filling and urine storage. The bladder receives sparse sympathetic innervation through the hypogastric nerve (Igawa, 2023). Sensory innervation detects distention or fullness of the bladder (Yoshimura and Chancellor, 2003). When the bladder reaches capacity, sensory nerves transmit signals to the central nervous system, alerting the brain of the need for voiding (Comperat *et al.,* 2007).

Acetylcholine (ACh), released from parasympathetic cholinergic nerve endings, binds to muscarinic receptors located on DSMC (detrusor smooth muscle cells), leading to contraction (Yoshimura & Chancellor, 2003). DSM from various species express muscarinic receptors, primarily M_2 and M_3 subtypes (Hegde & Eglen, 1999; Chess-Williams, 2002; Andersson & Arner, 2004). In human bladder, mRNA for all five muscarinic receptor subtypes has been detected (Sigala *et al.,* 2002), with M_2 and M_3 receptors most abundantly expressed (Yamaguchi *et al.,* 1996; Sigala *et al.,* 2002). M_3 receptors (M_3R) activation is the primary mechanism responsible for DSMC contraction, mediated by G_q signalling that elevates cytosolic calcium (Ca^{2+}) through sarcoplasmic reticulam (SR) Ca^{2+} release via IP_3 receptors (Choppin & Eglen, 2001; Andersson & Arner, 2004; De Groat & Yoshimura, 2015).

Sympathetic nerves induce relaxation of DSM, mediated by activation of β-adrenoceptors (β-ARs) in response to noradrenaline (NA) released from adrenergic nerve endings (Yoshimura & Chancellor, 2003). β-ARs are classified into three subtypes: β_1-AR, β_2-AR, and β_3-AR (Bylund *et al.,* 1994). β_3-AR is the most expressed and important subtype for relaxation in rat and human detrusor (Fujimura *et al.,* 1999; Michel and Vrydag, 2006; Igawa *et al.,* 2019). β_3-AR activation increases intracellular adenylate cyclase (AC), which triggers an increase in intracellular cyclic adenosine

monophosphate (cAMP) levels (Bylund *et al.,* 1994). This results in activation of either protein kinase A (PKA) or other effector molecules like EPAC (exchange protein activated by 3'-5'-cAMP) (Schmidt *et al.,* 2007), creating a sequential process resulting in relaxation of DSMC, enabling urine retention (Yoshimura & Chancellor, 2003; Frazier *et al.,* 2008). Previous studies reported that PKA activation causes relaxation by phosphorylating MLCK (myosin light chain kinase) (Stull *et al.,* 1993; Yamaguchi & Chapple, 2007) or by activating BK_{Ca} channels (large conductance potassium channels), which mediates DSM contractility (Xin *et al.,* 2014). In addition, increased PKA activity potentiates Ca^{2+} uptake from the cytosol to SR via SERCA (SR Ca^{2+}-ATPase) (Xin *et al.,* 2014; Krhut *et al.,* 2022). Subsequently, elevated PKA activity leads to ryanodine receptors (RyR) Ca^{2+} release, which activates BK_{Ca} channels, thereby modulates L-type Ca^{2+} channel (LTCC) activity (Xin *et al.,* 2014). Moreover, inhibition of EPAC blocks β-AR-induced or adenylate cyclase activator-induced relaxations in human and rat DSM, although the precise mechanism underlying these relaxations remains unclear (Silva *et al.,* 2020). M_2R activation by ACh can lead to inhibition of AC, offsetting β-ARs effect (Andersson & Arner, 2004; De Groat & Yoshimura, 2015).

DSM is also innervated by purinergic nerves. Purinergic signaling involves release of the neurotransmitter adenosine triphosphate (ATP), followed by its breakdown into adenosine monophosphate. ATP acts on P2 purinergic receptors, while adenosine influences P1 purinergic receptors (Ralevic, 2021). Purinergic receptors are distributed throughout the bladder and mediate numerous functions, including DSM contraction and relaxation. There are seven different P2X receptor types found in the bladder, the predominant subtype in both rat and human DSM is $P2X_1$ (De Groat & Yoshimura, 2015). The development of antagonists designed to block these specific P2X receptors is likely to have clinical utility in managing DSM over activity. Fong *et al.,* (2021) observed that activation of cAMP effector EPAC inhibited $P2X_1$ currents and enhanced $P2X_2$ currents (Fong *et al.,* 2021). The other type of purinergic receptors are P2Y which has eight subtypes: $P2Y_1$, $P2Y_2$, $P2Y_4$, $P2Y_6$, and $P2Y_{11\text{-}14}$. P2Y receptors respond to various extracellular purines and pyrimidines released by tissues (Lazarowski & Boucher, 2001; Chen *et al.,* 2010). P2Y receptors are present in DSM and bladder urothelium (Burnstock, 2014). P2Y receptors ($P2Y_1$) are present on

PDGFR-α$^+$ (platelet derived growth factor receptor alpha$^+$) cells and are believed to mediate DSM relaxation (Lee *et al.,* 2014).

2. Urethra:

The urethra is a tube connecting the bladder to the external urinary meatus through which urine is eliminated from the body (Fletcher & Bradley, 1978). In adult males, the urethra is ~20 cm long and divided into four parts: pre-prostatic, prostatic, membranous, and spongy urethra (Atala *et al.,* 2010). The pre-prostatic urethra serves as the sphincter to control urine flow. The prostatic urethra (approximately 3-4 cm long) passes through the prostate gland (Hickling *et al.,* 2015). The membranous urethra is the shortest part of the male urethra (approximately 1 cm), and passes through the urogenital diaphragm (Cheng *et al.,* 2020). The spongy urethra extends from the urogenital diaphragm to the external urethral orifice, and is the longest part of the male urethra (approximately 15 cm long) and runs through the corpus spongiosum of the penis (Hickling *et al.,* 2015). In females, the urethra is approximately 4 cm long, runs from the bladder neck to the external urethral orifice and is surrounded by an anterior vaginal wall (Mangera *et al.,* 2010; Pradidarcheep *et al.,* 2011; Jung *et al.,* 2012; Mahadevan, 2016).

The urethral wall comprises various tissue layers, arranged from outermost to innermost.

1. Outermost layer, adventitia, is composed of connective tissue that provides support and protection to the urethra (Mangera *et al.,* 2010; Pradidarcheep *et al.,* 2011).

2. Muscularis composed of two layers of USM: an inner longitudinal layer and an outer circular layer (Thind, 1995). The longitudinal muscle undergoes shortening during micturition, while circular USM contracts during bladder filling to ensure continence (Fry *et al.,* 2010).

3. Submucosa (lamina propria) is composed of connective tissue and numerous blood vessels, nerves, and lymphatics (Collins *et al.,* 2023). The Lamina propria

make direct contact with vascular, connective, and muscular tissues, and are proposed to play an important role in maintaining urinary continence by responding to physiological stimuli and communicating with afferent neurons (Birder and Andersson, 2013; Mueller *et al.,* 2025).

4. The innermost layer (mucosa), consists of transitional epithelium (urothelium). Urothelium is continuous with lining of the bladder and secretes mucus to protect the urethra from acidic urine (Khandelwal *et al.,* 2009). Urothelial cells have numerous microvilli on their apical surface and may communicate with the central nervous system (CNS) by activating afferent neurons in response to urethral distension (Birder *et al.,* 2014; Birder & Andersson, 2013; Mueller *et al.,* 2025).

Two urethral sphincters regulate urine flow: an internal urethral sphincter (IUS) made up of USM and an external urethral sphincter (EUS) also known as the rhabdosphincter, composed of striated muscle (Jung, *et al.,* 2012). The IUS is under involuntary control and regulates urine flow from the bladder during filling and voiding (Cooper *et al.,* 1986; Ashton-Miller *et al.,* 2001). The EUS is under voluntary control, and prevents urine leakage during sudden increases in abdominal and intravesical bladder pressure (guarding reflex) during sneezing, coughing and laughing (Fowler *et al.,* 2008). Urethral closure pressure should exceed intravesical bladder pressure to maintain continence during either resting conditions, or during increased abdominal pressure (Ashton-Miller *et al.,* 2001). The anterior vagina, endopelvic fascia, arcus tendineus fasciae pelvis, and levator ani muscle lie extrinsic to the urethra and form a urethral support system preventing urine leakage when abdominal pressure increases (Delancey & Ashton-Miller, 2004).

The urethral vasculature may facilitate continence by forming a watertight seal via coaptation of the mucosal surfaces (Ashton-Miller *et al.,* 2001). It has been observed that if blood flow through urethral arteries is interrupted, urethral pressure decreases (Keane & O'Sullivan, 2000). Recently, Hashitani *et al.,* (2024) found that nitric oxide (NO, inhibitory neurotransmitter) released from perivascular parasympathetic nerves inhibits sympathetic vasocontractions in rat urethral arterioles. Thus, vasorelaxation by NO aids in maintaining adequate blood flow and oxygen supply to contract USM,

sustaining their contractile state during bladder filling (Hashitani *et al.,* 2024). Hashitani and Mitsui (2025) proposed that induced NO-mediated sympatholysis (inhibition of sympathetic vasocontriction) may offer therapeutic and preventive potential for the ischaemic LUT (Hashitani & Mitsui, 2025).

Innervation of urethra

The urethra is innervated by three peripheral nerves- (i) Sympathetic nerves (hypogastric nerves) in the rostral lumbar region that supply noradrenergic excitatory input to USM (De Groat *et al.,* 2001), (ii) Parasympathetic (pelvic) nerves in the caudal lumbosacral region responsible for delivering nitrergic inhibitory signals to USM (De Groat *et al.,* 2001; Yoshimura & Chancellor, 2003), and (iii) Somatic nerves (pudendal nerves) in the caudal lumbosacral region that provide cholinergic excitatory input to striated muscle (Fig 1.2) (Strasser *et al.,* 2000; De Groat *et al.,* 2001).

Zeissl's (1893) studies demonstrated hypogastric nerve stimulation resulted in USM contraction, whereas pelvic nerve stimulation resulted in relaxations. This was further confirmed by Elliot (1907) and Barrington (1914). Histochemical studies indicate a high density of adrenergic fibres in the rat outer proximal USM, whereas the inner layer contains a combination of cholinergic fibres (34%) and adrenergic fibres (66%) (Gosling & Dixon, 1975; Watanabe *et al.,* 1979). However, in a study performed on male mouse USM tissues, the α1 adrenergic agonist, phenylephrine (PE) contracted the tissue, but a cholinergic agonist carbachol did not, indicating that cholinergic control in mice is minimal or functionally absent (Drumm *et al.,* 2018; Rembetski *et al.,* 2018). In contrast, in pig and rabbit, both carbachol and PE induces USM contraction (Bridgewater *et al.,* 1993; Nagahama *et al.,* 1998; Rembetski *et al.,* 2020). These findings indicated a species-specific differences in functional contributions of adrenergic and cholinergic receptors to USM contractility. In urethral striated muscle, there is a high density of cholinergic nerves and absence of adrenergic nerve fibres (Lincoln *et al.,* 1986; Von *et al.,* 1998, Watanabe *et al.,* 1979; Crowe *et al.,* 1989). The cholinergic innervation of EUS comprises of a combination of parasympathetic (pelvic nerve, involuntary control) and somatic nervous controls (pudendal nerve, voluntary control) (Lincoln *et al.,* 1986).

NO synthase (NOS) within parasympathetics nerve releases NO, the primary inhibitory neurotransmitter that relaxes USM (Andersson, 2001). Immunohistochemistry revealed a rich supply of NOS-immunoreactive nerve fibres in rabbit USM (Waldeck *et al.,* 1998). NO mediates USM relaxation primarily through activation of NO-sensitive soluble guanylyl cyclase (sGC) and subsequent cGMP production (Lies *et al.,* 2013). Electrical field stimulation (EFS) evoked relaxations of female pig and sheep USM were blocked by NOS inhibitors such as NG-nitro-L-arginine (L-NNA), implicating NO as a key neurotransmitter in this process (Garcia-Pascual *et al.,* 1991; Bridgewater *et al.,* 1993; Andersson & Persson, 1994). Spontaneous basal Ca^{2+} activity in mouse USM cells (USMC) was inhibited (>90%) by a NO donor, DEA-NONOate (Drumm *et al.,* 2018). This NO-dependent pathway is further supported by studies showing that L-NNA attenuates non-adrenergic, non-cholinergic (NANC) relaxation in rabbit and sheep USM (Dokita *et al.,* 1991; Thornbury *et al.,* 1992).

Functional coupling of NO to cGMP is evident in sheep and rabbit USM, where NO mediated relaxation correlates with increased cGMP levels (Dokita *et al.,* 1994; García-Pascual & Triguero, 1994), and is mimicked by cGMP analogs such as 8-Br-cGMP (García-Pascual & Triguero, 1994). However, in female dog urethra, partial relaxation persists despite NOS inhibition, suggesting co-existence of NO-independent pathways (Hashimoto *et al.,* 1993). A knockout mice lacking cGMP-dependent PKG I ($cGKI^{-/-}$), confirmed the necessity of the NO-cGMP-PKG axis, as these animals exhibit impaired USM relaxation despite intact NO synthesis (Persson *et al.,* 2000). These findings suggest NO is a critical mediator of USM tone regulation.

Sympathetic nerves release NA, which binds to adrenoreceptors (AR) on USM, leading to contraction (Fowler *et al.,* 2008). There are two subtypes of AR - α and β, further subdivided into α_1, α_2, β_1, β_2, and β_3 (Michel & Vrydag, 2006). α_1-AR has three distinct subtypes - α_{1a}, α_{1b}, α_{1d} (Yamada & Ito, 2011). The predominant subtype of AR present in male proximal urethra are α_{1a}-AR, which mediates USM contraction by activating G_q-coupled signalling upon binding with NA (Andersson, 2001; Hsieh *et al.,* 2023). However, in female mice, unlike males, α_1-AR agonists do not induce USM contraction (Alexandre *et al.,* 2017; Hsieh *et al.,* 2023). Previous studies showed that SM area is 15% smaller in female mouse in comparison to males (Alexandre *et al.,*

2017). In addition, transcriptional studies on mouse USM reported 84% higher mRNA expression of α_1-AR and 95% higher mRNA expression of tyrosine hydroxylase in male in comparison to female (Alexandre *et al.,* 2017), providing an explanation for the lack of α_1-AR-mediated contraction in female mice. However, another previous study demonstrated that female mouse USM contract in response to NA only after pre-incubation with propranolol, a β-AR antagonist (Hsieh *et al.,* 2023), suggesting that β-AR-mediated relaxation masks adrenergic contraction. In contrast, previous studies performed on male and female dogs showed that nerve stimulations-induced USM relaxation were primarily mediated by NO, and β-AR dependent mechanisms account for a minor component of relaxation (Van Der Werf & Creed, 2002; Michel & Vrydag, 2006). Similarly, β-AR density in male and female rabbit USM was much lower than DSM (Latifpour *et al.,* 1989; Michel & Vrydag, 2006).

In contrast to female mouse, female pig and rabbit USM contract in response to α_1-AR agonists (Andersson *et al.,* 1984; Alberts *et al.,* 1999). Radio ligand receptor binding assay demonstrated that densities of α_1-AR were similar in male and female rabbit USM, however, female rabbit USM exhibited a higher density of α2-AR compared to males (Morita *et al.,* 1987). Moreover, α_2-AR agonist (clonidine) induced a greater contraction in female rabbit USM compared to males (Morita *et al.,* 1987). RNase protection assays and *in situ* hybridization studies in USM of human patients with invasive bladder cancer showed α_{1a} as the predominant subtype mRNA, and no significant differences in the cross-sectional distribution of α_1-AR mRNA in both male and female urethral samples (Nasu *et al.,* 1998). Overall, the previous studies highlighted species- and sex-specific differences in adrenergic regulation of USM.

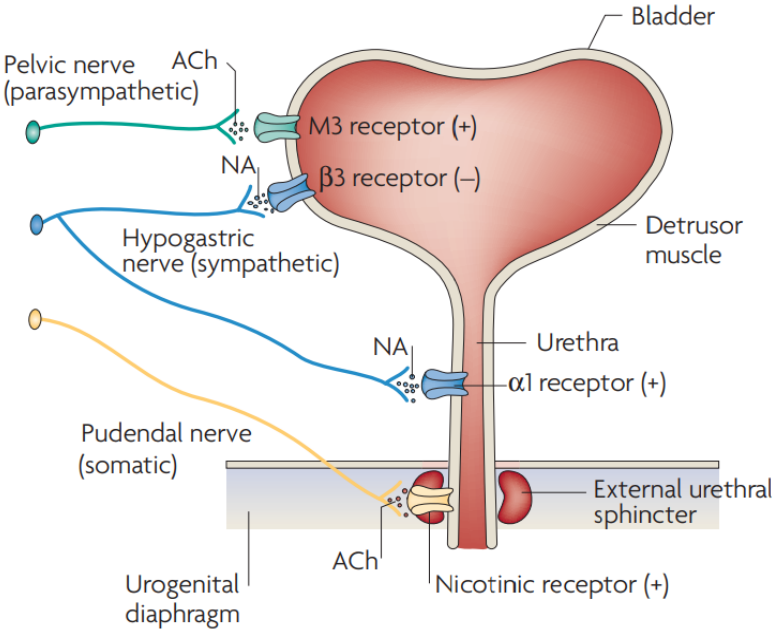

Fig 1.2: Neural pathways of the LUT. Parasympathetic postganglionic axons in the pelvic nerve release ACh to contract the bladder via M_3 muscarinic receptors. Sympathetic neurons release NA, activating β_3 adrenergic receptors to relax detrusor and α1 adrenergic receptors to contract USM. Somatic axons in pudendal nerve release ACh to contract the EUS via nicotinic receptors. Parasympathetic nerves release ATP to excite detrusor, and NO to relax USM. (Figure adapted from Fowler *et al.,* 2008)

1.3 Role of USM in maintaining continence

Though the connective tissues and other urethral support systems (such as the skeletal muscle of the rhabdosphincter) aid in maintaining continence, it is increasingly apparent that USM contraction plays a major role in maintaining continence (Donker *et al.,* 1972). Closure of the urethra during rest and bladder filling is a joint effort by both circular and longitudinal SM (Mistry *et al.,* 2020; Venema *et al.,* 2023).

Donker *et al.,* (1972) conducted investigations on adult men and women to study the urethral pressure profile (UPP) by pressure measurement with the help of a balloon catheter, electromyography of the urethra, and drug administration. Their findings revealed that elimination or impairment of striated muscle did not impact UPP, whereas pressure decreased significantly after injection of phentolamine, which would

antagonise α-adrenoreceptors on USM. Urethral pressure was restored after administration of α-adrenoreceptor agonists (Donker *et al.,* 1972). Cass and Hinman (1968) conducted an experiment where a device designed to sustain a consistent flow through the urethra to assess vesical pressure, urethral resistance and exit (meatus) pressure in female dogs following constriction of either the external meatus or vesical neck. They found vesical neck constriction greatly increased urethral resistance and upstream pressure compared to constricting the external meatus. This finding indirectly suggested that USM, present in vesicle neck, regulates urine flow, whereas striated muscle closer to the external meatus likely played a supportive or secondary role in maintaining continence or modulating flow (Cass & Hinman, 1968).

Dortermann and Bauer (1955), and later Lapides *et al.,* (1957), observed no change in urethral tone after inhibiting striated muscles using muscle-relaxant drugs. Lapides (1958) performed experiments on dogs where a series of incisions of urethra were made and found that leakage did not occur until the bladder neck outlet, rich in USM, was severed. Greenland (1996) found that pharmacological inhibition of striated muscle did not impact urethral closure pressure of female pig. Conversely, drugs that targeted USM significantly decreased urethral pressure (Greenland *et al.,* 1996).

Conte *et al.,* (1991) performed experiments on urethane-anesthetized rats in which the proximal urethra was surgically dissected to form a disconnection of bladder from the urethra. They recorded vesical and EUS pressure and found that administration of gallamine (skeletal muscle relaxant) and D-tubocurarine (skeletal muscle paralytic) caused no change in intraurethral pressure. Bridgewater *et al.,* (1993) conducted cystometry and urethral pressure profilometry on female pigs, which revealed that the mid-urethra (rich in USM) exhibited highest pressure in females, and circular USM excised from this region displayed spontaneous tone, which could be intensified by adrenergic and cholinergic input or suppressed by NO (Bridgewater *et al.,* 1993).

Venema *et al.,* (2025) demonstrated that USM contributes to closure of urethra during bladder filling by comparing a female patient with urethral instability to a control female with normal micturition. Urethral pressure measurement and needle electromyography recordings revealed early relaxation of USM during bladder filling and also rapid

fluctuation in urethral pressure in the patient. The subsequent entry of urine into the proximal urethra then triggers reflex contractions of the external sphincter in an effort to prevent leakage. In contrast, the control subject showed a smooth and gradual decline in urethral pressure without instability. These findings support USM as a potential therapeutic target for urethral instability (Venema *et al.,* 2023, 2025; Andersson & Uvelius, 2024).

In summary, the extensive array of studies presented illuminates the importance of USM in maintaining continence and underscores its potential as a crucial target for interventions aimed at managing UI, offering promising avenues for future research and therapeutic strategies.

1.4 Intracellular Ca^{2+} signalling

SM contracts involuntarily and is present not only in the LUT but also throughout the body, making up gastrointestinal (GI) organs, male and female reproductive systems, vascular / lymphatic systems, and airways (De Groat *et al.,* 2001; Fry *et al.,* 2010). Regardless of their location within the body, the contractile state of smooth muscle cell (SMC) is regulated by intracellular Ca^{2+}, with contractions initiated by increases in intracellular Ca^{2+} (Adelstein & Sellers, 1987).

Intracellularly, Ca^{2+} forms a complex with calmodulin, activating MLCK, which in turn phosphorylates myosin light chain (MLC), leading to its binding with actin and initiating SMC contraction (Adelstein & Sellers, 1987). Increased intracellular Ca^{2+} also activates protein kinase C (PKC), which can also phosphorylate MLC leading to muscle contraction (Nishikawas *et al.,* 1984). Ca^{2+} rises in SMC can be sourced intracellularly, extracellularly, or both (Triggle, 1985). A major intracellular Ca^{2+} source is the sarcoplasmic reticulum (SR), which mobilizes Ca^{2+} into the cytoplasm (Triggle, 1985; Somlyo & Himpens, 1989). Ca^{2+} present in the extracellular medium enters SMC through various plasmalemmal membrane channels activated by agonists, stretch or changes in membrane potential (Triggle, 1985; Hill-Eubanks *et al.,* 2011).

NA (excitatory neurotransmitter) or adrenergic agonists, such as PE, when bound to α_1-AR trigger G_q signalling pathways, activating phospholipase C (PLC). PLC

hydrolyses phosphatidylinositol-4, 5-biphosphate (PIP_2) in the plasma membrane (PM) into two intracellular messengers: inositol-1, 4, 5-triphosphate (IP_3) and 1, 2-diacylglycerol (DAG) (Exton, 1985; Woll & Van Petegem, 2022). IP_3 binds to IP_3 receptors (IP_3R) on the SR, which leads to release of Ca^{2+} into the cytoplasm (Woll & Van Petegem, 2022). Restoration of SR Ca^{2+} levels is maintained by sarcoplasmic reticulum Ca^{2+} ATPase (SERCA), which pumps cytosolic Ca^{2+} back into the SR (Thastrup, 1990). In contrast, NO, an inhibitory neurotransmitter, binds to sGC forming cGMP, which activates protein kinase G (PKG) leading to activation of myosin phosphatase which dephosphorylates MLC and relaxes USMC (Koesling & Friebe, 2000; Andersson, 2001).

1.5 Spontaneous activity in urethral smooth muscle

USM generates spontaneous tone in various animal models such as sheep (Thornbury *et al.,* 1992), pig (Bridgewater *et al.,* 1993), human (Brading, 1999) and rabbit (Bradley *et al.,* 2004). Urethral tone arises from spontaneous myogenic activity modulated by neural inputs (Ito and Kimoto, 1985; Persson & Andersson, 1992; Sergeant *et al.,* 2019). Different studies have characterized spontaneous activity in USM using a variety of experimental approaches. In 1981, intracellular microelectrode recordings in guinea-pig USM by Callahan and Creed revealed spontaneous electrical activity comprised of infrequent bursts of depolarising spikes at 1-7 minutes intervals. Their findings also demonstrated that unlike DSM, electrical activity in USM was uncoordinated and asynchronous. During quiescent periods, the mean resting membrane potential (RMP) of guinea pig USM was -42 mV (Callahan & Creed, 1981). Spontaneous electrical activity in rabbit USM consists of regular, single or compound spikes occurring at a frequency of 9 to 30 per minutes (Creed *et al.,* 1997). It was subsequently reported that rabbit USM developed infrequent spontaneous action potentials and spontaneous depolarisations of amplitude ~16mV, with a mean RMP of -39 mV (Creed *et al.,* 1997).

Hashitani *et al.,* (1996) characterized spontaneous electrical activity in rabbit circular USM recorded from intracellular microelectrodes into two types of myogenic depolarisations, large regularly occurring depolarisations termed slow waves (SW)

and small irregular events termed spontaneous transient depolarisations (STD). SW lasted 1-3 sec every 3-15 sec, and were up to 40 mV in amplitude. In contrast, STD lasted <1 sec. Inhibitors of neural input such as tetrodotoxin (TTX), atropine, guanethidine and phentolamine had no effect on STD and SW, indicating they were myogenic. Cyclopiazonic acid (CPA, SERCA pump inhibitor), caffeine (increase Ca^{2+} release from stores via ryanodine receptors, RyR) and procaine (inhibits Ca^{2+} release from stores) inhibited both SW and STD, suggesting Ca^{2+} release from stores was required for their generation. Nifedipine (LTCC inhibitor) reduced duration of SW but did not inhibit generation of SW or STD. In contrast, low chloride solutions and Ca^{2+}-activated-Cl^{-}channel (CaCC) inhibitors, niflumic acid and 4,4'-diisothiocyanstilbene-2,2'-disulphonic acid (DIDS) inhibited SW and STD. These findings suggested Ca^{2+} release from intracellular stores activated CaCC, which mediated spontaneous electrical activity in USM (Hashitani *et al.,* 1996). Similar findings were reported in guinea-pig USM, where SW and STD were abolished by niflumic acid, low chloride solution, CPA and caffeine (Hashitani & Edwards, 1999).

In 2007, Hashitani and Suzuki studied USMC spontaneous activity utilizing a Ca^{2+} indicator dye, flou-4-AM loaded into rabbit USM tissues. They observed that USMC generated spontaneous non-propagating Ca^{2+} transients at a frequency of ~11 per min. The Ca^{2+} events were asynchronous and did not spread between bundles unlike DSM, where Ca^{2+} waves originating from a single site spread across the muscle bundle (Hashitani *et al.,* 2001). Drumm *et al.,* (2018) demonstrated spontaneous intracellular Ca^{2+} events in murine USMC using a transgenic mouse model, SmMHC-Cre-GCaMP3, in which the genetically encoded Ca^{2+} sensor GCaMP3 was specifically expressed in USMC. This Ca^{2+} activity was not synchronized with that of adjacent USMC, and these Ca^{2+} events did not propagate from cell to cell across the muscle bundles (Drumm *et al.,* 2018). This out-of-phase and asynchronous firing of multiple USMC leads to multiple small rhythmic contractions across the bundle over the same period, which averages as uniform tone (Drumm *et al.,* 2018, 2024; Sergeant *et al.,* 2019). Urethral tone is thus myogenic and does not require continuous neural input (Brading, 1999). However, urethral tone can be modulated by excitatory adrenergic (Alberts *et al.,* 1999; Andersson, 2001; Michel & Vrydag, 2006) or in some species, cholinergic neural input (Ek *et al.,* 1977; Ito & Kimoto, 1985; Bridgewater *et al.,* 1993)

and relaxed by inhibitory nitrergic input (Thornbury *et al.,* 1992; Zygmunt *et al.,* 1995; Waldeck *et al.,* 1998; De Groat *et al.,* 2001).

These findings raised several important questions regarding the mechanisms underlying urethral physiology. In other SM organs, such as the GI tract, spontaneous activity in SMC is regulated by a complex interplay of various ionic conductances and specialized cell types. In the following sections, I will briefly review such regulatory mechanisms in the gut, before discussing how this might relate to urethral physiology.

1.6 Interstitial cells of Cajal (ICC)

In the late 1900s, a Spanish histologist, Santiago Ramón y Cajal, discovered a population of cells (interstitial cells of Cajal, ICC) embedded in tunica muscularis between nerve ganglia and SM in the gut. Electron microscopy revealed ICC ultrastructure, exhibiting numerous agranular vesicles and tubules on their outer surface, along with membrane-bounded bodies containing dense granular material. Mitochondria were numerous, short and oval, with sparse distribution, and dense granules are scattered between vesicles (Rogers & Burnstock, 1966).

Thuneberg (1982) proposed ICC may act as pacemakers and fulfill a "conductive function" within GI muscles. This idea was supported by studies in the small intestine, where electron microscopy and immunohistochemistry demonstrated gap junctions connecting ICC to SMC in both the circular and longitudinal layers, providing a structural basis for electrical coupling and coordinated contraction (Rumessen *et al.,* 1993). ICC are now recognized as pacemaker cells of the GI tract, generating and propagating electrical SW that coordinate SMC contractions and underlie fundamental motility patterns such as peristalsis and segmentation (Sanders *et al.,* 2014, 2022, 2023). Their roles are supported by specialized ionic conductances and Ca^{2+} signalling mechanisms that enable ICC to mediate rhythmic electrical activity and neurotransduction in the GI tract (Sanders *et al.,* 2014, 2022, 2023). In gut, ICC are a heterogeneous population with distinct subtypes discussed below:

1. Myenteric ICC (ICC-MY) are multipolar cells with branched processes found in networks between circular and longitudinal muscle layers of the myenteron and surround myenteric ganglia, and have a pacemaker role in stomach, small bowel, and colon (Sanders *et al.,* 2014). ICC-MY generate spontaneous SW which initiate rhythmic contractions (Sanders, 1996; Hennig *et al.,* 2010). The RMP of GI SMC between each SW ranges between −80 and −40 mV, which is generally negative to the range of potentials required for substantive activation of voltage-dependent Ca^{2+} channels (Sanders *et al.,* 2014). The role of SW is to depolarise SMC enough to activate Ca^{2+} influx through LTCC to trigger excitation-contraction coupling (Ozaki *et al.,* 1991; Sanders *et al.,* 2014).

2. Intramuscular ICC (ICC-IM) are spindle shaped with bipolar branching and do not form interconnections with each other as illustrated in Fig 1.3 (Kito, 2011). They are found within the muscle bundles of oesophagus, internal anal sphincter (IAS), lower oesophageal sphincter (LES), stomach, small intestine, colon (Chen *et al.,* 2007; Kito, 2011; Drumm *et al.,* 2019a, 2022; Hannigan *et al.,* 2020; Ni Bhraonain *et al.,* 2025a). ICC-IM receive signals from both excitatory cholinergic and inhibitory nitrergic nerves (Ward *et al.,* 2006a; Sanders *et al.,* 2006; Al-Shboul, 2013). ICC-IM are in close proximity to enteric nerve varicosities, and establish gap junctions with surrounding SMC, allowing them to mediate enteric motor neurotransmission to SMC (Burns *et al.,* 1996; Sanders *et al.,* 2014;). In addition to neuromodulatory role, ICC-IM were also observed to play a role in tone generation in LES and IAS (Cobine *et al.,* 2017; Drumm *et al.,* 2022; Hannigan *et al.,* 2020; Ni Bhraonain *et al.,* 2025b). In LES and IAS, two distinct population of ICC-IM was observed where one subtype exhibited asynchronous Ca^{2+} activity due to endoplasmic reticulum (ER) Ca^{2+} release, contributing to tone generation required for sphincter closure, such as preventing gastric reflux at the LES, while other subtype of ICC-IM displayed synchronous Ca^{2+} activity which participates in SW generation, and also ER-mediated asynchronous Ca^{2+} activity (Hannigan *et al.,* 2020; Drumm *et al.,* 2022; Ni Bhraonain *et al.,* 2025b).

In addition to major ICC subtypes, region-specific populations have been identified based on their anatomical locations within the GI tract (Sanders *et al.,* 2014; Sanders,

2019). ICC-DMP, a subtype of ICC-IM, are located in the deep muscular plexus of the small intestine (Ward *et al.,* 2006b). ICC-SM at the submucosal border of the circular SMC layer generate pacemaker activity in the colon. ICC-SS are situated in the serosal layer of the longitudinal SM, while ICC-SEP reside in the septal spaces between muscle bundles (Baker *et al.,* 2021; Lee *et al.,* 2007). ICC-SEP are believed to be extensions of ICC-MY or ICC-SM and contribute to the propagation of slow waves, however they are only present in larger mammals such as dogs and human (Sanders, 2019; Ward & Sanders, 1990; Lee *et al.,* 2007).

The proto-oncogene *kit* (CD117), a tyrosine kinase receptor, serves as a non-selective cellular marker for ICC, as it is also expressed in other cell types, including mast cells (Torihashi *et al.,* 1995). Mutant mice with defects in *kit* and lesions of pacemaker ICC-MY or neuromodulator ICC-IM in specific GI organs, manifest as a loss of pacemaker activity, rhythmic contractions, and postjunctional neural responses in affected tissues (Ward *et al.,* 1994, 2000; Burns *et al.,* 1996). Burns *et al.,* (1996) reported that *c-kit* mutant mice (W/W^V) lacked ICC-IM in the stomach (gastric fundus). In wild-type (WT) mice, EFS evoked inhibitory junction potentials (IJP) and muscle relaxation, whereas in *c-kit* mutants, IJPs were attenuated, and relaxation was minimal or absent, despite a normal distribution of inhibitory nerves in the stomach of *c-kit* mutants (Burns *et al.,* 1996). Similar findings were reported in murine lower esophageal (LES) and pyloric sphincter, where ICC-IM were absent in *c-kit* mutant mice and NO-dependent inhibitory neurotransmission was also reduced (Ward *et al.,* 1998). These findings suggest that the absence of ICC-IM markedly impairs nitrergic neurotransmission.

Subsequent immunolabelling with anti-vesicular acetylcholine transporter (vAChT) and Kit antibodies demonstrated that vAChT-positive nerve fibers were closely associated with ICC-IM in the murine gastric fundus (Ward *et al.,* 2000). Double-labelling with neuronal nitric oxide synthase (nNOS) and Kit antibodies further revealed that this close morphological association extended to inhibitory enteric neurons, indicating that ICC-IM interact with both excitatory and inhibitory nerve fibers (Ward *et al.,* 2000). Moreover, cholinergic nerve-mediated excitatory junction potentials (EJPs) evoked by EFS or electrical vagal nerve stimulation in the gastric fundus muscle of *c-kit* mutant mice were markedly reduced or absent compared to those observed in wild-type mice (Ward *et al.,* 2000; Beckett *et al.,* 2017).

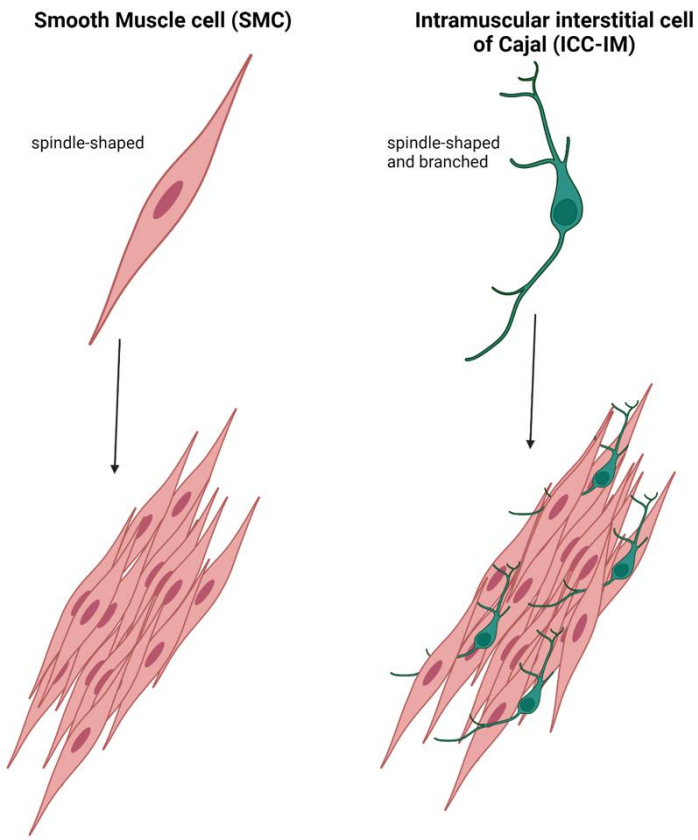

Fig 1.3: Schematic illustration of SMC and ICC-IM in the gut. SMC are spindle-shaped and organized in bundles, whereas ICC-IM are elongated with branched processes but do not form interconnections.

1.7 Role of chloride conductances in ICC

Tokutomi *et al.,* (1995) reported that the reversal potential of rhythmic inward currents in intestinal *Kit*$^+$ cells was close to the Cl^- equilibrium potential (E_{Cl}) ~ -10 mV, indicating a primary role for a Cl^- conductance (Tokutomi *et al.,* 1995). These currents were significantly inhibited by the anion transport inhibitor SITS (4-acetoamido-4-isothiocyanatostilbene-2,2'-disulfonic acid). Later, a high-conductance Cl^- channel in ICC was identified, that was spontaneously and rhythmically active at a frequency of 20–30 cycles per min at room temperature (RT), matching the frequency of pacemaker activity, thereby reinforcing the role of Cl^- channels in ICC-mediated SW generation (Huizinga *et al.,* 2002).

In 2002, it was reported in guinea pig stomach ICC that Ca^{2+} release from the internal stores activates CaCC (Hirst *et al.,* 2002; Kito *et al.,* 2002). Kito *et al.,* (2002) showed

that inhibition of SERCA pumps by CPA inhibited the plateau phase of SW and inhibiting IP_3R with 2-APB abolished SW. Moreover, DIDS (4,4′-diisothiocyano-2,2′-stilbene disulphonic acid) and low chloride solution also inhibited the plateau phase of SW (Kito *et al.,* 2002). Similar findings were reported by Hirst *et al.,* 2002 in a combination of Ca^{2+} imaging and electrophysiological recordings in single bundles of circular muscle isolated from the gastric antrum of guinea-pigs (Hirst *et al.,* 2002).

The previous studies on gut identified ICC based on the expression of Kit; however, as mast cells also express Kit (Metzger *et al.,* 2008), this marker lacked specificity. Later, a specific CaCC family member, Anoctamin 1 (ANO1), was identified and found to be selectively expressed in ICC in the gut (Chen *et al.,* 2007; Gomez-Pinilla *et al.,* 2009; Hwang *et al.,* 2009). ANO1 co-localized with Kit in the GI tract but was absent in mast cells, making it a more specific marker for ICC (Gomez-Pinilla *et al.,* 2009; Zhu *et al.,* 2009).

Hwang *et al.,* (2009) observed that loss or inhibition of ANO1 results in ablation of SW in GI muscles (Hwang *et al.,* 2009). Moreover, Sung *et al.,* (2018) observed that cholinergic contractions evoked by nerve stimulation were reduced in gastric fundus muscle of mice with conditional knockdown of ANO1 in Kit^{+} cells ($Kit^{CreERT2/+}$; $Ano1^{tm1jrr/-}$, (*i*$Ano1^{-/-}$)) (Sung *et al.,* 2018). In addition, blocking ANO1 inhibited post stimulus depolarisations in colonic muscles and colonic migrating motor complexes in intact colons (Koh *et al.,* 2022). Hwang *et al.,* (2016) observed differences in the sensitivity to ANO1 antagonists between gastric and small intestinal muscles, and predicted this was due to variations in ANO1 splice variants or intracellular Ca^{2+} levels (Hwang *et al.,* 2016). However, subsequent work showed that ANO1 knockdown ($Kit^{CreERT2/+}$; $Ano1^{tm2jrr/+}$) was similar in both tissues, yet SW were retained in the small intestine but largely absent in the stomach (Hwang *et al.,* 2019). In a comparison between adult and juvenile mice, ANO1 antagonists were less effective at inhibiting SW in adult small intestinal muscles than juveniles, suggesting age-dependent compensation by other conductances (Hwang *et al.,* 2019).

ANO1 channels have also been reported to contribute to pacemaker activity, and maintenance of tone in GI sphincters such as the LES and IAS. Pharmacological inhibition of ANO1 with CaCCinh-A01 or Ani9 inhibited rhythmic Ca^{2+} activity in a

secondary subtype of murine ICC-IM in LES and IAS (Hannigan *et al.,* 2020; Ni Bhraonain *et al.,* 2025b). Blockade of ANO1 channels with Ani9 also resulted in decline in tone in IAS tissue from mouse and monkey (Drumm *et al.,* 2022).

The findings above highlight the critical role ANO1 in identifying and characterizing gut ICC. ANO1, in particular, has emerged as a more selective marker and functional contributor to ICC activity and will be discussed in greater detail in a later section. Interestingly, ICC-like cells (ICC-LC) have also been identified in various organs across multiple species, and their presence and potential functions in other organs including urethra will be explored in the following section.

1.8 Interstitial cells of Cajal- like cells (ICC-LC)

Kit$^+$ ICC-like cells (ICC-LC) are found in mouse ureter (Pezzone *et al.,* 2003), prostate (Exintaris *et al.,* 2004), lymphatics (McCloskey & Gurney, 2002), blood vessels (Harhun *et al.,* 2004), fallopian tube (Popescu *et al.,* 2005) and renal pelvis (Lang *et al.,* 2007). The nomenclature for these cells varies among research groups; they have been referred to as pacemaker cells, Cajal cells, or ICC-like cells (ICC-LC). In this thesis, I use the term ICC-LC to describe these cells in organs other than the GI tract.

As mentioned earlier, Hashitani *et al.,* (1996, 1999) demonstrated SW and STD in rabbit and guinea pig urethra. However, no specialized pacemaking cells were known in urethra at that time. Later, Smet *et al.,* (1996) reported cGMP and vimentin$^+$ branched cells in the bladder and urethra of human and guinea-pig. The presence of vimentin$^+$ ICC-LC in rabbit urethra was shown by Sergeant *et al.,* (2000). When strips of rabbit urethral tissues were enzymatically treated to yield isolated cells, two distinct cell populations were found. 85-90% of cells were contractile USMC, which were electrically quiescent. A second, non-contractile cell type, which stained for the intermediate filament marker vimentin (but not myosin), were termed interstitial cells (hence forth termed ICC-LC in this thesis) (Sergeant *et al.,* 2000). Later, immunolabelling with anti-kit antibody revealed a population of *kit*$^+$ cells in rabbit USM similar to the ICC-IM present in gut (McHale *et al.,* 2006; Lyons *et al.,* 2007).

In current clamp recordings, STD occurred in rabbit ICC-LC (Sergeant *et al.,* 2000). In voltage clamp at -60 mV, ICC-LC exhibited spontaneous transient inward currents (STIC), which were attenuated by niflumic acid in both frequency and amplitude (Sergeant *et al.,* 2000), and increased by NA (Sergeant *et al.,* 2002). This led to the hypothesis that similar to ICC in the GI tract, spontaneous activity in urethral ICC-LC may depolarise USMC and increase the probability of LTCC opening, facilitating contraction. Spontaneous activity of ICC-LC was inhibited by CPA, ryanodine (RyR inhibitor), PLC inhibitors, 2-APB and anoctamin-1 inhibitors (ANO1, a family of CaCC) such as T16Ainh-A01 and CaCCinh-A01 (Sergeant *et al.,* 2000, 2001a, 2001b; Fedigan *et al.,* 2017). These findings suggested that spontaneous electrical activity of rabbit ICC-LC resulted from CaCC activation, specifically ANO1 channel activation via intracellular store Ca^{2+} release. Moreover, ANO1 mRNA expression was found exclusively in ICC-LC and not on USMC in rabbit (Fedigan *et al.,* 2017). In contrast, Sancho *et al.,* (2012) demonstrated ANO1 was expressed in USMC and not on vimentin^{+} ICC-LC in sheep, rat and mouse urethra. Moreover, application of SITS (anion transport inhibitor) had no effect on EFS-evoked or NA-induced dose dependent contractions, however other non-selective CaCC inhibitor such as niflumic acid and anthracene chloride (9-AC) inhibited EFS-or agonist-induced contractions in mouse, rat and sheep (Sancho *et al.,* 2012). Taken together, these findings indicate that ANO1 expression in the urethra, whether on ICC-LC or USMC, varies across species.

When rabbit urethral ICC-LC were held under voltage clamp at -30 mV, STIC and two types of STOC (slow spontaneous transient outward currents) developed: fast and slow (Sergeant *et al.,* 2001a). Application of penitrem A, antagonist of large conductance Ca^{2+}-activated-K^{+}channels (BK channels) completely blocked STOC and unmasked larger STIC, suggesting that BK channel activity was partially inhibiting STIC. Caffeine, CPA or ryanodine blocked STIC and both fast and slow STOC, suggesting that they were activated by ER Ca^{2+} release. However blocking IP_3R with 2-APB abolished only STIC and slow STOC, which led to the proposal that pacemaker activity in ICC-LC is driven by IP_3 sensitive stores (Sergeant *et al.,* 2001a). Further investigation using voltage clamp and Ca^{2+} imaging simultaneously, revealed that STIC were associated with intracellular Ca^{2+} waves, as 2-APB abolished STIC, but only reduced spatial spread of Ca^{2+} wave (Johnston *et al.,* 2005). However, inhibition

of RyR with either tetracaine or ryanodine abolished all spontaneous Ca^{2+} events (Johnston *et al.,* 2005). Together, these results indicate that Ca^{2+} release through RyR initiates local Ca^{2+} transients, but these microdomain signals are not sufficient to activate CaCC. STIC require a larger, global rise in intracellular Ca^{2+}, which depends on recruitment of IP_3-mediated Ca^{2+} release to amplify the RyR-initiated signal, resulting in propagation of intracellular Ca^{2+} wave. Thus, RyR provide the trigger for Ca^{2+} event initiation, while IP_3-dependent Ca^{2+} release is essential for generating the global Ca^{2+} elevations required to activate CaCC and produce STIC.

Subsequent studies reported that Ca^{2+} influx through NCX (sodium-calcium exchanger) also participate in the intracellular Ca^{2+} wave propagation (Bradley *et al.,* 2006; Drumm *et al.,* 2015). NCX is a bi-directional regulator of cytosolic Ca^{2+}, causing Ca^{2+} efflux in forward-mode and Ca^{2+} influx in reverse-mode (Tykocki *et al.,* 2012). Ca^{2+} release from RyR is an absolute requirement in all cases to provide the initial Ca^{2+} wave signal, while under normal conditions enhanced Ca^{2+} influx from NCX sensitize both or either IP_3R/RyR to facilitate Ca^{2+} wave propagation (Drumm *et al.,* 2015). Thus, the integrated contribution of RyR, IP_3R and NCX supports the global Ca^{2+} signals that underlie CaCC opening and the generation of STIC within rabbit urethral ICC-LC. This, in turn, enhances the excitability of electrically coupled USMC, leading to voltage-dependent Ca^{2+} channel activation and contraction, analogous to the role of pacemaker ICC in the gut.

Exogenous ATP increased frequency of STIC and Ca^{2+} waves via activation of P2Y receptors in rabbit urethral ICC-LC (Bradley *et al.,* 2010). NA also increased frequency of STIC, STD (Sergeant *et al.,* 2002), and Ca^{2+} waves in rabbit ICC-LC (Hashitani & Suzuki, 2007), while NO donors reduced STIC and STD frequency by reducing Ca^{2+} wave spatial spread (Sergeant *et al.,* 2006a). This suggested ICC-LC may mediate neural signals to USMC, as do ICC-IM in GI organs (Ward *et al.,* 2000; Suzuki *et al.,* 2003). This was supported by close anatomical associations between *kit*$^+$ ICC-LC and nitrergic nerves in rabbit urethra (Lyons *et al.,* 2007). In rat and sheep urethra, cGMP immunoreactivity was induced in both ICC-LC and USMC upon nitrergic nerve stimulation, suggesting that both cell type act as targets of NO (García-Pascual *et al.,* 2008). Further studies confirmed the expression of gap junctions in SMC and ICC-LC, however their inhibition with antagonist such as 18α-glycyrrhetinic acid did not alter

either agonist- or EFS-induced responses in sheep and rat urethra (Sancho *et al.,* 2011), suggesting that gap junctions may not play a significant role in urethral neurotransmission. In contrast to rabbit USM, NO-GC (NO-sensitive guanylyl cyclase) staining in WT mouse USM was co-localized with USMC, and no NO-GC expression was detected in SM-GCKO (smooth muscle cell-specific guanylyl cyclase knockout) USM tissue (Lies *et al.,* 2013). Application of DEA-NONOate (NO donor) induced dose-dependent relaxation on PE-induced contraction in WT mice urethra, but had no effect in SM-GCKO or global GCKO mice urethra (Lies *et al.,* 2013). These findings indicate that, in mouse urethra, USMC but not ICC-LC mediate nitrergic relaxation and highlight species-specific differences in nerve innervation of USMC and ICC-LC.

Hashitani *et al.,* (2007) performed experiments on intact rabbit urethral tissues, which were loaded with a Ca^{2+} dye (Fluo4-AM) to investigate ICC-LC Ca^{2+} activity *in situ*. They observed ICC-LC were sparsely distributed in rabbit USM and were not present in networks. ICC-LC activity did not exhibit a close temporal relationship with USMC but often fired synchronous Ca^{2+} activity (while USMC activity was asynchronous). ICC-LC Ca^{2+} activity was not sensitive to nicardipine (LTCC inhibitor), but was abolished by CPA, 2-APB and ryanodine. ICC-LC Ca^{2+} activity was enhanced by PE and abolished by SIN-1 (NO donor) (Hashitani & Suzuki, 2007). These findings indicated ICC-LC Ca^{2+} activity relied on Ca^{2+} release from stores and does not depend on Ca^{2+} influx by LTCC.

However, most of the above studies on rabbit ICC-LC were performed on isolated single cells, which were recognized as ICC-LC based on morphology, lacking detection based on a cellular marker. Hashitani *et al.,* (2007) conducted Ca^{2+} imaging on intact rabbit urethral tissue using Flou4-AM, cell permeable Ca^{2+} indicator dye that loads into all cell types without discrimination. As a result, the specific identity of the cells generating the observed Ca^{2+} signals could not be confirmed. In addition, their assessment of neural regulation relied on exogenous application of neurotransmitters or receptor agonists rather than direct stimulation of intramural nerves. ICC-LC were therefore never examined under conditions that mimic physiological neurotransmission. This leaves a significant gap in our understanding of how ICC-LC behave within intact urethral tissue and whether they function as direct targets of neural input in the urethra.

A defining feature of ICC in the gut and ICC-LC across multiple organ systems is the functional expression of CaCC, which are critical for generating spontaneous electrical activity. These channels contribute to pacemaker currents and neuromodulation, playing a central role in regulating excitability and contractility, as demonstrated by the findings mentioned in above sections. Among the known CaCC, ANO1 has been identified as a key protein mediating these functions. The following section focuses on ANO1, outlining its role in SM physiology across various organs, including the urethra.

1.9 Anoctamin 1 (ANO1) channels

A chloride (Cl^-) conductance, activated by an increase in intracellular Ca^{2+}, was first identified in the early 1980s in *Xenopus* oocytes (Barish, 1983) and salamander retinas (Bader *et al.,* 1982). In oocytes, CaCC induced membrane depolarisation, preventing polyspermy following fertilization (Barish, 1983), though the exact mechanism remained unclear. Anoctamin1 (ANO1) or TMEM16A or DOG1, a type of CaCC, is the most studied member of the anoctamin family. ANO1 was discovered by three research group in the same year independently (Caputo *et al.,* 2008; Schroeder *et al.,* 2008; Yang *et al.,* 2008). ANO1 is a homodimeric CaCC with a complex transmembrane structure consists of 10 transmembrane domains (TMDs), with both N- and C-termini located intracellularly (Pedemonte & Galietta, 2014). A key structural feature is the re-entrant loop between TMD5 and TMD6, which forms the anion-selective pore critical for ion permeability (Pedemonte & Galietta, 2014; Hawn *et al.,* 2021). Structural models also suggest lateral association of transmembrane helices (TMD3-TMD8) to create the ion conduction pathway, with alternative splicing (e.g., segments *a-d*) modifying intracellular domains to regulate Ca^{2+} sensitivity and gating kinetics (Hawn *et al.,* 2021).

Human ANO1 has four key splice segments: *a*, *b*, *c*, and *d*, encoded by different exons (Caputo *et al.,* 2008; Sung *et al.,* 2016). Segment *a* is involved in protein trafficking and plasma membrane expression, while segment *b* (encoded by exon 6b) reduces Ca^{2+} sensitivity by nearly fourfold, though the mechanism remains unclear (O'Driscoll *et al.,* 2011). Segment *c* (exon 13) alters voltage and time dependence and influences Ca^{2+} sensitivity of ANO1 (Ferrera *et al.,* 2009; Xiao *et al.,* 2011), and segment *d* (exon 15) slows activation / deactivation kinetics without affecting current magnitude

(O'Driscoll *et al.,* 2011). Additionally, exon 0, upstream of exon 1, enhances ANO1 expression and adds amino acids to the N-terminal domain (Wang *et al.,* 2017; Hawn *et al.,* 2021). These splice variants contribute to tissue-specific functionality and influence ANO1's biophysical properties, such as differential Ca^{2+} sensitivity and gating behaviour.

When activated by intracellular Ca^{2+}, ANO1 channels allow Cl^- movement according to the prevailing electrochemical gradient. In SMC and ICC, the intracellular Cl^- concentration is maintained above its electrochemical equilibrium, typically via active transport mechanisms such as Na^+-K^+-$2Cl^-$ cotransporter 1 (NKCC1) and Cl^-/HCO_3^- exchange (Wray *et al.,* 2021; Goto *et al.,* 2022; Zhu *et al.,* 2009). Under these conditions, if ANO1 channels open, it leads to Cl^- efflux, resulting in membrane depolarisation, which can subsequently activate voltage-dependent LTCC, if present (Leblanc *et al.,* 2005; Dunford *et al.,* 2020; Drumm *et al.,* 2021; Wray *et al.,* 2021).

ANO1 is expressed in various SMC including vascular SMC (Davis *et al.,* 2010), and inhibition of ANO1 results in vasorelaxation in murine and human arteries (Davis *et al.,* 2013). A previous study reported that ANO1 mediates the myogenic response, defined as pressure-induced vasoconstriction, in cerebral arteries (Bulley *et al.,* 2012). Knockdown of ANO1 suppressed myogenic responses, significantly reducing both pressure-induced vasoconstriction and membrane depolarisation in vascular SMC (Bulley *et al.,* 2012). Huang *et al.,* (2009) found ANO1 is expressed in airway SM, oviduct SM and ductus epididymis SM. A previous study reported an increase in expression of ANO1 in murine asthmatic models and human asthmatic patients (Huang *et al.,* 2012). Inhibition of ANO1 by benzbromarone significantly attenuated mouse and human airway SM contractions in response to cholinergic agonists (Huang *et al.,* 2012). In murine airway SM, M_2R mediated contractions were inhibited by blocking ANO1 channels by Ani9 and CaCCinh-A01 (Ghosh *et al.,* 2025). In mouse renal pelvis, inhibition of ANO1 by CaCCinh-A01 and benzbromarone resulted in significant reduction in frequency and Ca^{2+} wave propagation in SMC, inhibiting proximal to distal peristaltic propagations (Grainger *et al.,* 2022).

ANO1 protein is abundantly and specifically expressed in ICC throughout the murine, non-human primate (*Macaca fascicularis*), and human GI (gastrointestinal) tracts

(Gomez-Pinilla *et al.,* 2009; Hwang *et al.,* 2009). Pharmacological blockade of CaCC with niflumic acid and DIDS reduced SW frequency and amplitude in a concentration-dependent manner across species (Hwang *et al.,* 2009). Moreover, SW failed to develop by birth in Tmem16a$^{-/-}$ mice (Tmem16a$^{tm1Bdh/tm1Bdh}$) (Hwang *et al.,* 2009). CaCCinh-A01 and T16Ainh-A01 caused a reduction in SW of murine IAS (Cobine *et al.,* 2017). Cholinergic stimulation of isolated ICC-IM by CCh activated Cl^- conductance, which were blocked by benzbromorone and T16Ainh-A01 in gastric fundus. In addition, cholinergic nerve stimulation-evoked contractions were significantly reduced in ANO1 knockout mice (Tmem16a$^{-/-}$ mice) (Sung *et al.,* 2018).

Hwang *et al.,* (2016) observed differences in the sensitivity of gastric and small intestinal muscles to ANO1 antagonists and proposed that these variations might reflect differences in ANO1 splice variants or intracellular Ca^{2+} levels. However, subsequent work using ANO1 knockdown mice (Kit$^{CreERT2/+;}$ Ano1$^{tm2jrr/+}$) demonstrated that SW were preserved in the small intestine but were largely absent in the stomach, despite comparable reduction of ANO1 in both tissues (Hwang *et al.,* 2019). Further comparison between adult and juvenile mice showed that ANO1 antagonists were less effective in suppressing SW in adult small intestine compared with juveniles, suggesting that compensatory conductances emerge with age (Hwang *et al.,* 2019).

Recent work in the murine gastric corpus showed that ANO1-mediated STD play an important role in setting the RMP. In these experiments, longitudinal muscle and ICC-MY were removed so that STD could be recorded specifically from ICC-IM within circular muscle bundles (Hwang *et al.,* 2024). STD generated by ICC-IM provided a depolarizing drive that spread to neighbouring SMC. These events were eliminated by Ani9 or CaCCinh-A01, and inhibition of ANO1 produced a marked hyperpolarisation of muscle bundles (Hwang *et al.,* 2024). Together, these findings indicate that ANO1 activity regulates RMP in GI muscles.

Role of ANO1 channels in urethral smooth muscle

In urethra, the role of CaCC, was first reported in rabbit and guinea pig USM, where STD and SW were observed to be dependent on intracellular Ca^{2+} release, as they were abolished by Ca^{2+}-free solution, BAPTA-AM (Ca^{2+} chelator), and CPA (Hashitani

et al., 1996; Hashitani & Edwards, 1999). Pharmacological evidence suggested that Ca^{2+} release from ER stores activated CaCC, leading to depolarisation (Hashitani *et al.,* 1996; Hashitani & Edwards, 1999). This was supported by inhibition of STD and SW by low-Cl^- solution and non-selective CaCC blockers such as niflumic acid and DIDS (Hashitani *et al.,* 1996; Hashitani & Edwards, 1999).

Further evidence came from perforated patch-clamp recordings in isolated sheep USMC, which revealed a functional I_{ClCa} (Cotton *et al.,* 1997). Under step protocol from −80 to +50 mV, sheep USMC evoked two inward currents: a fast component peaking near 0 mV (reversed at +50 mV), and a slower current reversing near 0 mV and becoming outward at positive potentials (Cotton *et al.,* 1997). The fast current showed characteristics of LTCC, while the slower was identified as I_{ClCa} based on reversal shift in low-Cl^- solution and inhibition by niflumic acid and 9-AC, without affecting the fast current (Cotton *et al.,* 1997). Moreover, caffeine evoked I_{ClCa}, which was blocked by niflumic acid, confirming the role of SR Ca^{2+} release in its activation. In contrast, rabbit USMC were electrically quiescent (Sergeant *et al.,* 2000). However rabbit ICC-LC showed I_{ClCa} when held at -60 mV, followed by step protocols from −80 to +50 mV, which was reversed at the Cl^- equilibrium potential (0 mV) and reduced by niflumic acid and 9-AC (Sergeant *et al.,* 2000). When held at −60 mV, rabbit USM ICC-LC elicited STIC that were abolished by niflumic acid, CPA, high doses caffeine, ryanodine and 2-APB (Sergeant *et al.,* 2000; Sergeant *et al.,* 2001a). This indicated Ca^{2+} release from stores activated CaCC, generating STD & STIC in rabbit ICC-LC.

Sancho *et al.,* (2012) found high immunoreactivity of ANO1 on USMC and urothelia of multiple species (mouse, rat, sheep), whereas ANO1 was not found on vimentin$^+$ ICC-LC. Niflumic acid and 9-AC reduced EFS-evoked and NA induced dose-dependent responses in sheep, mouse and rat USM (Sancho *et al.,* 2012). In contrast, Fedigan *et al.,* (2017) reported ANO1 was exclusively expressed in rabbit ICC-LC and not in USMC through qPCR studies. While recording rabbit urethral ICC-LC at -60 mV in a patch-clamp experiment, both STIC and STD were inhibited by $CACC_{inh}$-A01 and $T16A_{inh}$-A01 (Fedigan *et al.,* 2017). Moreover, $CACC_{inh}$-A01 and $T16A_{inh}$-A01 attenuated EFS-evoked contractions in strips of rabbit USM (Fedigan *et al.,* 2017). In contrast, inhibition of ANO1 by $CACC_{inh}$-A01 and Ani9 (selective ANO1 inhibitor) had

no effects on urethral tone and EFS-evoked contractions in pig (Rembetski *et al.,* 2020).

A previous study suggested that in mouse and human urethra, ANO1 contributes to sex differences in relation to spontaneous USM tone generation. They reported that ANO1 expression in mouse and human USMC was nearly twice as high in females compared to males, which corresponded with greater spontaneous tone in female urethra (Chen *et al.,* 2020). They further demonstrated that Cl^- current recorded in isolated female mice USMC were greater than male and application of $T16A_{inh}$-A01 suppressed it. Genetic deletion of ANO1 in SM ($TMEM16A^{SMKO}$) resulted in impaired urethral tone in mice. In addition, spontaneous tone in human and WT mouse urethra was diminished by T16Ainh-A01, ryanodine, or nifedipine, and caffeine-evoked contractions were similarly reduced by these interventions (Feng *et al.,* 2019). Together, these findings led the authors to propose that Ca^{2+} release through RyR activates ANO1, and that ANO1 activity subsequently promotes LTCC activation, thereby supporting USM tone.

Previous studies on USM shown importance of ANO1 in pathological conditions. Chen *et al*., (2022) reported that female mice with hypertriglyceridemia, induced by a high-fat diet, lost spontaneous USM tone and showed reduced contractions to EACT, which they attributed to downregulated ANO1 expression in USMC. A separate recent study showed that ANO1 expression co-localised with c-kit in mouse and human urethral stromal cells, which the authors interpreted as ICC-LC (Ambrogi *et al.,* 2025). However, these stromal cells did not display the typical elongated or branched morphology characteristic of gut ICC (Hwang *et al.,* 2009) or the ICC-LC previously described in rabbit urethra (Sergeant *et al.,* 2000). This study further proposed a mechanism in which TRPA1 activation in urethral neuroendocrine cells during *E. coli* infection triggers Ca^{2+} influx and release of serotonin (5- hydroxytryptamine, 5-HT) (Ambrogi *et al.,* 2025). 5-HT then acts on HTR3 and HTR2B receptors and on ANO1 channels expressed in urethral stromal cells to produce contractions that aid in bacterial expulsion. The proposal was supported by observations that female mice deficient in 5-HT synthesis (Tph1 knockout) or lacking neuroendocrine cells (Ascl1 conditional knockout) developed more severe infections than WT females (Ambrogi *et al.,* 2025). They also showed that 5-HT-evoked contractions were blocked by Ani9 and

that both EACT and the HTR2B agonist BW723C86 hydrochloride produced contractions even in the absence of 5-HT (Ambrogi *et al.,* 2025).

Although ANO1 function in ICC is well established in the GI tract, its role in the urethra is more difficult to define because the available evidence varies considerably among species. Some studies report ANO1 expression and function primarily in ICC-LC, whereas others identify its expression mainly in USMC. These species-dependent patterns lead to different interpretations of how ANO1 contributes to urethral excitability and tone. Most of the existing evidence for a functional contribution of ANO1 to USM contractility comes from studies that used pharmacological inhibitors such as DIDS, MONNA, niflumic acid, CaCCinh-A01, and T16inh-A01. These agents are now known to exert substantial off-target effects on LTCC and SR Ca^{2+} release mechanisms (Cruickshank, Baxter and Drummond, 2003; Boedtkjer *et al.,* 2015; Genovese *et al.,* 2023; Dwivedi *et al.,* 2023), which could affect interpretation of earlier findings. This highlights the need for studies employing more selective pharmacological tools and refined experimental approaches to clarify the precise role of ANO1 in USM contractility. Previous studies in other SM organs showed ANO1 depolarise the membrane potential, which in turn opens voltage gated Ca^{2+} channels leading to Ca^{2+} influx in SMC. Given this close interplay, the following section explores the role and mechanisms of voltage-gated Ca^{2+} channels in SM tissues, including their potential contribution to urethral contractility in different species.

1.10 Voltage-gated Ca^{2+} channels (VGCC)

Voltage-gated Ca^{2+} channels (VGCC) regulate Ca^{2+} influx in SMC, which in turn controls their contraction (Brading, 1999). There are two types of VGCC in rabbit and human urethra, L-type and T-type (Hollywood *et al.,* 2003; Bradley *et al.,* 2004).

- **L-type Ca^{2+} channels**

Long-lasting voltage-gated Ca^{2+} channels (L-type Ca^{2+} channels, LTCC) are activated at voltages from -20 mV to -40 mV and inactivate at -50 to -70 mV (Kopecky *et al.,* 2014). LTCC are composed of a voltage sensing α1 subunit forming a pore through which Ca^{2+} passes, and β, α2δ, and γ regulatory subunits (Catterall, 2011; Hill-

Eubanks *et al.,* 2011; Dolphin, 2012; Striessnig *et al.,* 2014). α1 subunits of LTCC forms a pseudotetrameric structure, consisting of four repeat domains (I-IV), each containing six transmembrane segments (S1-S6) and intracellular N- and C-termini (Catterall, 2000; Hill-Eubanks *et al.,* 2011), analogous to individual subunits of tetrameric voltage-gated potassium (K^+) channels (Hill-Eubanks *et al.,* 2011).

The most common isoforms of the LTCC α1 subunit are: Cav1.1, Cav1.2, Cav1.3, and Cav1.4 (Striessnig *et al.,* 2014). In SM, Cav1.2 is the dominant subtype, where it mediates Ca^{2+} influx essential for contraction (Moosmang *et al.,* 2003; Sommer *et al.,* 2016; Yu, 2022). Moosmang *et al.,* (2003) reported reduced mean arterial blood pressure in transgenic mice with knocked out Cav1.2 from SM. Moreover, agonist-induced contractions in human bronchial and tracheal SM were inhibited by nifedipine (LTCC inhibitor) (Drazen *et al.,* 1983; Kohrogi *et al.,* 1985), indicating an important role of LTCC in mediating these contractions. Similarly, esophageal manometery studies showed decreased LES pressure after oral doses of nifedipine in humans (Hongo *et al.,* 1984). In murine colon, inhibition of LTCC resulted in 95% reduction of spontaneous contractions in amplitude (Fida *et al.,* 1997). A previous study showed that LTCC were responsible for Ca^{2+} store refilling in guinea pig detrusor DSMC, as store refilling was enhanced by sustained depolarisation and attenuated by LTCC antagonists (Wu *et al.,* 2002).

Several studies have examined the contribution of LTCC to USM function across species. In pig USM, dihydropyridines such as nifedipine lowered basal tone, reduced agonist-evoked contraction and diminished nerve-evoked responses (Brading, 1999; Greenland *et al.,* 1996; Rembetski *et al.,* 2020). Electrophysiological studies also supported a role for LTCC in rabbit and human USMC that exhibited LTCC currents which were sensitive to nifedipine (Bradley *et al.,* 2004; Hollywood *et al.,* 2003). Ca^{2+} imaging studies further indicated LTCC involvement, as nicardipine decreased Ca^{2+} activity in rabbit USMC (Hashitani & Suzuki, 2007), and nifedipine shortened slow-wave duration in guinea pig USM (Hashitani & Edwards, 1999).

However, LTCC involvement in USM tone generation and maintenance of contractions is not consistent across all species and the underlying reasons for these differences remain unclear. Oral nifedipine did not alter urethral pressure in male cats or human

females (Forman *et al.,* 1978; Mawby *et al.,* 1991). Likewise, NA-evoked contraction in rabbit and sheep urethra persisted despite LTCC block (Larsson *et al.,* 1984; Garcia-Pascual *et al.,* 1991). In male mouse, LTCC inhibition did not affect agonist-induced contraction, and neither LTCC block nor activation changed intracellular Ca^{2+} activity *in situ* in USMC (Drumm *et al.,* 2018).

Introduction of extracellular Ca^{2+} after thapsigargin treatment in Ca^{2+}-free conditions, which prevents SR store refilling, produced a marked overshoot in USM tone in male mice. This response is characteristic of SOCE (Putney, 1986) and was unaffected by nifedipine, yet completely abolished by GSK-7975A (Orai channel antagonist), indicating that SOCE in mouse USM is mediated predominantly by Orai channels rather than LTCC. In contrast, applying the same protocol to pig USM showed that the tone overshoot was eliminated by nifedipine (Drumm *et al.,* 2018), suggesting that SOCE in pig relies primarily on LTCC. These observations point to species-specific differences in the Ca^{2+} entry pathways that support SOCE in the urethra (Rembetski *et al.,* 2020). Taken together, previous evidences suggests that LTCC support contractile behaviour in certain species such as pig, rabbit and guinea pig, but alternative Ca^{2+} entry pathways may dominate USM regulation in others.

LTCC activity is regulated by interplay of various ion channels, including ANO1 and potassium channels (Drumm *et al.,* 2021). ANO1 channels contributes to membrane depolarisation, which facilitates activation of LTCC (Hashitani *et al.,* 1996; Hashitani & Edwards, 1999; Bulley *et al.,* 2012). In contrast, opening of potassium channels, such as large-conductance Ca^{2+}-activated potassium (BK_{Ca}) channels and voltage-gated Kv7 channels, induces membrane hyperpolarisation, leading to inactivation of LTCC (Jackson, 2016; Sancho and Kyle, 2021). These opposing influences are likely to differ among species, and such differences may explain why LTCC appear to contribute strongly to urethral contractility in some species but play a more limited role in others. However, at present, there are no definitive evidences that define how these mechanisms modulate LTCC activity in murine USM.

- **T-type Ca^{2+} channels**

Transient-lasting VGCC (T-type, TTCC) or low voltage activated channels, open between -80 to -40 mV (Hollywood *et al.,* 2003; Kopecky *et al.,* 2014; Kyle, 2014). TTCC are distinct from other VGCC due to their rapid activation and inactivation kinetics, as well as their slow deactivation (Perez-Reyes, 2003; Ono & Iijima, 2005). In vertebrates, the TTCC family is composed of three distinct genes encoding the α1 subunit: CACNA1G, CACNA1H, and CACNA1I (Iftinca, 2011). These genes correspond to α1G, α1H, and α1I subunits, respectively (McRory *et al.,* 2001). According to the current nomenclature, these subunits are designated as Cav3.1, Cav3.2, and Cav3.3 (Iftinca, 2011).

TTCC controls the pacemaking activity of the sinoatrial (SA) node in the heart, allowing for continuous rhythmic bursts (Ono & Iijima, 2005). Blocking TTCC with mibefradil or Ni^{2+} reduced the upstroke component and propagation of SW in ICC networks in the gut, suggesting Ca^{2+} influx through TTCC contributes to the upstroke phase and propagation of SW in ICC (Ward *et al.,* 2004; Park *et al.,* 2006; Bayguinov *et al.,* 2007; Zheng *et al.,* 2014). Previous work on murine mid and distal colon showed that EFS-evoked contractions were abolished, and propagation of colonic migrating motor complexes was inhibited by the application of NNC 55-0396 (TTCC inhibitor) (Koh *et al.,* 2024), indicating that TTCC influence neurally-evoked contractions and propagation of colonic migrating motor complexes in these regions. Spontaneous Ca^{2+} activity of ICC-MY in small intestine were also attenuated by NNC 55-0396 and TTA-A2 (TTCC inhibitor) (Drumm *et al.,* 2017). These previous studies on GI muscles proposed a mechanism that the initiation and propagation of SW result in depolarisation, which activates TTCC. Ca^{2+} influx through TTCC then triggers Ca^{2+} release from RyR with amplification from IP_3R via Ca^{2+}-induced-Ca^{2+} release (CICR), sustaining ANO1 activation and thereby supporting SW propagation (Drumm *et al.,* 2017; Koh *et al.,* 2024).

The role of TTCC in modulating USM contractility appears to vary between species. Shafei *et al.,* (2003) demonstrated that nifedipine or Ni^{2+} significantly reduced tone in an isolated rat whole urethra preparation, implying Ca^{2+} influx via both TTCC and LTCC contributes to urethral tone (Shafei *et al.,* 2003). Rabbit and human USMC exhibited currents with electrophysiological properties typical of LTCC and TTCC,

which were sensitive to nifedipine and Ni^{2+}, respectively (Hollywood *et al.,* 2003; Bradley *et al.,* 2004). In rabbit USMC, inhibition of TTCC using Ni^{2+} and mibefradil reduced the frequency of STD (Bradley *et al.,* 2004). In contrast, inhibition of TTCC using NNC 55-0396 and TTA-A2 in male murine USM had no effect on basal spontaneous Ca^{2+} activity (Drumm *et al.,* 2018). However, to date, effects of TTCC inhibition on agonist-induced or nerve-evoked stimulation of USM are unknown. Moreover, most of the previous work investigating role of TTCC in USM contractility utilized pharmacological agents such as Ni^{2+} and mibefradil which are now recognized to have various off-target effects (Brimblecombe & Cragg, 2015; Wang *et al.,* 2015; Li *et al.,* 2019; Pfaffendorf *et al.,* 2000), this may affect the interpretation of their data. The limitations and gaps in earlier studies presents an opportunity to examine whether TTCC contribute to agonist-induced and EFS-evoked contractions in USM, using more selective pharmacological tools.

The following section discusses major potassium channels that plays a critical role in various SM organs, including LUT, by maintaining membrane potential and thereby regulating the activity of voltage gated Ca^{2+} channels.

1.11 Kv7 channels (Voltage gated potassium channels)

Kv7 channels (KCNQ) are a family of voltage-gated K^+ channels that modulate RMP in SMC such as airways (Jepps *et al.,* 2013), myometrium (Mccallum *et al.,* 2010), corpus cavernosum (Lee *et al.,* 2020; Mercer *et al.,* 2025) and vascular SM (Tsai *et al.,* 2020). Kv7 channels activate at membrane potentials starting as negative as -60 mV in SM (Stott *et al.,* 2014; Tykocki *et al.,* 2018). There are five subtypes of mammalian Kv7 (Kv7.1- Kv7.5) (Gutman *et al.,* 2003). α subunits of Kv7 channel assemble as tetramers of homo- (Kv7.1) or hetero-tetrameric subunits with preferential combinations such as: Kv7.2/Kv7.3 and Kv7.3/Kv7.5 complexes (Soldovieri *et al.,* 2011).

Several report Kv7 channels regulate activity of VGCC in SMC through hyperpolarisation of membrane potential (Mccallum *et al.,* 2010; Brueggemann *et al.,* 2012; Lee *et al.,* 2020; Tsai *et al.,* 2020; Mercer *et al.,* 2025). In murine and human

vascular SMC, inhibition of Kv7 by XE991 initiated Ca^{2+} oscillations that were sensitive to nifedipine and NNC 55-0396 (Tsai *et al.,* 2020). In human lung slices, application of XE991 induced robust airway constrictions which was reversed by inhibition of LTCC with verapamil (Brueggemann *et al.,* 2012). In murine myometrium, inhibition of Kv7 channels enhanced basal contractions, and activation of Kv7 channels abolished them, indicating Kv7 channels regulate rhythmic myometrial activity (Mccallum *et al.,* 2010). Lee *et al.,* (2020) demonstrated increased basal Ca^{2+} upon inhibition of Kv7 channels by XE991 in human corpus cavernosum SMC. In murine corpus cavernosum SMC, XE991 increased phasic contractions and this was reversed by nifedipine (Mercer *et al.,* 2025). In guinea pig DSMC, addition of retigabine (Kv7 channel activator) and L-364373 (Kv7.1 channel activator) inhibited action potentials by membrane hyperpolarisation (Afeli *et al.,* 2013). Conversely, XE991 and linopirdine increased DSMC spontaneous and EFS-evoked contractions (Afeli *et al.,* 2013). Application of XE991 on bladder strips from mouse, guinea pig, rat, pig, and human increased spontaneous contractions, whereas as retagabine or flupirtine (Kv7 channels activators) supressed it (Anderson *et al.,* 2013; Rode *et al.,* 2010; Svalø *et al.,* 2013, 2015; Tykocki *et al.,* 2018).

Expression of Kv7 subtypes varies across different organs. Kv7.1 is expressed in heart (Ng *et al.,* 2011), pancreas (Lubberding *et al.,* 2022), thyroid gland (Fröhlich *et al.,* 2011; Purtell *et al.,* 2012), brain (Celentano *et al.,* 2024), GI tract (Lee *et al.,* 2000; Dedek & Waldegger, 2001), portal vein (Serrano-Novillo *et al.,* 2020), and inner ear (Lee *et al.,* 2000). Kv7.2, Kv7.3, Kv7.4 and Kv7.5 are predominantly expressed in neural tissues (Miceli *et al.,* 2011; King & Scherer, 2012; Celentano *et al.,* 2024). In guinea pig DSM, expression of Kv7.1 was highest among all five subtypes whereas Kv7.4 was low or non-detectable (Afeli *et al.,* 2013). However, in rat DSM, a higher expression of Kv7.4 and lower expression of Kv7.1 and Kv7.5 was detected, whereas Kv7.2 and Kv7.3 were completely undetected (Malysz & Petkov, 2020).

While there is a growing research on the role of Kv7 channels in various SM tissues, including urinary bladder, studies specifically investigating their functional expression in USM are notably lacking. This gap in the literature presents an opportunity to explore the potential roles of Kv7 channels in USM.

1.12 BK channels (Ca^{2+} activated K^+ channels)

Large-conductance Ca^{2+} activated K^+ (BK) channels, also referred to as MaxiK channels are voltage and Ca^{2+} dependent (Ghatta *et al.,* 2006; Wu & Marx, 2010). The structure of BK channels consists of a tetramer of α-subunits forming the pore of the channel and four auxillary β and γ-subunits (Ghatta *et al.,* 2006; Latorre & Brauchi, 2006; Wu & Marx, 2010; Yan & Aldrich, 2012; Li & Yan, 2016). KCNMA1 gene encodes α-subunits (BKα) and KCNMB 1-4 genes encodes four β-subunits of BK channels, respectively (Gonzalez-Perez & Lingle, 2019). Dudem *et al.,* (2020) found that LINGO1 is another regulatory subunit of BK channels. LINGO1 and γ-subunit are both leucine-rich repeat (LRRC) gene encoded proteins (Dudem *et al.,* 2020). γ1-4 subunit encoded by gene LRRC26, LRRC52, LRRC55 and LRRC38, respectively (Yan & Aldrich, 2012; Li & Yan, 2016; Gonzalez-Perez *et al.,* 2022).

BK channel activation generates an outward K^+ current that hyperpolarises membrane potential, and thereby inhibiting Ca^{2+} influx through VGCC (Latorre & Brauchi, 2006; Dopico *et al.,* 2018). This negative feedback mechanism promotes relaxation of SM. BK channels are activated by Ca^{2+} release by RyR in the form of Ca^{2+} sparks (Herrera *et al.,* 2001; Lifshitz *et al.,* 2011) or by Ca^{2+} influx through VGCC (Herrera and Nelson, 2002). BK channels are found in vascular (Sausbier *et al.,* 2005), airway (Liu *et al.,* 2007), corpus cavernosum (Hannigan *et al.,* 2016) and DSMC (Meredith *et al.,* 2004). The repolarisation phase of the DSM action potential is significantly influenced by BK channels (Heppner *et al.,* 1997). Iberiotoxin (BK channel inhibitor) prolongs action potentials and depolarises RMP (Heppner *et al.,* 1997). Furthermore, iberiotoxin increased amplitude but decreased frequency of phasic contractions in guinea pig DSM strips (Herrera *et al.,* 2000). Meredith *et al.,* (2004) reported enhanced basal and nerve-mediated DSM contractions in $Slo^{-/-}$ mice, which lacked both Ca^{2+}- and voltage-activated BK currents.

Hollywood *et al.,* (2000) recorded outward transient current and a component of sustained current in sheep USMC, which were blocked by iberiotoxin, penitrem A and nifedipine but unaffected by apamin (small conductance Ca^{2+} activated potassium channel (SK channel) blocker) or 4-aminopyridine (non-selective Kv channel blocker). Teramoto *et al.,* (2004) observed a high-frequency large amplitude channel current in

outside-out configuration patch-clamp experiment in pig urethra at +30 mV which were reversibly inhibited by iberiotoxin, indicating that the outward currents observed in sheep USMC are primarily mediated by BK_{Ca} channels and are functionally coupled to Ca^{2+} entry through LTCC. Kyle *et al.,* (2013) showed that RyR mediated-Ca^{2+} release contributes to activation of BK channels in rabbit USMC. They performed perforated patch clamp studies on rabbit USMC, and found that BK currents were inhibited by ryanodine (30 μM), tetracaine (100 μM), caffeine (10 mM) but were unaffected by 2-APB (Kyle *et al.,* 2013). Griffin *et al.,* (2020) detected that isolated murine USMC exhibited Ca^{2+} sparks activity which were abolished by ryanodine, indicating that these Ca^{2+} sparks events are mediated by RyR in USMC. Taken together, BK_{Ca} act as a modulator of LUT SMC excitability and Ca^{2+} dynamics (Ridlon *et al.,* 2025). However, direct evidence demonstrating functional coupling between BK_{Ca} channels and LTCC in murine USM is currently lacking, and this interaction remains to be defined.

1.13 K_{ATP} channels (ATP-sensitive potassium channels)

Adenosine triphosphate (ATP)-sensitive K^+ (K_{ATP}) channels belong to the K_{ir} superfamily of K^+ channels, and conduct weak inward rectifier K^+ current. K_{ATP} channels are hetero-octameric complexes composed of four pore-forming subunits (Kir6.1 or Kir6.2, encoded by KCNJ8 and KCNJ11, respectively) and four regulatory sulfonylurea receptor (SUR) subunits from the ATP-binding cassette subfamily C, which include SUR1, SUR2A, or SUR2B (Szeto *et al.,* 2018). K_{ATP} channels are inhibited by intracellular ATP and activated by Mg-ADP, enabling the cell to couple its metabolic state (reflected by ATP/ADP ratio) to electrical activity of the plasma membrane (Szeto *et al.,* 2018).

In SM, high ATP levels close K_{ATP} channels, leading to depolarisation and increased excitability (Quayle *et al.,* 1997). Conversely, during metabolic stress or hypoxia, ATP levels drop and Mg-ADP levels rise, opening K_{ATP} channels, causing hyperpolarisation and relaxation of SMC (Quayle *et al.,* 1997). K_{ATP} channel activation in vascular SM regulates vasodilation by relaxing the muscle and increasing arterial diameter (Cole & Clément-Chomienne, 2003). In guinea pig, activation of K_{ATP} by cromakalim and

pinacidil supresses amplitude and frequency of spontaneous contractions in DSM (Foster *et al.,* 1989; Seki *et al.,* 1992). Electrophysiological experiments showed that cromakalim and pinacidil induced dose-dependent hyperpolarisations and loss of spike activity in DSMC; these effects were reversed by glibenclamide (K_{ATP} inhibitor) (Andersson & Arner, 2004; Foster *et al.,* 1989; Seki *et al.,* 1992). These findings highlight importance of K_{ATP} channels in modulating spontaneous contractions in DSM. In corpus cavernosum SM, activators of K_{ATP}, cromakalim and levcromakalim, dose-dependently abolished agonist-induced contractions, which was reversed by glibenclamide (Ruiz Rubio *et al.,* 2004). During labor, expression of K_{ATP} decreases in human myometrium, possibly contributing to the increased excitability required for coordinated contractions (Xu *et al.,* 2011).

In pig urethra, levcromakalim induced relaxation to resting tone, which was reversed by glibenclamide (Teramoto & Brading, 1996). In patch-clamp recording of isolated pig USMC, levcromakalim evoked concentration dependent hyperpolarisation, which was abolished by glibenclamide (Teramoto & Brading, 1996). K_{ATP} openers such as Diazoxide, a SUR1 activator, and pinacidil, a selective SUR2 activator, induced glibenclamide-sensitive inward K^+ currents in pig USMC. Similar findings was reported by Rembetski *et al.,* (2020) in pig urethra, where pinacidil and nifedipine inhibited USM tone, suggesting that K_{ATP} channels opening inhibit LTCC activity (Rembetski *et al.,* 2020). While KATP channels played a major role in pig USM, its functional role is not investigated in other species such as mouse where inhibition of LTCC had no effect on spontaneous Ca^{2+} activity and agonist-induced contractions.

The following section discusses Ca^{2+} release-activated Ca^{2+} channel, another important ion channel in various SM and also in urethra. These channels are responsible for refilling intracellular stores with Ca^{2+}, hence mediating various Ca^{2+} signalling pathway across various SM organs.

1.14 CRAC (Ca^{2+} release-activated Ca^{2+} channel)

Ca^{2+} release-activated Ca^{2+} channel (CRAC) also known as Orai channels, are voltage independent channels that play a crucial role in store-operated calcium entry (SOCE)

in various cell types (Parekh, 2010; Prakriya & Lewis, 2015; Drumm *et al.,* 2018). The concept that depletion of intracellular Ca^{2+} stores triggers Ca^{2+} influx from the extracellular space was first proposed by Putney (Putney *et al.,* 1981; Putney, 1986, 1990). This hypothesis, often referred to as the 'capacitative Ca^{2+} entry' model, laid the foundation for our current understanding of SOCE (Putney, 1990).

Later, CRAC was discovered in rat peritoneal mast cell where emptying the store induced activation of a sustained inward current that was highly selective for Ca^{2+} ions and showed a characteristic inward rectification (Hoth & Penner, 1992). Orai channels function in conjunction with stromal interaction molecules (STIM), which act as Ca^{2+} sensors in the SR (Liou *et al.,* 2005). STIM has two homologs, STIM1 and STIM2 which are single-pass transmembrane proteins with a putative Ca^{2+}-binding EF-hand domain located in the lumen of the ER (Liou *et al.,* 2005). The key functional distinction between STIM isoforms lies in their Ca^{2+} affinity. STIM2 has a lower Ca^{2+} affinity than STIM1, making it more sensitive to small reductions in ER Ca^{2+} content (Berna-Erro *et al.,* 2017). As a result, STIM2 redistributes to ER-PM junctions in response to modest deviations from resting ER Ca^{2+} levels by triggering a minor but sustained activation of SOCE, thus overcoming slight fluctuation in ER Ca^{2+} levels (Berna-Erro *et al.,* 2017; Sallinger *et al.,* 2024). In contrast, STIM1 is recruited only during substantial ER Ca^{2+} depletion and drives a robust yet transient SOCE response that rapidly restores ER Ca^{2+} stores (Berna-Erro *et al.,* 2017; Liou *et al.,* 2007; Sallinger *et al.,* 2024).

Bindings of Ca^{2+} to luminal domains of STIM maintains the protein in a monomeric state (Stathopulos *et al.,* 2008). Depletion of SR Ca^{2+} causes Ca^{2+} dissociation from STIM, triggering conformational change, oligomerisation, and translocation to plasma membrane (Gudlur *et al.,* 2019). The C-terminal binding hands of STIM (STIM Orai-activating region (SOAR)) binds to Orai channels (Yuan *et al.,* 2009), leading to channel opening and Ca^{2+} influx. The resulting rise in cytosolic Ca^{2+} promotes refilling of SR Ca^{2+} stores via SERCA-mediated uptake (Parekh, 2003). Orai1 forms the membrane pore through which Ca^{2+} enters (Parekh, 2010).

Previous studies reported importance of STIM 1 in SOCE as knock down of STIM1 inhibited CRAC activity in Jurkat T cells and HEK293 cells (Roos *et al.,* 2005; Liou *et*

al., 2005). Feske *et al.,* (2006) reported that Orai1 is an important component of CRAC as Orai1 mutation in T cells of severe combined immune deficiency patients had defective SOCE (Feske *et al.,* 2006).

Other homologs of Orai identified were Orai2 and Orai3 (Feske *et al.,* 2006; Mercer *et al.,* 2006). A previous study reported great reduction in SOCE in knockdown of either Orai1 or STIM1 in rat vascular SMC, whereas knockdown of Orai2 or Orai3 had no effect (Potier *et al.,* 2009). Recent studies in mammalian cells (HEK 293), reported CRAC is formed by heteromerization of Orai2 and Orai3 with Orai1 (Yoast *et al.,* 2020; Zhang *et al.,* 2020). Using single, double and triple knockout of Orai isoforms in HEK 293 cells, it was demonstrated Orai3 and Orai2 are critical for low- and mid-range oscillatory Ca^{2+} responses, whereas Orai1 mediates high-range Ca^{2+} plateaus (Yoast *et al.,* 2020). These findings indicate that Orai2 and Orai3 along with Orai1 are essential for the proper functioning of CRAC.

Previous studies reported critical role of Orai and STIM mediated SOCE in various SM such as vascular (Grosse *et al.,* 2007; Potier *et al.,* 2009; Tanwar *et al.,* 2017), airway (Spinelli *et al.,* 2012; Chen and Sanderson, 2016), myometrium (Murtazina *et al.,* 2011; Tica *et al.,* 2011). In rat myometrium, store depletion with thapsigargin (SERCA inhibitor) induced robust SOCE, which was insensitive to nifedipine, indicating that the Ca^{2+} influx was primarily due to CRAC activity (Tica *et al.,* 2011). Moreover, mRNA knockdown of STIM1 and Orai1-Orai3 in human myometrial cells had significantly attenuated oxytocin and CPA-stimulated SOCE (Murtazina *et al.,* 2011).

Knockdown of STIM1 and Orai1 significantly inhibited proliferation and migration of cultured rat vascular SMC, whereas knockdown of STIM2, Orai2, or Orai3 had no appreciable effect (Potier *et al.,* 2009). Previous studies reported that STIM1 and Orai1 mediates the increase in platelet Ca^{2+} concentration, and thereby mediates thrombosis (Grosse *et al.,* 2007; Ahmad *et al.,* 2011), which is essential as increase in cytosolic Ca^{2+} concentration is required for platelet aggregation at the site of thrombus formation (Mazzucato *et al.,* 2002; Tanwar *et al.,* 2017). Upregulation of SOCE and Orai1 contributed to aberrant proliferation, apoptosis resistance, exacerbated migration, and arterial contractility in pulmonary artery SMC from patients with pulmonary arterial hypertension, which was reversed by either knockdown of STIM1 or Orai1, or by

inhibitors of Orai channels (Masson *et al.,* 2022). In mesenteric artery SM, Ca^{2+} influx via Orai1 stimulates BK_{Ca} channels, leading to membrane hyperpolarisation (Chen *et al.,* 2016).

STIM1 and Orai1 protein levels were significantly increased in airway SMC isolated from allergen-induced asthmatic mice, compared to controls (Spinelli *et al.,* 2012). Moreover, platelet-derived growth factor (PDGF), which is secreted by asthmatic airways, was tested on cultured rat airway SMC, where it induced Ca^{2+} entry resembling SOCE. This PDGF-evoked Ca^{2+} influx was inhibited by gadolinium (a non-selective SOCE blocker) and was markedly reduced in either Orai1 or STIM1 knockdowns (Spinelli *et al.,* 2012). Collectively, these data suggest that increased STIM1 and Orai1 dependent SOCE is a key mechanism underlying enhanced Ca^{2+} entry in airway SMC during asthma. In murine airway SM, GSK-7975A (Orai inhibitor) inhibited agonist-induced contractions by abolishing Ca^{2+} oscillations, suggesting a potential role of Orai channels in mediating Ca^{2+} influx essential for airway SM contractile activity (Chen & Sanderson, 2016). In another study, inhibition of Orai channels by GSK-7975A suppressed greater proportion of agonist induced dose-dependent contractions in comparison to LTCC blockade by nifedipine in murine airway SM. In addition, application of GSK-7975A and nifedipine together abolished agonist induced dose-dependent contractions (Dwivedi, *et al.,* 2023).

In the gut, inhibiting Orai channels reduced basal Ca^{2+} activity and pacemaker activity in ICC (Zheng *et al.,* 2018; Drumm *et al.,* 2020, 2022; Baker *et al.,* 2021). Blockade of Orai channels inhibited STIC in small intestinal ICC (Zheng *et al.,* 2018). Reintroduction of extracellular Ca^{2+} in store-depleted ICC resulted in CaCC activation (Zheng *et al.,* 2018). Subsequent, inhibition of CaCC by 5-nitro-2-(3-phenylpropylamino)-benzoic acid revealed an inwardly rectifying current with properties of a Ca^{2+} release-activated current (I_{CRAC}) which were abolished by GSK-7975A and 2-APB (Zheng *et al.,* 2018). In HEK293 cells expressing Orai1 and STIM1, I_{CRAC} was inhibited by inhibitory peptide (CC2, cytoplasmic coiled-coil domain) that interfered with STIM-Orai interaction. CC2 also inhibited STIC and SW in small intestinal ICC (Zheng *et al.,* 2018). These findings indicate that SOCE-mediated by Orai-STIM channels are crucial for sustaining pacemaker activity of ICC.

In rabbit urethral ICC-LC, spontaneous intracellular Ca^{2+} waves were insensitive to LTCC inhibition (Johnston *et al.,* 2005; Bradley *et al.,* 2005; Hashitani & Suzuki, 2007), but were abolished by Ca^{2+} free solutions and reduced in frequency by SKF 96365 (non-selective SOCE inhibitor) (Johnston *et al.,* 2005; Hashitani & Suzuki, 2007). Intracellular microelectrode recordings revealed that generation of SW and STD in rabbit USM were inhibited by application of Ca^{2+} free solution, BAPTA-AM, CPA, caffeine and procaine (Hashitani *et al.,* 1996). Similarly, SW and STD were also abolished in guinea pig USM by CPA, BAPTA, and caffeine (Hashitani & Edwards, 1999). These findings indicate that Ca^{2+} release from intracellular stores were required for CaCC activation and thereby driving the generation of SW and STD.

Consistent with this, Johnston *et al.,* (2005) reported that spontaneous Ca^{2+} waves in rabbit urethral ICC-LC were inhibited by the non-selective SOCE inhibitors SKF 96365, La^{3+} and Cd^{2+}. In contrast, Bradley *et al.,* (2005) demonstrated that although rabbit urethral ICC-LC are capable of mediating capacitative Ca^{2+} entry (SOCE) following store depletion, inhibition of SOCE with Gd^{3+} or La^{3+} did not suppress spontaneous activity. These contrasting observations suggest uncertainty regarding the contribution of SOCE to ICC-LC Ca^{2+} signalling in the urethra. Importantly, these earlier studies relied on non-selective Ca^{2+} influx and SOCE inhibitors with well-documented off-target effects (Blaustein & Lederer, 1999; Brommundt & Kavaler, 1987; Hobai *et al.,* 1997; Lacampagne *et al.,* 1994; Singh *et al.,* 2010), complicating interpretation of their findings. Consequently, there remains a need to directly examine the role of Orai-mediated SOCE in USM ICC-LC using more selective pharmacological approaches.

In pig, inhibiting Orai channels significantly decreased USM tone and contractions-evoked by nerve stimulation and PE, emphasizing the significance of Orai channels in influencing USM contractions through SOCE (Rembetski *et al.,* 2020). Moreover, SKF 96365 and GSK-7975A decreased spontaneous intracellular Ca^{2+} waves in murine USMC*,* and reduced PE-induced concentration dependent contractions in intact urethral rings (Drumm *et al.,* 2018). After incubating male mouse USM in thapsigargin and Ca^{2+}-free solution, reintroduction of Ca^{2+} to the bath in the continued presence of thapsigargin induced tonic contraction attributed to SOCE (Putney, 1986). This tonic USM contraction was insensitive to nifedipine but were dose-dependently inhibited by GSK-7975A (Drumm *et al.,* 2018). Transcriptional studies revealed that Orai1 and

Orai3 are the predominant Orai subtypes expressed in the male mouse urethra, whereas Orai2 is the least expressed subtype (Drumm *et al.,* 2018).

Collectively, these findings indicate a critical role for Orai channels in SM function and contractility. However, the function of Orai channels in female USM, particularly in species such as the mouse, remains unexplored. In addition, the effects of Orai channel inhibition have been investigated only under conditions of exogenous neurotransmitter / agonist application, with no studies addressing their contribution to EFS-evoked contractions in either male or female USM. Furthermore, the role of Orai channels in urethral ICC-LC has not been definitively established, owing to discrepancies in earlier studies on rabbit urethral ICC-LC that predominantly relied on non-selective Ca^{2+} influx and SOCE inhibitors.This gap in knowledge provides a clear rationale for addressing these limitations in the present thesis using selective pharmacological tools.

1.15 Current gaps in literature in urethral physiology

Previous studies have identified a novel population of ICC-LC within the USM that resemble ICC found in the GI tract. These urethral ICC-LC, often vimentin^{+} and/or Kit^{+}, have been implicated in modulating USM activity through interactions with neurotransmitters, suggesting a potential neuromodulatory role. However, significant gaps remain in our understanding of identity and function of ICC-LC in urethra. One major limitation in earlier work was reliance on morphological identification of ICC-LC within enzymatically dispersed USM cell preparations, without the use of specific cellular markers. This raised concerns about cell type purity and functional attribution. Furthermore, most studies employed non-specific Ca^{2+} dyes such as Fluo-4 AM, which indiscriminately load all cell types and obscure cell-specific Ca^{2+} dynamics. No studies to date have employed direct electrical or optogenetic stimulation of ICC-LC to assess whether they are modulated by nerve inputs, leaving their physiological responsiveness to neural signalling unresolved.

Furthermore, earlier studies suggested ICC-LC in USM generate spontaneous depolarisations which are sensitive to CaCC antagonists. Subsequent research identified ANO1 as the specific member of CaCC family expressed on ICC in the gut

where it contributes to depolarisation, and subsequent activation of LTCC in electrically coupled SMC through gap junctions. In the urethra, expression of ANO1 on ICC-LC has been reported in rabbits but not consistently across other species. In mouse, rat and sheep, for example, ANO1 expression appears limited to USMC rather than vimentin^{+} ICC-LC. Conversely, recent work has shown ANO1 and c-Kit co-expression in mouse urethral stromal cells thought to be ICC-LC, but their morphology differs markedly from gut ICC or rabbit urethral ICC-LC. These discrepancies point to species-specific variation in the identity and function of ANO1-expressing cells in the urethra. Moreover, early pharmacological studies on CaCC relied on non-selective blockers (e.g., niflumic acid), which are now known to have significant off-target effects (Cruickshank *et al.,* 2003; Genovese *et al.,* 2023; Oba, 1997). The role of ANO1 in urethral contractility thus requires re-evaluation using more selective inhibitors such as Ani9 to ensure accurate functional attribution.

Ca^{2+} influx pathways also remain incompletely understood in USM. While inhibition of LTCC has been shown to reduce urethral tone in human, rabbit, and pig, *in situ* Ca^{2+} recording using mouse models expressing GCaMP (Ca^{2+} sensor) in USMC reported that LTCC blockade has no effect on USMC intracellular Ca^{2+} signalling, even in the presence of adrenergic agonists. In contrast, inhibition of Orai channels has been suppresses USMC Ca^{2+} responses, suggesting SOCE may play a more dominant role in urethral tone regulation. The role of VGCC and Orai channels have largely been unexplored on EFS responses in urethra, which is critical to understand as it closely resemble physiological signalling than application of exogenous agonist. Moreover, most previous studies on ionic regulation in USM have been conducted in male mice, leaving a significant gap in our understanding of the underlying mechanisms in female USM physiology.

Furthermore, the role of potassium channels in urethral excitability has been largely inferred from bladder studies. Although BK_{Ca} channels are well established regulators of DSM excitability, their role in USM remains largely uncharacterized. K_{ATP} channels were examined in pig urethra, where they play an important role in mediating urethral contractility. However, the role of K_{ATP} channels were not explored in mouse USM. Despite progress in SM research, critical gaps remain in our understanding of the ionic and neural regulation of USM, warranting detailed and targeted studies.

1.16 Aims

This study aims to address longstanding gaps and methodological limitations in our understanding of murine USM physiology, structured around five core objectives:

- Identify and characterize ICC-LC in intact mouse urethra with a transgenic Kit-GCaMP6f mice, whose GCaMP (Ca^{2+}) sensor is driven by the Kit promoter enabling specific and dynamic visualization of ICC-LC Ca^{2+} activity *in situ*, overcoming limitations of morphology-based cell identification and indiscriminate loading of Ca^{2+} dyes in multicellular tissue preparations.

- Evaluate functional coupling of ICC-LC with neural inputs by combining real-time *in situ* Ca^{2+} imaging and visualization of ICC-LC during excitatory and inhibitory EFS protocols, revealing whether ICC-LC are targets of endogenous neurotransmission within USM tissues.

- Define cellular expression and role of ANO1 channels in USM tissues, distinguishing between ICC-LC and USMC localization, and investigating ANO1 contribution to basal tone and spontaneous activity using selective inhibitors such as Ani9, in contrast to previous studies that used non-specific blockers.

- Assess the contribution of Orai-mediated SOCE and voltage-gated Ca^{2+} channels in USM contractility under agonist and EFS evoked conditions that better mimic physiological signalling and have been insufficiently explored.

- Examine the regulatory role of K^+ channels in modulating USM excitability and contractility, given their well-established function in bladder physiology but largely uncharacterized role in the urethra.

2. Materials & Methods

2.1 Ethical approval

All experiments were carried out at:

1. Smooth Muscle Research Centre, Dundalk Institute of Technology, Ireland- All animal procedures were approved by the Dundalk Institute of Technology Animal Care and Use Committee and complied with EU directive 2010//63/EU.
2. Department of Physiology and Cell Biology, Reno School of Medicine, University of Nevada, Reno, USA. All animal procedures were approved by Institutional Animal Use and Care Committee at University of Nevada, Reno in accordance with National Institutes of Health Guide for Care and Use of Laboratory Animals.

2.2 Tissue preparation

Wild type (WT) C57BL/6 mice were purchased from the Jackson Laboratory (Bar Harbor, ME, USA) and bred in house. GCaMP6flox/$^{+}$ mice (B6; 129S-Gt(ROSA)26Sortm95.1(CAG-GCaMP6f)Hze/J) were purchased from the Jackson Laboratory (Bar Harbor, ME, USA) and crossed with Kit-iCre expressing mice (Kit-tm1cre/ERT2Dsa, gifted from Dr. Dieter Saur of Technical University Munich, Germany) to generate Kit-GCaMP6f mice (Fig 2.1) for conditional expression of GCaMP6f in *c-Kit*$^{+}$ cells. Kit-GCaMP6f mice were injected with tamoxifen between 6 - 8 weeks of age, as previously described (Drumm *et al.,* 2019a, 2019b) to induce expression of GCaMP6f in *kit*-expressing cells by licensed and trained personnel. For experiments conducted at University of Nevada, Reno, mice were anaesthetized by inhalation of isoflurane (Baxter, Deerfield, IL, USA) and killed by cervical dislocation prior to experimentation by licensed and trained personnel, in accordance with institutional and national ethical guidelines.

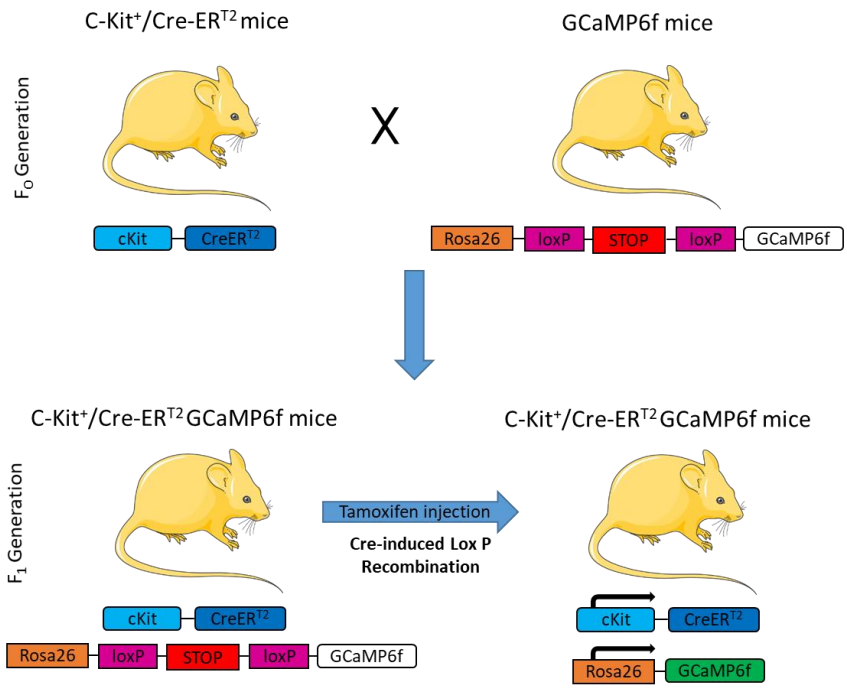

Fig 2.1: Diagrammatic representation of Generation of Kit-GCaMP6F mice by Cre-LoxP technology: by crossing Ai95 (RCL-GCaMP6f)-D (GCaMP6f mice) with c-Kit$^+$/CreER^{T2} (Kit-Cre mice). At the age of 6-8 weeks, these mice are administered tamoxifen to activate Cre Recombinase, resulting in exclusive expression of GCaMP6f in c-Kit$^+$ cells.

At DkIT, male / female C57BL/6 mice (Envigo, USA) and Acta2-GCaMP8.1mice (Jackson Laboratory, USA), were euthanized by intraperitoneal application of pentobarbital, by HPRA (Health Products Regulatory Authority) authorized laboratory animal technician. A closed-circuit system was used to control environmental conditions in the animal storage room with temperatures from 18-20°C and humidity at 50%. In all experiments, the urethra and bladder were removed immediately and dissected free of fat and connective tissue and placed in a Sylgard plate filled with oxygenated Krebs' solution (95% O_2 and 5% CO_2). The proximal urethra (1-1.5 mm, Fig. 2.2) was dissected from the bladder. In male mice, prostate glands were removed to expose proximal urethra, and overlying striated muscle from the EUS was carefully trimmed using fine micro-scissors. In female mice, proximal urethra was freed from surrounding pelvic floor muscle attachments, and segments with minimal striated layer were gently dissected away. For positive test controls in isometric tension experiments (described below), proximal colon was removed from the animal. Proximal colon was opened along the mesenteric border via a longitudinal incision and pinned flat, mucosal side up. Mucosal layers were carefully removed by peeling using fine forceps,

revealing transparent underlying SM layers. Two circularly oriented strips (5-8 mm) were cut and used for experiments.

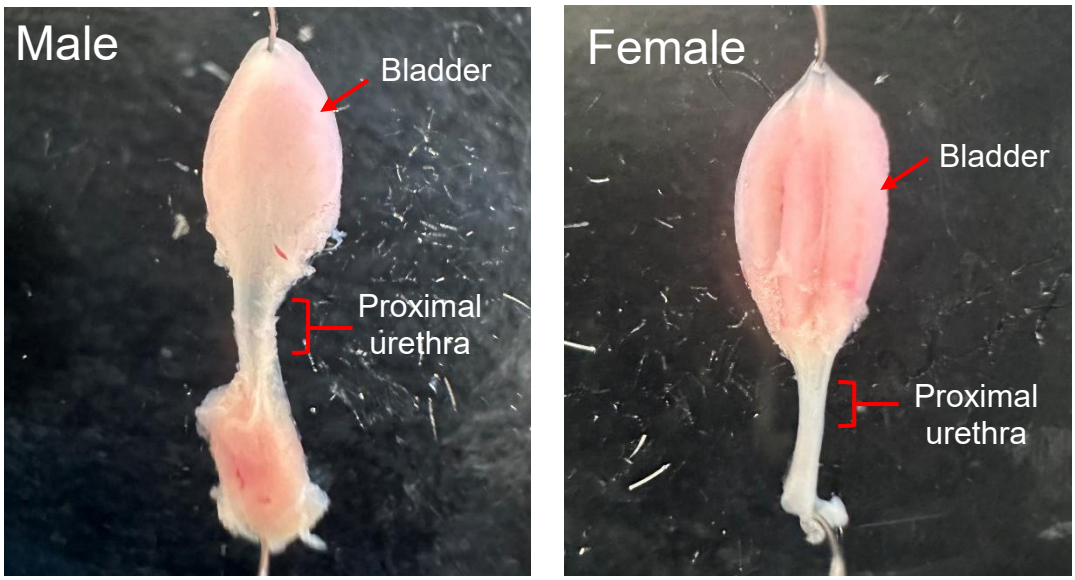

Fig 2.2: Murine male & female lower urinary tract. The lower urinary tracts (LUT) of male and female mice were excised and placed in Kreb's solution on a Sylgard plate for dissection. The male LUT was carefully dissected to isolate the proximal urethra from the surrounding prostate gland. Similarly, the female urethra was dissected free from the adjacent uterine body.

GCaMP mice and its mechanism of action

GCaMP mice harbours a genetically encoded Ca^{2+} sensor, GCaMP, a fusion protein composed of green fluorescent protein (GFP), calmodulin (CaM), and M13, a peptide sequence from MLCK (Nakai *et al.,* 2001). GCaMP6f is a fast-kinetics, genetically encoded Ca^{2+} indicator that acts by binding intracellular Ca^{2+} to a calmodulin domain, causing a conformational change that increases the fluorescence of a circularly permuted enhanced GFP (cpEGFP) (Chen *et al.,* 2013). It enables real-time monitoring of rapid Ca^{2+} transients in cells (Chen *et al.,* 2013). The GCaMP6f was expressed in c-Kit^{+} cells using Cre-Lox recombination technology (Fig 2.1) as described above.

GCaMP8.1 consists of a polyHis plasmid leader sequence essential for thermal stability, a 20 residue peptide of chicken smooth muscle MLCK (M13), a circularly

permutated GFP (cpGFP) and a rat calmodulin DNA fragment (CaM). GCaMP8.1 is a sensitive variant of GCaMP range with high dynamic range and fast response kinetics as well as improved Ca^{2+} binding affinity. They were designed in the Kotlikoff laboratory in Cornell University. The Acta2-GCaMP8.1 mice express the GCaMP8.1/mVermilion fusion protein under control of the Acta2 locus promoter regions within the mouse bacterial artificial chromosome (BAC) transgene. Acta2-GCaMP8.1 were obtained from Jackson Laboratory. These transgenic mice express the GCaMP8.1/mVermilion fusion protein which is a basic red fluorescent protein, and is a mCherry derivative with approximately a 2 fold brighter emission. It remains at a constant level, allowing for ratiometric measurements of Ca^{2+} signalling in various SM.

These genetically encoded Ca^{2+} indicator mice have several advantages over the Ca^{2+} dye Fluo-4AM, including cell specific Ca^{2+} indicator expression, reduced photobleaching, even distribution of fluorescent indicator throughout the specific cell type, and the ability to perform longer experiments since the fluorescent indicator does not leave the cells.

2.3 Isometric tension recording

Proximal urethral rings were mounted to force transducers in a water-jacketed (37° C) organ baths filled with oxygenated Krebs' solution, which was continuously bubbled with 95% O_2 and 5% CO_2. Urethral rings were held by two stainless steel hooks and placed between two platinum electrodes (5 mm length, 2.5 mm apart) on a tissue holder, see Fig. 2.3. Initial 2 mN of tension was applied and tissues left to equilibrate for 45 minutes before experimentation. A multi-channel myobath system was used to record contractions and LabScribe software (version 4.340000) was used to acquire data. Electrical field stimulation (EFS) was generated by a MultiStim system-D330 stimulator (Digitimer Ltd, England) via the platinum electrodes (pulse width 0.3 ms).

Male urethral rings could be contracted by applying various concentrations of the α1-adrenoreceptor agonist phenylephrine (PE, 30 nM to 30 μM) or arginine vasopressin (AVP, 10 nM) or by EFS (1 Hz, 2 Hz, 5 Hz, 10 Hz, 20 Hz) for 30 sec with a time interval of 2 minutes between each stimulation. Female urethral rings were contracted by 10 nM of AVP. All experiments were carried out in the presence of indomethacin (10 μM)

to prevent release of endogenous prostaglandins. Contractions were quantified by measuring area under curve (AUC), amplitude (mN) or frequency (min^{-1}) in LabScribe software (version 4.340000).

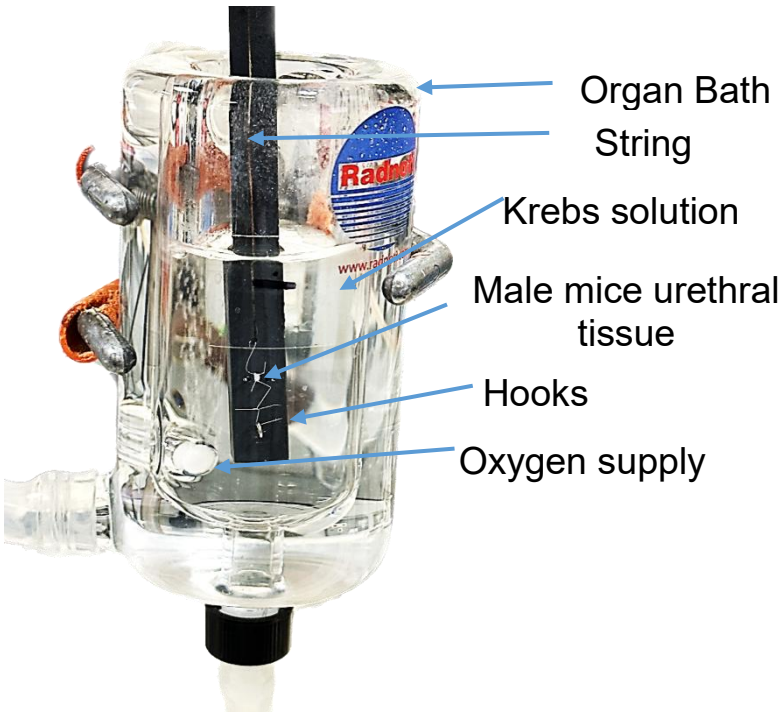

Fig. 2.3: Isometric tension setup: Urethral tissue is positioned between the electrodes on the transducer using hooks and strings to enable electric field stimulation (EFS). USM rings are immersed in an organ bath containing Krebs solution and is continually oxygenated and maintained at 37°C.

2.4 Tissue Ca^{2+} Imaging

The proximal urethra from KitGCaMP6f or Acta2-GCaMP8.1mice was opened along a longitudinal incision and the urothelium was carefully removed by sharp dissection. The muscular coat of the urethra was pinned to the base of a 5 ml volume, 60 mm diameter Sylgard-coated dish. The urethra preparation was continuously perfused with warmed Krebs' solution at 37°C for an equilibration period of 1 h before experiments were initiated. ICC-LC and USMC were visualized within tissues due to cell specific promoter driving GCaMP expression (*kit* and *acta2*). ICC-LC were visualized using an Eclipse E600FN microscope equipped with a 40× 1.0 CFI Fluor lens (Nikon) Fluor lens

and a FITC HQ series fluorescence filter cube equipped with a 510 nm dichroic, with a barrier filter of 535 nm. USMC were visualised using an Olympus BX51WI microscope equipped with Olympus LUMPLFLN40XW lens. Fluorescence was captured by excitation of GCaMP6f and GCaMP8.1 at 488 nm, and fluorescence emission was >510 nm. Images of ICC-LC were captured at 33 frames per sec using a high-speed EMCCD camera and TILLvisION software. USMC images were captured at 15 FPS using iXon^{EM} + EMCCD camera (Andor Technology, Belfast, UK) coupled to a Nipkow spinning disk confocal head (CSU-X1, Yokogawa, Japan) and IQ software (Andor, Belfast, UK).

Analysis of recordings were performed as per Drumm *et al.,* 2019c. Recordings (30 - 60 sec) of *in situ* ICC-LC and USMC Ca^{2+} activity were converted to a stack of TIFF (tagged image file format) images and imported into ImageJ (version1.54e, National Institutes of Health, MD, USA). Spatio-temporal maps (STMs) of Ca^{2+} activity in ICC-LC and USMC were generated by drawing a segmented line along the mid axis of the cell and applying the 'reslice' function in ImageJ; this generated an STM which was calibrated for distance and time. Basal Ca^{2+} fluorescence was acquired from regions of the cell displaying most uniform and least intense fluorescence (F_0). Fluorescence values throughout the cell was divided by the calculated F_0 value to calibrate the STM for amplitude of Ca^{2+} events as $\Delta F/F_0$. Frequency of Ca^{2+} events in ICC-LC and USMC was expressed as number of events fired per cell (min^{-1}). Duration of Ca^{2+} events was expressed as full duration at half-maximum amplitude (FDHM) and spatial spread of Ca^{2+} events was expressed as micrometres (μm) of cell propagated per Ca^{2+} event.

2.5 Total RNA isolation

Male and female mouse urethras were collected and pooled into three groups (6 urethras per group / biological replicate, n=3, N=18) for each sex prior to RNA extraction. Additionally, for Chapter 4 qPCR studies, proximal colons were collected as a positive control (n=3, N=3). Total RNA was isolated from tissue samples using the TRIZOL method. Tissue pieces were flash frozen in liquid nitrogen and homogenised using a chilled pestle and mortar. The tissue was then transferred into a ribonuclease (RNase) free eppendorf tube containing 1 mL Trizol reagent, followed by gentle trituration through an 18-gauge needle and then a 21-gauge needle to

physically disrupt cell membranes. The sample was then incubated for 5 min at room temperature (RT). After that, 200 µL chloroform was added to cause organic and aqueous phase separation. The sample was capped and agitated for 15 sec, followed by incubation at RT for 3 min, and then centrifugation at 14500 RPM in a cold room for 15 minutes. Centrifugation separated the sample into a lower layer of red phenol-chloroform, an interlayer, and a clear upper aqueous layer. Upper aqueous layer containing RNA was transferred into a sterile Eppendorf tube. Care was taken to avoid touching inter-layers. The addition of 500 µL isopropanol then precipitated RNA. The sample was then vortexed briefly before incubation at RT for 10 min and then centrifuged for 10 min in a cold room. Next, the pellet was recovered and washed with 1 mL 75% ethanol. Then, the sample was vortexed and centrifuged for 5 min in a cold room. This was followed by supernatant removal and air-drying for 5 min. Finally, the pellet was resuspended in 25 µL RNase free water by trituration.

All isolated RNA samples were treated with deoxyribonuclease (DNase) to eliminate DNA contamination. 1 µL DNase 1 enzyme was added per 10 µL dissolved RNA before incubation at RT for 15 min. The enzymatic reaction was inactivated by EDTA and 10 min of heating (65°C). After DNase treatment, samples were deemed suitable for cDNA synthesis. RNA yield was quantified using a NanoDrop Spectrophotometer. Nucleic acids and proteins absorb ultraviolet light at 260 nm/280 nm, respectively. On the other hand, absorbance at 230 nm is typically the result of salt contamination. Hence, A260/A280 and A260/A230 ratios are used to estimate sample purity. Thus, RNA samples with an A260/A280 ratio between the range of 1.8 and 2 and a A260/A230 ratio between 2.0 and 2.2 were considered pure.

2.6 cDNA synthesis

Complimentary DNA (cDNA) is double-stranded DNA synthesised from single-stranded RNA in a reaction catalysed by reverse transcriptase enzymes. A total reaction volume of 20 µL was used to synthesise cDNA from 1 µg of total sample RNA. First, random hexamers (200 µg), DNase 1 treated RNA (1 µg), and dNTP mix (10 mM) were added into a nuclease-free microcentrifuge tube. Samples were heated initially to 65°C for 5 min, followed by a quick chill on ice. Then, contents were collected by brief centrifugation, followed by addition of 4 µL 5x First-Strand Buffer and 2 µL of

0.1 M DTT. Contents were mixed gently by trituration and incubated at 25°C for 2 min. Then, 1 µL of Superscript II RNase-H Reverse Transcriptase (Invitrogen) was added and mixed by gentle trituration. The incubation temperature was set at 25°C for 10 min and then 42°C for 50 min. Finally, inactivation of the reaction was carried out by heating to 70˚C for 15 min. All cDNA samples were stored at -20°C until further use. # Genomic DNA contamination cannot be fully excluded as no-Reverse transcriptase (no-RT) controls were not included during cDNA generation.

2.7 Real-time quantitative PCR

A commercially available qPCR mastermix – SYBR™ Green Universal Master Mix (Applied Biosystem) was used for qPCR experiments. The PCR reaction also required three components the cDNA template, forward and reverse primers (Table 2.1). SYBR Green is a dye that binds to double-stranded DNA (dsDNA) with high specificity. This dye absorbs light at 488 nm and emits light at 522 nm when dye-DNA interaction occurs. Therefore, fluorescence intensity is proportional to dsDNA quantity. Efficiency of each primer pair was calculated by constructing a standard curve from amplicons obtained from a series of serial dilutions of template cDNA. Standard curves for each individual primer set was obtained from mouse brain cDNA used at concentrations of 1:3, 1:10, 1:30 and 1:100. Primer efficiency was calculated from each standard curve using StepOne™ software (version 2.3, Applied Biosystems). Only primers possessing efficiency values within a 90-110% range were used for qPCR. Details of each primer sequence, including their accession number and expected amplicon size, are listed above in Table 2.3.

The qPCR reactions were carried out in triplicate with three biological replicates using Applied biosystems thermal cycler and StepOne™ software (version 2.3, Applied Biosystems). Non-template controls (NTCs) were also included in triplicates in each run to confirm the absence of contamination or non-specific amplification. The temperature-programmed protocol used is shown below in Table 2.2. To validate that observed fluorescence was amplicon-based, melting curve analysis was performed on each reaction. This involved ramping the temperature from 70°C to 90°C to melt dsDNA. The presence of one peak indicated one PCR product was produced in the

reaction. Each gene and their subsequent standard curve were compared to a standard curve generated from a reference housekeeping gene (*β-actin*). qPCR data were normalised to *β-actin* and analysed using $2^{-\Delta\Delta CT}$ method (Livak & Schmittgen, 2001).

Reagents	Volume (µL)
SYBR™ Green Universal Master Mix	12.5
PCR grade water	8.5
Forward Primer	1
Reverse Primer	1
cDNA template	2
Total volume	25

Table 2.1: PCR reaction reagents.

Step	Temperature (˚C)	Time (minutes)
Initial denaturation	95	5
Denaturation	95	0.5
Annealing	56	0.5
Extension (x40 cycles)	72	0.5
Final extension	72	7

Table 2.2: Thermal steps used in qPCR amplification.

Gene	Sequence	Accession no.	Product size
Ano1-F	TAACCCTGCCACCGTCTTCT	NM_178642	145 bp
Ano1-R	ATGATCCTTGACAGCTTCCTCC		
β – *actin-F*	CTAGGCACCAGGGTGTG	NM_007393.3	205 bp
β – *actin-R*	GTGAGCAGCACAGGGT		
Cacna1a-F	CCTCATCATCATCGGCTCCT	NM_007578	190 bp
Cacna1a-R	CGCAAGAATCACCTCTTCTGC		
Cacna1c-F	GTAAGGATGAGTGAAGAAGCCGAGTAC	NM_009781	157 bp
Cacna1c-R	CAGAGCGAAGGAAACTCCTCTTTGG		
Cacna1d-F	ACCAAAGAAACAGAAGGCGG	NM_028981	122 bp
Cacna1d-R	TGTAAACTGGGCACTCCTGA		
Cacna1f-F	AGCCCTCCTCACTGTCTTTC	NM_019582	155 bp
Cacna1f-R	TCAGCAGGATGTAGTTGCCA		
Orai1-F	GTTCACTTCTACCGCTCCCT	NM_175423	131 bp
Orai1-R	GTGCCCGGTGTTAGAGAATG		
Orai2-F	CACAAGGGCATGGATTACCG	NM_178751	112 bp
Orai2-R	CCCTGCTCAGGTAGAGCTTC		
Orai3-F	GGCTGAAGTTGTTCTGGTGG	NM_198424	173 bp
Orai3-R	TGGAAGGCTGTTGTGATGTG		
Kcnq1-F	AGCACACCCCATTTCTTGAG	NM_008434.2	274 bp
Kcnq1-R	ACTGATCCAGCCTTCTCTGT		

Kcnq2-F	CGGCAGAATTCAGAAGAAGCA	NM_010611.3	211 bp
Kcnq2-R	CCGAGTACTGTTCGATGACG		
Kcnq3-F	CCAGCAGTCTCCAAGGAATG	NM_152923.2	204 bp
Kcnq3-R	GCCCCCTTAGTTGGGTAGTA		
Kcnq4-F	CGATCACACTGACGACCATT	NM_001081142.2	216 bp
Kcnq4-R	ACGCAGCCTGGATGAGATTA		
Kcnq5-F	TCTTGGCTCAGGTTTTGCAT	NM_001160139.1	193 bp
Kcnq5-R	CTTCTGATTGGTAGGGCTGC		
Kcnma1-F	CTCCAATGAAATGTACACAG	NM_001253358.1	71 bp
Kcnma1-R	CAGGAGCTTAAGCTTCACA		

Table 2.3: List of primers used during qPCR.

2.8 Immunohistochemistry

Proximal urethral rings were longitudinally opened and pinned at all four corners with thin tungsten wire on a Sylgard-based dish, and urothelium was removed by sharp dissection. Tissues were fixed in 4% paraformaldehyde (PFA) for 20-30 min at RT. Tissues were washed in phosphate buffered saline (PBS, 0.01 M, pH 7.2) for 5 hours and PBS changed every hour. Tissues were subsequently incubated in donkey serum (10%; 2 hour at RT) to reduce non-specific antibody binding. The first incubation was carried out for 48 hours at 4°C with primary antibody (diluted 1:500 in 0.5% Triton-X 100). Tissues were subsequently washed in PBS for 5 hours and PBS changed every hour before incubating in secondary antibody (1:1000 in PBS) for 1 hour at RT, and washes were repeated with PBS for 5 hours. Tissues were then mounted on glass slides using Vectashield mounting media and a thin coverslip was placed over tissues. Each mount was then examined on a Leica Stellaris 5 confocal system with DMi8 inverted automated fluorescence microscope. Leica Application Suite X (LAS X) Software was used to capture Z-stack images of various depths of tissue at objective of 20X and 40X. Final images were constructed using the LAS X software (version 5.1.0.25593) and converted to TIFF files.

2.9 Isolation of mouse smooth muscle cells

SMCs from tissue such as USM were isolated enzymatically using 1 mg/ml of papain (Sigma), 1 mg/ml bovine serum albumin (BSA; Sigma), 1 mg/ml dithioerythritol (DTE; Sigma) and 1 mg/ml collagenase (type II; Sigma). Tissue dissection (Section 2.1) was performed in ice cold Dissection solution. Isolated tissues were finely chopped into fragments and placed in a 35mm Nunclon dish containing dissection solution, for 15-20 min at 4°C. Tissue fragments were transferred to a 1.5 ml Eppendorf for enzymatic dispersion, completed in two steps. Firstly, tissue fragments were incubated in primary dispersal medium comprising 1 mg/ml papain (Sigma), 1 mg/ml dithioerythritol (DTE; Sigma), 1 mg/ml BSA (Sigma) dissolved in 1 ml of dissection solution for 30 min at 37°C. The suspension was then washed with dissection solution before incubation in a second dispersal medium containing 1mg/ml collagenase type-2 (Sigma, 1 mg/ml BSA (Sigma) and 100 µM Ca^{2+} dissolved in 1 ml of Dissection solution. This incubation was performed for 7 min at 37°C. After 10 min, tissue was thoroughly rinsed and allowed to rest on ice for 10 min. SMCs were released from tissue fragments by gentle trituration with three glass pipettes of decreasing diameter. Isolated cells were stored in Dissection solution at 4°C

2.10 Immunocytochemistry

SMCs were dispersed from WT mouse urethra (male and female), bladder and corpus cavernosum. After dispersal, cells were adhered to coverslips coated with poly-l-lysine on ice. Cells were fixed with 2% PFA for 30 minutes and washed three times with 1% PBS. Cells were permeabilized with 0.1% Triton X (Sigma life science) for 10 minutes and washed thrice with 1% PBS. Blocking was performed with 50% SEA block (Thermo Fisher Scientific). Cells were co-stained with primary antibodies (Table 2.4) overnight at 4° C. Cells were washed with 20% blocking reagent (SEA block, Thermo Scientific) followed by incubation with secondary antibodies (Table 2.5) for 2 hours. Cells were then washed and mounted on slides using Vectashield mounting media. Appropriate positive and negative controls were included to verify antibody specificity. In Chapter 4, bladder SMC were used as negative controls, while corpus cavernosum SMC were used as positive controls for ANO1 expression. In Chapter 6, HEK293 cells

transfected with Kv7.1 or Kv7.5 were used as positive controls for Kv7.1 and Kv7.5 expression, respectively, while untransfected HEK293 cells were used as negative controls. Antibody specificity was further assessed using secondary only control preparations in which the primary antibody was omitted and tissues were incubated with secondary antibody only, to confirm that any observed fluorescence was not due to non-specific secondary antibody binding. Mounted cells were imaged on Axioskop 2 LSM 510 Meta confocal microscope (Zeiss, Germany, 20X objective). Confocal micrographs were generated from z-series scans taken at 0.5 µm depth intervals. Final images were constructed using Fiji by Image J (version1.54f, National Institutes of Health, MD, USA).

Primary antibody	Supplier	Dilution	Host
ANO1	Abcam, Alomone lab	1:500, 1:100	Rabbit polyclonal
Anti-GFP	Aveslabs	1:1000	Chicken polyclonal
Alpha-actin	Dako, Agilent	1:100	Mouse monoclonal
PDGFR-alpha	R and D Systems	1:200	Goat polyclonal
Kv7.5	Invitrogen	1:100	Rabbit polyclonal
Kv7.1	Alomone lab	1:100	Rabbit polyclonal

Table 2.4: List of primary antibodies used in experiments.

Secondary antibody	Supplier	Dilution	Wavelength
Alexa Fluor anti-rabbit	Invitrogen	1:1000	594 nm
Alexa Fluor anti-chicken	Jackson Immunoresearch Laboratories, Inc.	1:1000	488 nm
Alexa Fluor anti-mouse	Life technologies	1:1000	555 nm
Alexa Fluor anti-rabbit	Invitrogen	1:1000	488 nm
Alexa Fluor anti-goat	Invitrogen	1:1000	488 nm

Table 2.5: List of secondary antibodies used in experiments.

2.11 Solutions

Krebs' solution for isometric tension: NaCl (120 mM), KCl (5.9 mM) $NaHCO_3$ (25.0 mM), glucose (5.5 mM), NaH_2PO_4 (1.2 mM), $MgCl_2$ (1.2 mM), $CaCl_2$ (2.5 mM). Bubbled with 95% O_2 and 5% CO_2 to maintain a pH of 7.4.

Krebs' solution for Ca^{2+} imaging: NaCl (120.35 mM), $NaHCO_3$ (15.5 mM), KCl (5.9 mM) $MgCl_2$ (1.2 mM), NaH_2PO_4 (1.2 mM), $CaCl_2$ (2.5 mM) and glucose (11.5 mM). Bubbled with a mixture of 97% O_2 and 3% CO_2.

High potassium Krebs' solution: NaCl (65.8 mM), KCl (60 mM), $NaHCO_3$ (25.0 mM), Glucose (5.5 mM), NaH_2PO_4 (1.2 mM), $MgCl_2$ (1.2 mM), $CaCl_2$ (2.5). Bubbled with 95% O_2 and 5% CO_2 to maintain a pH of 7.4.

Ca^{2+} free Krebs' solution for isometric tension: NaCl (120 mM), KCl (5.9 mM) $NaHCO_3$ (25.0 mM), glucose (5.5 mM), NaH_2PO_4 (1.2 mM), $MgCl_2$ (1.2 mM), EGTA (0.5 mM). Bubbled with 95% O_2 and 5% CO_2 to maintain a pH of 7.4.

Dissection solution for cell dispersal: Monosodium glutamate (80 mM), NaCl (55 mM), KCl (6 mM), Glucose (10 mM), $MgCl_2.6H_2O$ (2 mM), HEPES- free acid (10 mM). pH to 7.3 with NaOH.

2.12 Drugs

The following drugs were used in the experiments such as isometric tension recordings and Ca^{2+} imaging (Table 2.6):

Drug Name	Supplier	Solvent
Indomethacin	Tocris	Ethanol
Ani9	Tocris	DMSO
GSK-7975A	MCE, Tocris	DMSO
Phenylephrine	Sigma Aldrich	H_2O
Nifedipine	Sigma Aldrich	DMSO
Nω-Nitro-L-arginine (L-NNA)	Sigma Aldrich	H_2O
Arginine Vasopressin	Tocris	H_2O
2-Aminoethoxydiphenylborate (2-APB)	Sigma Aldrich	Ethanol
Guanethidine	Sigma Aldrich	H_2O
Atropine	Sigma Aldrich	DMSO
Cyclopiazonic acid (CPA)	Tocris	DMSO
DEA-NONOate	Sigma Aldrich	H_2O
Tetrodotoxin (TTX)	Alomone labs	H_2O
CaCCinh-A01	Tocris	DMSO
Niflumic acid	MCE	DMSO
FPL64176	Tocris	Ethanol
Synta66	MCE	DMSO
TTA-A2	MCE	DMSO
XE991 dihydrochloride	Tocris	H_2O
Iberiotoxin	Smartox biotech	H_2O
Glibenclamide	MCE	DMSO

Table 2.6: List of drugs used in the experiments.

2.13 Statistical analysis

The statistics were applied to independent experiments and not on replicates or sum of replicates throughout the thesis. Experimental data for isometric tension were obtained from a minimum of six animals in most experiments, with the number of animals referred to as 'n.' In Ca^{2+} imaging experiments, intracellular Ca^{2+} activity was measured in the same cells within a FOV under control conditions and following pharmacological treatment or EFS in USM tissues, allowing paired comparisons at the cellular level. Statistics were applied to compare control and treatment conditions within the same cells which is refered to as "c" and the number of animals used refered to as "n". Summary data is presented as mean ± standard deviation (SD). Statistical analyses were performed using GraphPad Prism (version 10, GraphPad Software, USA). Normality of data distribution was assessed using the Shapiro-Wilk test. For normally distributed data, parametric tests were applied, including paired or unpaired Student's t-tests, when comparing two groups, one-way ANOVA for comparisons involving a single independent variable and two-way ANOVA for datasets involving two independent variables across more than two groups. Non-parametric tests (Wilcoxon signed rank test) were applied when data were not normally distributed.

Post hoc analyses were chosen according to the type of multiple comparisons required. Bonferroni's testing was applied for selected pairwise comparisons, Dunnett's test was used when multiple treatment groups were compared to a single control, and Tukey's test was employed when all groups were compared against one another. Non-linear regression followed by an extra-sum-of-squares F-test was used to compare EC_{50} values. Statistical significance was defined as $P<0.05$.

3. Identification and classification of interstitial cell of Cajal like cells (ICC-LC) in murine urethra

3.1 Introduction

ICC in the GI tract are pacemakers and neuromodulators of SMC, generating slow waves driving regular contractions of the GI tract (Thuneberg, 1982; Sanders, 1996, Dickens, 1999). In the GI tract, ICC express ANO1 and c-kit (Hulzinga *et al.,* 1995; Hwang *et al.,* 2009). The gene *c-kit* (proto-oncogene), located at the W locus, encodes a receptor tyrosine kinase (Takeda *et al.,* 1992). *Kit* signalling plays a crucial role in regulating development and survival of ICC. Disrupting c-kit with neutralizing antibodies (ACK2) or mutation causes loss of ICC and pacemaking activity (Ward *et al.,* 1994; Torihashi *et al.,* 1995; Ördög *et al.,* 1999).

Sergeant *et al.,* (2000) first identified ICC-LC in pools of enzymatically isolated USMC in rabbit urethra. These ICC-LC appeared morphologically similar to gut intramuscular ICC (ICC-IM) and were proposed to serve a pacemaker role, as they also generated spontaneous depolarisations (Sergeant *et al.,* 2000; Mchale *et al.,* 2006). ICC-LC were vimentin^{+}, and later Kit^{+} ICC-LC were also identified in rabbit USM (Sergeant *et al.,* 2000; McHale *et al.,* 2006). ICC-IM in the gut are innervated by cholinergic and nitrergic nerves (Ward & Sanders, 2006). Similarly, previous studies on isolated rabbit urethra ICC-LC suggested they were under control of adrenergic and nitrergic neurotransmission, as their spontaneous activity was increased by adrenergic agonists and decreased by NO donors (Sergeant *et al.,* 2002; Sergeant *et al.,* 2006a). Later, immunolabelling studies revealed close spatial interaction between ICC-LC with nitrergic nerves in rabbit USM (Lyons *et al.,* 2007; Smet *et al.,* 1996). Hashitani and Suzuki (2007) performed studies on whole rabbit USM tissue, utilizing the Ca^{2+} dye fluo-4-AM for visualization of USMC and ICC-LC. They observed Ca^{2+} activity in ICC-LC (identified based on morphology) was also increased with adrenergic agonists and reduced by NO donors (Hashitani & Suzuki, 2007).

Previous research on urethral ICC-LC has primarily utilized Ca^{2+} dyes such as fluo4-AM on isolated cells or tissue. However, permeable dyes load all cells in tissues indiscriminately. In addition, previous electrophysiological studies in rabbit USM were also performed on isolated cells. Identification of ICC-LC in previous rabbit USM studies, were based largely on morphology, which is not definitive due to the lack of any cellular marker. Moreover, direct visualization and direct nerve stimulation of ICC-

LC in intact urethral tissue was lacking. Thus, although ICC-LC responded to exogenous neurotransmitters, evidence for functional innervation was unclear.

To address these limitations, a transgenic mouse was utilised, Kit-GCaMP6f (Fig 2.1) which express a genetically encoded Ca^{2+} reporter (GCaMP6f). GCaMP6f is driven by expression of $CreER^{T2}$ linked to the *Kit* promotor, and expression of GCaMP is exclusively induced in *c-kit*$^{+}$ cells after tamoxifen injection and recombination of lox p sites by Cre recombinase. This mouse model was used previously in studying ICC-IM in colon (Drumm *et al.,* 2019a; 2019b), ICC in IAS (Hannigan *et al.,* 2020) and ICC-LC in renal pelvis (Grainger *et al.,* 2020). This model would enable us to record *in situ* Ca^{2+} activity from ICC- LC within intact mouse urethral tissue, and identify cells with confidence, without contaminating signals from non-ICC-LC. With this, I could visualize intercellular behaviour of ICC-LC and study the nerve stimulation responses.

The objectives of this chapter were to investigate whether ICC-LC are present in mouse urethra, and to study their distribution in the tissue. I sought to determine if ICC-LC were spontaneously active, and if their activity was coordinated. Finally, I aimed to clarify whether ICC-LC were functionally innervated.

* Data presented in Fig. 3.1, 3.2A&B, 3.3- 3.12 was published in the following peer-reviewed article prior to submission of this thesis: Gupta N, Baker SA, Sanders KM, Griffin CS, Sergeant GP, Hollywood MA, Thornbury KD, Drumm BT (2024). Interstitial cell of Cajal-like cells (ICC-LC) exhibit dynamic spontaneous activity but are not functionally innervated in mouse urethra. *Cell Calcium*. 2024 Nov;123:102931. doi: 10.1016/j.ceca.2024.102931. Epub 2024 Jul 22. PMID: 39068674.

* Data presented in Fig. 3.13 was published in the following peer-reviewed article prior to submission of this thesis: Gupta N, Baker SA, Sanders KM, Rabab KE, Thean DK, Alkawadri T, Griffin CS, Sergeant GP, Hollywood MA, Thornbury KD, Drumm BT (2025). ANO1 channels are expressed in mouse urethral smooth muscle but do not contribute to agonist or neurally evoked contractions. *Sci Rep*. 2025 May 19;15(1):17365. doi: 10.1038/s41598-025-00953-z. PMID: 40389459; PMCID: PMC12089485.

* Data presented in Figure 3.11A were performed and analysed jointly with Dr. Bernard Drumm at the Smooth Muscle Research Centre, Dundalk Institute of Technology, and at the University of Nevada, Reno School of Medicine. Data presented in Figure 3.12A were performed and analysed by Dr. Bernard Drumm, while data shown in Figure 3.13B were performed by Dr. Peter Blair in the laboratories of Prof. Kenton M. Sanders and Dr. Salah A. Baker at the University of Nevada, Reno School of Medicine.

3.2 Results

3.2.1 Urethral ICC-LC imaged using Kit-GCaMP6f mice

Kit-GCaMP6f mice were employed to visualize urethral ICC-LC *in situ*. Dissected urethral tissues (urothelium removed) were incubated with anti-GFP antibodies as outlined in the Methods section. These antibodies were utilized to specifically bind to green fluorescent protein (GFP), a constituent component of the GCaMP molecule (Nakai *et al.,* 2001), thereby facilitating selective labelling of Kit-GCaMP6f^{+} cells (ICC-LC) within the tissue.

Employing one of the features of the Leica microscope and software (LAS X), I secured images of every tissue section at a magnification of 20x, resulting in a single, composite picture of urethras from Kit-GCaMP6f mice. This revealed a dense population of slender, spindle-shaped ICC-LC distributed throughout the tissue (Fig 3.1A). ICC-LC could be positioned in close vicinity to one another, yet remained separate and dispersed across different planes (Fig 3.1B). At 40x magnification, ICC-LC morphology appeared thin, elongated, and spindle-shaped (Fig 3.1C). As an alternative to performing immunohistochemistry, I visualized ICC-LC by summating the fluorescent signals from Ca^{2+} events (described below) recorded over a 20-30 sec period. This generated a single summated picture of ICC-LC that was colour-coded green (Fig 3.1D). ICC-LC could be present in clusters, without any physical connection with each other. While ICC-LC could be in close proximity, I found no obvious network or interconnected plexus of ICC-LC.

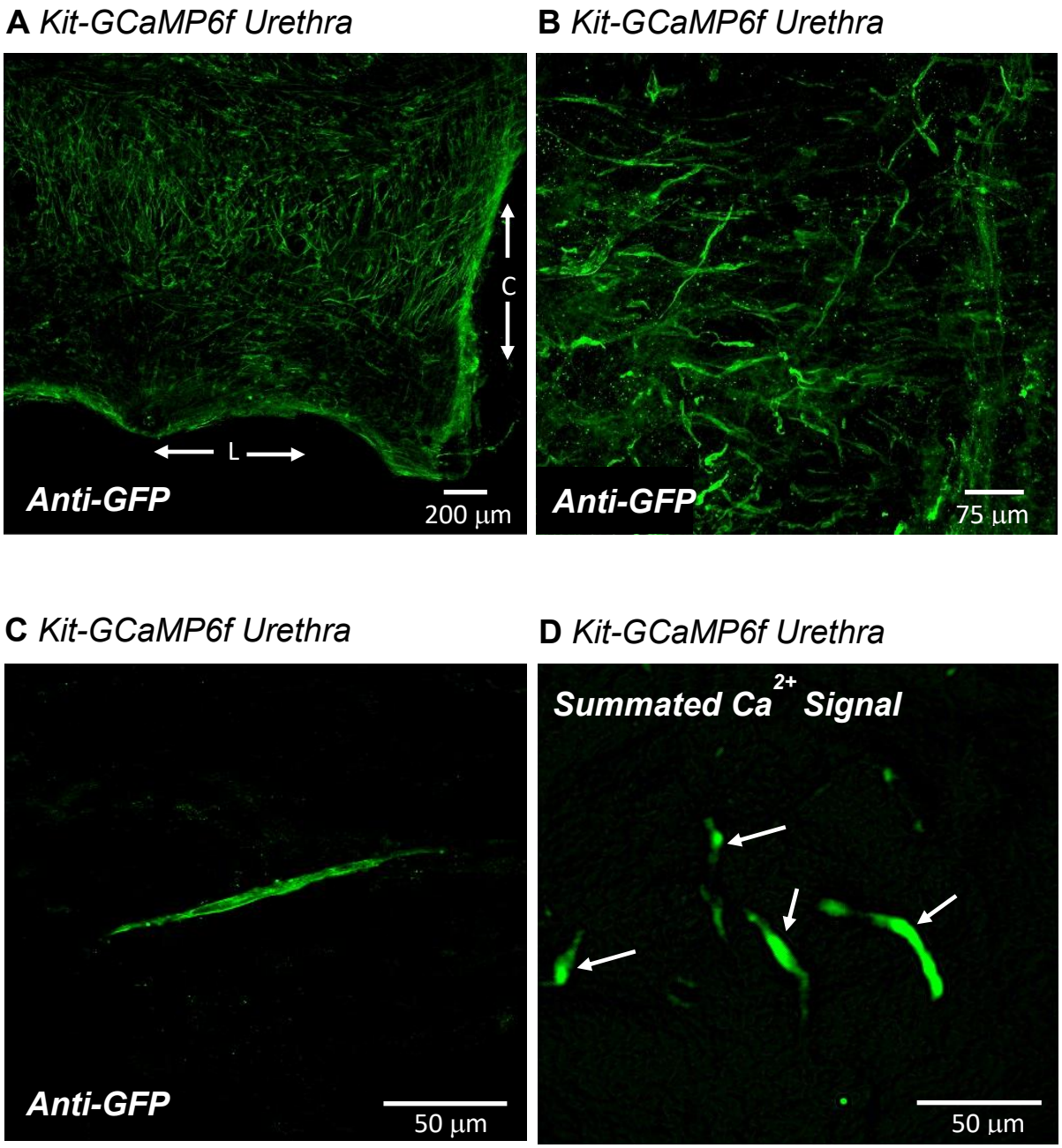

Fig 3.1: Visualizing ICC-LC morphology in Kit-GCaMP6f mouse urethra by immunohistochemical staining and Ca^{2+} imaging. **A** Single composite image capturing all sections of anti-GFP labelled urethral tissue from a Kit-GCaMP6f mouse at 20x magnification, depicting dense population of ICC-LC, longitudinal axis (L) & circular axis (C). **B** 20x magnification image from Kit-GCaMP6f urethra showing ICC-LC present in different planes and not interconnected to each other. **C** A single spindle shaped ICC-LC from a Kit-GCaMP6f mouse captured at 40x magnification using anti-GFP labelling. **D** Summated-Ca^{2+} signal image from a 20 sec recording of spontaneous activity from the urethra of a Kit-GCaMP6f mouse, showing multiple ICC-LC present (examples indicated by white arrows) in a field of view (FOV) demonstrating ICC-LC do not form a network.

By visualizing USMC with Acta2-GCaMP8.1 mice (Methods), I compared cellular distribution of USMC with ICC-LC in Kit-GCaMP6f mice. Acta2-GCaMP8.1 mice express an *acta2* promotor, which encodes *α-actin* of SM attached to the GCaMP sensor and was utilized for recording USMC Ca^{2+} activity. Images in Fig 3.2 were created by summation of 20 sec control recording of spontaneous Ca^{2+} activity in urethral tissue of both Acta2-GCaMP8.1and Kit-GCaMP6f mice and were depicted as a green signal. These images demonstrated USMC were arranged in bundles in circular, longitudinal and transversal orientations (Fig 3.2A&C). In Acta2-GCaMP8.1mice, Ca^{2+} signals occurred throughout the USMC bundles as described previously (Drumm *et al.,* 2018). In contrast, ICC-LC were not arranged in bundles and Ca^{2+} signals from Kit-GCaMP6f mice were confined to elongated, sometimes branched ICC-LC described above (Fig 3.2B&D).

Ca^{2+} imaging of ICC-LC was performed using a 40x objective at 33 frames per second. An example of a spontaneously active ICC-LC present in a FOV is illustrated in Fig 3.3A&B. Analysis of ICC-LC intracellular Ca^{2+} activity was performed by preparing STMs of Ca^{2+} activity (Methods). The STM of Ca^{2+} activity from the cell highlighted and referred to as cell 1 in Fig. 3.3B is shown in Fig. 3.3C. This STM illustrated spontaneous intracellular Ca^{2+} events occurring from multiple discrete sites within the cell. Some Ca^{2+} events propagated long distances, whereas others were spatially and temporally confined. A portion of the STM was expanded (white dashed box, Fig 3.3D), and its 3-D plot was also created (Fig. 3.3E) to display a representative example of the range of Ca^{2+} events (1-5) on an expanded time-scale. In contrast to extended and wave-like appearance of Ca^{2+} events 4 and 5, short and ephemeral Ca^{2+} events 2, and 3 were similar to Ca^{2+} sparks or puffs, which arise from activation of ryanodine receptors (RyR) or IP_3Rs respectively (Fig 3.3D&E). Ca^{2+} events propagated either unidirectionally (event 1) or bidirectionally (event 4 or 5) in ICC-LC (Fig 3.3D).

A *Acta2-GCaMP8.1 Urethra*

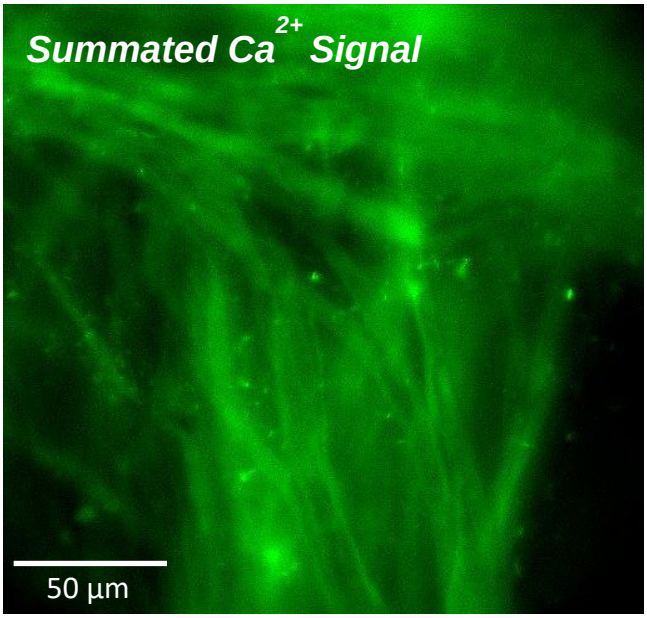

B *Kit-GCaMP6f Urethra*

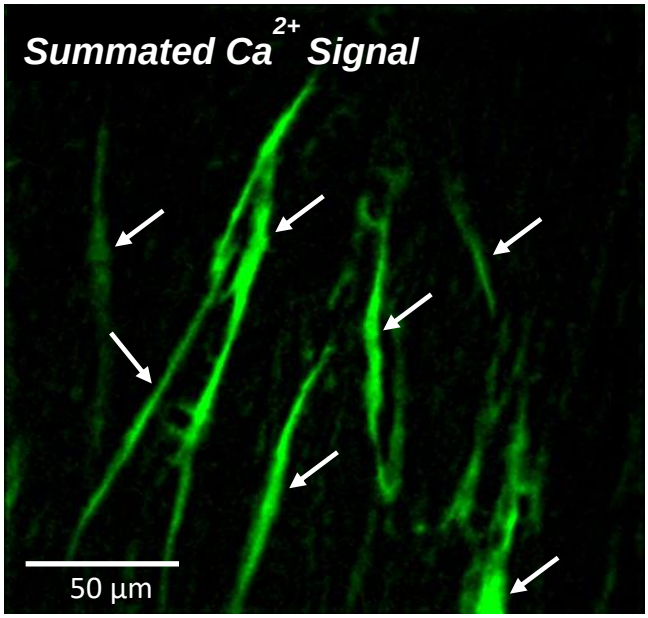

C *Acta2-GCaMP8.1 Urethra*

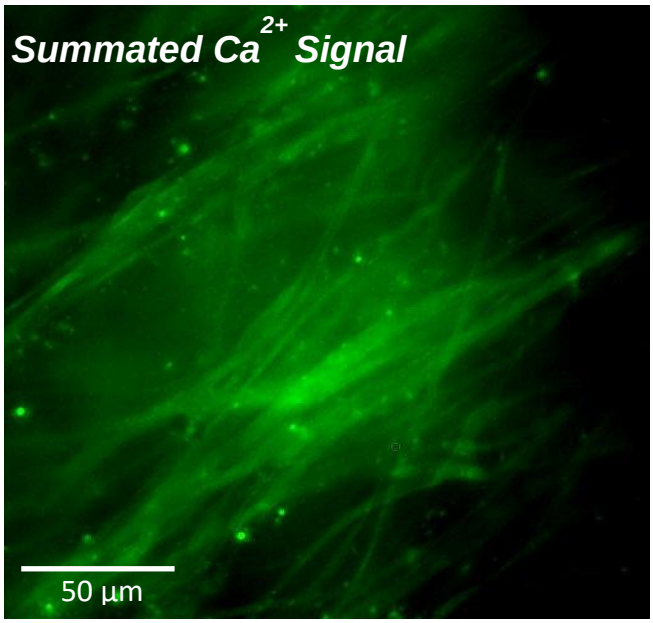

D *Kit-GCaMP6f Urethra*

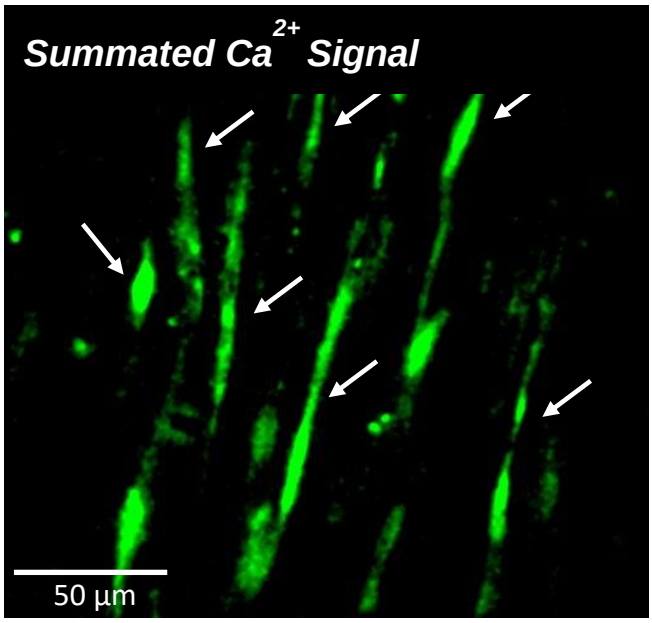

Fig 3.2: Comparison of cellular distribution of USMC and ICC-LC using Acta2-GCaMP8.1 and Kit-GCaMP6f mice respectively. A&C Summated image of Ca^{2+} signal from 30 sec control recording of Acta2-GCaMP8.1 mice urethra showing USMC present in bundles in a crisscross orientation. **B&D** Summated Ca^{2+} signal image of ICC-LC in a FOV from a Kit-GCaMP6f mouse showing thin, spindle-shaped cells, some but not all appeared branched.

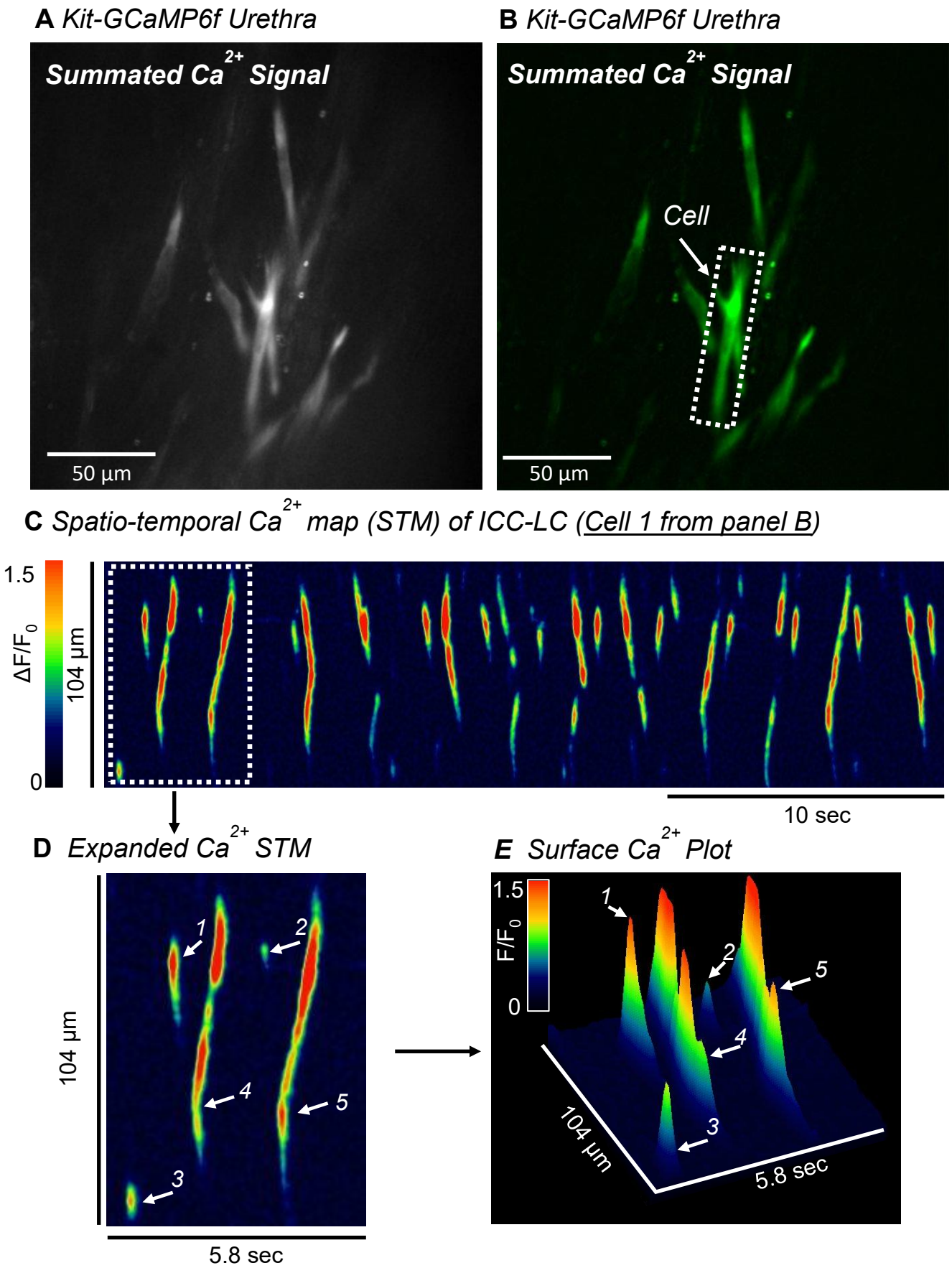

Fig 3.3: Spontaneous Ca^{2+} waves in ICC-LC of murine urethra. A&B, summated Ca^{2+} signals image showing ICC-LC in a FOV firing spontaneous Ca^{2+} events out of which one cell was selected for analysis demonstration. **C** STM generated from selected cell 1 (B) showing Ca^{2+} events originating from multiple firing sites. White dashed box represents section of the STM displayed on an expanded timescale in **D** and as a 3-D plot representation in **E**.

ICC-LC fired spontaneous intracellular Ca^{2+} events arising from multiple firing sites. To illustrate this, an STM from a single ICC-LC was generated, illustrating firing of Ca^{2+} events from multiple points of origin (Fig 3.4A). Six firing sites were indicated by coloured arrows to the left of the STM, and activity occurring in these regions was plotted as colour-coded traces (Fig 3.4B). These traces were merged (Fig 3.4C) to investigate any obvious synchronicity or coordination between Ca^{2+} events. This demonstrated Ca^{2+} events initiated at one firing site could propagate to another region, but there was no apparent relationship between the timing of Ca^{2+} events firing at different sites (Fig 3.4B). Instead, Ca^{2+} events appeared to fire in a stochastic manner, with little to no temporal coordination (Fig 3.4C).

Asynchronous firing of Ca^{2+} events between adjacent ICC-LC was also observed. As shown in Fig. 3.5A, multiple ICC-LC were present within a single FOV, and four ICC-LC were selected and marked with equal-sized coloured regions of interest (ROIs) (red, green, pink, and blue; Fig 3.5B) and STMs generated in representative colours for selected cells (Fig. 3.5C). STMs were merged (bottom panel Fig 3.5C), which revealed Ca^{2+} signalling patterns between ICC-LC exhibited no discernible overlap or intercellular coordination. This indicated intracellular activity of ICC-LC was largely independent of activity occurring in adjacent ICC-LC.

Quantitative analysis of Ca^{2+} activity in 54 cells from 13 animals (displayed as summary histograms (Fig. 3.6), revealed ICC-LC fired Ca^{2+} events on average 70 ± 8.1 min^{-1} (range 6 - 324 min^{-1}; Fig. 3.6A). Amplitudes of Ca^{2+} events averaged 0.4 ± 0.008 $\Delta F/F_0$ (range 0.08 - 1.96 $\Delta F/F_0$; Fig. 3.6B, 1243 events). Ca^{2+} events had an average FDHM of 0.2 ± 0.001 sec (range 0.04 - 0.7 sec; Fig. 3.6C, 1243 events). Ca^{2+} event propagation also showed considerable variation, with some events propagating <10 µm, while others could propagate ≥ 100 µm. On average, spatial spread of Ca^{2+} events was 40 ± 0.7 µm (Fig. 3.6D; n=13, c=54, 1243 events). While ICC-LC could have up to 10 firing sites per cell, most cells recorded (72%) contained 2-4 firing sites, with an average of 3 firing sites per ICC-LC (Fig. 3.6E; n=13, c=54).

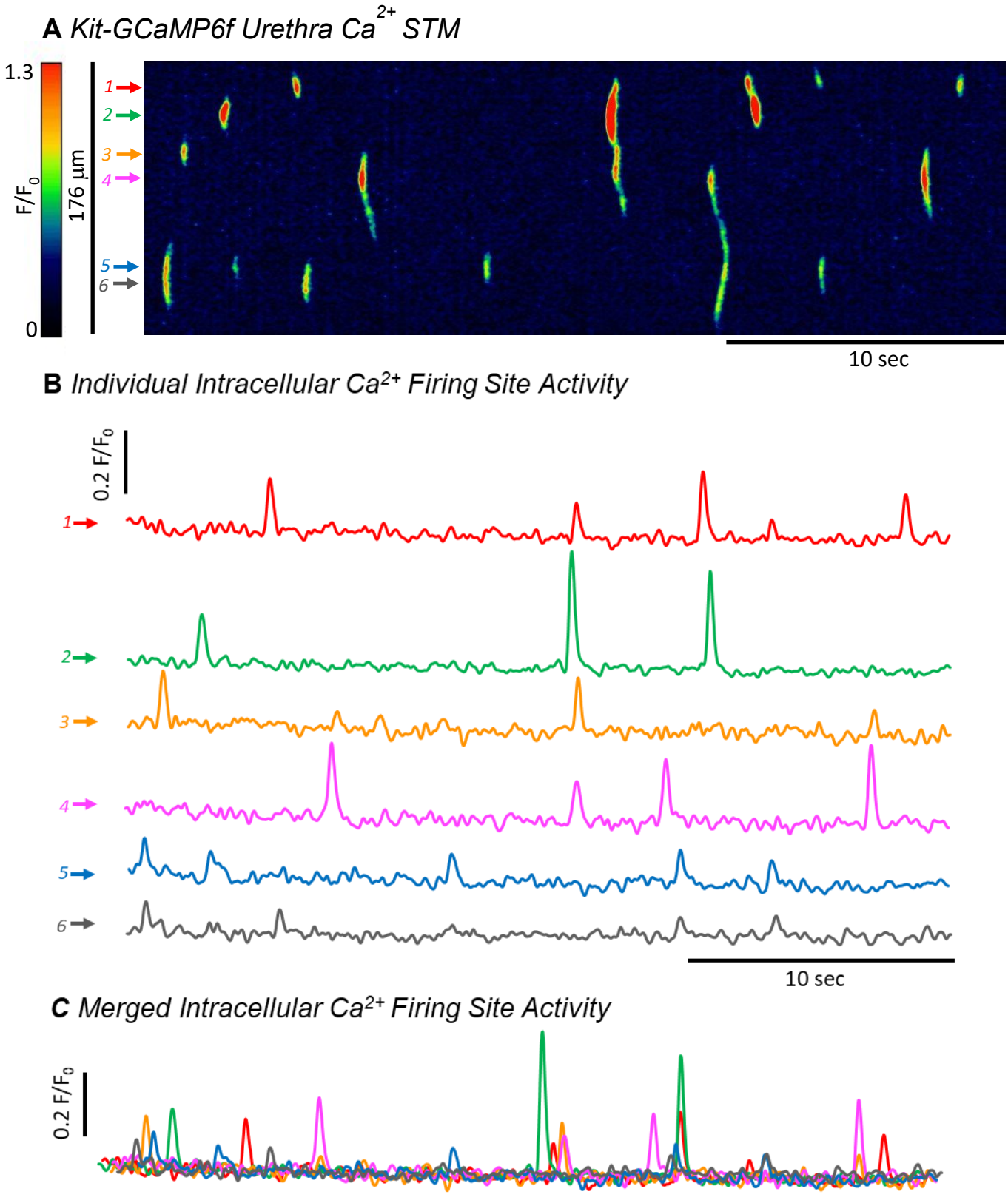

Fig 3.4: Multiple intracellular Ca^{2+} firing sites of ICC-LC. A Representative STM of ICC-LC Ca^{2+} activity showing multiple Ca^{2+} firing sites along the length of the cell, 6 of which are indicated by the red, green, orange, pink, blue and grey arrows. **B** Colour coded plot profiles of the Ca^{2+} activity at each of the corresponding colour coded Ca^{2+} firing sites indicated in (A). **C** Merged colour coded plot profiles showing intracellular Ca^{2+} firing sites activity.

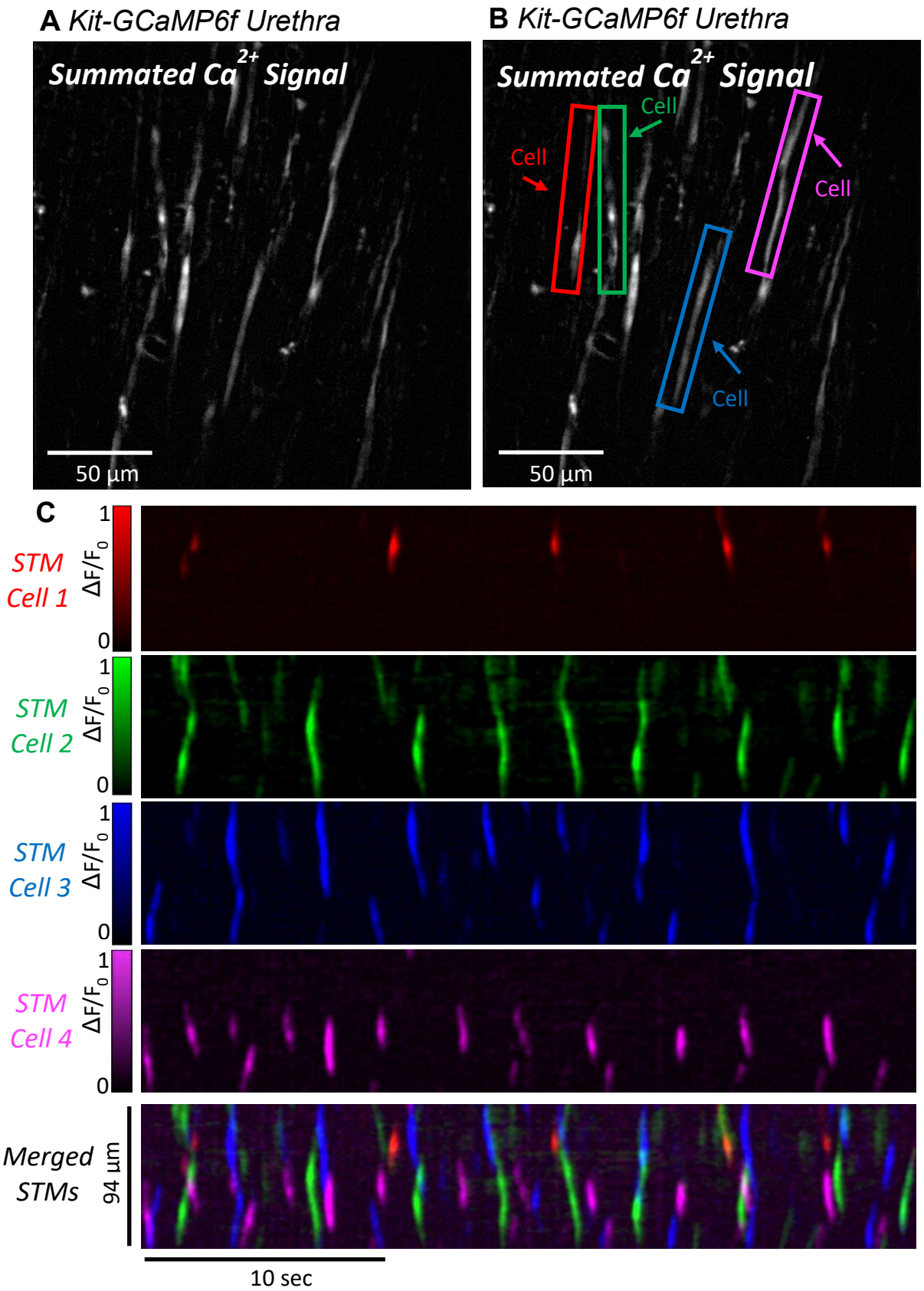

Fig 3.5: Urethral ICC-LC activity is not coordinated across the tissue. A Summated Ca^{2+} signal from a 20 sec recording with multiple ICC-LC in a FOV. **B** Four ICC-LC were selected and highlighted in red, green, blue and pink colours. **C** Uniformly coloured STMs were generated to show Ca^{2+} events in the selected four cells and were merged in the bottom panel to highlight asynchronous firing of ICC-LC and lack of intercellular coordination.

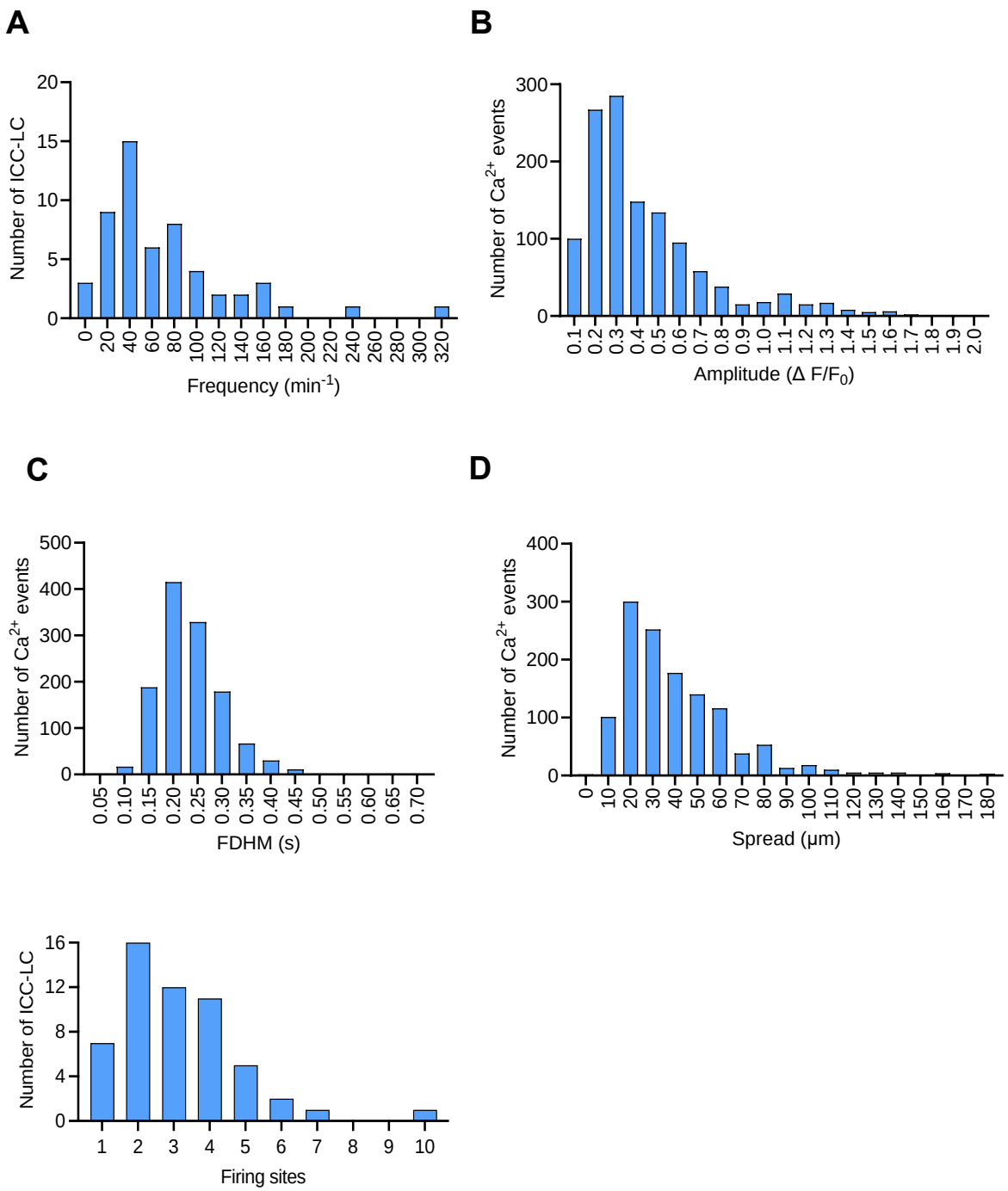

Fig 3.6: Quantification of ICC-LC Ca^{2+} signaling in the urethra. A-E, Histograms display quantitative analysis of Ca^{2+} events, **A** frequency (min^{-1}), **B** amplitude (F/F_0), **C** duration (s), **D** spatial spread (µm), **E** firing sites (1243 events, n=13, c=54).

3.2.2 Extracellular and intracellular Ca^{2+} sources for ICC-LC Ca^{2+} activity

In rabbit urethral ICC-LC, spontaneous Ca^{2+} activity occurs through ER mediated Ca^{2+} store release, sustained by Ca^{2+} influx from the extracellular space (Bradley *et al.,* 2005, 2006; Johnston *et al.,* 2005; Sergeant *et al.,* 2006b; Drumm *et al.,* 2014; Drumm *et al.,* 2014; Drumm *et al.,* 2015; Sancho *et al.,* 2017). To verify if similar mechanisms were responsible for generating activity in mouse urethral ICC-LC, I tested effects of blocking ER Ca^{2+} refilling and influx pathways.

Initially, 30 sec control recordings were obtained and the same FOV was recorded for 30 sec after 15 min of administration of the L-type Ca^{2+} channel blocker nifedipine (1 μM). Nifedipine failed to cause any significant change in Ca^{2+} activity (n=5, c=8, Fig 3.7A). It did not affect frequency (P=0.25), amplitude (P=0.18), duration (P=0.43), or spread (P>0.9) of ICC-LC Ca^{2+} events (n=5, c=8, Fig. 3.7B). Next, I examined effects of an Orai channel inhibitor (GSK-7975A) to determine if ICC-LC Ca^{2+} activity was due to store operated Ca^{2+} entry (SOCE). GSK-7975A reduced Ca^{2+} event frequency by 83% (n=6, c=16, Fig. 3.7C&D), lowering frequency from 67.7 ± 50.4 min^{-1} to 11.4 ± 10.9 min^{-1} (P=0.0002). Amplitude was reduced from 0.4 ± 0.2 to 0.25 ± 0.15 $\Delta F/F_0$ (P<0.0001), half maximal duration from 0.2 ± 0.04 to 0.2 ± 1 sec (P= 0.008) and spatial spread of Ca^{2+} events from 43.6 ± 36.3 to 18.2 ± 10 μM (P=0.0003).

Next, I tested effects of cyclopiazonic acid (CPA; 10 μM; SERCA pump inhibitor). CPA eliminated Ca^{2+} activity in ICC-LC within 15 min (n=6, c=12, Fig. 3.8 A&B). These findings align with studies conducted on rabbit urethra, which concluded ICC-LC depend on intracellular stores for initiating Ca^{2+} activity (Johnston *et al.,* 2005; Hashitani & Suzuki, 2007; Drumm *et al.,* 2015).

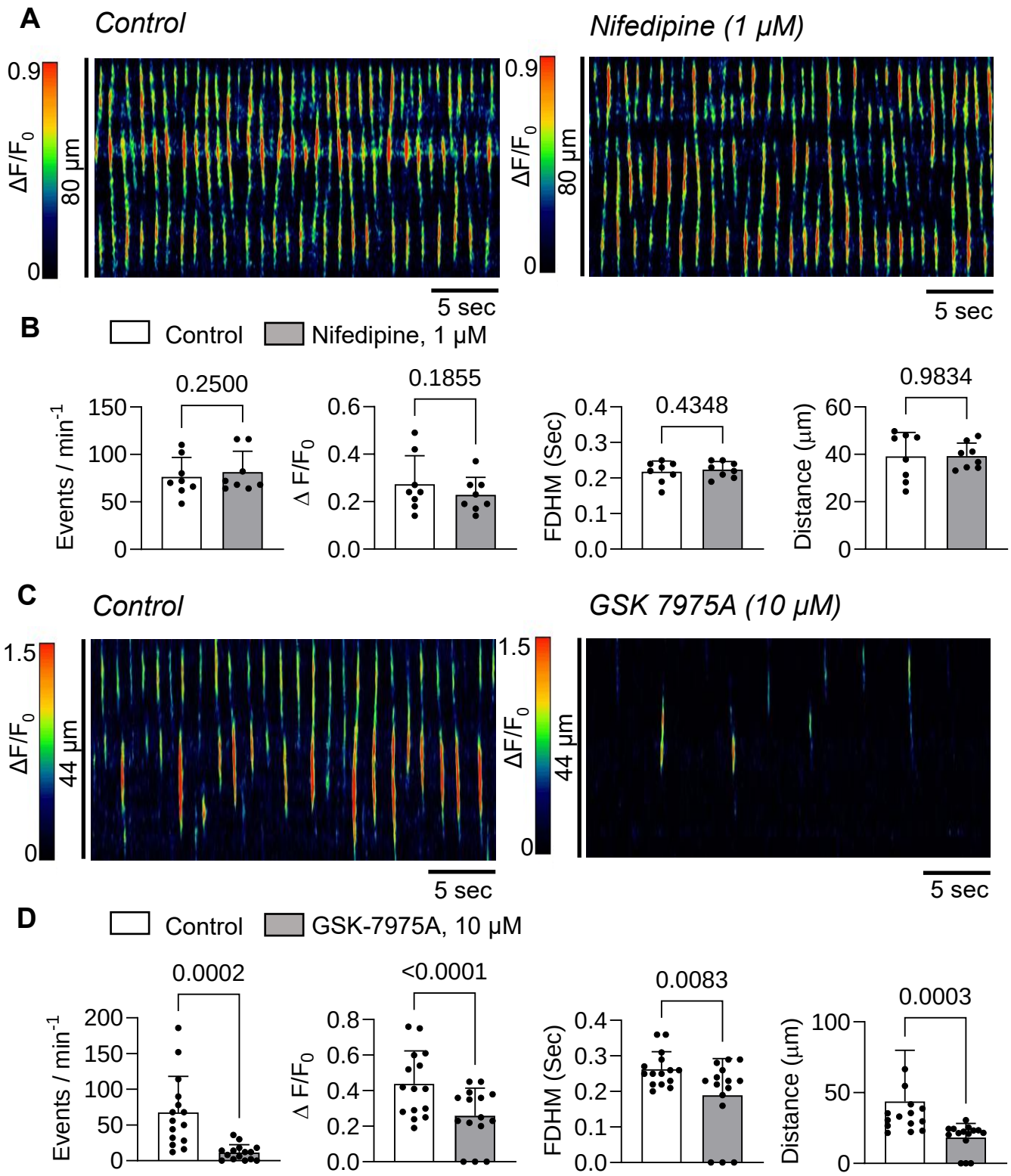

Fig 3.7: Spontaneous Ca^{2+} events in ICC-LC rely on SOCE via Orai channels but not LTCC. A STMs of Ca^{2+} events in ICC-LC recorded in situ during control conditions and after incubation with 1 µM nifedipine. **B** Summary of 1 µM nifedipine effects on frequency, amplitude, duration and spatial spread of ICC-LC Ca^{2+} events (n = 5, c=8), **C** STMs of Ca^{2+} events in ICC-LC recorded in situ during control conditions and after incubation with 10 µM GSK-7975A. **D** Summary data of 10 µM GSK-7975A effects on frequency, amplitude, duration and spatial spread of ICC-LC Ca^{2+} events (n=6, c=16).

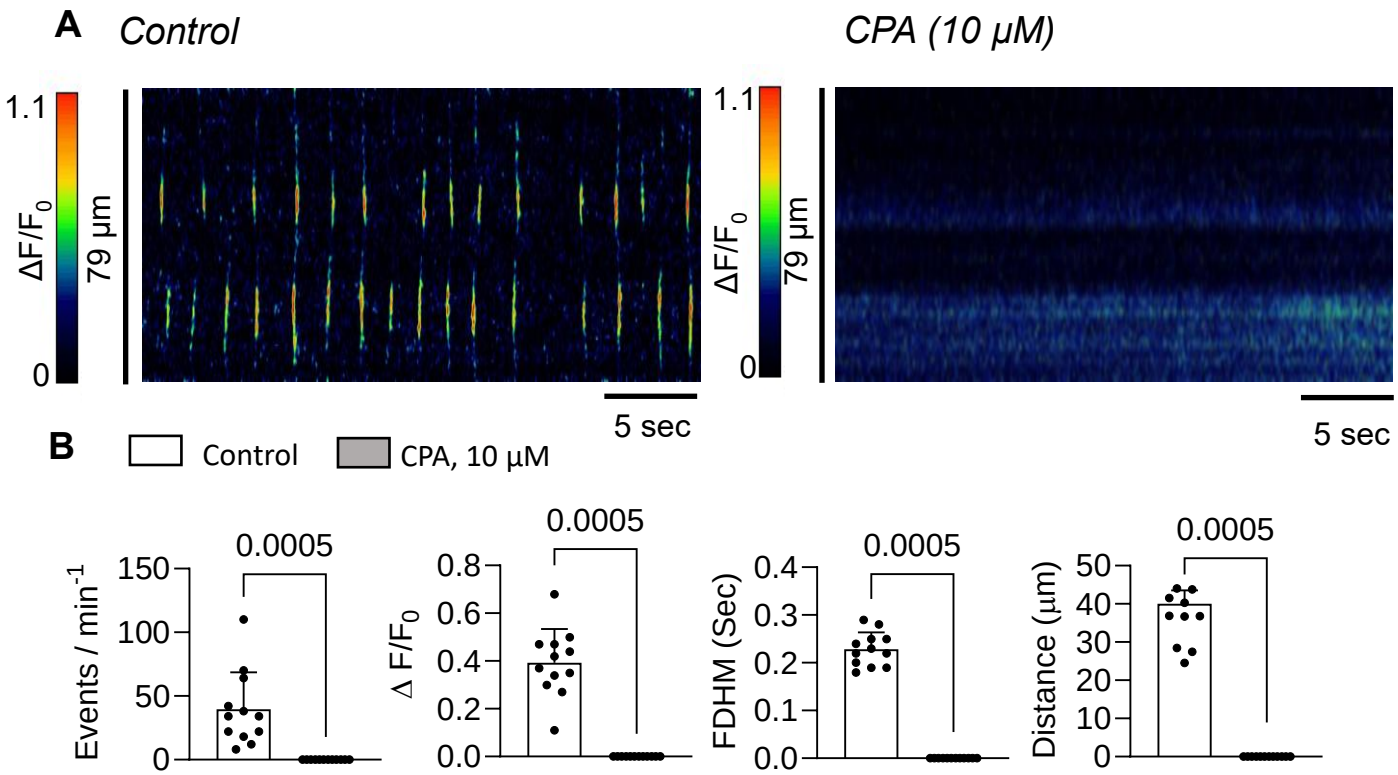

Fig 3.8: Ca^{2+} events in ICC-LC rely on ER stores. A Representative STM of Ca^{2+} event firing within a single ICC-LC recorded *in situ* during control conditions and after incubation with 10 µM CPA. **B** Summary data 10 µM CPA effects on frequency, amplitude, duration and spatial spread of ICC-LC Ca^{2+} events (n=6, c=12).

3.2.3 Neuronal control of ICC-LC Ca^{2+} activity

NO and NA are the main inhibitory and excitatory neurotransmitters for USMC, respectively (Andersson, 2001; De Groat *et al.,* 2001). In previous studies, DEA-NONOate (NO donor) suppressed Ca^{2+} events in USMC (Drumm *et al.,* 2018). DEA-NONOate, also reduced STD, STIC and Ca^{2+} waves in isolated rabbit ICC-LC (Sergeant *et al.,* 2006a). Similarly, another NO donor, SIN-1, reduced the amplitude of ICC-LC Ca^{2+} activity in intact rabbit urethra (Hashitani & Suzuki, 2007). Rabbit ICC-LC also responded to adrenergic agonists (increased STIC, STD and Ca^{2+} wave frequency (Sergeant *et al.,* 2002; Hashitani & Suzuki, 2007; Drumm *et al.,* 2014)). Moreover, previous immunolabelling studies demonstrated rabbit urethral ICC-LC were in close anatomical association with nitrergic nerve endings (Smet *et al.,* 1996; Lyons *et al.,* 2007), suggesting ICC-LC might be innervated, similar to ICC-IM in the gut. However, direct stimulation of ICC-LC in intact tissues has not yet been tested. Therefore, I aimed to determine whether ICC-LC were targets of neurotransmission.

In contrast to previous findings on rabbit ICC-LC, I found that DEA-NONOate (10 µM) failed to inhibit ICC-LC Ca^{2+} events (Fig. 3.9A). As shown in Fig 3.9B DEA-NONOate did not affect frequency (P=0.85), amplitude (P=0.5), duration (P=0.08), or spread (P=0.95) of Ca^{2+} events (n=7, c=15). Conversely, the α1-adrenoreceptor agonist phenylephrine (PE, 1 µM) increased Ca^{2+} activity (n=6, c=13, Fig 3.9C) by doubling firing frequency from 92.2 ± 83.3 to 170 ± 92.95 min^{-1} (P=0.001). PE also significantly increased amplitude (P=0.03, 0.7 ± 0.3 to 1 ± 0.7 $\Delta F/F_0$) and FDHM (P=0.06, 0.2 ± 0.03 to 0.27 ± 0.09 sec) of Ca^{2+} events, without significantly affecting spatial spread (P=0.08, Fig 3.9D).

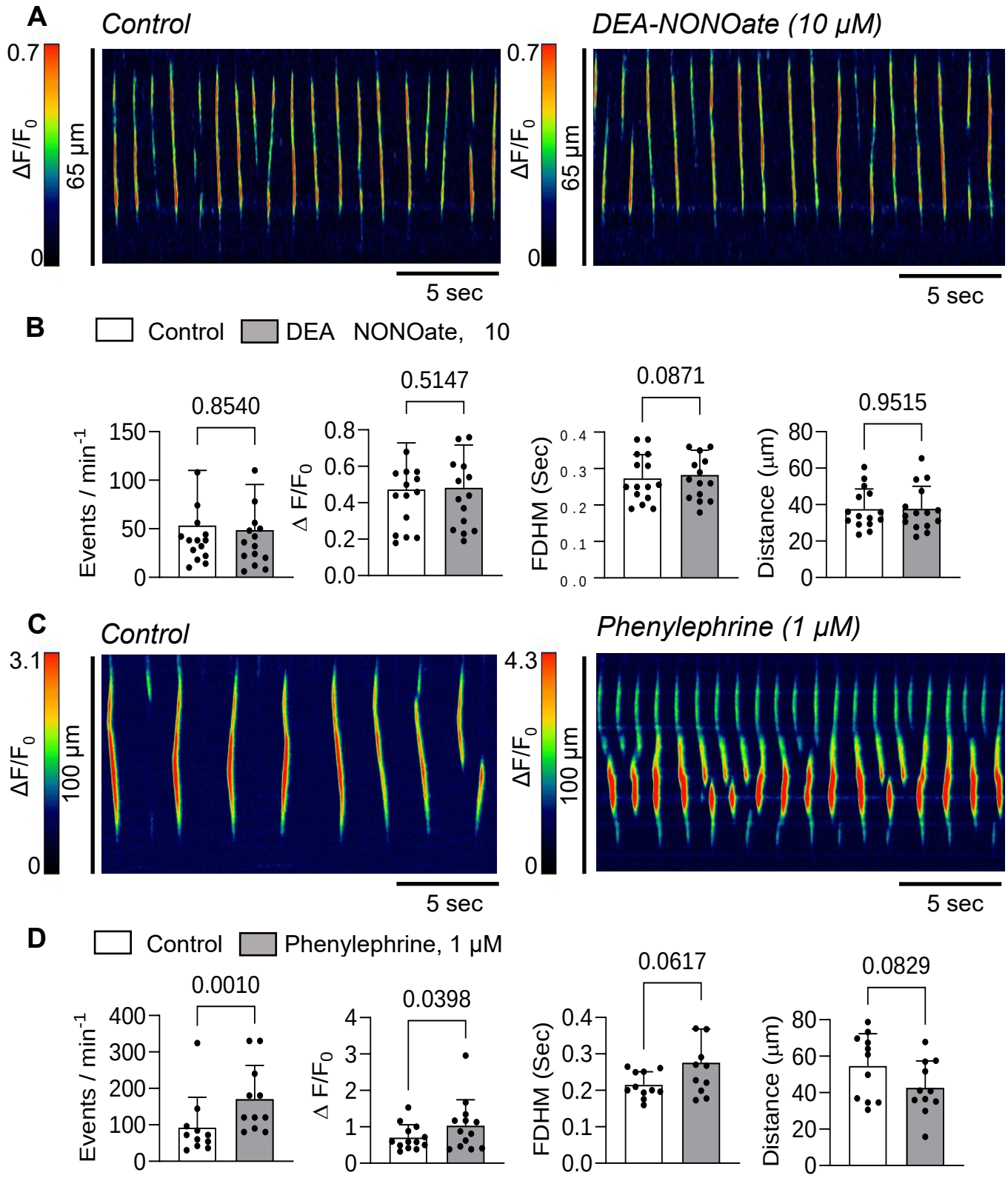

Fig 3.9: ICC-LC activity is modulated by an exogenously applied adrenergic agonist but not an NO donor. A STMs of Ca^{2+} events in ICC-LC recorded *in situ* during control conditions and after incubation with 10 µM DEA-NONOate. **B** Summary data showing the effect of 10 µM DEA-NONOate on frequency, amplitude, duration and spatial spread of ICC-LC Ca^{2+} events (n=7, c=15). **C** STMs of Ca^{2+} events in ICC-LC recorded *in situ* during control conditions and after incubation with 1 µM phenylephrine. **D** Summary of 1 µM phenylephrine effects on frequency, amplitude, duration, and spatial spread of ICC-LC Ca^{2+} events (n=6, c=13).

In isometric tension recordings, intact murine urethral rings exhibited contractile responses to electrical field stimulation (EFS) across a frequency range of 1-20 Hz (Fig. 3.10A&B). The amplitude of EFS-evoked contractions increased progressively with stimulation frequency. Lower frequencies such as 1 Hz and 2 Hz elicited relatively small contractions, whereas higher frequencies, such as 10 Hz and 20 Hz, produced the large contractile responses. From 5 Hz onwards, the EFS evoked contractions became significantly different ($P<0.0001$, Fig 3.10B). Increasing the stimulation frequency from 5 to 10 Hz enhanced the amplitude of EFS-evoked contractions from 0.13 ± 0.10 mN to 0.50 ± 0.20 mN, corresponding to a ~3.85-fold increase (Fig. 3.10B). We next tested the effect of EFS under these conditions on spontaneous Ca^{2+} activity of ICC-LC and USMC within intact urethral tissue. When EFS was applied to Acta2-GCaMP8.1urethral tissues at 10 Hz, (n=3, c=6, Fig. 3.11A&B), USMC Ca^{2+} event frequency significantly increased from 25.7 ± 11 to 44 ± 15 min^{-1} ($P=0.03$, Fig. 3.11A&B). In contrast, EFS elicited no change in frequency ($P=0.35$), amplitude ($P=0.06$), FDHM ($P=0.14$), or spatial spread ($P=0.06$) of ICC-LC Ca^{2+} events (n=11, c=20, Fig. 3.11C&D).

In experiments above, EFS in the absence of specific neuronal blockers would release both NA and NO neurotransmitters, which may counteract each other, making effects difficult to discern. Therefore, EFS at 10 Hz for 30 sec in ICC-LC under conditions favouring excitatory effects of NA, by inhibiting NO production with L-NNA (NO synthase inhibitor, 100 µM) was tested. However, this failed to elicit any effect on ICC-LC Ca^{2+} activity (n=6, c=16, Fig. 3.12A&B). Next, I tested EFS at 10 Hz for 30 sec under inhibitory conditions (non-adrenergic-non-cholinergic (NANC) conditions), by applying 1 µM atropine (muscarinic antagonist) and 10 µM guanethidine (adrenergic nerve inhibitor) (Fig 3.12C). Under NANC conditions, EFS also failed to affect frequency, amplitude, duration or spread of ICC-LC Ca^{2+} events (Fig. 3.12D, n=7, c=20).

A *EFS evoked contractions of USM*

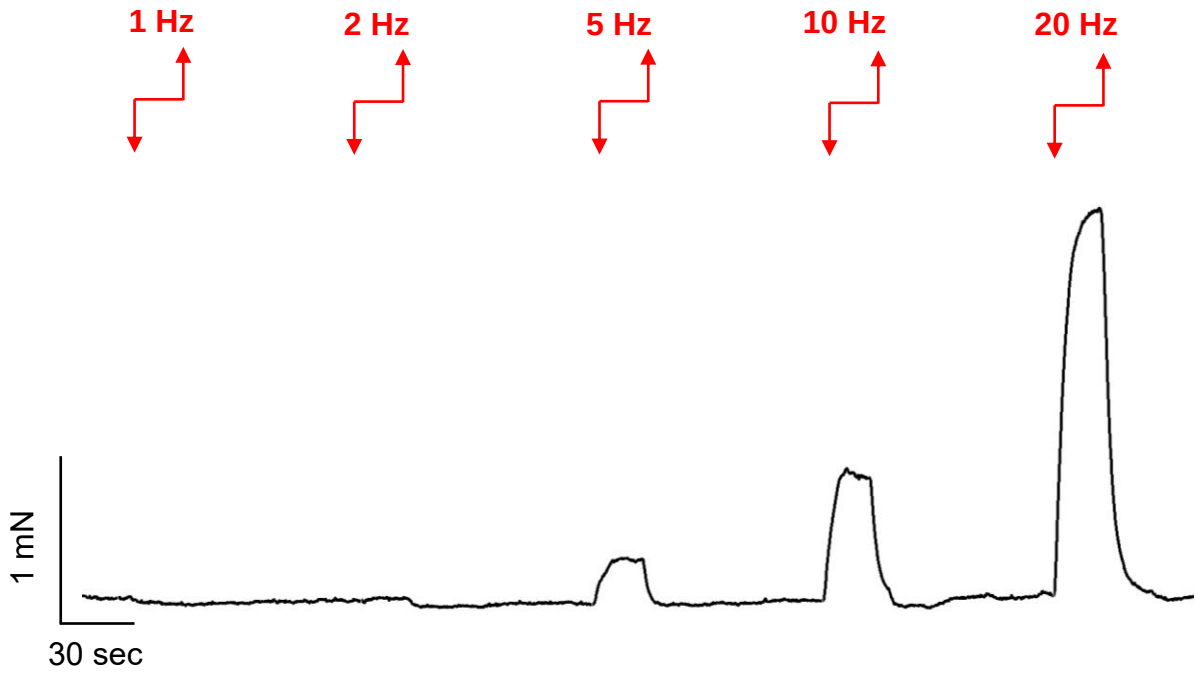

B

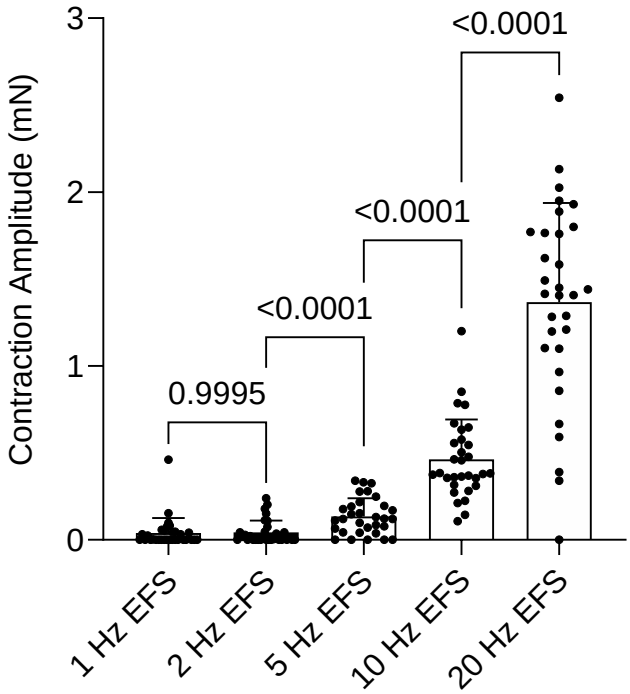

Fig 3.10: EFS evokes contractions of urethral tissues. A Isometric tension experiment, displaying a contractile trace of male wild type (WT) USM rings showing that EFS (30 sec) evokes robust contractions of USM tissues which increase according to EFS frequency (1-20Hz). **B** Summary data of EFS stimulation on USM contraction amplitude (1-20 Hz, n=31). (One-way ANOVA, Bonferroni's post-hoc test).

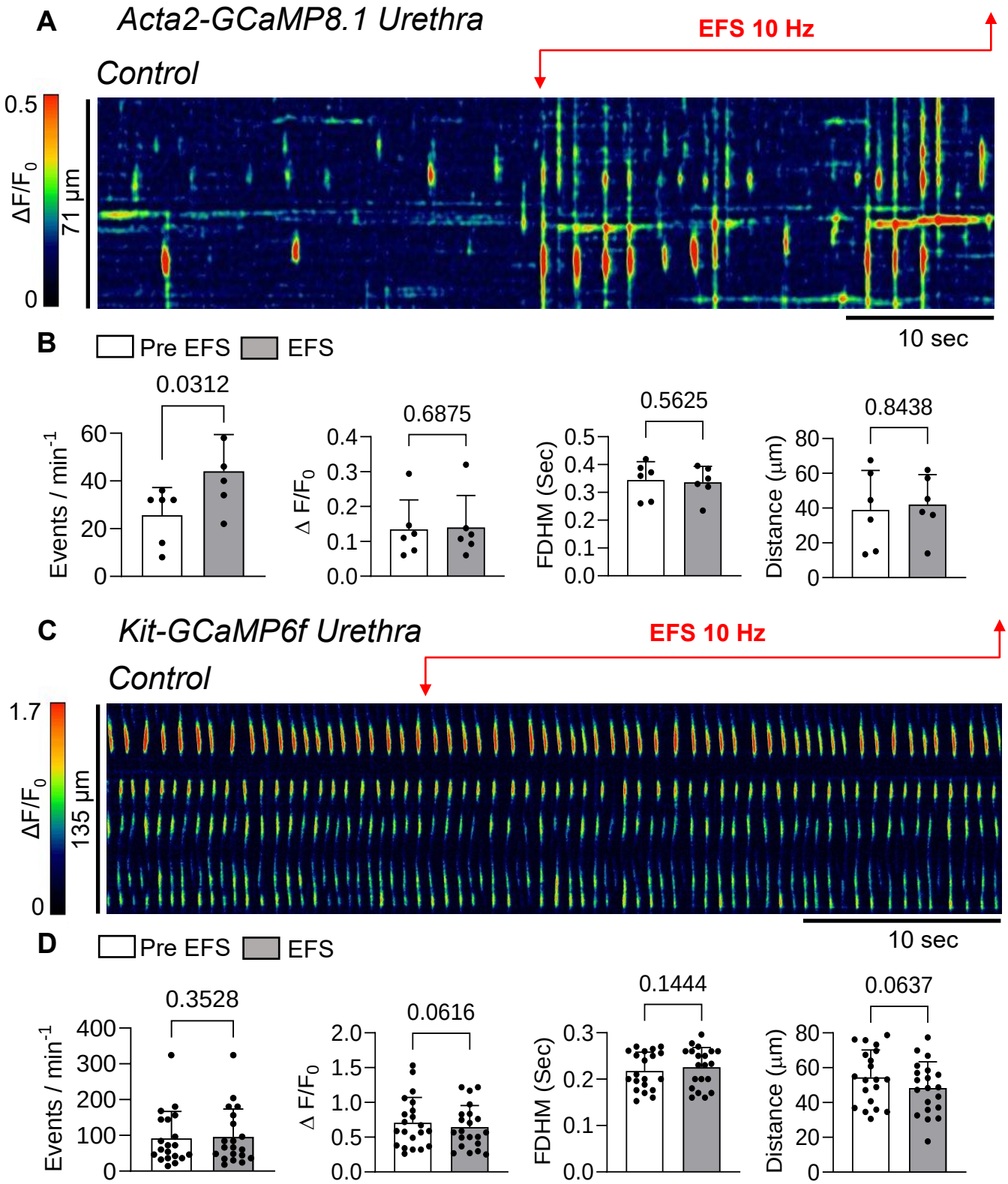

Fig 3.11: EFS (10 Hz) elicits responses in USMC but does not affect ICC-LC Ca^{2+} activity. **A** Representative STM of Ca^{2+} events in USMC recorded from an Acta2-GCaMP8.1 mice, note the increased activity during EFS (10Hz, 30 sec) indicated by the double pointed arrows. **B** Summary data of EFS stimulation on USMC Ca^{2+} events (10Hz, n=3, c=6) **C** STM of Ca^{2+} events in ICC-LC showing a lack of effects of EFS (10 Hz, 30 sec) on ICC-LC in the absence of any pharmacological agent. **D** Summary data of EFS effects on frequency, amplitude, duration, and spatial spread of ICC-LC Ca^{2+} events (c=20, n=11).

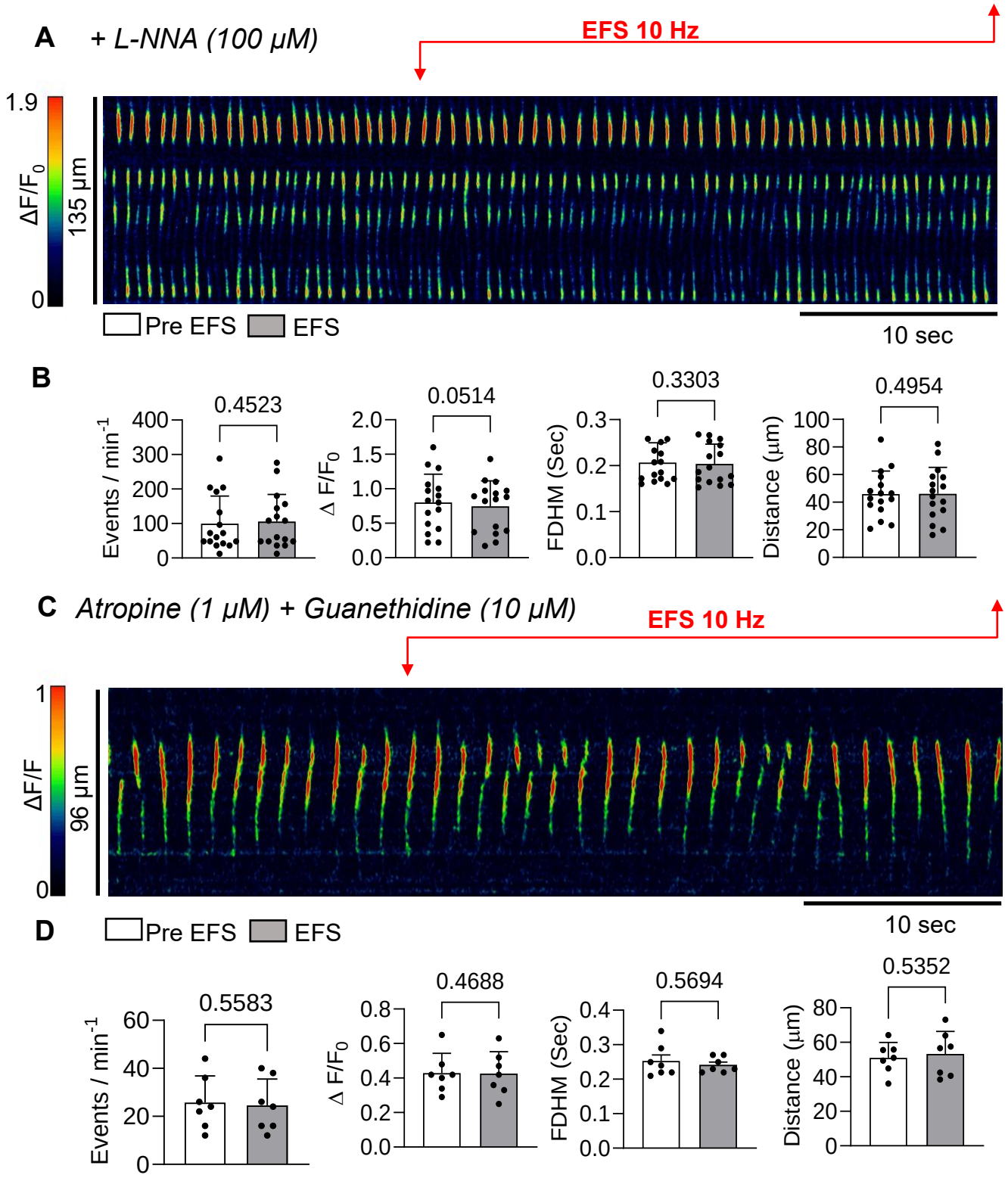

Fig 3.12: EFS failed to affect urethral ICC-LC activity when excitatory or inhibitory neural pathways are isolated. A Representative STM of Ca^{2+} events in ICC-LC in the presence of L-NNA (100 µM) and EFS 10 Hz, 30 sec. **B** Summary effects of EFS on ICC-LC in the presence of L-NNA (c=16, n=6). **C** Representative STM of Ca^{2+} events in ICC-LC in the presence of atropine (1 µM) and guanethidine (10 µM) and EFS at 10 Hz for 30 sec. **D** Summary effects of EFS on ICC-LC in the presence of atropine and guanethidine (NANC condition) (c=7, n=7).

3.2.4 ANO1 Expression in ICC-LC

In the gut, physiological functions of ICC as pacemakers and neuroeffectors, relies on expression of the Ca^{2+}-activated-Cl^- channel (CaCC) ANO1 (Hwang et al, 2009, Sung et al, 2018), and evidence suggests rabbit urethral ICC-LC also express this conductance (Fedigan *et al.,* 2017) and their intracellular Ca^{2+} activity is coupled to CaCC (Sergeant *et al.,* 2000, 2002, Johnston *et al.,* 2005). To investigate cellular location of ANO1 expression in mouse tissues, I performed double immunolabelling of anti-GFP and ANO1 antibodies on Kit-GCaMP6f mouse urethra (Methods). I found ANO1 labelling was not co-localized with ICC-LC, instead ANO1 antibodies appeared to label underlying USMC bundles (Fig. 3.13A, n=5). In upper urinary and male reproductive tracts, ANO1 expression is localized within PDGFRα$^+$ interstitial cells (Grainger *et al.,* 2020; Kudo *et al.,* 2024). To test if such cells expressed ANO1 in urethra, co-incubation of WT urethral muscle preparations with antibodies against PDGFRα and ANO1 was performed. PDGFRα$^+$ cells were abundant in urethral tissues (Fig. 3.13B), however no evidence of co-labelling with ANO1 was observed, and ANO1 appeared once again to be confined to USMC bundles (Fig. 3.13B, n=3).

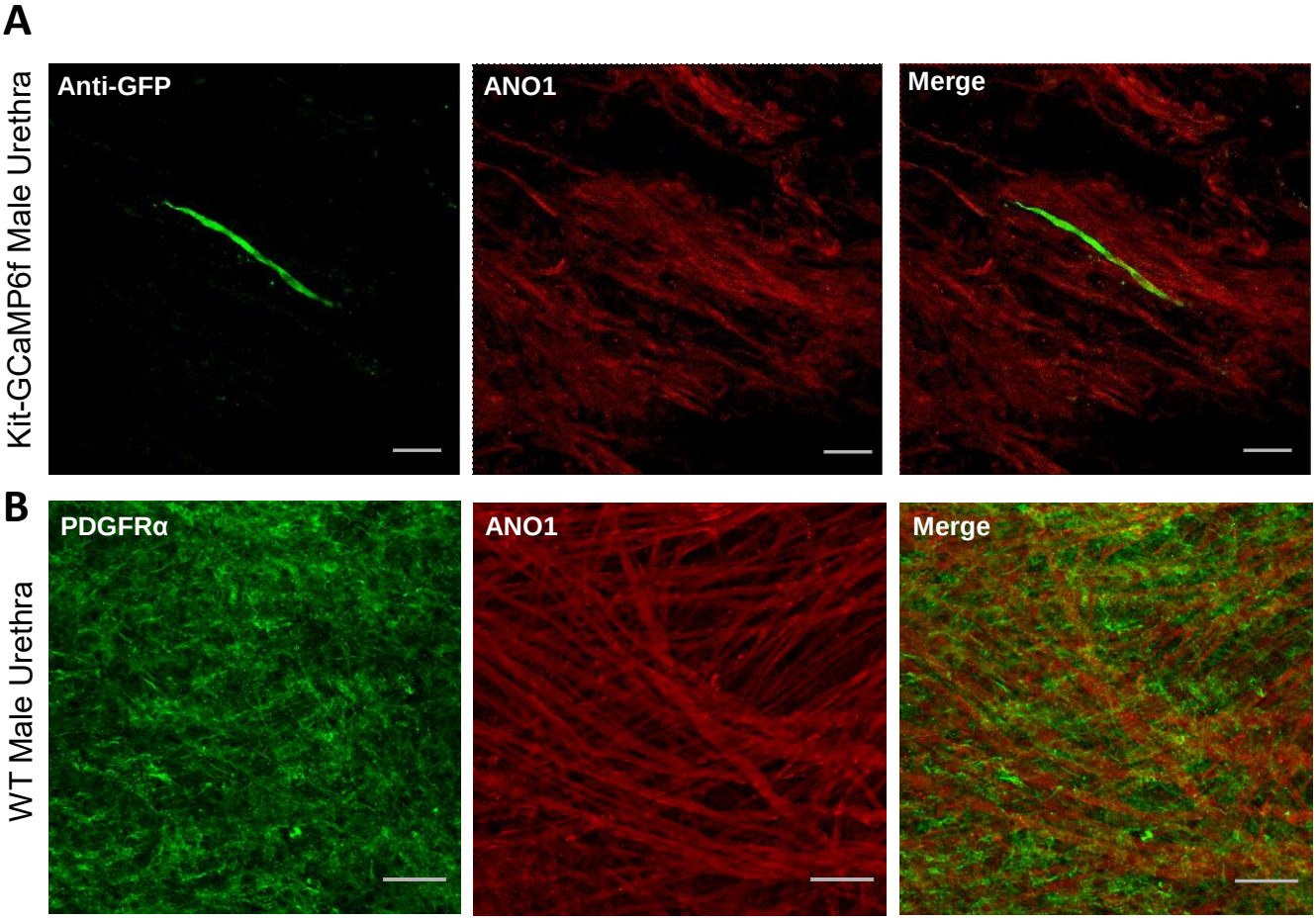

Fig 3.13: ANO1 is not expressed in mouse urethral interstitial cells. A Representative images of double immuno-labelling for anti-GFP (ICC-LC, green) and ANO1 (red) in Kit-GCaMP6f mouse urethra (n=5) captured at 40x magnification. **B** Representative images of PDGFRα^{+} cells (green) and ANO1 (red) in WT male mouse urethra (n=3) captured at 20x magnification. Scale bar: 50 µm in all panels.

3.3 Discussion

ICC-LC have been reported in various organs such as prostate (Exintaris, Klemm and Lang, 2004), lymphatics (McCloskey *et al.,* 2002), blood vessels (Harhun *et al.,* 2004), fallopian tube (Popescu *et al.,* 2005) and renal pelvis (Lang *et al.,* 2007). In rabbit urethra, ICC-LC were proposed to serve as pacemaker cells, regulating behaviour of USMC (Sergeant *et al.,* 2000). Subsequent studies on rabbit urethral ICC-LC demonstrated these cells exhibit STIC and STD similar to spontaneous depolarisations recorded from ICC in the GI tract (Mchale *et al.,* 2006; Sanders *et al.,* 2006). Application of NA increased frequency of STIC and STD (Sergeant *et al.,* 2002), while NO donors reduced STIC and STD frequency by reducing Ca^{2+} wave spatial spread (Sergeant *et al.,* 2006a). Although these studies demonstrated the presence of ICC-LC in the urethra based on their morphological appearance, definitive identification of ICC-LC using cellular markers were lacking. ICC-LC were also studied previously in intact rabbit urethral tissues using a Ca^{2+} dye flou-4-AM. However, this dye loads into all cells, meaning cell identification could be ambiguous (Hashitani & Suzuki, 2007). Nonetheless, this study found that exogenous application of SIN-1 (NO donor) reduced the amplitude of ICC-LC Ca^{2+} events and PE increased the frequency of ICC-LC Ca^{2+} events. This previous study concluded that ICC-LC were targets of neurotransmission in urethra, however, recordings of responses of ICC-LC to direct nerve stimulation were not attempted.

Our study demonstrates a novel approach to observe and characterize ICC-LC in urethra, as I utilized a transgenic mouse (Kit-GCaMP6f), to identify and study ICC-LC within intact tissues. Kit-GCaMP6f mice harbours a genetically encoded Ca^{2+} sensor, GCaMP, a fusion protein composed of green fluorescent protein (GFP), calmodulin (CaM), and M13, a peptide sequence from myosin light-chain kinase (Nakai *et al.,* 2001). In Kit-GCaMP6f transgenic mice, GCaMP6f is driven by expression of Cre^{ERT2} linked to the *Kit* promotor, and expression of GCaMP is exclusively induced in *c-kit*$^{+}$ cells after tamoxifen injection (Grainger *et al.,* 2020). This enabled us to capture high-resolution images of spontaneous Ca^{2+} activity in *Kit*$^{+}$ urethral ICC-LC *in situ*. Additionally, the GFP component of GCaMP allowed for reliable immunolabelling with anti-GFP antibodies, thereby facilitating visualization of ICC-LC. These transgenic mice have been employed to study ICC in the gut (Drumm *et al.,* 2019a; 2019b; Hwang

et al., 2022; Sanders *et al.,* 2024) and renal pelvis (Grainger *et al.,* 2020). In our study, this model allowed us to identify ICC-LC with confidence, allowing visualization of their distribution, spontaneous activity, intercellular coordination and Ca^{2+} mobilization pathways.

Our findings unveiled ICC-LC exhibited an elongated and spindle-shaped morphology, with some displaying branching similar to ICC-LC in rabbit as described by Sergeant *et al.,* (2000). ICC-LC did not form a network or plexus, and there was no physical connection between them, a characteristic also observed in ICC-IM in the GI tract (Burns *et al.,* 1997). This suggests ICC-LC do not work as coordinated pacemaker cells like ICC-MY, that generate and propagate electrical SW throughout SMC in the gut (Dickens *et al.,* 1999). Using Ca^{2+} imaging, I observed ICC-LC generated spontaneous Ca^{2+} events. Ca^{2+} events originated from multiple initiation sites. Some Ca^{2+} events were short in duration and localized in spread, while others propagated over a greater distance and lasted much longer. Ca^{2+} events were asynchronous among cells in close proximity to one another, which contrasts with rabbit urethral ICC-LC, where most of the tissue preparation (17 out of 22) exhibited synchronous Ca^{2+} activity among ICC-LC (Hashitani & Suzuki, 2007).

Previous studies on rabbit urethral isolated ICC-LC demonstrated that spontaneous activity was due to Ca^{2+} release from intracellular stores (Bradley *et al.,* 2005, 2006; Johnston *et al.,* 2005; Sergeant *et al.,* 2006a; Sergeant *et al.,* 2006b; Hashitani & Suzuki, 2007; Drumm *et al.,* 2014; Drumm *et al.,* 2015). Ca^{2+} influx in rabbit urethral ICC-LC occurred through non-LTCC (Bradley *et al.,* 2005; Hashitani & Suzuki, 2007). In our study, I tested sources of Ca^{2+} in ICC-LC in intact mouse urethra *in situ* using various pharmacological agents. ICC-LC activity was insensitive to nifedipine, similar to ICC-LC in rabbit urethra (Johnston *et al.,* 2005; Bradley *et al.,* 2005; Hashitani & Suzuki, 2007). Johnston *et al.,* (2005) reported that in rabbit urethral ICC-LC, spontaneous Ca^{2+} waves were inhibited by non-selective SOCE inhibitors SKF 96365, La^{3+}, and Cd^{2+} (Johnston *et al.,* 2005). In contrast, Bradley *et al.,* (2005) demonstrated that while rabbit urethral ICC-LC have the capability to mediate SOCE, but blocking SOCE with Gd^{3+} or La^{3+} did not affect spontaneous activity in these cells. The discrepancy in previous findings (Johnston *et al.,* 2005; Bradley *et al.,* 2005) regarding the role of SOCE may result from the use of non-selective Ca^{2+} influx and SOCE

inhibitors, which have various off-target effects, including blockade of Ca^{2+} entry via NCX and stretch-activated ion channels (Blaustein & Lederer, 1999; Brommundt & Kavaler, 1987; Hobai *et al.,* 1997; Lacampagne *et al.,* 1994; Singh *et al.,* 2010). The present study utilized a specific inhibitor of Orai, GSK-7975A, which reduced frequency of Ca^{2+} events by 83.1% in murine ICC-LC, indicating SOCE as a major extracellular source of Ca^{2+} influx in ICC-LC. I also found that the major intracellular source of Ca^{2+} source in ICC-LC were ER stores, as CPA blocked all Ca^{2+} events. This aligns with findings from rabbit ICC-LC which concluded ER stores are the predominant supplier of Ca^{2+} into the cytosol for spontaneous activity (Sergeant *et al.,* 2001a; Johnston *et al.,* 2005; Hashitani & Suzuki, 2007; Drumm *et al.,* 2015).

An important question I sought to address in this study was whether urethral ICC-LC are target of neurotransmission. Previous studies reported that USM contract in response of adrenergic stimulation (Andersson, 2001; Ito & Kimoto, 1985; Rembetski *et al.,* 2018, 2020), and relaxes in response to NO released from nitrergic nerves (Andersson, 2001; Garcia-Pascual *et al.,* 1991; Persson & Andersson, 1992; Waldeck *et al.,* 1998). In rabbit and guinea pigs, urethral ICC-LC respond to exogenous application of adrenergic and nitrergic neurotransmitters (Waldeck *et al.,* 1998; Sergeant *et al.,* 2002; Sergeant *et al.,* 2006a; Hashitani & Suzuki, 2007). Moreover, previous immunolabelling studies demonstrated $cGMP^{+}$ ICC-LC in human, guinea pig and rabbit bladder/proximal urethra were closely associated with nitrergic nerves, suggesting ICC-LC in urethra were innervated (Smet *et al.,* 1996; Lyons *et al.,* 2007).

In present study, I found spontaneous Ca^{2+} events in ICC-LC were not affected by application of NO donor, DEA-NONOate. In contrast, spontaneous Ca^{2+} events in murine USMC suppressed in reponse to similar NO donor, as previously reported (Drumm *et al.,* 2018). Similar findings were reported by Lies et al. (2013), who demonstrated that NO-GC immunofluorescence was confined to murine USMC, and that deletion of NO-GC in SMC abolished NO-induced relaxations in mouse urethra. In contrast, c-Kit^{+} and $PDGFR\alpha^{+}$ cells did not co-localise with NO-GC. Furthermore, NO-mediated relaxations evoked by DEA-NONOate were preserved in Kit-specific NO-GC knockout mice, indicating that NO-dependent urethral relaxation is mediated primarily via NO-GC expressed in USMC rather than ICC-LC (Lies *et al.,* 2013). In contrast, in sheep and rat USM electrical stimulation of nitrergic nerves increased

cGMP immunoreactivity in both ICC-LC and USMC. This response was abolished by NO synthase and GC inhibitors, confirming its dependence on NO-cGMP signalling (García-Pascual *et al.,* 2008). In our study, a α1-adrenergic agonist increased ICC-LC Ca^{2+} activity, suggesting α1-adrenoreceptors are present in ICC-LC. However, when functional innervation of ICC-LC was tested with EFS, ICC-LC were non-responsive under the same conditions that evoked responses in USMC and contractile responses in whole tissue rings. We tested EFS under NANC conditions to favour NO release and also in the presence of L-NNA, but no effect was observed in ICC-LC under either condition. This suggests that in murine urethra, ICC-LC Ca^{2+} activity is not modulated by neural input.

The expression and function of ANO1 channels in urethral cells appears to be species-dependent (Drumm *et al.,* 2021). Previous studies suggested ANO1, expressed in ICC-LC, may act as a pacemaker conductance to modulate USMC excitability, similar to ANO1 in gastrointestinal ICC (Sergeant *et al.,* 2000). In rabbits, ANO1 is exclusively found in ICC-LC, which exhibit large CaCC currents, while ANO1 is absent in USMC (Sergeant *et al.,* 2000; Fedigan *et al.,* 2017). However, in sheep and rodents, ANO1 is expressed in USMC, but not in vimentin^{+} ICC-LC (Sancho *et al.,* 2012). In contrast, Ambrogi *et al.,* (2025) reported co-expression of ANO1 and c-kit^{+} cells through immunostaining studies in mouse and human female urethral stromal cells, which they presumed as ICC-LC (Ambrogi *et al.,* 2025). However, the stromal cells described in this study were morphologically distinct from the elongated, spindle-shaped murine urethral ICC-LC (localized in muscle bundles) observed in Chapter 3 of this thesis and rabbit urethra (Sergeant *et al.,* 2000). Consistent with findings of Sancho *et al.,* (2012), I observed ICC-LC did not co-label with ANO1. Additionally, PDGFRα^{+} cells also did not co-localized with ANO1 in our study. ANO1 immunoreactivity was clearly observed in the surrounding muscle bundles, indicating ANO1 was abundantly expressed in USMC. This finding suggests that in murine urethra, any influence ICC-LC exert on USMC occurs through an ANO1-independent mechanism. Nonetheless, it is possible that ANO1 expressed on USMC alone is sufficient to depolarise the membrane, activate LTCC, and thereby modulate USM contractility.

This raises the question of how murine ICC-LC might contribute to urethral contractility if they are not directly innervated or express ANO1 as do rabbit ICC-LC. In the murine

urethra, spontaneous Ca^{2+} signalling in ICC-LC driven by Orai-mediated SOCE and SR Ca^{2+} release may contribute to the maintenance of basal USM tone. A comparable mechanism has been described in other sphincter SM, such as LES and IAS, where ER Ca^{2+} release in subsets of ICC-IM supports tone generation essential for sphincter closure (Hannigan *et al.,* 2020; Drumm *et al.,* 2022; Ni Bhraonáin *et al.,* 2025b).

Another possibility is that diffusible messengers such as Ca^{2+} or IP_3 could be released from ICC-LC and transmitted to adjacent USMC, thereby modulating their contractile activity (Boitano *et al.,* 1992). In pancreatic acinar cells, coordinated Ca^{2+} waves occur without traditional electrical pacemaking (Takano & Yule, 2023). Instead, intercellular diffusion of IP_3 and Ca^{2+} through gap junctions helps synchronize activity between cells (Takano & Yule, 2023; Yule & Takano, 2024). ATP also contributes by being released extracellularly in paracrine manner and activating purinergic receptors on neighboring cells, which triggers IP_3 production and Ca^{2+} release (Takano & Yule, 2023). Similarly, in vascular endothelium, signalling can switch between ATP diffusion and regenerative IP_3 production to sustain coordinated Ca^{2+} responses across cells (Buckley *et al.,* 2024). ATP can also be released by via vesicles extracellularly or can also be released via gap junctions (Leybaert & Sanderson, 2012). Expression studies confirmed presence of different connexins in ICC-LC and USMC in sheep and rat urethra, indicating presence of gap junctions (Sancho *et al.,* 2011). In murine and rabbit urethra, ATP is already known to enhance basal tone, suggesting it could be part of this signalling (Bradley *et al.,* 2010; Drumm *et al.,* 2018). Similarly, diffusion of IP_3 or Ca^{2+} from ICC-LC may raise Ca^{2+} in USMC sufficiently to trigger Ca^{2+}-induced-Ca^{2+}-release (CICR), thereby support sustained contraction, although direct evidence for this mechanism in USM is currently lacking and warrants further investigation.

It could be possible that a distinct population of ICC-LC becomes active in pathological conditions such as bacterial infections in murine urethra (Ambrogi *et al.,* 2025). Ambrogi and colleagues reported that neuroendocrine cells in female mouse and human urethra synthesize serotonin (5-HT), which induces urethral contraction in response to infection. These 5-HT induced contractions were inhibited by the ANO1 blocker Ani9, and also reduced by imatinib, a tyrosine kinase inhibitor (non-selective c-kit inhibitor). Immunolabelling revealed that stromal ICC-LC, a population distinct from the spindle-shaped ICC-LC characterized in this thesis, expressed ANO1. The

authors proposed that ANO1 activity in stromal ICC-LC contributes to bacterial expulsion by modulating USMC activity through gap junctions, and thereby LTCC activation (Ambrogi *et al.,* 2025).

In conclusion, spindle-shaped ICC-LC were distributed throughout mouse USM but did not form networks. They were spontaneously active due to Ca^{2+} release from intracellular stores, sustained by Orai-mediated SOCE (Fig. 3.14), and displayed asynchronous activity with no temporal coordination. ICC-LC responded to exogenous α1-adrenoreceptor agonists but not to endogenous neurotransmitters, unlike USMC. Unlike gut ICC, urethral ICC-LC lacked ANO1 expression, which was instead present in surrounding USM bundles. The following chapter examines ANO1 localization in isolated USMC and its functional role in urethral contractions using the selective pharmacological agent (Ani9, (Seo *et al.,* 2016)).

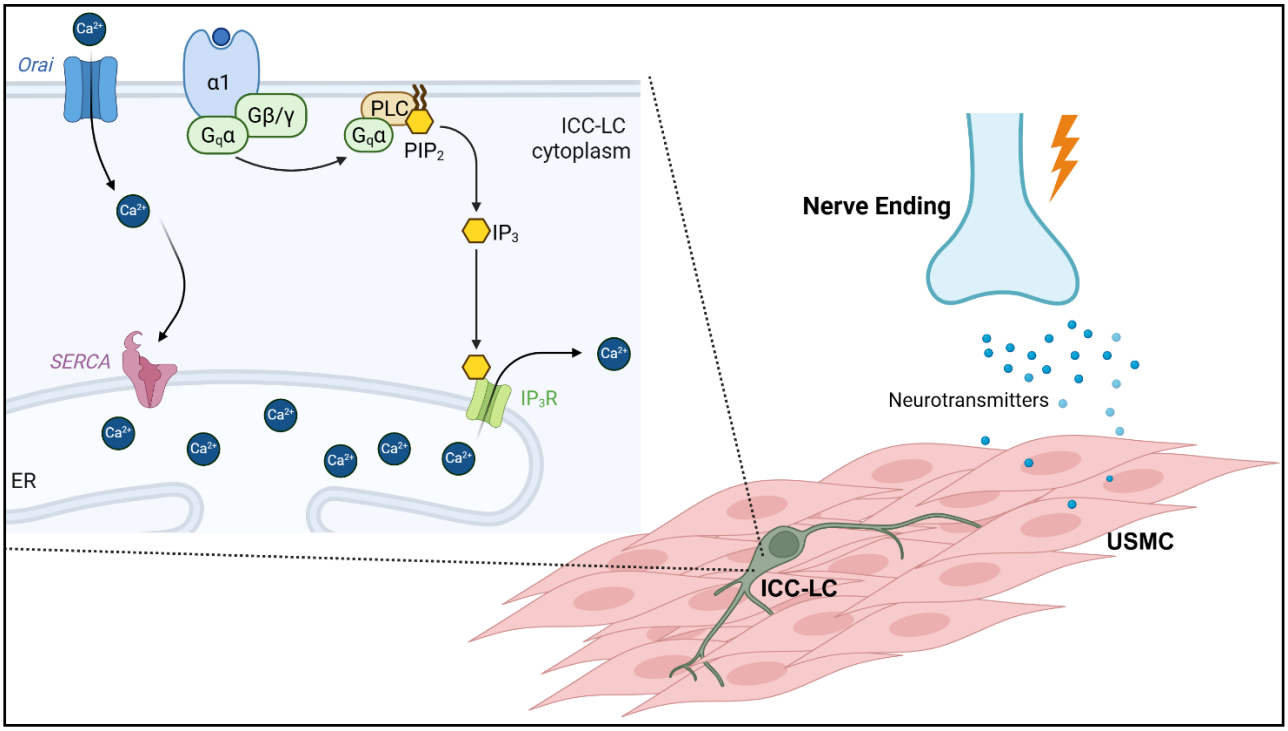

Fig 3.14: ICC-LC in mouse urethra are not functionally innervated and their spontaneous Ca^{2+} activity depends predominantly on Orai-mediated SOCE and ER Ca^{2+} release. Spontaneous Ca^{2+} activity in ICC-LC enhance in response to adrenergic-agonist but were unaffected by NO donor. In addition, ICC-LC do not respond to nerve stimulation, unlike USMC.

4. Do ANO1 channels contribute to murine urethral smooth muscle contractility?

4.1 Introduction

ANO1 channels modulate SMC contractions in various SM tissues such as corpus cavernosum (Hannigan *et al.,* 2017; Lim *et al.,* 2022), epididymis (Kudo *et al.,* 2024), lymphatics (Zawieja *et al.,* 2019), renal pelvis (Grainger *et al.,* 2022), cerebral arteries (Bulley *et al.,* 2012), stomach (Kito, 2011), LES (Drumm *et al.,* 2022), colon (Drumm *et al.,* 2019a; 2019b), IAS (Cobine *et al.,* 2017) and small intestine (Hwang *et al.,* 2019). Even before the specific identification of ANO1, evidence suggested CaCC played a vital role in USM contractility of certain species.

Rabbit and guinea pig USM tissues exhibit SW and STD, induced by activation of CaCC due to Ca^{2+} release from intracellular stores (Hashitani *et al.,* 1996; Hashitani & Edwards, 1999). Similar events to STD were also found in sheep USMC using perforated patch clamp recording, which fired action potentials superimposed on the plateau (Cotton *et al.,* 1997). STD in sheep urethra were unaffected by nifedipine, but reduced in amplitude by niflumic acid (non-selective CaCC blocker), suggesting they were due to Cl^- currents. In contrast, action potentials were blocked by nifedipine, suggesting they were due to LTCC (Cotton *et al.,* 1997). Sergeant *et. al* (2001) found STIC in ≥10% of isolated sheep USMC, which were inhibited by 100 µM niflumic acid and 1 µM anthracene-9-carboxylic acid (Cl^- transport inhibitor), Ca^{2+} free solution, 10 mM caffeine and 30 µM ryanodine (Sergeant *et al.,* 2001b). Furthermore, they observed amplitude and frequency of STIC were unaffected by nifedipine.

Sergeant *et al.,* (2000) discovered ICC-LC in suspensions of isolated rabbit USM tissues. In voltage clamp experiments, a stepping protocol was followed in which ICC-LC were held at -60 mV and stepped from -80 to +50 mV in 10 mV steps of 500 ms duration, resulting in generation of inward currents. Steps to -10 mV evoked a fast inward LTCC current which peaked within 50 ms, followed by a slower inward Cl^- current. The fast LTCC current peaked at 0 mV and reversed around +40 mV, while the slow Cl^- current reversed near 0 mV (calculated E_{Cl}), generating large outward currents at more positive potentials. Upon returning to -80 mV, large, slowly decaying tail currents were observed (Sergeant *et al.,* 2000). In contrast, slow inward currents and tail currents were not observed in USMC under identical conditions. These slow inward, outward and tail currents in ICC-LC were sensitive to niflumic acid (Sergeant

et al., 2000). Moreover, niflumic acid reduced EFS-evoked (10 Hz) contractions in rabbit USM (Sergeant *et al.,* 2002). Further studies in rabbit ICC-LC found STIC were generated under voltage clamp at -60 mV, while STD were generated under current clamp, and were sensitive to niflumic acid, CPA, ryanodine and 2-APB, suggesting that Ca^{2+} release from intracellular store were required to activate CaCC (Sergeant *et al.,* 2001b; Sergeant *et al.,* 2002; Sergeant *et al.,* 2006b; Sergeant *et al.,* 2006c).

In 2008, three independent research groups showed ANO1 was an intrinsic constituent of CaCCs (Caputo *et al.,* 2008; Schroeder *et al.,* 2008; Yang *et al.,* 2008). Later, ANO1 was found to be a selective marker for ICC in gut (Espinosa *et al.,* 2008; Gomez-Pinilla *et al.,* 2009; Hwang *et al.,* 2009). Hwang (2009) found that inhibiting CaCC with niflumic acid reduced the frequency of SWs in gastric antrum of mouse and monkey (Hwang *et al.,* 2009). TMEM16A$^{-/-}$ mice failed to develop SWs in spite of the presence of normal ICC networks (Hwang *et al.,* 2009). Moreover, knock down of ANO1 expression specifically in ICC (Kit$^{CreERT2/+}$; Ano1tm2jrr$^{/+}$) with Cre/LoxP technology severely altered gastric motor activity, including interrupted SWs, aberrant phasic contractions, and delayed gastric emptying (Hwang *et al.,* 2019).

Sancho *et al.,* (2012) reported ANO1 expression on USMC but not on vimentin^{+} urethral ICC-LC of mouse, sheep and rat (Sancho *et al.,* 2012). In contrast, Fedigan *et al.,* (2017) found ANO1 transcript was highly expressed in rabbit urethral ICC-LC and not in USMC. Moreover, in rabbit USMC, CaCC currents were not detected (Sergeant *et al.,* 2000; Fedigan *et al.,* 2017). STD and STIC recorded from rabbit urethral ICC-LC were inhibited by ANO1 inhibitors CaCCinh-A01 and T16Ainh-A01 (Fedigan *et al.,* 2017). CACCinh-A01 and T16Ainh-A01 also reduced myogenic tone and EFS evoked contractions of rabbit USM (Fedigan *et al.,* 2017). In contrast, in pig urethra, ANO1 inhibitors including Ani9 and CaCCinh-A01 had no effects on tone or EFS induced contractions (Rembetski *et al.,* 2020). These findings indicate a potential species difference in expression and function of ANO1 in USM (Drumm *et al.,* 2021).

Chen *et al.,* (2022) observed a downregulation of ANO1 expression in female mice with hypertriglyceridemia, resulting in decreased urethral tone (Chen *et al.,* 2022). Another study by the same group reported ANO1 expression was two-fold higher in USMC of female mice and humans compared to males, therefore contributing to

reported higher basal tone in females. Furthermore, they observed activation of ANO1 by EACT triggered a weak spontaneous tone in male USM, and patch clamp recordings revealed ANO1 activation induced larger Cl^- currents in female as compared to male (Chen *et al.,* 2020). Feng et al. (2019) reported impaired urethral tone in ANO1 SM knockout mice ($TMEM16A^{SMKO}$). In patch-clamp recording, caffeine evoked currents in WT USMC but not in knockouts. Caffeine-induced contractions were reduced by nifedipine in a dose-dependent manner, and abolished when combined with T16Ainh-01. In both human and WT mouse, T16Ainh-01, nifedipine, and ryanodine each abolished spontaneous tone. Together, these studies suggest that RyR-dependent Ca^{2+} release activates ANO1, causing depolarisation and subsequent LTCC-mediated Ca^{2+} entry to support urethral tone.

From the literature described, there are evidential species differences in cellular ANO1 expression and function in USM. In many studies, evidence for ANO1 involvement in urethral activity has relied on what are now known non-specific pharmacological drugs that inhibits VGCC or activate/inhibit SR Ca^{2+} release (Boedtkjer *et al.,* 2015; Dwivedi *et al.,* 2023; Genovese *et al.,* 2023). These include niflumic acid, benzbromarone, MONNA, CACCinh-A01 and T16Ainh-A01 (Ottolia & Toro, 1994; Wang *et al.,* 1997; Greenwood & Leblanc, 2007; Bradley *et al.,* 2014; Fedigan *et al.,* 2017; Dwivedi *et al.,* 2023). In the previous chapter, I illustrated how Kit-GCaMP6f mice, allowed robust identification of ICC-LC in intact tissues. I found ANO1 was not expressed on ICC-LC nor $PDGFR\alpha^+$ cells in mouse urethra but labelled underlying USMC bundles.

In the next series of experiments, I will examine expression of ANO1 in isolated USMC. To investigate functional roles of ANO1 in mouse urethra, I employed a specific and potent ANO1 antagonist (Ani9) along with traditional ANO1 antagonists such as CACCinh-A01 and niflumic acid (Seo *et al.,* 2016; Dwivedi *et al.,* 2023), and examined effects on agonist and EFS-evoked contractions of USM tissues. A previous study reported significant effect of LTCC inhibition at lower concentrations of agonist in airway SMC than at supramaximal doses (Dwivedi *et al.,* 2023), likely due to large SR Ca^{2+} release masking LTCC effects. Therefore, I tested effects of Ani9 at a range of agonist concentrations to examine its effect on physiologically relevant concentrations of agonist and also on supramaximal doses. In addition, I also tested the effects of Ani9 at various frequencies of EFS.

* Data presented in Fig. 4.1, 4.2, 4.4-4.8, 4.11, 4.12 was published in the following peer-reviewed article prior to submission of this thesis: Gupta N, Baker SA, Sanders KM, Rabab KE, Thean DK, Alkawadri T, Griffin CS, Sergeant GP, Hollywood MA, Thornbury KD, Drumm BT (2025). ANO1 channels are expressed in mouse urethral smooth muscle but do not contribute to agonist or neurally evoked contractions. *Sci Rep*. 2025 May 19; 15(1):17365. doi: 10.1038/s41598-025-00953-z. PMID: 40389459; PMCID: PMC12089485.

* Experiments presented in Fig. 4.5A, 4.11B, 4.12A&B were performed jointly with Denzel Thean in the Smooth Muscle Research Centre, DkIT. The analyses of the data and preparation of the figures were carried out independently by the author of this thesis.

4.2 Results

4.2.1 ANO1 expression in urethral tissues

I first evaluated expression of *Ano1* gene and ANO1 protein in male vs female mouse urethra. In qPCR, fold change expression of *Ano1* transcript relative to colon (normalized to housekeeping gene *β-actin*) in male vs female USM was 2.9 ± 0.5 (n=3, P=0.03; Fig. 4.1) and 2.9 ± 0.7 (n=3, P=0.03; Fig. 4.1) respectively. There was no statistical difference in *ANO1* expression between male vs females (P>0.99; Fig. 4.1).

Data from the previous chapter suggested ANO1 was expressed in murine USMC, and not ICC-LC or PDGFRα^+ cells (Fig. 3.13). To confirm this, immunocytochemical staining was performed on enzymatically isolated male and female USMC with SM α-actin and ANO1 antibodies. I found USMC from both male and female tissues were readily labelled with antibodies against α-actin and ANO1 (Fig. 4.2A&B, n=3). Negative controls using bladder SMC (lacking ANO1 expression) and positive controls using corpus cavernosum SMC (known to express ANO1) were included to validate immunocytochemistry antibodies, as previously described (Lim *et al.,* 2022). Corpus cavernosum SMC showed clear ANO1 expression colocalized with α-actin (Fig 4.2C, n=3), whereas ANO1 expression was not detected in bladder SMC (Fig. 4.2D, n=3).

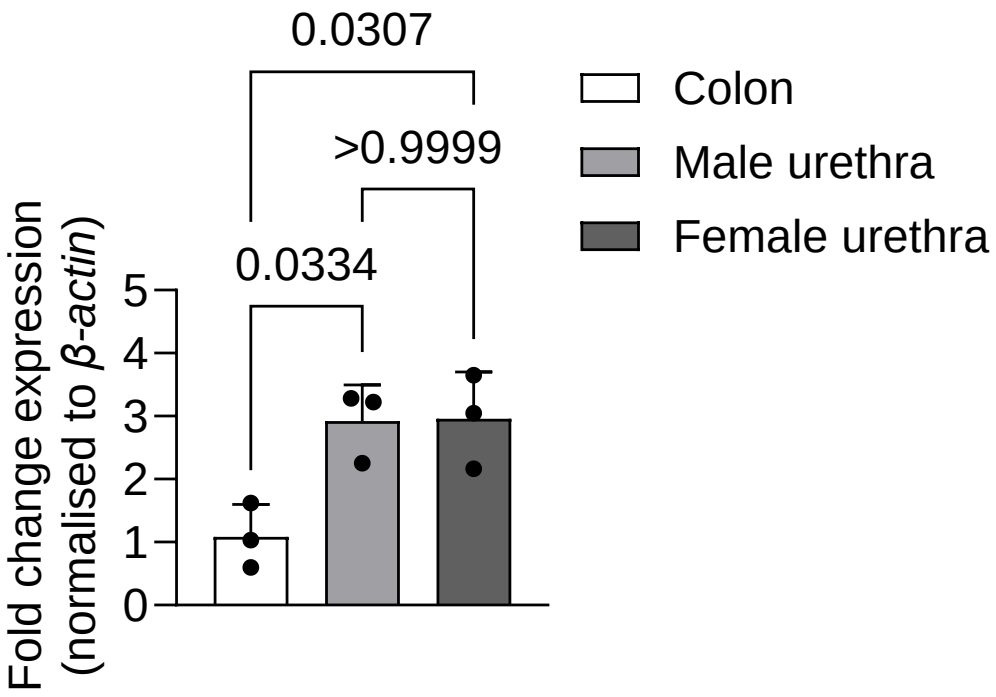

Fig 4.1: Relative expression of *Ano1* in WT male, female urethra compared to proximal colon through qPCR. Real-time PCR analyses showing gene expression of *Ano1* normalized to *β-actin* gene expression (endogenous control) in male, female urethra and proximal colon. Fold change was calculated by $2^{-\Delta\Delta CT}$. Data represents comparison of *Ano1* fold change expression relative to colon (n=3) and normalized to *β-actin* in male (n=3), female urethra (n=3) (One-way ANOVA, Tukey's test).

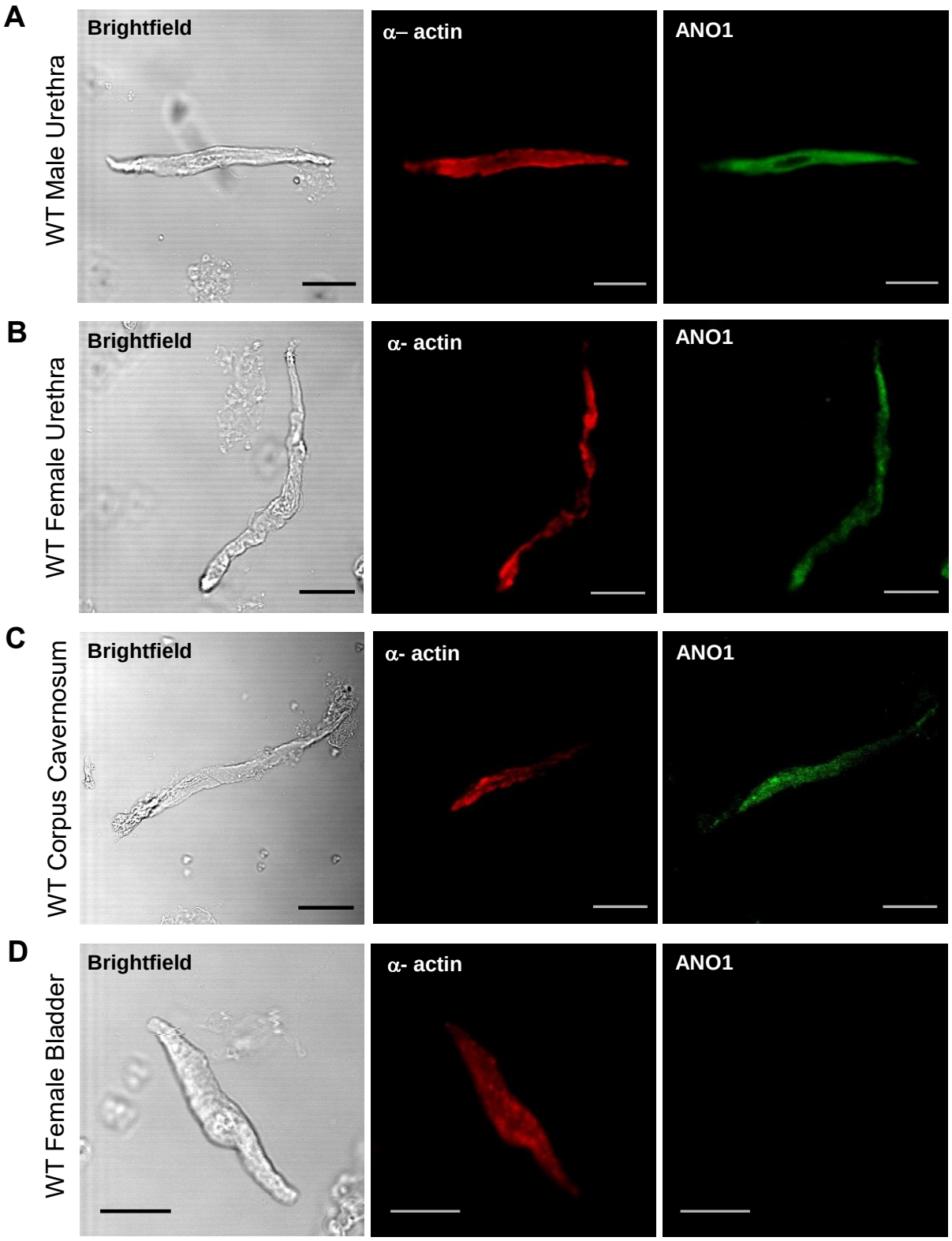

Fig 4.2: ANO1 is expressed in urethral smooth muscle cells. A Representative images of urethral SMC (USMC) captured in brightfield and at different wavelengths (488 nm and 555 nm) to show double immuno-labelling for α-actin (red) and ANO1 (green) from WT male urethra (n=3), **B** female urethra (n=3), **C** corpus cavernosum (n=3), and **D** bladder (n=3). Scale bar: 20 µm in all panels.

4.2.2 Effects of ANO1 inhibition on agonist evoked urethral contractions

I firstly conducted isometric tension recordings of urethral rings of male WT mice to investigate effects of ANO1 inhibition on contractile responses. Initially, I precontracted tissues with an α1-adrenoreceptor (PE) agonist at various concentrations. Specifically, I performed PE concentration-dependent response curves ranging from 30 nM to 30 µM PE (n=6; Fig 4.3A). At concentrations of 100 nM PE, sustained contractions, averaging 34.2 ± 29.9 mN.s (AUC) were observed, which were largely sustained over 10 mins. As the concentration of PE increased beyond 300 nM, evoked contractions developed a biphasic nature, consisting of an initial peak, followed by partial decline and sustained contraction (Fig. 4.3A). In many instances, amplitude of the initial peak and rate of the subsequent decline increased as PE concentration increased. These characteristics could be somewhat variable between tissues, with some responses consisting mostly of sustained contractions, without obvious initial peaks. To analyse these traces and encompass the entire contraction regardless of variability, I quantified PE responses as area under the curve (AUC). I found increased PE concentrations reliably increased AUC in a dose-dependent manner. For example, at PE concentrations of 300 nM, average AUC was 101.1 ± 63.4 mN.s and at 1 µM PE, this was increased to 255.133 ± 143.3 mN.s (Fig 4.3C). Across 6 experiments, the EC_{50} value for PE was 1.3 µM (n=6; Fig. 4.3C). To verify that such responses were reproducible, the PE application were repeated on the same tissue after 4 x 15 min washes (Fig. 4.3B). When contractions of both responses curves were compared, there was no statistical difference in AUC (P>0.7 at all concentrations) or EC_{50} values (P=0.6, n=6; Fig. 4.3C).

I next tested effects of the potent and selective ANO1 inhibitor Ani9 (Seo *et al.,* 2016) on PE-induced contractions of male USM. I performed PE response curves on USM as described above, followed by application of 3 µM Ani9 for 30 minutes, and then repeated the PE applications in the continued presence of Ani9 (Fig. 4.4A&B). Ani9 did not impact the EC_{50} value (P=0.6) or AUC (P>0.7) of PE responses at any concentration (n=6; Fig. 4.4D). I further examined effects of Ani9 on basal tone (Fig and found no significant change (n=6, P=0.9; Fig 4.4C&E). These findings suggest that ANO1 channels do not modulate agonist-induced responses in male USM.

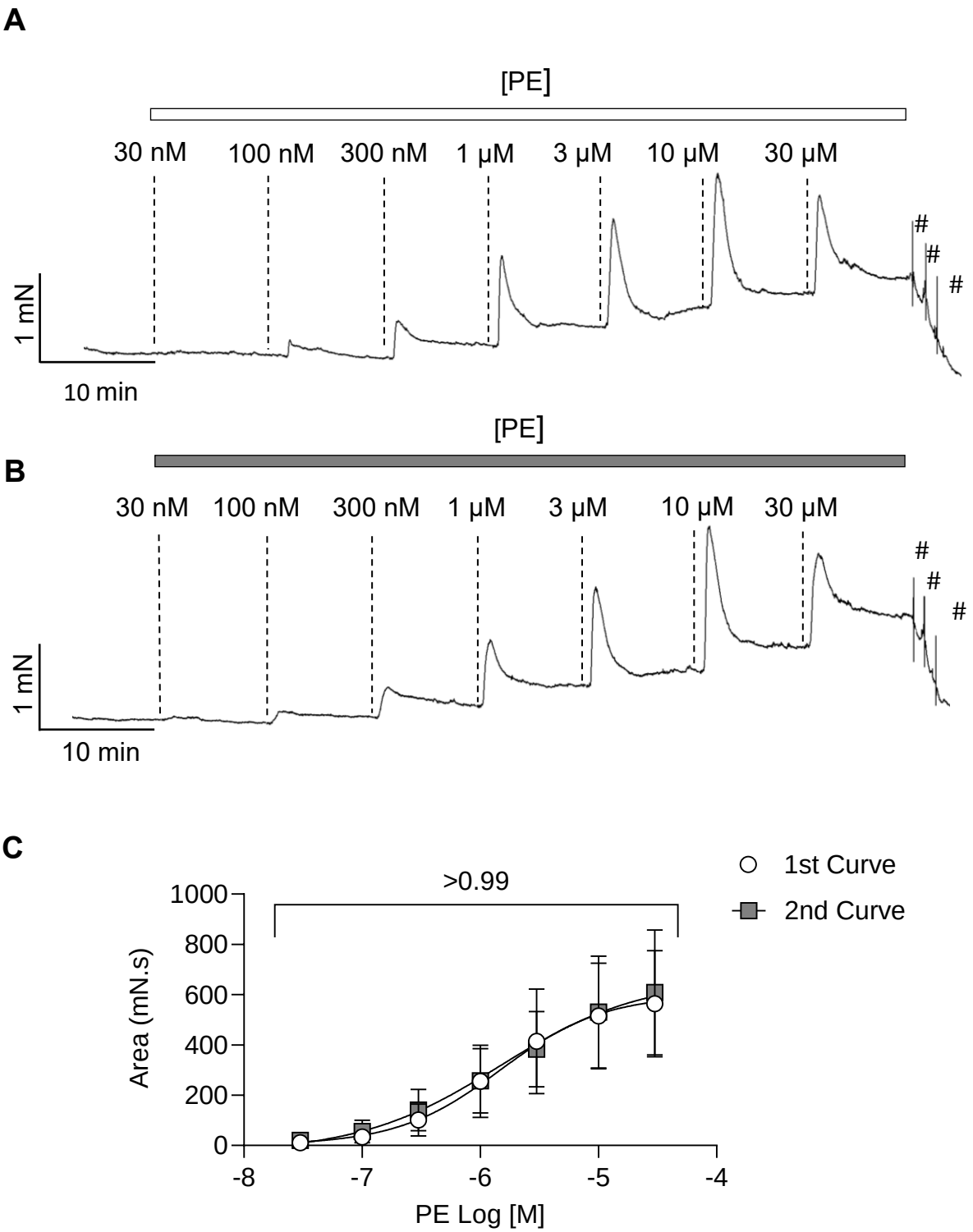

Fig 4.3: PE concentration-dependent curves were reproducible in male mouse USM. A Representative contractile data showing contractions of intact tissue of male mice urethra induced by increasing concentrations of PE (30 nM - 30 µM). **B** Reproducible contractile responses elicited by PE (30 nM - 30 µM) in the same male USM tissues after washing 4 times at an interval of 15 mins for an hour. **C** Summary data (n=6, Two-way ANOVA, Bonferroni's test). (# represents washing)

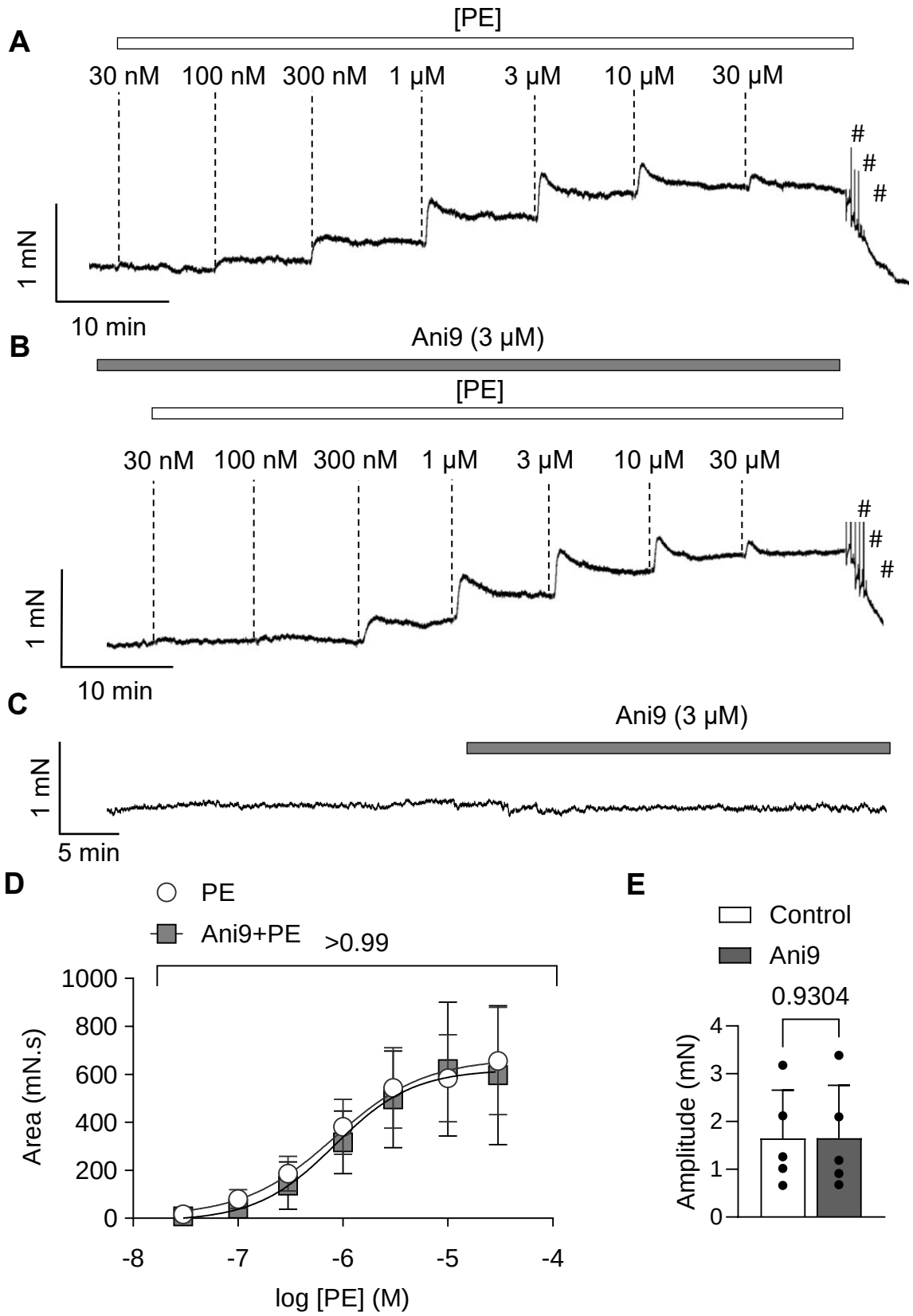

Fig 4.4: ANO1 inhibitor Ani9 does not affect PE responses nor basal tone in male USM. A-B Representative data showing PE dose dependent contractile responses of males USM (30 nM - 30 μM) in control (A) and in the presence of Ani9 (3 μM). **C** Representative trace of Ani9 (3 μM) effect on male USM basal tone. **D** Summary effect of Ani9 on PE dose responses curves in male USM (n=6, Two-way ANOVA, Bonferroni's post-hoc test) **E** Summary effect of Ani9 on basal tone in male USM (n=6, paired t-test). (# represents washing).

4.2.3 Effects of ANO1 inhibition on EFS evoked urethral contractions

I next sought to investigate effects of Ani9 on EFS (1, 2, 5, 10, and 20 Hz) evoked responses of male USM. EFS-evoked contractions were abolished by the fast Na^+ channel blocker tetrodotoxin (TTX, 1 μM; Fig. 4.5A&C; n=6), confirming EFS evoked contractions were neurogenic. EFS-evoked contractions were also reproducible when tested after a 30-min interval (n=6, P>0.1 at all frequencies; data not shown). To test effects of ANO1 inhibition on neurogenic responses, EFS was first applied under control conditions, followed by a 30-min incubation in Ani9 (3 μM), after which the EFS protocol was repeated (n=6; Fig 4.5B). Ani9 did not affect EFS-induced contractions at any frequency in male USM (n=6, P>0.1; Fig 4.5B&D), suggesting that ANO1 channel activity do not influence neurogenic responses.

4.2.4 Effects of ANO1 inhibition on USM Ca^{2+} signals

The underlying cellular behaviour that generates urethral tone is firing of asynchronous intracellular Ca^{2+} events in USMC (Drumm *et al.,* 2018), which are increased in frequency by PE (Drumm *et al.,* 2018) or EFS as showed in previous Chapter. I next tested effects of Ani9 on these USMC Ca^{2+} events. USMC recorded from Acta2-GCaMP8.1 mice *in situ* were spontaneously active and exhibited asynchronous Ca^{2+} activity throughout the muscle bundle, as previously described in male USM tissues imaged with GCaMP3 (Drumm *et al.,* 2018). Ani9 (3 μM) failed to significantly change this Ca^{2+} activity of either male (n=5, c=10; Fig. 4.6A&B) or female USMC (n=6, c=15; Fig. 4.6C&D). Ani9 (3 μM) did not affect frequency (P=0.7), amplitude (P=0.9), duration (P=0.7), or spread (P=0.7) of male USMC Ca^{2+} events (n=5, c=10; Fig. 4.6B). Similarly, in female USMC, there was no significant change in frequency (P=0.1), amplitude (P=0.9), duration (P=0.1) or spread (P=0.9, n=6, c=15; Fig. 4.6D) after incubation in Ani9 (3 μM).

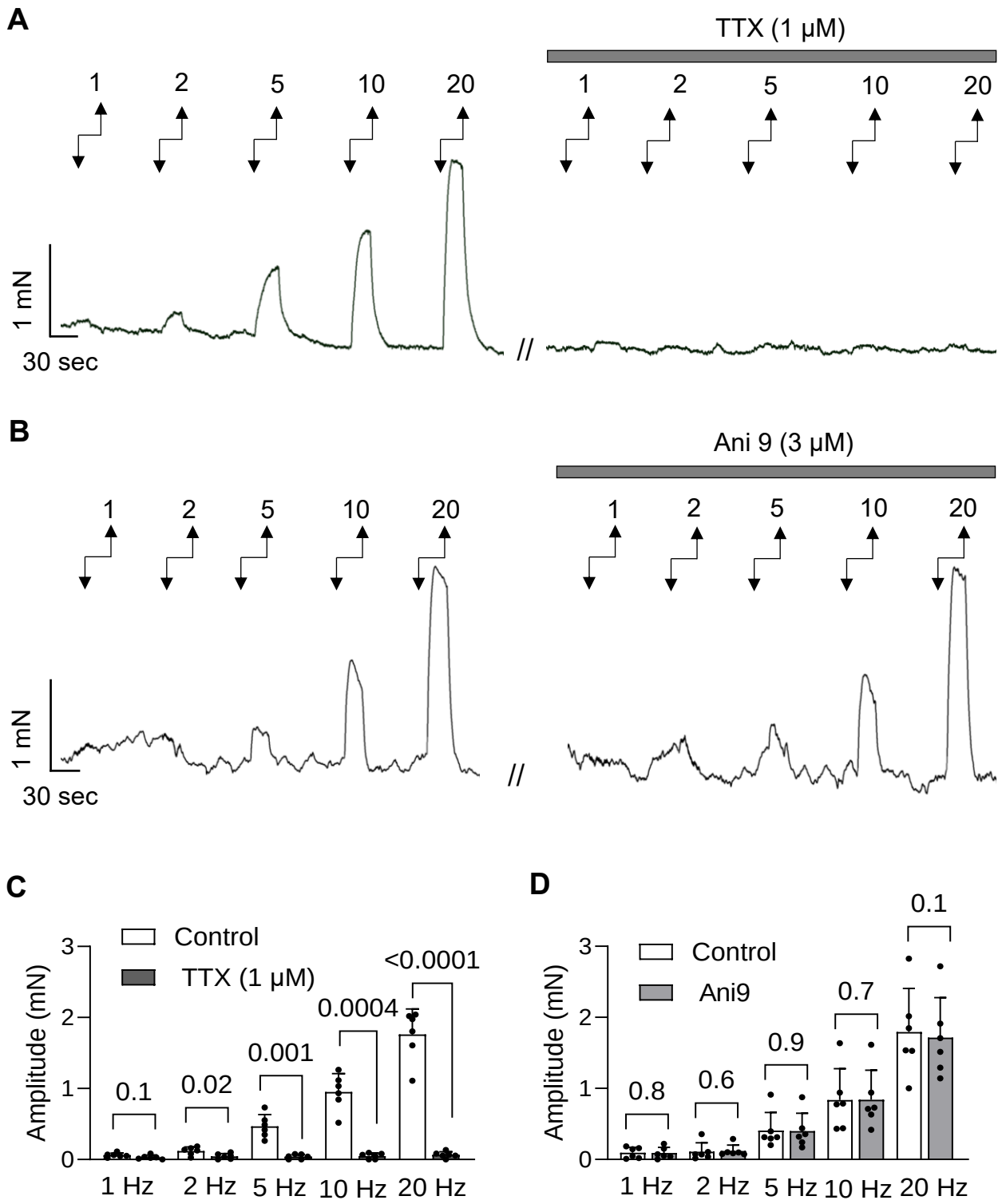

Fig 4.5: ANO1 channels inhibition does not affect the EFS-evoked contractions of male mouse USM. EFS evokes contractions of male USM, which are increased in amplitude as EFS frequency is increased. **A** These responses were abolished by tetrodotoxin (TTX, 1μM), whereas **B** inhibiting ANO1 channels with application of Ani9 (3 μM) had no effect on amplitude of EFS-evoked contractions of USM. Summary data showing **C** effects of TTX (n=6, Paired t-test), and **D** Ani9 on EFS-evoked contractions in USM (n=6, Paired t-test). Double-headed arrow represents EFS frequencies (Hz).

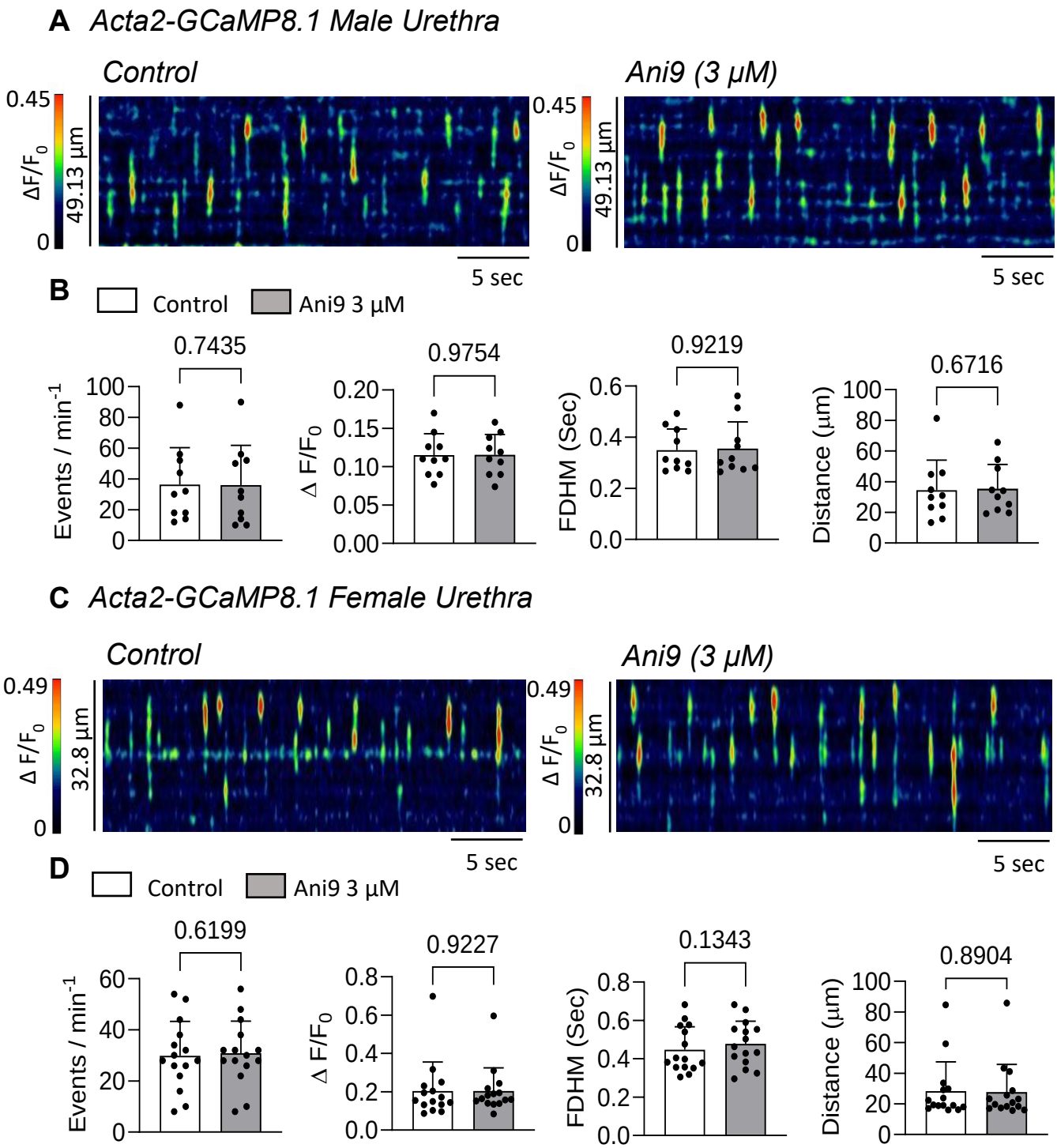

Fig 4.6: Spontaneous USMC Ca^{2+} events do not depend on ANO1 channels. A Spatiotemporal maps of Ca^{2+} events in male USMC recorded *in situ* from an Acta2-GCaMP8.1 mouse during control conditions and after incubation with 3 µM Ani9. **B** Summary effects of Ani9 on male USMC Ca^{2+} event frequency, amplitude, duration and spatial spread (n=5, c=10, paired t-test). **C** STMs of Ca^{2+} events in female USMC recorded *in situ* from an Acta2-GCaMP8.1 mouse during control conditions and after incubation with 3 µM Ani9. **D** Summary effects of Ani9 on female USMC Ca^{2+} event frequency, amplitude, duration and spatial spread (n=6, c=15, paired t-test).

4.2.5 Effects of ANO1 inhibition on colonic contractions & Ca^{2+} signals

Given the lack of Ani9 effects on USM, I evaluated the efficacy of Ani9 on contractions of mouse proximal colon, as ANO1 channels (expressed in ICC) play a major role in colonic motility (Drumm *et al.,* 2019a; 2019b; Koh *et al.,* 2022). Under control conditions, proximal colon preparations exhibited rhythmic phasic contractions during isometric tension recording. Ani9 (3 μM) significantly attenuated colonic phasic contractions (n=6; Fig. 4.7A), evidenced by a marked reduction in amplitude from 11.6 ± 7.2 to 4.6 ± 3.3 mN (n=6, P=0.02; Fig 4.7B), and frequency from 3.4 ± 1.6 to 1.7 ± 1.1 min^{-1} (n=6, P=0.004; Fig 4.7C). These experiments suggested Ani9 was effective in inhibiting contractions in organ bath experiments with other tissues. I also examined effects of Ani9 on Ca^{2+} signals generated in proximal colon from Acta2-GCaMP8.1 mice. In these recordings (40x objective), strips of circular orientated proximal colon SMC generated regular propagating Ca^{2+} waves or Ca^{2+} flashes that lasted up to 5 sec, and propagated rapidly across the tissue ~ 5 times per minute. These colonic Ca^{2+} signals induced massive contractions of colonic muscles, making analysis of individual cells impossible. Instead, Ca^{2+} signals across the entire FOV in a 30 sec recording were plotted against time to generate plots of Ca^{2+} activity from which amplitude, frequency and duration of Ca^{2+} waves across the whole FOV were quantified. Plots of this activity in Fig. 4.7D (summated Ca^{2+} signal from entire 30 sec recording) shows reduced Ca^{2+} activity in the presence of Ani9 compared to control (Fig. 4.7D-E, n=7). Ani9 significantly reduced Ca^{2+} event frequency from 5.4 ± 2.2 to 2.8 ± 1.9 min^{-1} (P= 0.01), amplitude from 1 ± 0.8 to 0.3 ± 0.2 $\Delta F/F_0$ (P=0.04) and duration from 4.9 ± 2.8 to 2.5 ± 1.9 sec (P=0.03).

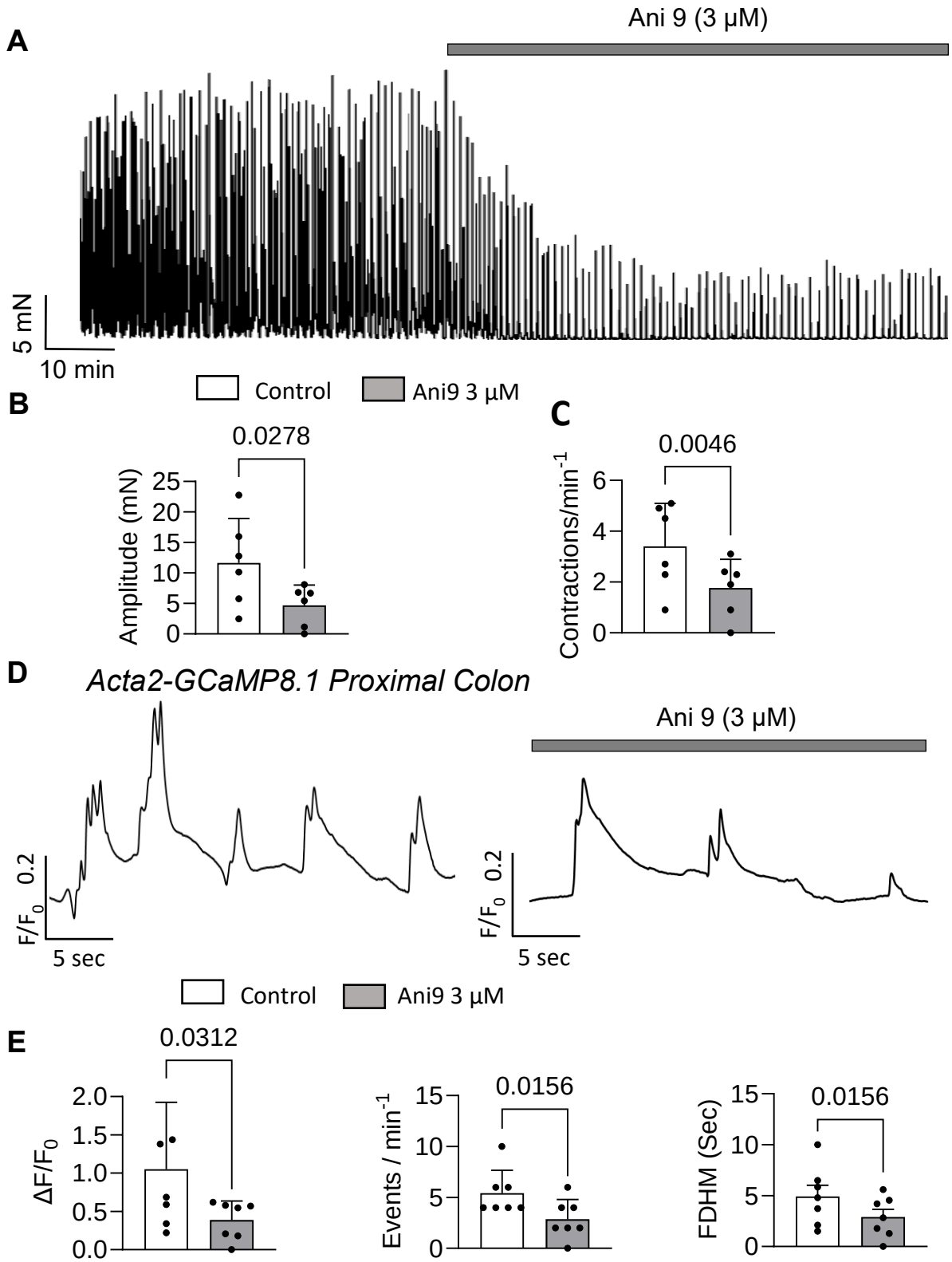

Fig 4.7: Ani9 inhibits phasic contractions and basal Ca^{2+} activity of mouse proximal colon. A Representative contractile data from mouse proximal colon in the absence and presence of Ani9 (3 µM). **B** Summary effects of Ani9 on amplitude and frequency of phasic contractions (n=6, paired t test). **D** Plot profile of spontaneous Ca^{2+} signals recorded from an entire field of view (40x objective) of proximal colon from an Acta2-GCaMP8.1 mouse in the absence and presence of 3 µM Ani9. **E** Summary of Ani9 effects on amplitude, frequency and duration of Ca^{2+} events in proximal colon (n=7, paired t-test).

4.2.6 PE & EFS-evoked contractions are abolished by IP_3R antagonist

To demonstrate if USM contractions evoked by PE or EFS could be reduced by appropriate means, I tested effects of the IP_3R antagonist 2-APB (2-aminoethoxydiphenyl borate, non-selective IP_3 inhibitor), which should reduce contractions of USM induced by exogenous application of PE or release of NA following stimulation of intramural nerves. 2-APB (100 μM) effectively reduced PE-evoked contractions at all concentrations tested (n=6; Fig. 4.8A,B&C). For example, at 300 nM PE, contractile AUC was reduced from 335.8 ± 225.8 to 4.68 ± 10.2 mN.s (P= 0.0005; Fig. 4.8C, n=6) and at 30 μM PE, AUC of evoked responses were reduced from 1128.3 ± 424.8 to 83.7 ± 142 mN.s (P<0.0001; Fig 4.8 C, n=6). Similarly, 2-APB abolished EFS-evoked contractions at all stimulation frequencies (n=6; Fig.4.8A&B). These controls established agonist and EFS responses could be inhibited by pharmacological agents.

4.2.7 Arginine vasopressin but not phenylephrine contracts female urethra

To investigate effect of ANO1 inhibition on female USM, I looked for a suitable agonist as female USM did not contract in response to PE (n=6), unlike males (n=6; Fig. 4.9A,B&D). To check the tissue viability, high KCl (60 mM) was applied before testing PE. High K^+ induces depolarisation in membrane potential, and directly activates LTCC-mediated Ca^{2+} entry, which generates SM contraction (Ishida *et al.,* 2017). Both male and female tissues responded to depolarisation-induced contractions. However, the magnitude of these responses differed markedly between sexes. Male USM generated approximately double the force observed in females, with an initial amplitude of 1.6 ± 0.6 mN (n=9) compared with 0.5 ± 0.1 mN in female tissues (n=11), see Fig 4.9A&B. This suggest that female USM express fewer functional LTCC than male USM (studied more in next Chapter). Our findings align with earlier work showing that high KCl produces larger contractions in male USM, while PE or epinephrine elicit little or no response in female USM in both mice and marmosets (Alexandre *et al.,* 2017). That study also reported higher expression of α1-adrenoceptors and tyrosine hydroxylase in males, with minimal expression in females, which explained why female does not respond to α1-adrenergic agonist, PE.

Previous studies demonstrated that PE majorly activates α_1-adrenergic agonist, however when α_1-adrenergic agonist were blocked PE acted on β2-adrenergic receptors in human brachial arteries (Torp *et al.,* 2001). Similarly, another previous study reported that prior incubation with propranolol (β-adrenergic receptor inhibitor) induced PE-evoked contractions in murine female USM (Hsieh *et al.,* 2023). In our experiment, incubation with propranolol (1 hour) enabled PE to induce contractions in female USM but the response were markedly weak and occurred at higher concentrations of PE (3-30 µM, n=6; Fig 4.9C&D). This could be due to lower expression of α1-adrenergic receptors in female USM (Alexandre *et al.,* 2017). Therefore, to assess the effect of Ani9 in females, I needed a more reliable G_q-coupled agonist capable of producing robust contractions in female USM.

Therefore, I tested effects Ani9 on female USM on responses evoked by arginine vasopressin (AVP, antidiuretic hormone). AVP is a vasopressin 1_A receptors ($V1_AR$) agonist, which activates the G_q signalling pathway, thereby triggering IP_3Rs and SR Ca^{2+} release similar to PE, (Li *et al.,* 2001). I initially performed dose-response response curves with AVP (n=6, Fig 4.10A&C), which led to a dose-dependent contraction of female USM. The AVP-evoked responses in females appeared different from PE-induced responses in male. While higher concentrations of PE (≥300 nM) elicited an initial peak followed by a partial decline and a sustained contraction, AVP did not follow a consistent or structured pattern (Fig 4.10A). For example, at 1 nM AVP, a brief initial increase was observed, followed by a decline and then slightly elevated contraction. At higher concentrations (10-100 nM), AVP continued to evoke an initial peak followed by an elevated plateaued contraction, but without the sustained or clearly biphasic profile seen with PE. In contrast to PE-evoked responses in males, I found responses elicited by AVP were not reproducible. In order to examine effects of ANO1 inhibition on AVP responses, we were therefore required to take a different approach. I applied a single dose of AVP to female tissues (10 nM, EC_{50}), which immediately contracted the tissue (Fig 4.10B), and this contraction reached its maximum (897.6 ± 237.2 mN.s, n=6, Fig. 4.10D) in 10-20 min. 10 nM AVP responses were sustained even after 60 mins exposure. For example, as shown in in Fig. 4.10D, after 30 mins the average contraction AUC was 897.6 ± 237.2 mN.s and after 60 mins this had not significantly changed (856.6 ± 270 mN.s, P>0.2, Fig. 4.10D; n=6).

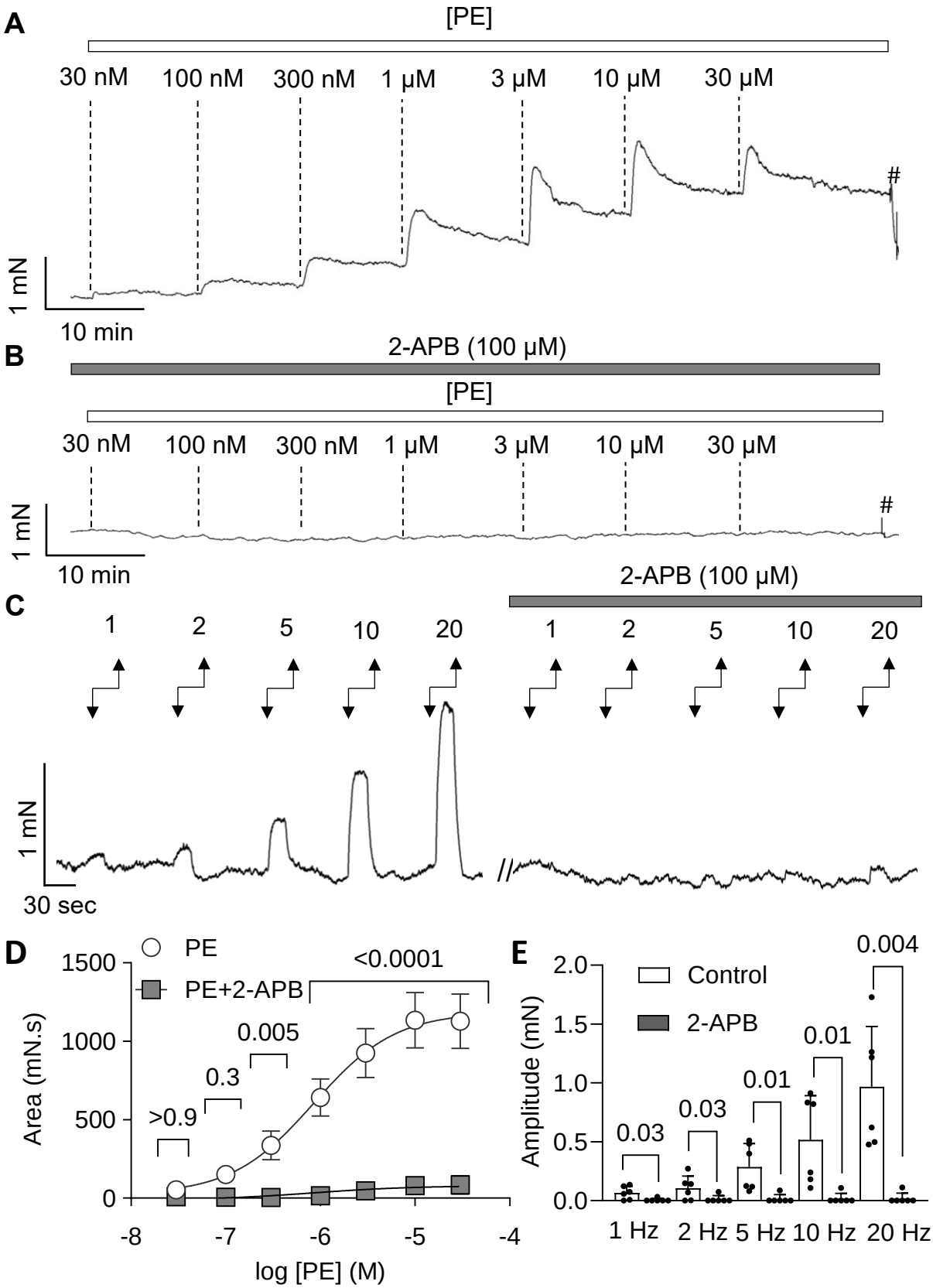

Fig. 4.8. IP_3R blockade with 2-APB (100 μM) abolished PE-evoked concentration-dependent contractions and EFS-induced contractions in male USM. (**A-B**) Representative trace of PE responses (30 nM-30 μM) under control conditions and in the presence of 2-APB. **C** Representative EFS traces demonstrating effect of 2-APB. Summary effects of 2-APB on PE- (n=6, two-way ANOVA; Bonferroni's test) and EFS-induced contractions (n=6; Paired t-test). Double-headed arrow represents EFS frequencies (Hz).

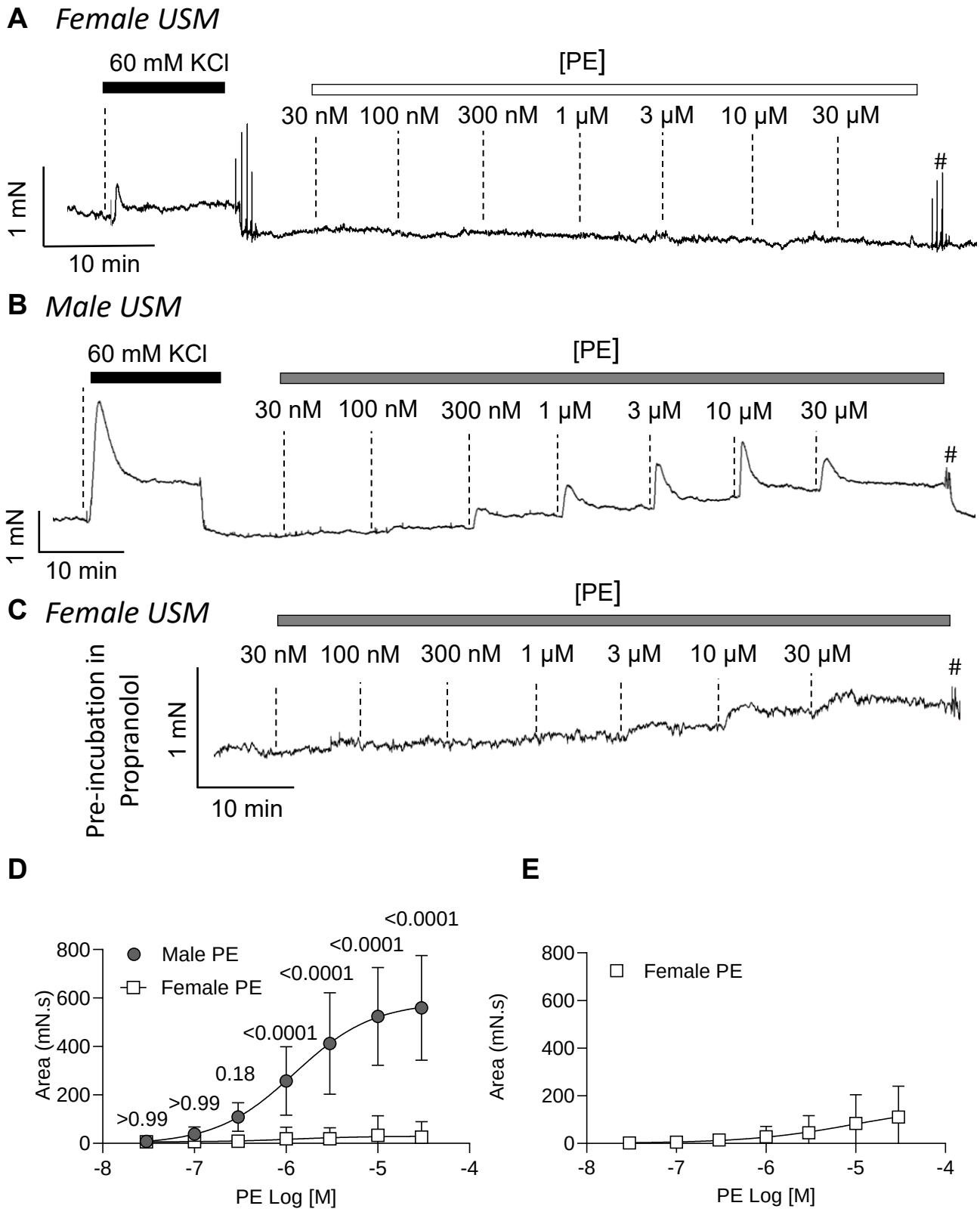

Fig. 4.9: The adrenergic agonist PE does not affect female USM unless β-adrenergic receptors are blocked, whereas it induces contraction in male USM. Representative contractile data showing responses induced by increasing PE concentrations (30 nM - 30 μM) **A** on female, **B** male USM, **C** and on female USM pre-incubated for 1 hour with propranolol. **D** Summary of PE effects on male and female USM (n=6, Two-way ANOVA, Bonferroni's test), **& E** effects of PE on propranolol pre-incubated female USM, measured as contraction area (n=6, Two-way ANOVA). (#represent washing). High KCl (60 mM) was used initially in panel A & B to check tissue viability.

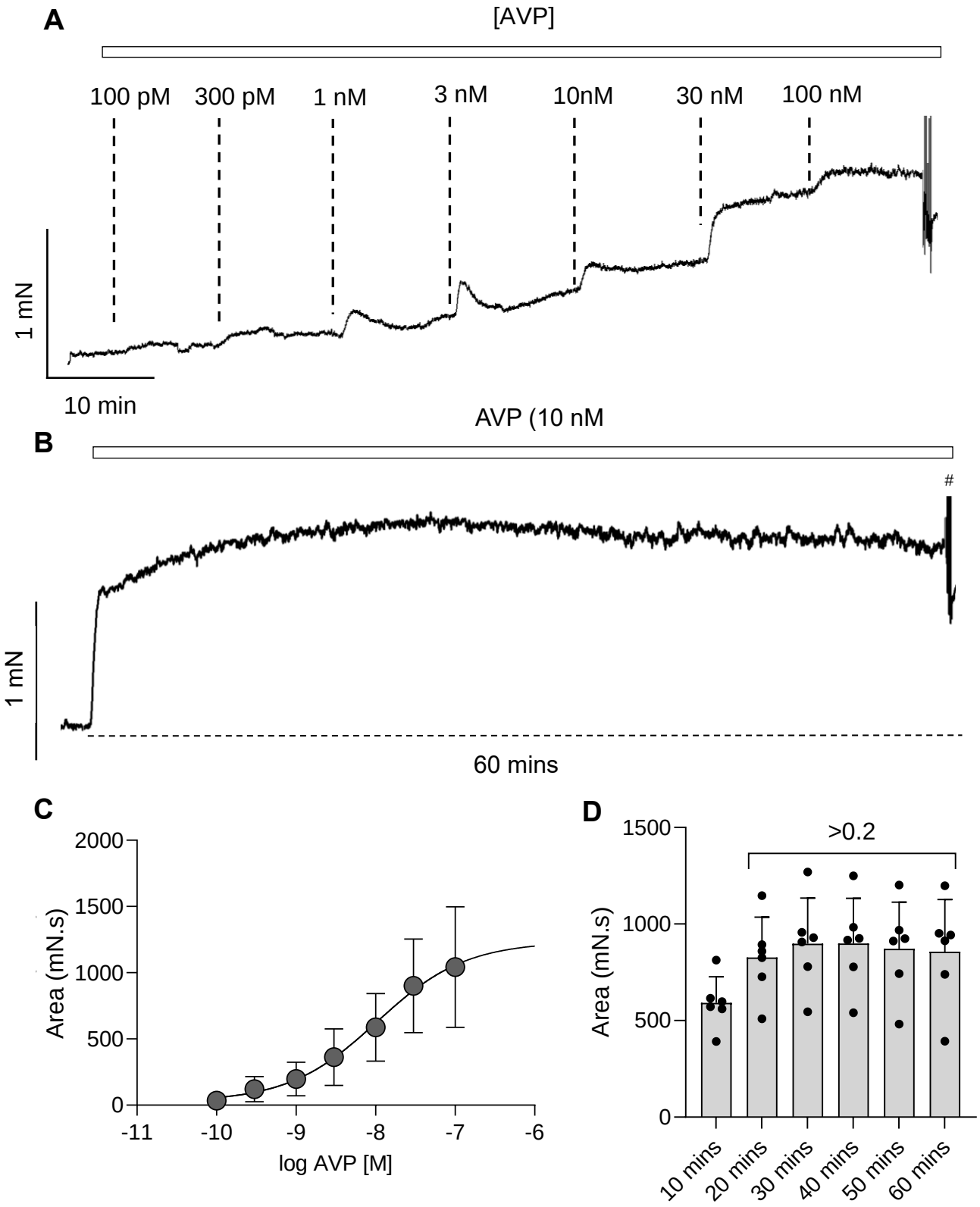

Fig 4.10: Female USM contract in response to AVP. A Representative contractile data showing contractions of female mouse urethra induced by increasing concentrations of arginine vasopressin (AVP) (100 pM - 100 µM). **B** AVP effects (10 nM) on female USM contractions can be sustained for periods over 1 hour. **C** Summary effects of increasing AVP concentration (n=6, non-linear fit curve), and **D** 10 nM AVP on female USM contractile area (n=6, one-way ANOVA, Tukey's test). (#represents washing)

In female USM precontracted with AVP in this manner, Ani9 failed to significantly affect AVP-induced contractions (P=0.09, n=6; Fig. 4.11A&C), whereas 2-APB (100 μM) abolished it (P=0.0005, n=6, Fig. 4.11A&C). This finding suggested agonist-induced contraction in female USM was not modulated by ANO1 channels but depend predominantly on IP_3-mediated Ca^{2+} release from the SR.

4.2.8 Investigating effects of other CaCC inhibitors on urethral contractions

In addition to Ani9, we also tested effects of other CaCC inhibitors on USMC contractions (CaCCinh-A01 and niflumic acid). On AVP-induced contractions of female USM, CaCCinh-A01 (10 μM) caused a non-significant, slow reduction in contraction from 1345 ± 425.3 mN.s to 1156 ± 246.9 mN.s (P=0.4, n=6, Fig. 4.11B&D). Subsequently, niflumic acid (100 μM) in the continued presence of CaCCinh-A01 resulted in an immediate decline in AVP-induced contractions (P<0.0001, n=6, Fig. 4.11B&D). This finding indicates an off-target effect of niflumic acid.

Niflumic acid (100 μM) also reduced EFS-evoked contractions of male USM by 40%-50% (5-20 Hz, P=0.0003 at 5 Hz and P<0.0001 at 20 Hz, n=5, Fig 4.12A&C). In a separate experiment, I firstly tested CaCCinh-A01 (10 μM) on EFS-evoked contractions in male USMC, which had no significant effect (P>0.2 at all frequencies, n=5, Fig. 4.12 B & D). However, in the continued presence of CaCCinh-A01, niflumic acid reduced contractions by 50%-60% (P=0.03 at 2 Hz, P=0.005 at 5 Hz, P=0.0005 at 10 Hz, n=5, Fig. 4.12 B&D). Again, suggesting off-target effects of niflumic acid.

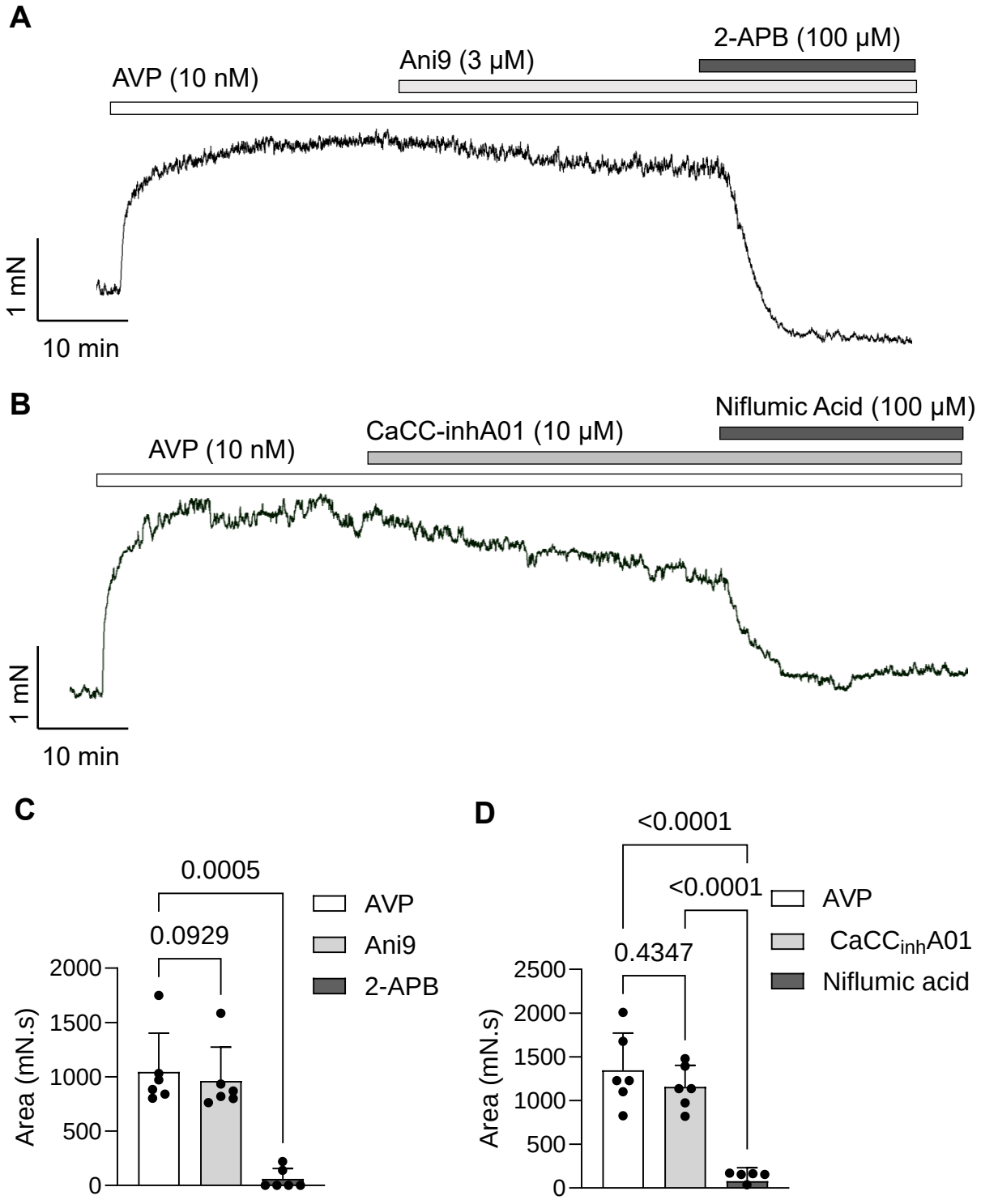

Fig 4.11: Ani9 and CaCC-inhA01 do not affect agonist induced contractions of female USM. A-B Representative data showing effects of Ani9 (3 μM) and 2-APB (100 μM), CaCC-inhA01 (10 μM) and 2-APB (100 μM) on AVP (10 nM) induced contractions of female USM. Summary effects of **C** Ani9 (n=6; One-way Anova, Bonferroni's test) & **D** CaCC-inhA01 on agonist-induced contraction in female USM (n=6, One-way ANOVA, Tukey's test).

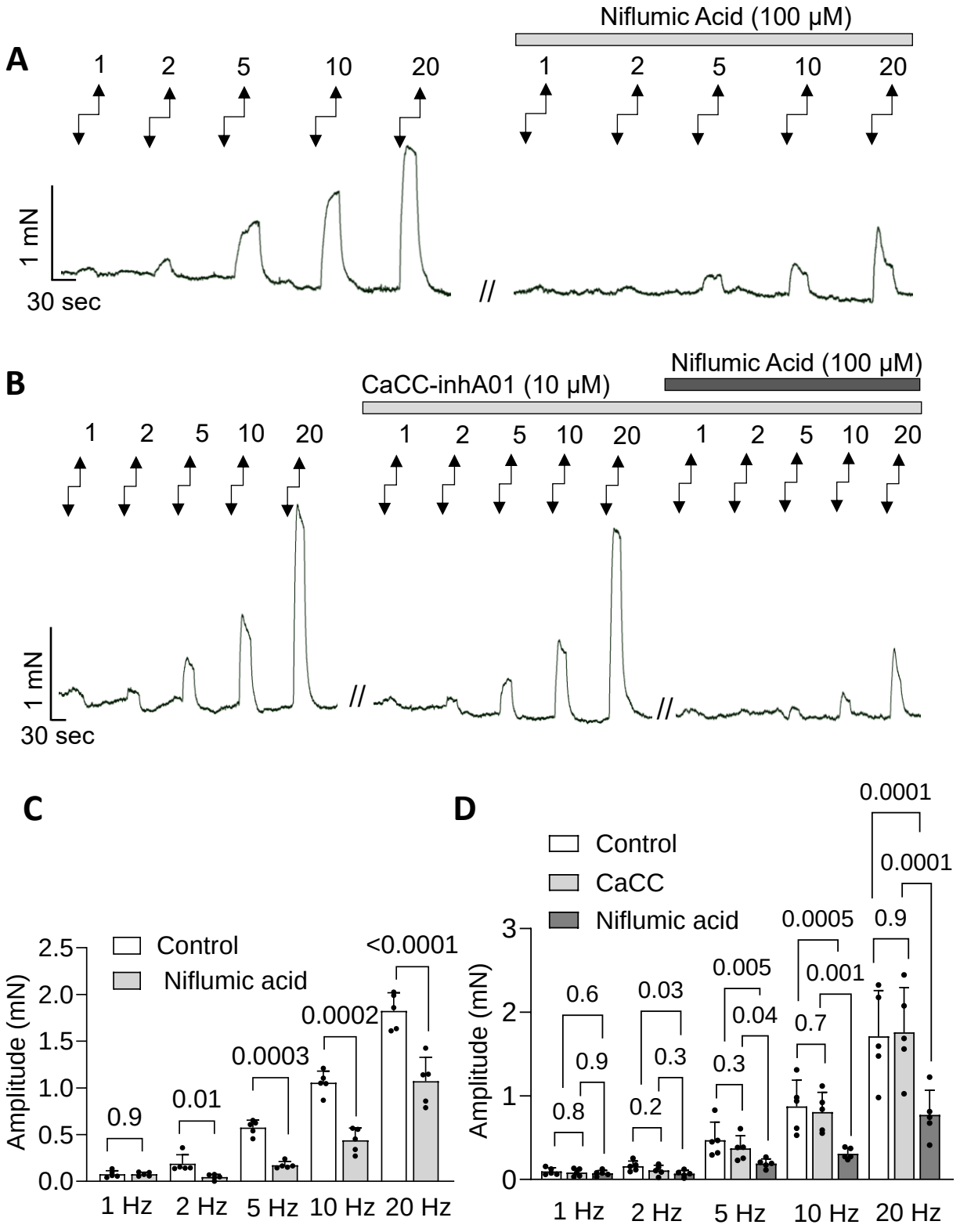

Fig 4.12: EFS-evoked contractions of male USM are inhibited by niflumic acid but not CaCCinh-A01. A Representative isometric tension recording from male USM showing effects of niflumic acid (100 μM) on contractions induced by EFS. **B** Representative isometric tension recording from male USM showing effects of CaCC-inhA01 (10 μM) and niflumic acid (100 μM) on contractions induced by EFS. **C** Summary effects of niflumic acid (n=5; Paired t-test), & **D** CaCC-inhA01 and niflumic acid on EFS evoked contractions of male USM (n=5, One-way ANOVA, Tukey's test)**.** Double-headed arrow represents EFS frequencies (Hz).

4.3 Discussion

CaCCs play crucial roles in numerous physiological processes including epithelial transport, SM contraction and sensory processing (Jin *et al.,* 2016). ANO1 contributes to parasympathetic-induced bronchi contractions (Huang *et al.,* 2012). In uterine SM, ANO1 contributes to spontaneous and oxytocin-mediated myometrium contractions (Bernstein *et al.,* 2014) and in lymphatic collecting vessels ANO1 mediates pressure-sensitive contractions (Zawieja *et al.,* 2019). ANO1 activation in ICC-IM of lower oesophageal sphincter (LES) and internal anal sphincter (IAS) contributes to depolarised membrane potentials, facilitating opening of LTCC on SMC leading to generation of tone (Cobine *et al.,* 2017; Drumm *et al.,* 2022). ANO1 has also been identified as a selective marker of ICC in the gut (Gomez-Pinilla *et al.,* 2009).

However, species-specific differences in ANO1 expression are observed in urethra. In rabbit USM, *Ano1* transcript expression is confined exclusively to ICC-LC (Fedigan *et al.,* 2017), whereas in rat, sheep, and mouse urethra, ANO1 is expressed in USMC rather than in vimentin^{+} ICC-LC, at protein level (Sancho *et al.,* 2012). Rabbit ICC-LC exhibit Cl^{-}currents, STIC and STD, which are not apparent in rabbit USMC (Sergeant *et al.,* 2000; Fedigan *et al.,* 2017). A recent study in mouse and human reported ANO1 channel expression co-localized with c-kit in urethral stromal cells, presumed to be ICC-LC (Ambrogi *et al.,* 2025). These stromal cells were proposed to contribute to bacterial expulsion during urinary tract infection, as female mouse urethral rings contracted in response to 5-HT, which were suppressed by the ANO1 inhibitor Ani9. Notably, these stromal cells appearred morphologically distinct from elongated, spindle-shaped murine ICC-LC observed in Chapter 3 of this thesis and rabbit urethra (Sergeant *et al.,* 2000). This suggests that ANO1^{+} stromal cells may represent a functionally distinct subset of ICC-LC, potentially modulating urethral excitability under pathological conditions differently from the canonical spindle-shaped ICC-LC characterized in this thesis. In contrast, in the previous chapter, I observed the absence of ANO1 expression in ICC-LC, as determined by anti-GFP and ANO1 antibody co-labelling on urethral tissue from Kit-GCaMP6f mice. However, ANO1 immunoreactivity appeared on USM bundles.

In this chapter, I investigated expression of ANO1 at the transcriptional and protein level in mouse USM. I found equivalent expression of ANO1 transcript in male and female urethra. Co-labelling of isolated USMC with α-actin and ANO1 antibodies confirmed similar levels of ANO1 expression in both male and female USMC. This contrasts with a previous study (Chen *et al.,* 2020) which reported nearly double ANO1 expression in female compared to male human and mouse USM using qPCR and western blotting (Chen *et al.,* 2020). The reasons for these differences are not yet clear but could be due to the type or specificity of ANO1 antibodies.

Chen *et al.,* (2020) postulated that differences in ANO1 expression accounted for sex-specific variation in urethral tone (Chen *et al.,* 2020). They further suggested females with hypertriglyceridemia have impaired urethral tone due to downregulation of ANO1 (Chen *et al.,* 2022). Evidence supporting these hypothesis included reduction of USM tone by the ANO1 inhibitor T16inh-A01 (Feng *et al.,* 2019), enhancement of tone by non-selective ANO1 activator EACT (Chen *et al.,* 2020), and reported loss of USM tone in animals with targeted deletion of ANO1 in USMC (Feng *et al.,* 2019). However, most of the previous evidences for ANO1's role in USM contractility is based on pharmacological inhibitors such as DIDS, MONNA, niflumic acid, CaCCinhA01 or T16 inhA01. These compounds are known to exhibit significant off-target effects on LTCC and SR Ca^{2+} release mechanisms, which may affect interpretation of earlier findings (Cruickshank *et al.,* 2003; Boedtkjer *et al.,* 2015; Dwivedi *et al.,* 2023; Genovese *et al.,* 2023). In addition, EACT, which was used as an ANO1 activator in these studies, has been reported to elevate intracellular Ca^{2+} through activation of TRPV1 and TRPV4 channels, thereby indirectly activating ANO1 rather than directly gating the channel (Liu *et al.,* 2016; Genovese *et al.,* 2019). This further limits interpretation of previous studies as being ANO1-specific.

In the present study, I used Ani9, a potent and selective antagonist of ANO1 channels which does not demonstrate off-target effects such as SR Ca^{2+} release or inhibition of ion channels such as VGCC in SM organs (Seo *et al.,* 2016; Lim *et al.,* 2022; Dwivedi *et al.,* 2023). Our findings demonstrated Ani9 did not affect PE-induced contractions in males nor AVP-induced contractions in females, similar to previous findings in pig urethra, where Ani9 failed to affect tone or EFS evoked contractions (Rembetski *et al.,* 2020). In contrast, 2-APB abolished PE and AVP induced contractions in USM.

Moreover, in our hands the same stock and concentration of Ani9 was effective in reducing phasic contractions and Ca^{2+} activity of mouse proximal colon, suggesting a lack of effect on USM was not due to insufficient efficacy of Ani9.

While Ani9 and CaCCinh-A01 had no significant effect on USM contractions, niflumic acid, a non-selective inhibitor of CaCC, reduced EFS evoked contractions in males and abolished AVP induced contractions in females. This finding might suggest other CaCCs may contribute to murine USM contractility. However, niflumic acid has off-target effects such as leakage of Ca^{2+} from SR (Cruickshank *et al.,* 2003; Genovese *et al.,* 2023), inhibiting VGCC (Balderas *et al.,* 2012), modulating RyR (Oba, 1997) and opening K^+ channels (Ottolia & Toro, 1994). Thus, niflumic acid effects may be attributable to such actions. I also observed a slight non-significant decrease in AVP evoked contraction due to CaCCinh-A01, which may be due to off-target effects as this compound leaks SR Ca^{2+}, depleting SR Ca^{2+} gradually (Cruickshank *et al.,* 2003; Dwivedi *et al.,* 2023) and might possibly inhibit IP_3R (Genovese *et al.,* 2023).

In this chapter, I observed ANO1 channels were expressed on USMC and not on ICC-LC (Sancho *et al.,* 2012). However they do not seem to play a functional role in modulating murine urethral contractility, whether male or female, under conditions of our experiments. It could be possible ANO1 channels become important only during certain pathological conditions or during specific stages of life. Previous studies have suggested that ANO1 channels play an important role in disease states, for example their upregulation during hyperglyceridaemia (Chen *et al.,* 2022), and their expression and function in c-kit$^+$ stromal cells leading to pathogen elimination by enhancing USM contractions in response to 5-HT (Ambrogi *et al.,* 2025). A comparison between juvenile and adult mice revealed that ANO1 antagonists were less effective in suppressing SW in adult small intestinal muscles than juvenile, indicating possible age-related compensatory mechanisms involving other conductances (Hwang *et al.,* 2019). A similar phenomenon may occur in mouse urethra, where ANO1-independent conductances might emerge with maturation. This can be examined in future studies by comparing ANO1 expression in juvenile and adult urethra, and by testing ANO1 inhibitors in juvenile tissues using isometric tension recordings and Ca^{2+} imaging to investigate whether ANO1 contributes to urethral function at juvenile stages of life.

Alternative splicing of ANO1 variants are thought to affect Ca^{2+} sensitivity, voltage dependence and kinetics of activation and deactivation in both physiological and pathological conditions (O'Driscoll *et al.,* 2011; Sung *et al.,* 2016). Previous studies demonstrated that in mouse and human there is an additional exon (exon 0) upstream of the first exon that could enhance ANO1 expression (Mazzone *et al.,* 2015). Differential expression of ANO1 splice variants may underlie variable sensitivity to ANO1 antagonists, potentially influenced further by differences in intracellular Ca^{2+} levels (Sung *et al.,* 2016). Hence, there is a possibility ANO1 splice variants and their regulation through alternative splicing contribute variably to urethral function. This could be investigated by examining the expression of ANO1 splice variants (exons a-d and exon 0) in male and female USM using qPCR or RNA-sequencing. Subsequent heterologous expression of these specific variants in HEK293 cells would allow isolation of their intrinsic biophysical properties, independent of the complex ionic environment of native tissue. Patch-clamp analysis could then determine how urethra-relevant ANO1 splice variants differ in Ca^{2+} sensitivity, voltage dependence, and pharmacological responsiveness to selective inhibitors such as Ani9. Collectively, this strategy would clarify whether variability in urethral ANO1 function reflects splice variant-dependent channel behaviour or instead arises from alternative regulatory mechanisms operating in USM.

Another important direction for investigation is assessing the role of LTCC in USM. Drumm *et al.,* 2018 reported LTCC inhibition did not affect spontaneous Ca^{2+} activity and agonist-induced contraction in male mouse USM, whereas Orai inhibition significantly reduced it. If LTCC inhibition does not impact Ca^{2+} dynamics, this could explain the minimal functional role of ANO1 channels in urethra, since previous studies reported that ANO1 channels activation contribute to membrane depolarisation in SMC that activates LTCC (Leblanc *et al.,* 2005; Dunford *et al.,* 2020; Drumm *et al.,* 2021; Wray *et al.,* 2021). However, LTCC modulation has not been tested during EFS-induced contractions in previous studies, which is a more physiological model. Also, prior work focused solely on male USM, with no data from females. Therefore, in the next chapter, I investigated involvement of VGCC and Orai channels in both male and female mouse USM, using PE-, EFS-evoked responses and *in situ* Ca^{2+} imaging to better understand the role of these channels in modulating murine USM contractility.

5. Role of VGCC and Orai channels in murine urethral smooth muscle contractility

5.1 Introduction

Voltage-gated calcium channels (VGCC) are transmembrane proteins critical for converting electrical signals into cellular responses via Ca^{2+} influx (Catterall, 2011). VGCC exhibit diverse roles across SM types, influencing physiological processes from vasoconstriction to gastrointestinal motility (Moosmang *et al.,* 2003; Jiang *et al.,* 2014; Striessnig *et al.,* 2014; Rodriguez-Tapia *et al.,* 2016; Liu *et al.,* 2024).

In USM, Ca^{2+} influx through LTCC (Cav 1.2 channels) has long been proposed as a key mechanism underlying myogenic tone and agonist evoked contraction (Brading, 1999; Greenland *et al.,* 1996; Hollywood *et al.,* 2003; Rembetski *et al.,* 2020). In pig USM, dihydropyridines such as nifedipine reduced urethral tone, agonist-induced contraction and nerve stimulation-induced responses (Brading, 1999; Greenland *et al.,* 1996; Rembetski *et al.,* 2020). Patch-clamp studies revealed rabbit and human USMC express currents elicited by LTCC and TTCC, which were sensitive to nifedipine and mibefradil or Ni^{2+} (non-selective TTCC antagonist), respectively (Bradley *et al.,* 2004; Hollywood *et al.,* 2003). Hashitani *et al.,* (2007) demonstrated nicardipine (Cav 1.2 antagonist) suppressed Ca^{2+} activity in rabbit USMC using membrane permeable dyes (Hashitani & Suzuki, 2007). In guinea pig USM, nifedipine reduced duration of slow waves (Hashitani & Edwards, 1999). Spontaneous USM tone in female mice urethra was reduced by nifedipine (Feng *et al.,* 2019).

In contrast, several studies suggested limited role of LTCC in urethral contractility of certain species. Oral administration of nifedipine failed to affect urethral pressure in male cats and human females (Forman *et al.,* 1978; Mawby *et al.,* 1991). Similarly, in female rabbit and sheep urethra, nifedipine did not abolish NA-induced contractions, suggesting the importance of alternative Ca^{2+} influx pathways (Larsson *et al.,* 1984; Garcia-Pascual *et al.,* 1991). Findings from male mice further support this view. Drumm *et al.,* (2018) showed that LTCC blockade with nifedipine had no effect on agonist-induced contraction, and LTCC inhibition with nifedipine, nicardipine or isradipine, nor activation with FPL64176, altered intracellular Ca^{2+} activity in male mouse USMC recorded *in situ.* Selective TTCC inhibition with TTA-A2 also had no effect on Ca^{2+} activity in male mouse USMC. Instead, the Orai inhibitor GSK-7975A significantly reduced agonist dependent responses and intracellular Ca^{2+} activity.

When SR Ca^{2+} stores were depleted, reintroduction of extracellular Ca^{2+} evoked a large tonic contraction (indicative of SOCE, Putney, 1986), that was nifedipine-insensitive but dose-dependently inhibited by GSK-7975A (Drumm *et al.,* 2018). These findings demonstrated that in male mouse urethra, Orai-mediated SOCE rather than VGCC serves as the main Ca^{2+} influx pathway supporting Ca^{2+} activity and agonist-evoked contractions.

However, these previous studies had certain limitations. The effect of nifedipine was assessed only at a single agonist concentration (10 μM PE) (Drumm *et al.,* 2018). Notably, Dwivedi *et al.,* (2023) reported that at supramaximal agonist concentrations (>1 μM, Carbachol), inhibition of LTCC produces little or no effect, whereas at lower, physiologically relevant concentrations (0.1-0.3 μM, Carbachol), inhibitory effects of LTCC were more evident in airway SMC (Dwivedi *et al.,* 2023). A similar possibility may exist in the male mouse urethra, where the use of a high concentration of PE (10 μM) could have masked the contribution of LTCC.

In addition, previous studies (Drumm *et al.,* 2018) on male mice USM did not examine effects of LTCC, TTCC, or Orai channel inhibition on nerve-stimulated contractions, which would represent a more physiological approach to evaluating urethral excitability. Moreover, it has been well established (Alexandre *et al.,* 2017), and also demonstrated in Chapter 4 of this thesis, that significant sex differences exist in mouse urethra. Therefore, role of VGCC and Orai channels should also be investigated in female mouse USM as it is less explored in previous studies. Another gap in the literature concerns gene expression profiles of LTCC subunits in male and female, and of Orai channels in the female as differences in channel expression can directly influence urethral excitability, Ca^{2+} signalling, and tone.

The present study was conducted to address existing knowledge gaps in mouse USM, and to further explore observations from Chapter 3, which demonstrated inhibition of ANO1 had no significant effect on mouse urethral contractility, which suggest that LTCC activation does not rely on ANO1 channels activity or might play a limited role in the mouse urethra. This observation provided the rationale to investigate LTCC function in the present chapter, along with other Ca^{2+} entry pathways, to better define mechanisms that sustain USM excitability and contraction.

5.2 Results

5.2.1 Expression of LTCC and Orai in murine USM

I first examined expression profiles of *Cacna* (*Cacna1a, Cacna1c, Cacna1d, and Cacna1f*) and *Orai* (*Orai1, Orai2, and Orai3*) gene subtypes in male and female urethra using qPCR. Statistical comparisons were not made between males and female samples due to considerable variability amongst the 3 qPCR n numbers, but results confirmed presence of *Cacna1c* (Cav 1.2) expression in both male and female urethra. *Cacna1c* (Cav 1.2) showed highest expression, with values of 0.003 ± 0.001 (n=3) in males and 0.003 ± 0.0007 (n=3) in females (Fig. 5.1A). In comparison *Cacna1d* (Cav1.3) showed lower expression, and *Cacna1f* (Cav 1.4) was the least expressed subtype, with 0.0004 ± 0.0003 (n = 3) in males and 0.00008 ± 0.00003 (n=3) in females (Fig. 5.1A). Among *Orai* genes, *Orai1* exhibited highest expression, with 0.016 ± 0.001 (n=3) in males and 0.02 ± 0.01 (n=3) in females (Fig. 5.1B), followed by *Orai 3* and least expressed was *Orai 2* in both male with 0.007 ± 0.001 and female with 0.01 ± 0.008 (Fig. 5.1B).

5.2.2 Effects of LTCC inhibition in murine USM

Given confirmed expression of LTCC, I next explored their functional relevance in USM. Previous work on male mice USM tested nifedipine at a single, high dose of PE (10 µM) (Drumm *et al.,* 2018). At such concentrations, strong IP_3R activation can trigger large SOCE responses, potentially masking any contribution from LTCC as previously described in airway SMC (Dwivedi *et al.,* 2023). In the present study, nifedipine was applied on a range of concentrations of PE (30 nM- 30 µM). As described in Chapter 3, PE concentration response curves (30 nM-30 µM) were generated under control conditions (Fig. 5.2A), and following a 30-minute incubation with 1 µM nifedipine (Fig. 5.2B). Nifedipine treatment did not affect AUC (P>0.6 at all concentrations) or EC_{50} (P=0.8) of PE concentrations dependent curves (n=6; Fig. 5.2D), suggesting blockade of LTCC does not alter α_1-adrenergic-mediated contractile responses in male urethra. Nifedipine also did not affect resting basal tone of male urethra (n=5, P=0.1; Fig.5.2C&E).

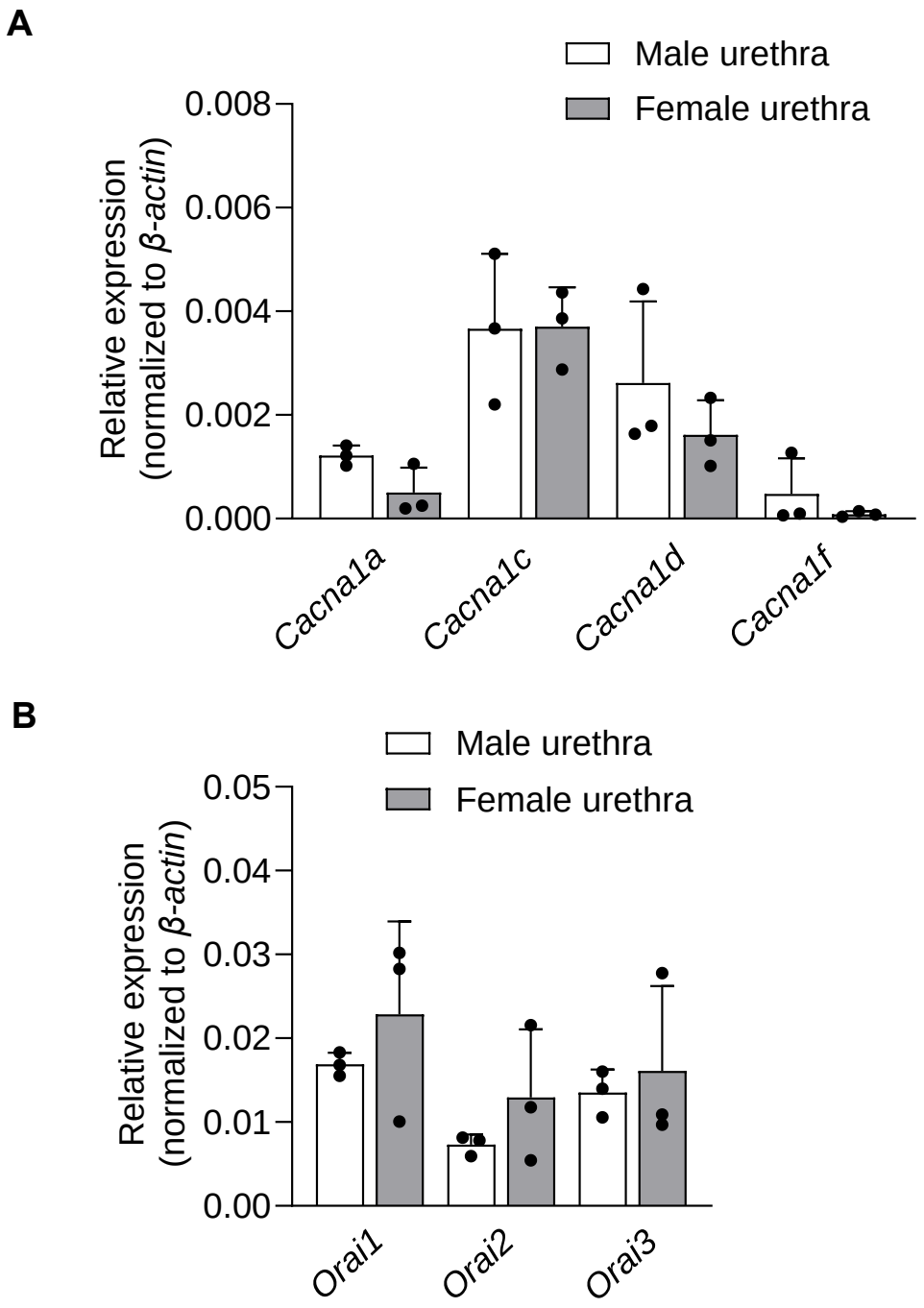

Fig 5.1: Relative expression of *Cacna1a, Cacna1c, Cacna1d, Cacna1f, Orai1, Orai2, Orai3* in WT male & female urethra. Real-time PCR analyses showing gene expression of **A** *Cacna1a, Cacna1c, Cacna1d, Cacna1f,* **B** *Orai1, Orai2, Orai3* normalized to *β-actin* gene expression (endogenous control) in male and female urethra. Data **A** & **B** represents the comparison of male and female urethra fold change expression of *Cacna1a, Cacna1c, Cacna1d, Cacna1f,* and *Orai1, Orai2, Orai3* relative to *β-actin* in male (n=3), female urethra (n=3; Unpaired t-test).

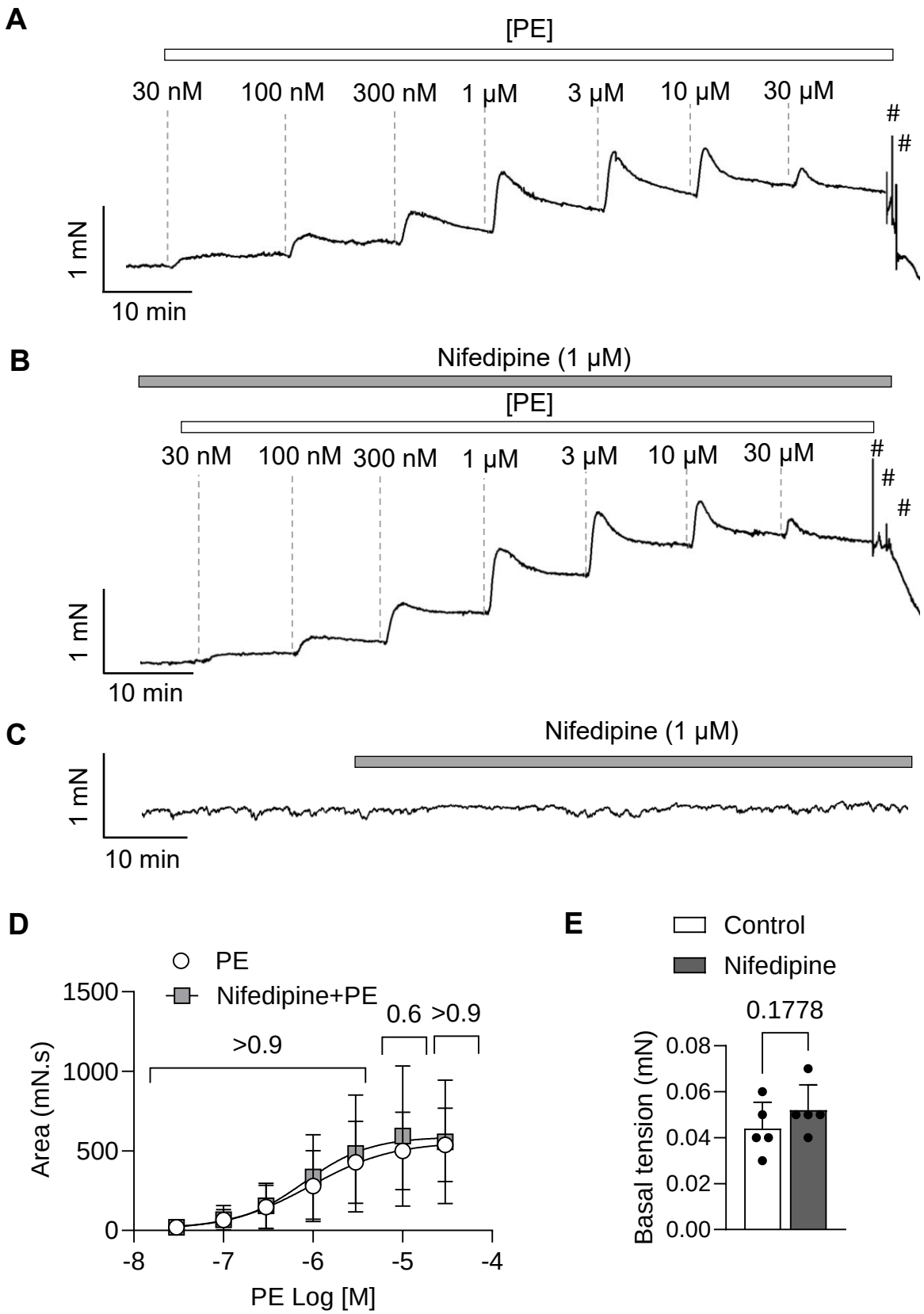

Fig 5.2: LTCC inhibitor nifedipine does not affect PE responses nor basal tone in male USM. A-B Representative PE dose dependent contractile responses of male USM (30 nM - 30 μM) **A**, and **B** in the presence of nifedipine (1 μM). **C** Representative trace showing application of nifedipine (1 μM) on basal tone. Summary effect of nifedipine on PE dose responses curves, **D** (n=6; Two-way ANOVA, Bonferroni's test), and **E** on basal tone (n=5; Paired t-test). (# represents washing).

I next sought to determine whether LTCC modulates neurally-evoked responses, as this was not attempted in previous studies. The effect of nifedipine was examined on EFS-evoked contractions at various frequencies (1 Hz, 2 Hz, 5 Hz, 10 Hz, 20 Hz) in male USM. However, nifedipine (1 µM) did not alter the amplitude of EFS-induced responses at any frequency (n=6, P=0.09 at 20 & 5 Hz, P>0.1 at 1, 2 & 10 Hz; Fig. 5.3A&C). This suggests LTCC does not modulate nerve-stimulated contractions in male mouse urethra. LTCC inhibition was next examined on female mice urethra. Female USM was precontracted with 10 nM AVP, followed by application of 1 µM nifedipine (n=5; Fig. 5.3B). Nifedipine produced no observable change in AUC of AVP-induced contractions (P=0.2), whereas 2-APB abolished it (Fig. 5.3B&D). These findings indicate that LTCC blockade does not influence agonist-induced contractility in female urethra. These observations in mouse urethra highlight species-specific differences, as previous studies in porcine, rabbit and human urethra have reported that LTCC inhibition markedly reduced urethral tone and contractions (Bridgewater, 1993; Hollywood *et al.,* 2003; Hashitani & Suzuki, 2007; Rembetski *et al.,* 2020).

To ensure that the lack of response in USM was not due to inactive nifedipine, I applied the same stock solution to male colon preparations. While 1 µM nifedipine had no effect on PE (1 µM)-induced contraction in male urethra (n=5, P=0.8; Fig. 5.4A&C), it effectively abolished phasic contractions in colon (n=5; Fig. 5.4B&D) by attenuating both amplitude (P=0.006) and frequency (P=0.01) of contractions. These results confirm functional effectiveness of nifedipine. 2-APB, however, abolished the PE-induced contractions in male USM (Fig. 5.4A), suggesting that the agonist-induced contractions relies primarily on SR Ca^{2+} release.

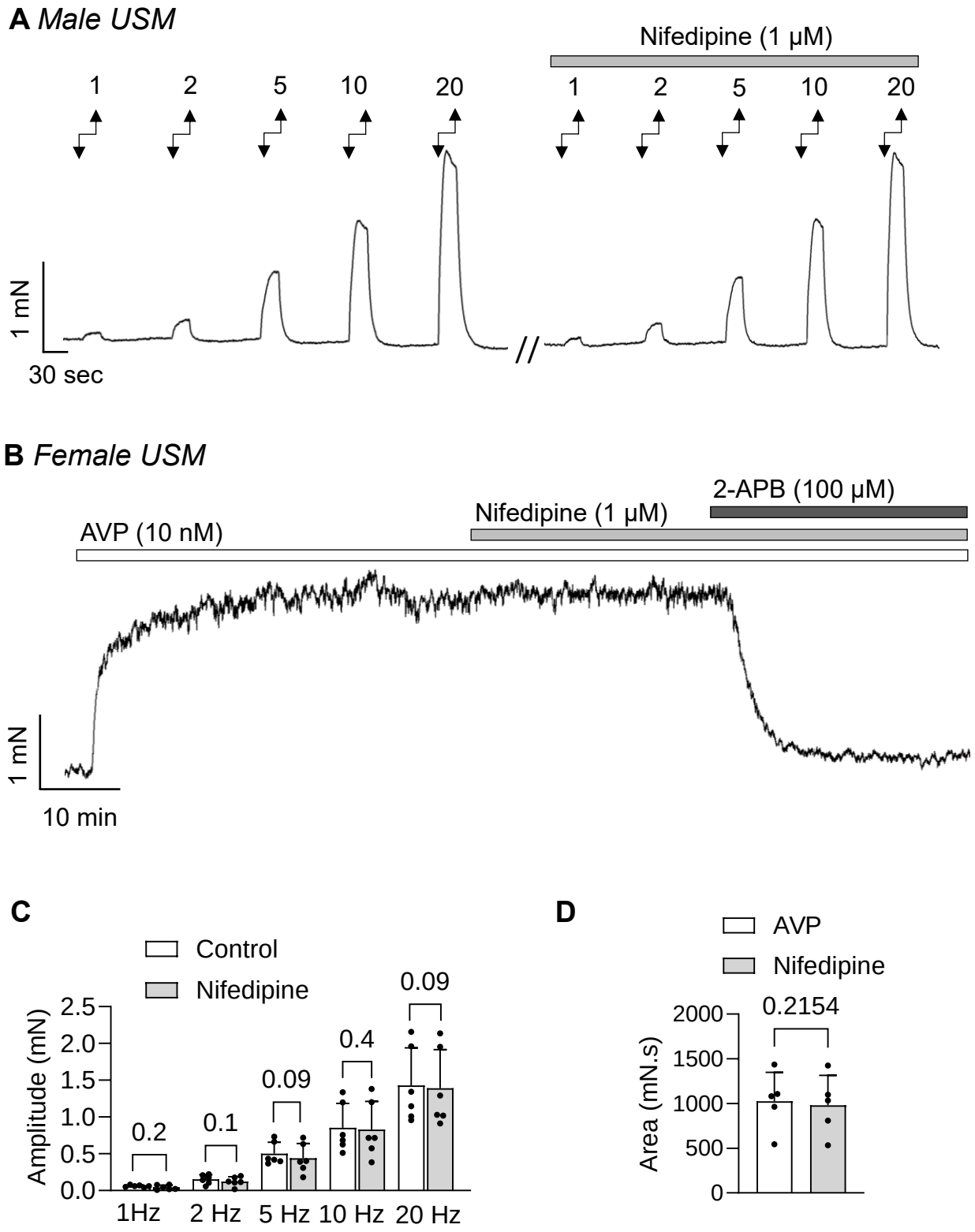

Fig. 5.3: LTCC inhibition by nifedipine does not affect EFS- or agonist-induced contractions in male or female urethra respectively. Representative traces show **A** EFS-evoked contractions in male USM under control conditions and after nifedipine (1 μM), and **B** AVP (10 nM)-induced contractions in female urethra under control and after nifedipine (1 μM). Summary effects of nifedipine on **C** EFS-evoked male USM contractions (n=6; Paired t-test) and **D** AVP-induced female urethra contractions (n=5; Paired t-test) are also shown. Double-headed arrows indicate EFS frequency (Hz).

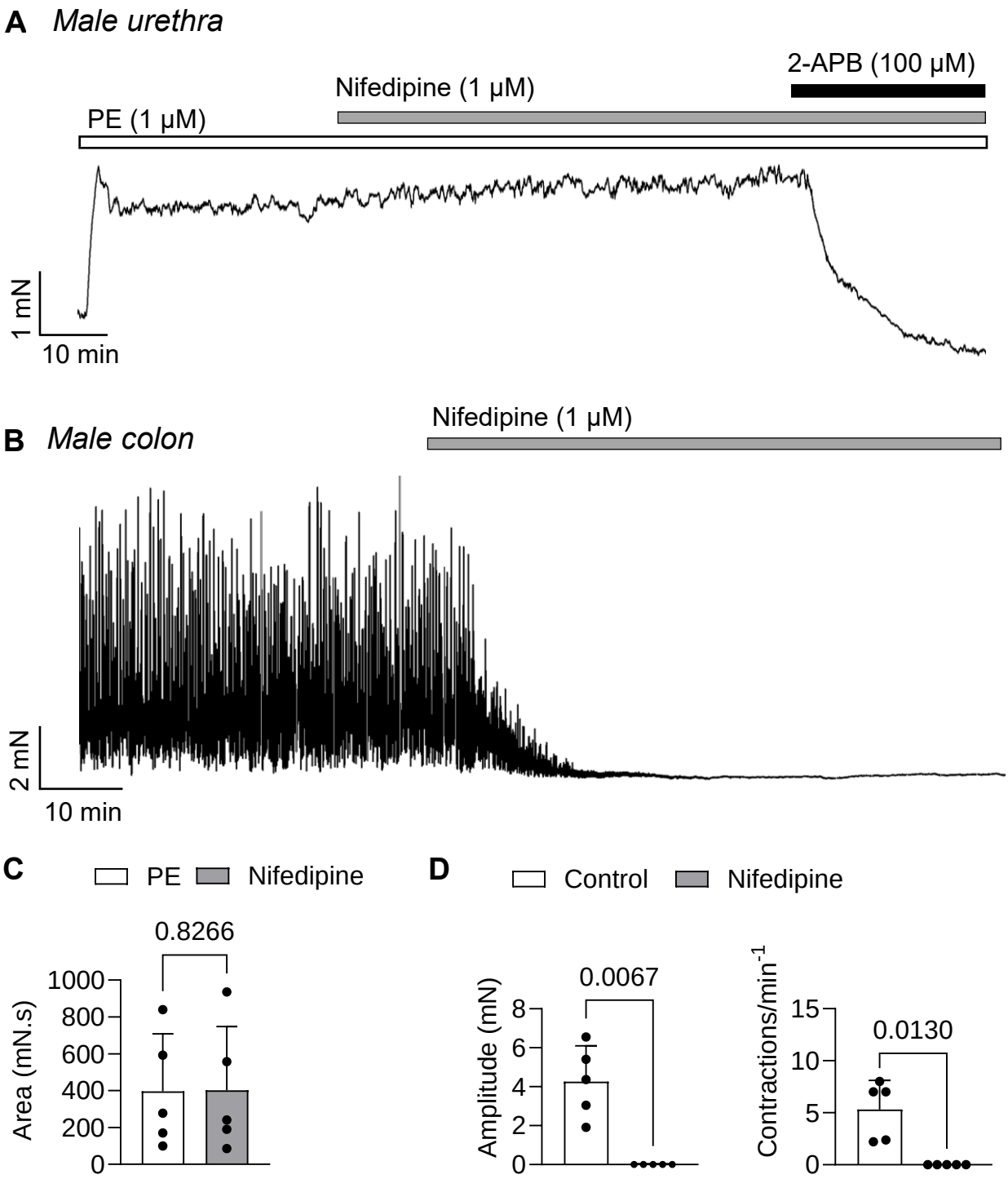

Fig 5.4: LTCC inhibition does not affect agonist response in male USM but abolished phasic contractions in colon. Representative data showing application of nifedipine (1 μM) on **A** PE (1 μM) induced contraction in male USM, and **B** phasic contractions of colon. Summary effects of nifedipine on **C** PE induced contraction in male USM (n=5; Paired t-test), and **D** amplitude and frequency of colonic contractions (n=5; Paired t-test).

To investigate whether LTCC are functionally active in response to depolarisation in mouse USM, tissues were exposed to a high KCl solution (60 mM) to induce membrane depolarisation. High K^+ depolarises SMC, leading to opening of LTCC and subsequent Ca^{2+} influx, which triggers contraction (Ishida *et al.,* 2017). High K^+ solution-induced contractions in both male (n=3; Fig. 5.5A) and female urethra (n=4; Fig. 5.5B), with a greater response in male (AUC= 569.7 ± 222.3 mN.s; Fig. 5.5C) than female tissue (AUC=185.1 ± 31.1 mN.s; Fig 5.5D). The mean initial amplitude of high K^+-induced contractions was also higher in males (1.6 ± 0.6 mN; n=9) as compared to female USM (0.5 ± 0.1 mN; n=11), also observed in previous chapter. Nifedipine (1 µM) was applied during the sustained phase of the high K^+-induced contraction in males (Fig. 5.5A). However, since the high K^+-evoked contractions in females were small and not well sustained, applying nifedipine directly during the response would not have clearly demonstrated its inhibitory effect. Therefore, high K^+-induced contraction was first obtained, then the tissue was washed and allowed a rest for 30-min interval before reapplying high K^+ to check if contractions were reproducible in females (Fig. 5.5 B). The high K^+-induced contractions were found reproducible in females (P=0.3, Fig 5.5 B&D). Following this, tissues were incubated with nifedipine (1 µM), and high K^+ was reapplied to assess the effect of LTCC inhibition (Fig. 5.5B&D). Application of nifedipine abolished high K^+-induced contractions in female (n=4; P=0.003) USM (Fig. 5.5A-D), confirming that depolarisation-induced contraction is primarily mediated through LTCC activity, and hence proves that LTCC are functionally present in USM.

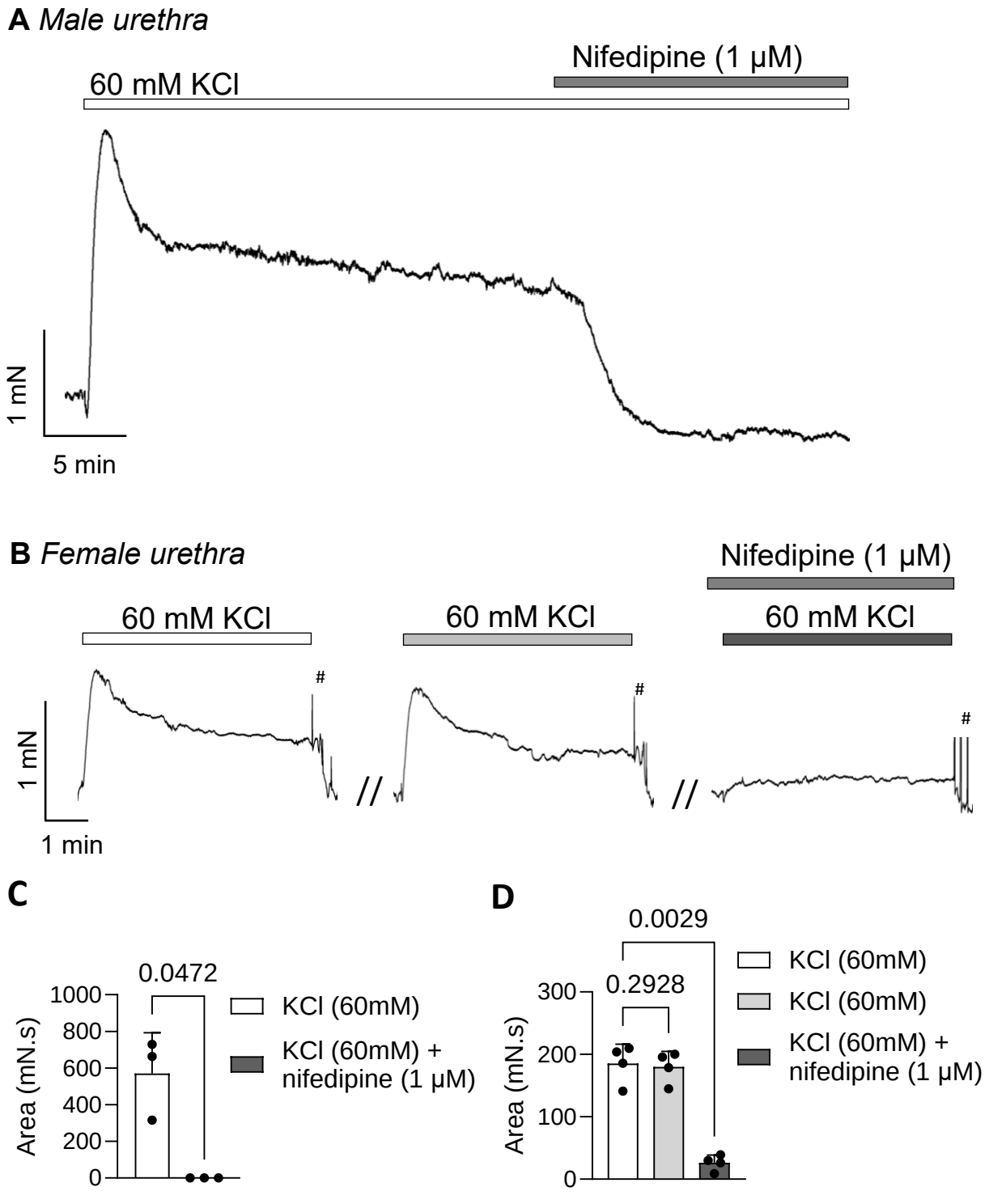

Fig. 5.5: Nifedipine abolished high potassium solution induced contraction in both male and female. Representative data shows inhibition of LTCC channels via nifedipine (1μM) in the presence of TTX (1μM) on high K^+ (60 mM) induced contraction **A** in male (n=3) & **B** in female urethra (n=4). **C & D** Summarized effects of nifedipine on high K^+ induced contractions in male (Paired t test) and female (one way ANOVA, Bonferroni's test). (# represent washing)

To examine the role of LTCC on Ca^{2+} activity in USM, *in situ* Ca^{2+} imaging was performed on male and female Acta2-GCaMP8.1 mice USM (Fig. 5.6A&C). Spontaneous USMC Ca^{2+} events were recorded in 30 sec segments under control conditions and after 25 min incubation with nifedipine (1 μM) in both male and female USM. Nifedipine had no effect on frequency (P=0.15), amplitude (P=0.14), duration (P=0.6) or spread (P=0.16) of male USMC Ca^{2+} events (n=3, c=9; Fig. 5.6A&B). These findings are consistent with Drumm *et al.,* 2018, which reported no effect of nifedipine on spontaneous Ca^{2+} male USMC using SmMHC-Cre-GCaMP3. Similar findings were observed in female USM (n=5, c=10; Fig. 5.6C&D), where nifedipine did not affect frequency (P=0.39), amplitude (P=0.76), duration (P=0.51) or spread (P=0.1) of spontaneous Ca^{2+} activity. This indicates basal Ca^{2+} activity in USMC is independent of LTCC-mediated Ca^{2+} entry and is likely driven by other Ca^{2+} influx mechanisms.

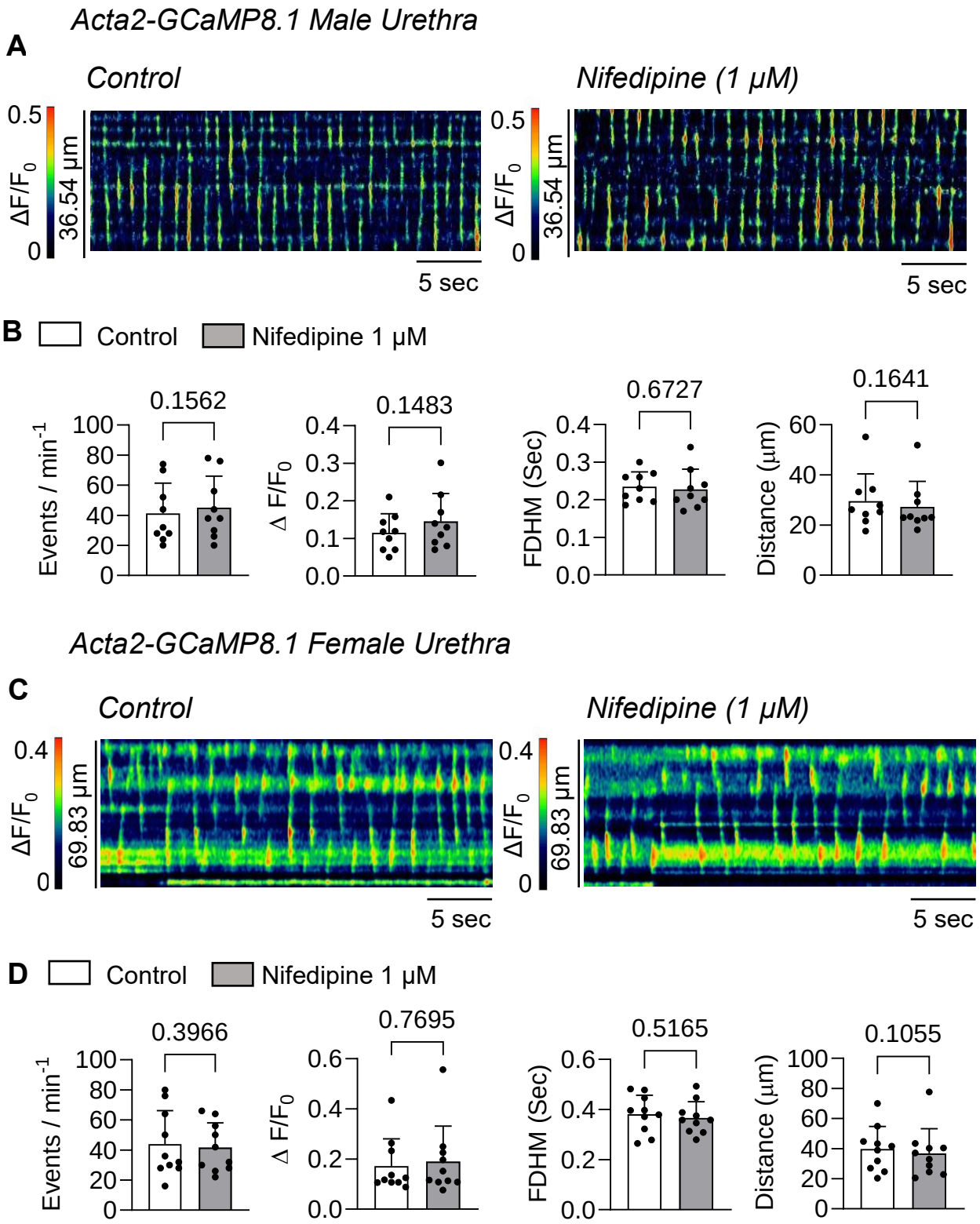

Fig. 5.6: LTCC inhibition does not affect basal Ca^{2+} activity in Acta2-GCaMP8.1 murine USM. Representative traces of spontaneous Ca^{2+} events in control conditions and in the presence of nifedipine (1 μM) in **A** male**,** and **B** female USM. Summary data showing frequency, amplitude, duration and spread of Ca^{2+} events in the presence of control conditions vs nifedipine **C** male (n=3, c=9; Paired t-test), and **D** female USM (n=5, c=10; Paired t-test).

5.2.3 Effects of LTCC activation in murine urethra

Since LTCC inhibition had no effect on agonist-induced, basal, spontaneous, or EFS-evoked activity, I next investigated whether their activation could modulate USM contractility. The selective LTCC activator FPL64176 (300 nM) was applied to evaluate its effect on both agonist-induced contractions and basal tone (Fig. 5.7A,B&C). FPL64176 markedly increased the AUC of PE-induced contractions by superimposing additional phasic contractions, which became apparent at PE concentrations ≥300 nM (Fig. 5.7 B&D). For instance, at 1 μM concentration of PE, the AUC was increased from 570.2 ± 277.2 mN.s in control to 758 ± 288.5 mN.s (n=7, P=0.003; Fig. 5.7 A,B&D) in presence of FPL64176 in male USM. The mean initial amplitude of PE concentration-response curves showed a noticeable increase in the presence of FPL64176, particularly at ≥300 nM of PE (Fig 5.7A&B). The summary graph is not shown, but at 1 μM PE, the mean initial amplitude increased from 0.9 ± 0.2 to 1.1 ± 0.4 mN (n=7; P=0.04), and at 3 μM PE, it further increased from 1 ± 0.2 to 1.3 ± 0.2 mN (n=7; P=0.001). However, FPL64176 did not produce a significant shift in the EC_{50}, changing only from 0.84 μM under control conditions to 0.67 μM after treatment (n=7, P=0.7; Fig. 5.7 A,B,D). In addition, FPL64176 did not affect resting basal tone of male USM (n=6, P=0.29; Fig. 5.7C&E). These findings indicate that direct LTCC activation can modulate agonist-evoked responses; however, basal opening of LTCC does not appear to contribute to the resting USM tone.

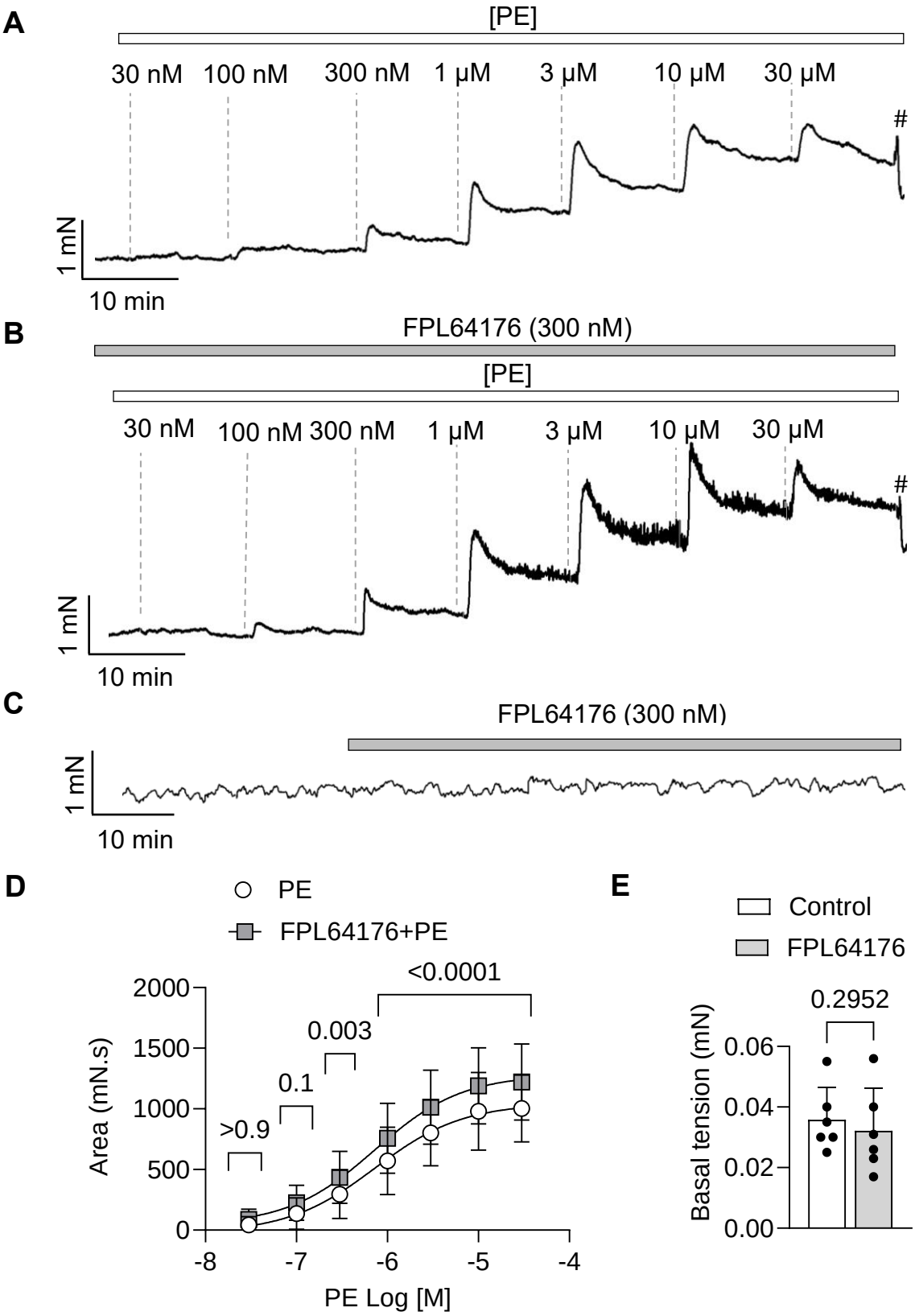

Fig 5.7: LTCC activator FPL64176 induced phasic contractions on PE responses but had no effect on basal tone in male USM. A-B Representative PE dose-dependent contractile responses of male USM (30 nM - 30 µM) **A** and **B** in the presence of FPL 64176 (300 nM). **C** Representative trace showing application of FPL 64176 (300 nM) on resting basal tone**.** Summary effect of FPL 64176 on PE dose responses curves, **D** (n=7; Two-way ANOVA, Bonferroni's test), and **E** basal tone (n=6; Paired t-test). (# represents washing).

Next, I investigated effects of LTCC activation on neurally-evoked contractions in male USM. I applied EFS (1 Hz, 2 Hz, 5 Hz, 10 Hz, 20 Hz) on male USM to induce contractions followed by incubation in FPL64176 (300 nM) and repeated EFS (Fig. 5.8A). FPL64176 significantly enhanced the amplitude of EFS-evoked contractions by ~30-40% from 5 Hz onwards (n=6; Fig. 5.8A&C). At 10 Hz, the amplitude was increased from 0.9 ± 0.4 mN to 1.3 ± 0.5 mN (P=0.0008), representing a ~36% increase and at 20 Hz, from 1.8 ± 0.7 mN to 2.3 ± 0.9 mN, representing a 28% increase (P=0.0002). Nifedipine reversed the FPL64176-induced increase in contraction amplitude, restoring responses to control levels (n=6; Fig. 5.8A&C), confirming that the FPL64176-induced enhancement was mediated through LTCC activity.

Effects of LTCC activation on female USM was next examined. FPL64176 (300 nM) was applied during AVP (10 nM)-induced contractions (n=5; Fig. 5.8B&D). FPL64176 did not alter the AUC of AVP-induced contractions (P=0.97). Subsequent application of nifedipine (1 μM) also had no additional effect (P=0.1), indicating LTCC do not contribute to agonist-evoked contractile activity in female USM. In contrast, 2-APB (100 μM) abolished AVP-induced contractions (Fig 5.8B), as previously shown (Chapter 3), suggesting that IP_3-mediated Ca^{2+} release is the dominant mechanism driving contraction in female urethra.

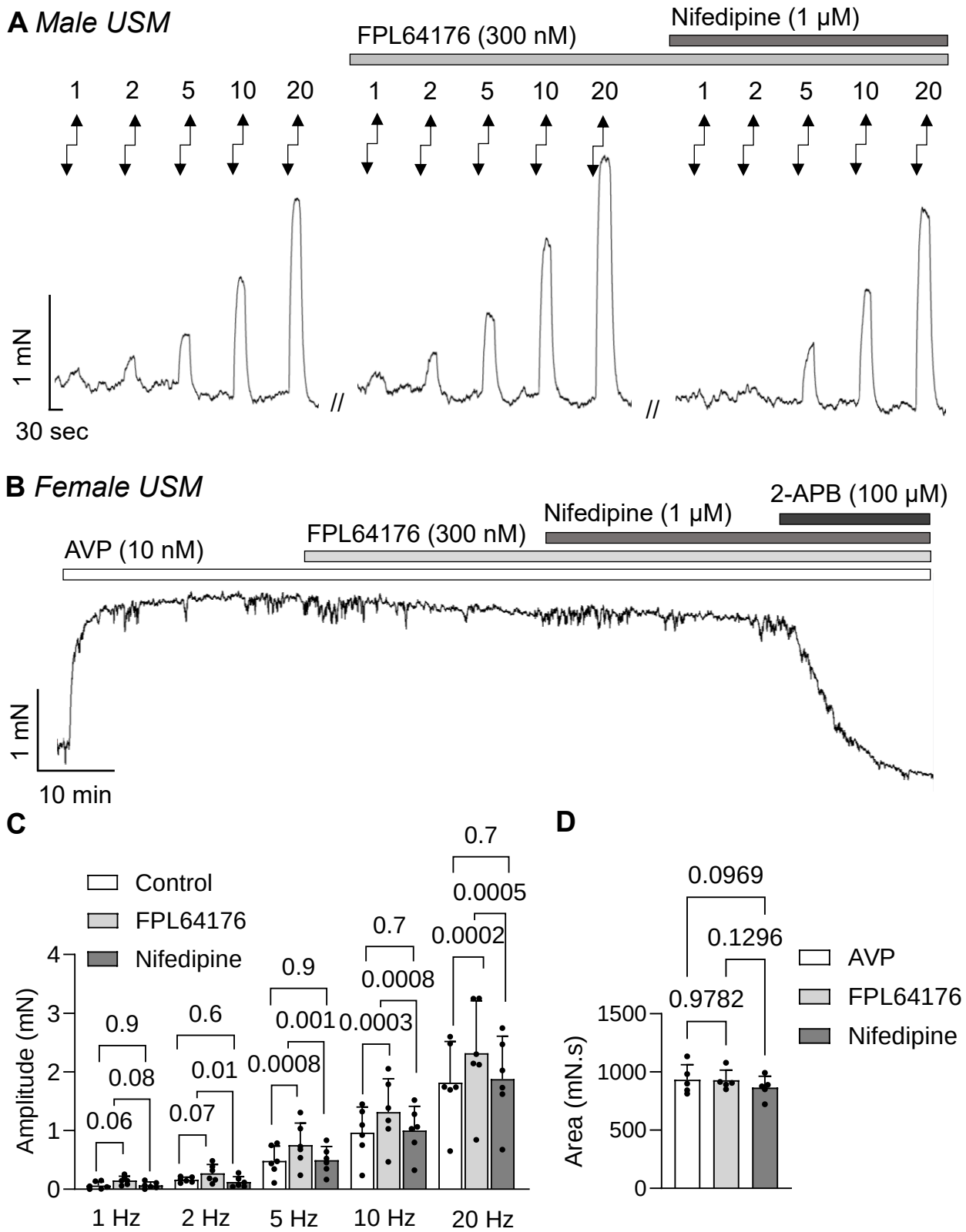

Fig. 5.8: LTCC activation enhances EFS-evoked contractions in male urethra, but has no effect on agonist-induced contractions in female urethra. Representative effects of FPL64176 (300 nM) followed by nifedipine (1 μM) on **A** EFS-induced contractions in male, and **B** AVP-induced contraction in female USM. In female USM, 2-APB (100 μM) was applied at the end of the experiment. Summary data for **C** EFS-evoked contractions in male (n=6, one-way ANOVA, Tukey's test), and **D** AVP-induced contractions in female (n=5, one-way ANOVA, Tukey's test). Double-headed arrows indicate EFS frequency (Hz).

5.2.4 Effect of T-type Ca^{2+} channel (TTCC) inhibition in murine USM

TTCC regulate excitability and pacemaker activity in several SM systems such as vascular and GI tissues (Ward *et al.,* 2004; Ono & Iijima, 2005; Park *et al.,* 2006; Bayguinov *et al.,* 2007; Zheng *et al.,* 2014; Drumm *et al.,* 2017; Koh *et al.,* 2024). However, earlier studies investigating TTCC function in urethra predominantly used non-selective inhibitors such as mibefradil and Ni^{2+} (Bradley *et al.,* 2004; Hollywood *et al.,* 2003; Shafei *et al.,* 2003), both of which are now recognised for off-target effects (Blaustein & Lederer, 1999; Brimblecombe & Cragg, 2015; Huang *et al.,* 2015; Li *et al.,* 2019; Pfaffendorf *et al.,* 2000). Drumm *et al.,* (2018) reported spontaneous Ca^{2+} events in male mouse USMC were insensitive to a selective TTCC blocker, TTA-A2. However, TTA-A2 was not tested on PE-induced or EFS-induced contractions to determine whether TTCC inhibition modulate agonist-or nerve-mediated responses.

Therefore, I investigated effects of TTA-A2 on agonist- and EFS-induced contractions in male, and on agonist-induced contraction on female USM. Male and female urethra were precontracted with PE (1 μM) and AVP (10 nM), respectively, followed by application of TTA-A2 (10 μM) (Fig. 5.9 A&B). TTA-A2 had no effect on either male (P=0.9, n=4; Fig. 5.9A&D) or female USM (P=0.7, n=5; Fig. 5.9B&E). Next, I tested TTA-A2 on EFS-evoked contractions in male USM (Fig. 5.9C&F). TTA-A2 failed to affect the amplitude of EFS-evoked contractions at any frequency (n=6, P=0.1 at 1 Hz & P=0.8 at 20 Hz; Fig. 5.9C&F). These findings suggest that TTCC do not modulate agonist-or EFS-evoked contractions in either male or female mouse USM.

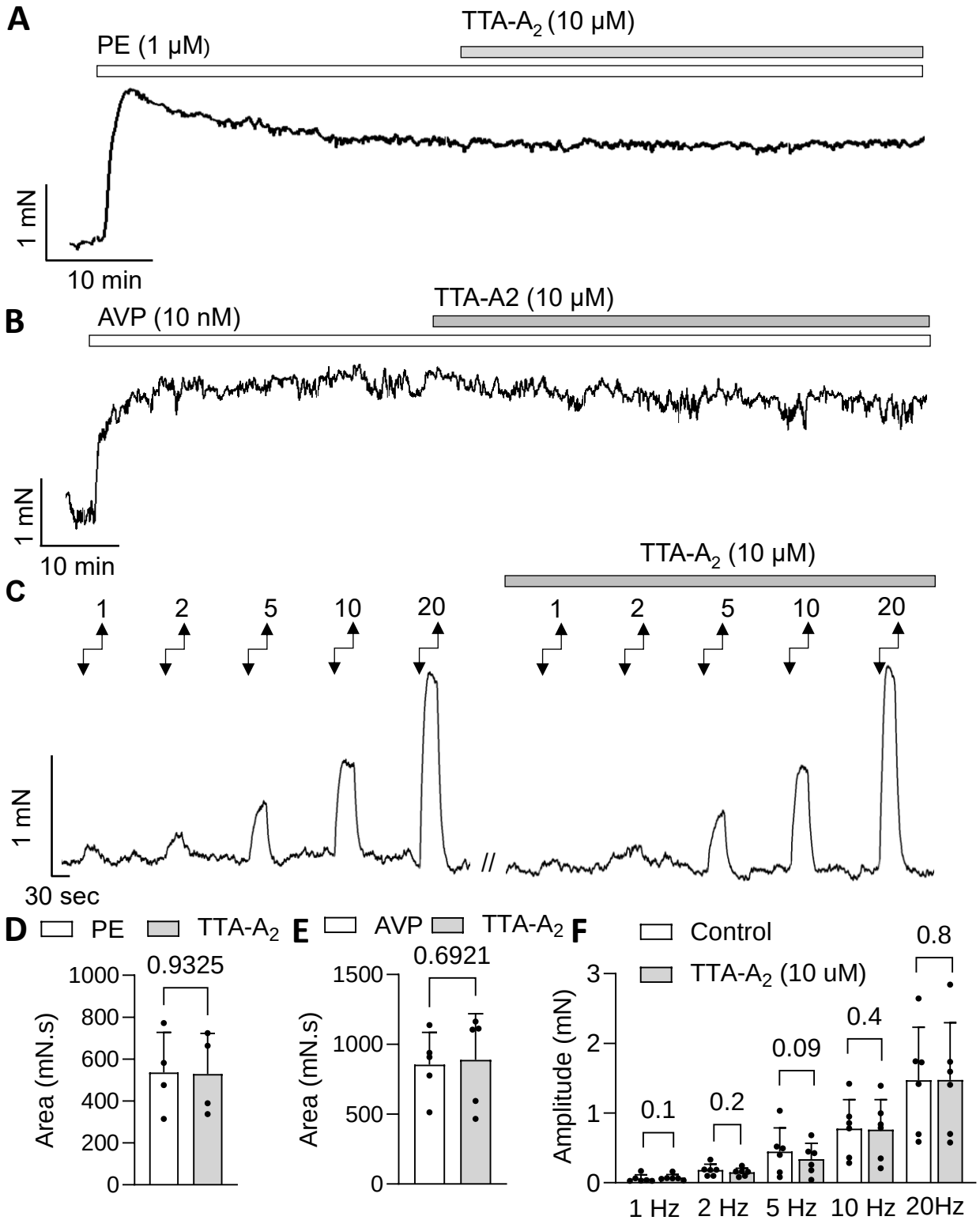

Fig. 5.9: TTCC blocker, TTA-A2 had no effect on agonist/EFS induced contractions in male or female urethra. Representative data shows inhibition of TTCC via TTA-A2 (10 μM) on **A** pre-contracted male USM by PE (1 μM), **B** AVP (10 nM)-induced contractions in female USM, and **C** EFS-evoked contractions in male. Summary effect of TTCC blockade on agonist-induced contraction **D** in male USM (n=4; Paired t-test), **E** female USM (n=5, Paired t-test), and **F** EFS-evoked contractions (n=6; Paired t-test). Double-headed arrows indicate EFS frequency (Hz).

5.2.5 Role of SOCE in murine urethra

Since inhibition of LTCC and TTCC had minimal effects on agonist- or EFS-evoked contractions and did not explain the mechanisms underlying sustained USM tone and contractions in either sex, I next investigated whether Ca^{2+} influx via SOCE contributes to urethral contractility in male and female mice. Orai channels are key mediators of SOCE in SMC, facilitating Ca^{2+} influx following depletion of intracellular Ca^{2+} stores (Potier *et al.,* 2009; Parekh, 2010; Murtazina *et al.,* 2011; Spinelli *et al.,* 2012; Rembetski *et al.,* 2020; Drumm *et al.,* 2018). Previous studies identified Orai-mediated SOCE as the predominant Ca^{2+} entry pathway sustaining USM contractility in male mouse (Drumm *et al.,* 2018). However, effects of Orai inhibition on EFS-evoked responses, which more closely resemble physiological conditions, had not been examined previously in male USM, and the role of Orai channels in contractile activity of female USM also remained unexplored. In our study, I examined the role of Orai channels in male and female urethra using two inhibitors GSK-7975A (inhibits Orai1, Orai2 and slightly inhibit Orai3; Zhang *et al.,* 2020) and Synta66 (inhibits Orai1 and potentiates Orai 2; Zhang *et al.,* 2020).

Tissues were exposed to GSK-7975A, and the effects on both agonist-concentration dependent responses, and resting basal tone were assessed (Fig. 5.10 A,B&C). GSK-7975A (10 μM) significantly reduced AUC of PE response curves from 100 nM onwards (Fig.5.10A,B&D). For instance, at 300 nM PE, AUC was reduced from 253.3 ± 168.7 to 76.4 ± 44 mN.s (n=3, P<0.0001) and at 10 μM PE, AUC was reduced from 763.9 ± 200.9 to 277.7 ± 117.3 mN.s (n=3, P<0.0001), see Fig. 5.10D. Application of GSK-7975A also caused a rightward shift in the PE concentration response curve, increasing EC_{50} from 1.05 μM to 4.3 μM (n=3, P<0.0001; Fig. 5.10D), indicating that Orai channel inhibition reduces the sensitivity of murine USM to PE. However, basal tone remained unaffected in response to GSK-7975A (n=6, P=0.9; Fig. 5.10E).

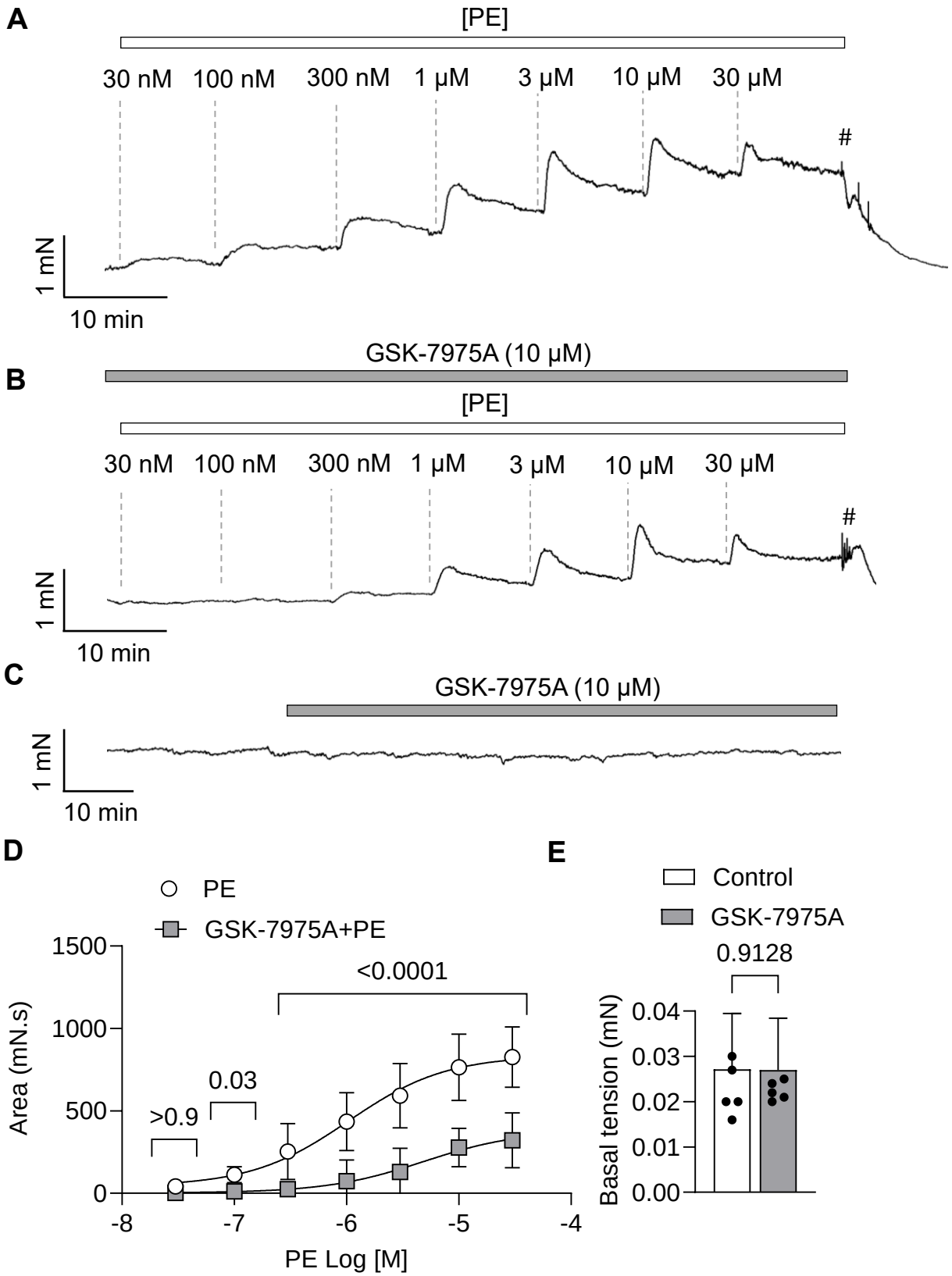

Fig 5.10: Orai channel inhibitor GSK-7975A reduces PE dose response curves but does not affect basal tone in male urethra. Representative data showing responses induced by increasing PE concentrations (30 nM - 30 μM) **A** in the presence of no drugs **B** in the presence of GSK-7975A (10 μM). **C** Representative trace showing application of GSK-7975A (10 μM) on basal tone**.** Summary effects of GSK-7975A on PE dose responses curves, **D** (n=3; Two-way ANOVA, Bonferroni's test), and **E** on basal tone (n=6; Paired t-test). (# represents washing).

I tested effects of GSK-7975A on neurally-evoked contractions in male urethra. I applied EFS (1, 2, 5, 10, 20 Hz), before and after incubation with GSK-7975A (10 μM) followed by 2-APB (Fig.5.11A). GSK-7975A attenuated the amplitude of higher frequencies EFS responses almost by half (n=13; Fig.5.11A&C), for example at 10 Hz, GSK-7975A reduced amplitude by 50% (0.6 ± 0.3 to 0.3 ± 0.2 mN; P=0.002) and at 20 Hz, amplitude was reduced by 46% (1.1 ± 0.5 to 0.6 ± 0.2 mN; P<0.0001). 2-APB abolished all remaining EFS contractions (Fig. 5.11A), suggesting residual contractions were dependent on Ca^{2+} release from intracellular stores.

Previous studies in airway SM reported that simultaneous blockade of Orai and LTCC suppresses a greater proportion of excitatory contractions than inhibition of either channel alone (Dwivedi *et al.,* 2023). To test if a similar mechanism operates in USM, I examined effects of GSK-7975A on EFS-evoked responses in male USM following LTCC block. As observed previously, nifedipine (1 μM) did not affect EFS responses (n=6, P>0.1 at all frequencies; Fig. 5.11B&D). However, GSK-7975A (10 μM) caused a slightly greater reduction in amplitude of higher frequencies EFS responses when LTCC were blocked (Fig. 5.11B&D). For example, at 10 Hz, GSK-7975A reduced EFS amplitude by 62.1% (P=0.01), and at 20 Hz by 58.3% (P=0.007) (Fig. 5.11D). Although the proportional reduction in contraction amplitude produced by Orai blockade appeared slightly greater (~12%) when LTCC were blocked, direct statistical comparison revealed that this difference was not significant (P=0.6 at 10 Hz, P=0.7 at 20 Hz, summary graph not included) in comparsion to when LTCC were not blocked.

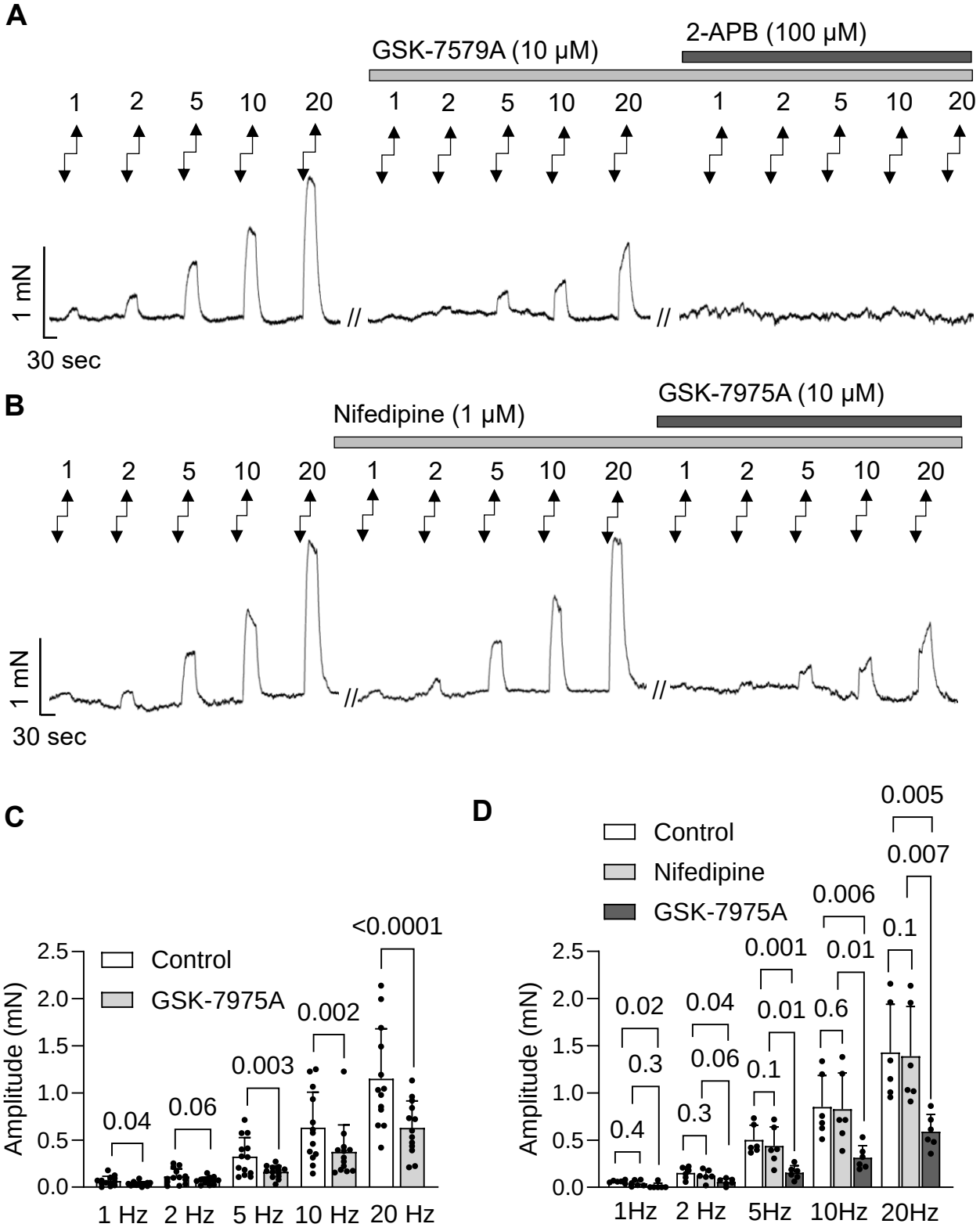

Fig 5.11: Orai channel inhibitor GSK-7975A reduces EFS-evoked contractions in male USM. A Representative trace of EFS-induced contractions in male USM under control conditions, followed by incubation with GSK-7975A (10 μM) and 2-APB (100 μM). **B** Representative EFS responses under control conditions, followed by application of nifedipine (1 μM) and GSK-7975A (10 μM). **C** Summary effects of Orai inhibition on EFS-induced contractions (n=13; Paired t-test). **D** Summary effects of nifedipine followed by GSK-7975A (n=6; One-way ANOVA, Tukey's test). Double-headed arrows indicate EFS frequency (Hz).

I then tested the reverse approach: Orai channels were first inhibited with GSK-7975A (10 μM), and EFS responses were recorded, followed by LTCC blockade with nifedipine (1 μM) (n=13; Fig. 5.12A&C). GSK-7975A significantly reduced the amplitude of EFS-induced contractions from 5 Hz onwards (Fig. 5.12A&C). For instance, at 5 Hz, the mean amplitude decreased from 0.3 ± 0.2 mN to 0.1 ± 0.06 mN (a reduction of 53%, P=0.009), which was further reduced by 26.6% (P=0.002) following nifedipine. At 20 Hz, GSK-7975A decreased mean contraction amplitude from 1.1 ± 0.5 to 0.6 ± 0.2 mN (45.4%, P<0.0001), and nifedipine produced a further 25.8% reduction (P<0.0001). A similar pattern was observed when the same protocol was repeated using another Orai channel blocker, Synta66 (10 μM, n=6; Fig. 5.12B&D). At 5 Hz, Synta66 reduced the mean amplitude of EFS-induced contractions from 0.55 ± 0.1 to 0.25 ± 0.1 mN (54.5%, P=0.008), followed by a further 24% reduction upon nifedipine treatment. At 20 Hz, Synta66 decreased the mean amplitude from 2 ± 0.3 to 1.1 ± 0.3 mN (44.3%, P<0.0001), with an additional 42.8% decrease (P=0.001) after LTCC blockade. These findings indicate that blockade of Orai channels by two different inhibitors GSK-7975A and Synta66 exerts similar effects to EFS-induced responses in male mouse USM. However, Orai inhibition by either inhibitor unmasked a compensatory role of LTCC in sustaining contractile activity.

I also tested the same protocol of EFS with Ani9 (3 μM) instead of nifedipine to see if ANO1 channels modulates nifedipine sensitive EFS responses (n=6; Fig. 5.13A). Unlike nifedipine, Ani9 failed to elicit any response when Orai channels were blocked (P=0.8 at 1 Hz, P=0.2 at 2-20 Hz, Fig. 5.13A&B), suggesting that LTCC activity is independent of ANO1 channel modulation in male mouse USM. This also indicates that inhibition of residual contractions observed after GSK-7975A treatment was entirely due to LTCC blockade and not a time-dependent effect of GSK-7975A. The presence of residual EFS-induced contractions after combined Orai and LTCC blockade prompted us to examine if they were mediated by TTCC activity. TTA-A2 (10 μM) was applied following Orai and LTCC inhibition during EFS-induced contractions (Fig. 5.14A). TTA-A2 had no further effect on residual contractile amplitude (n=6, P>0.5 at all frequencies; Fig. 5.14A&B), indicating TTCC do not contribute to these contractions.

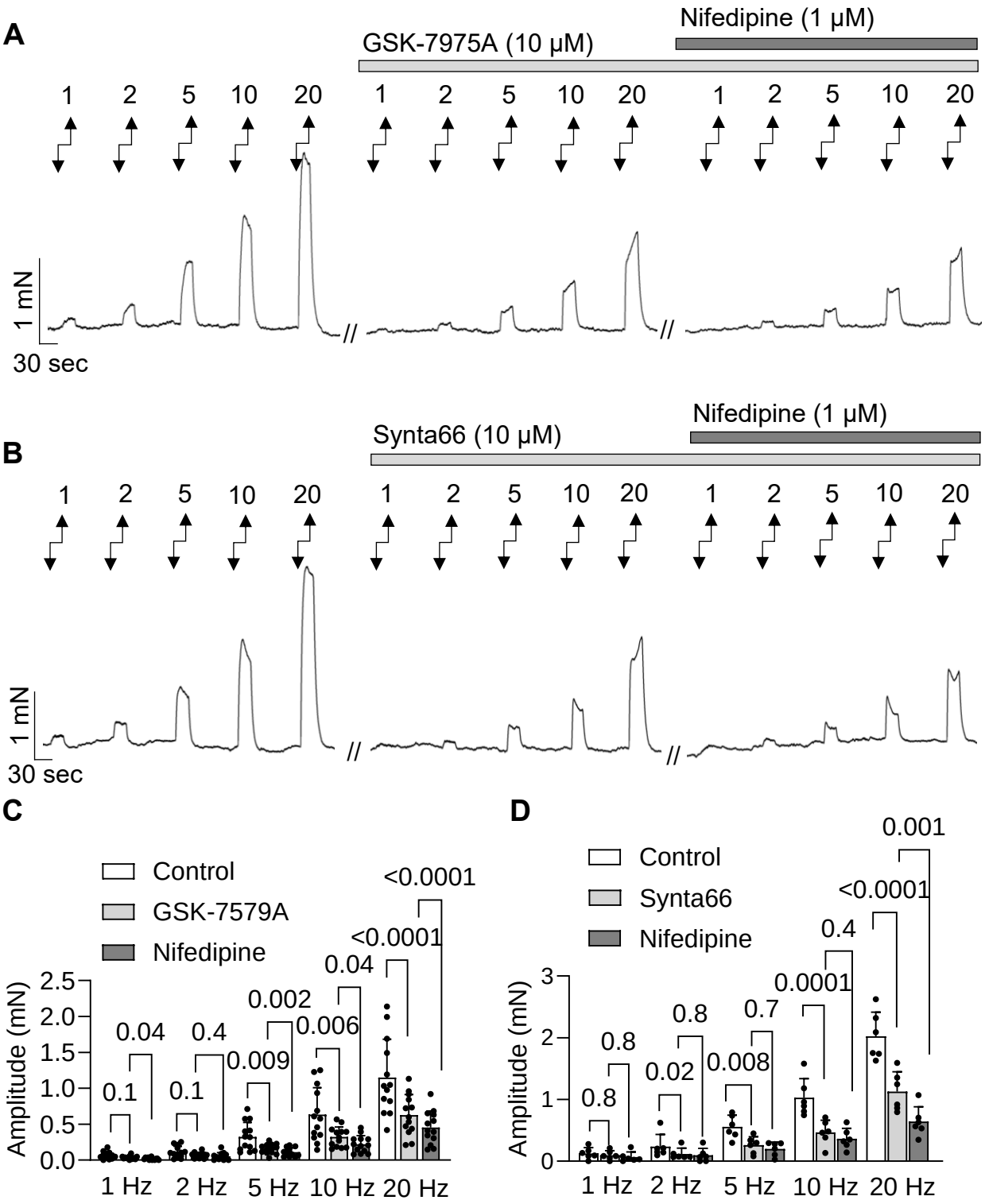

Fig. 5.12: LTCC inhibition reduced the higher frequencies of EFS responses when Orai channels were blocked in male USM. Representative traces of EFS-induced responses under control conditions followed by incubation with **A** GSK-7975A (10 μM) or **B**, Synta66 (10 μM), and subsequent addition of nifedipine (1 μM). Summary effects of nifedipine on EFS-induced contractions when Orai channels were inhibited by **C** GSK-7975A (n=13; One-way ANOVA, Bonferroni's test), and **D** Synta66 (n=6; One-way ANOVA, Bonferroni's test). Double-headed arrows represents EFS frequency (Hz).

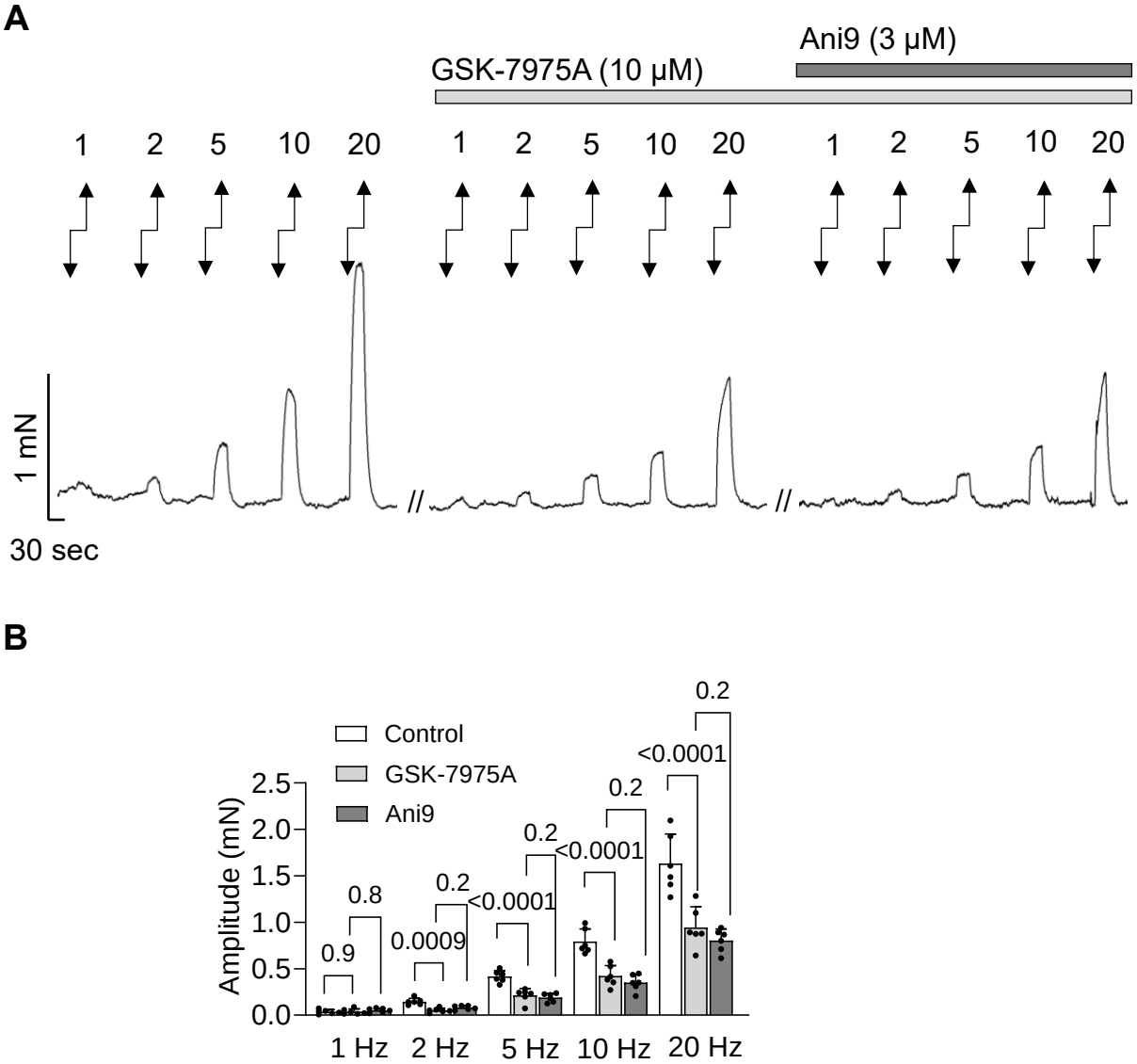

Fig. 5.13: ANO1 inhibition, unlike LTCC inhibition had no effect on EFS-induced contractions in the presence of Orai channel inhibitor in male USM. Representative traces shows EFS-induced contractions in the presence of **A**, no drugs followed by GSK-7975A (10 μM), and subsequent addition of Ani9 (3 μM). **B** Summary data showing the effects of Ani9 in presence of Orai inhibitor (n=6; One-way ANOVA, Bonferroni's test). Double-headed arrows represents EFS frequency (Hz).

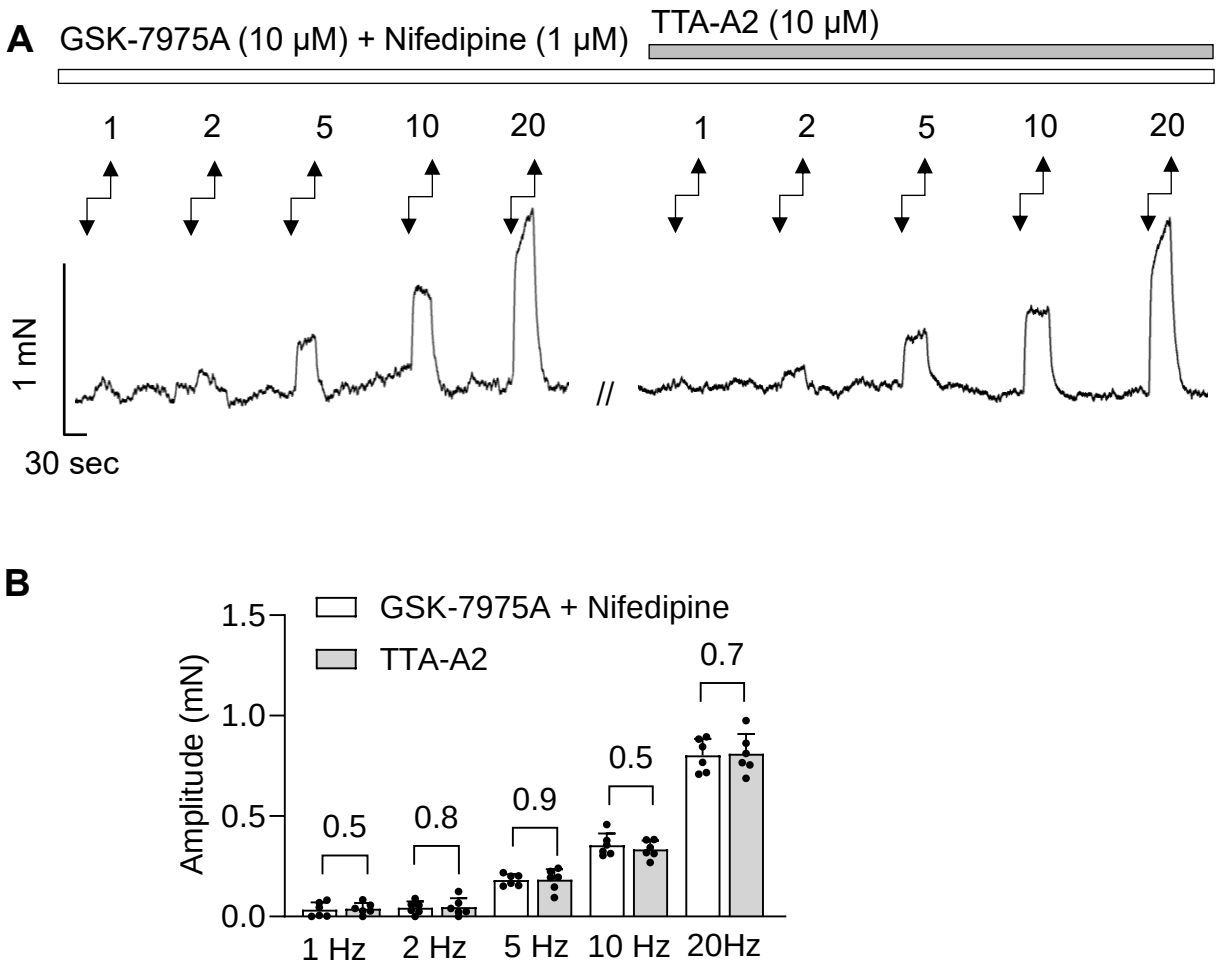

Fig. 5.14. Selective TTCC blocker TTA-A2 shows no effect on residual EFS-evoked contractions after blockade of LTCC and Orai channels in male urethra. **A** Representative trace showing the effect of TTA-A2 (10 μM) in the presence of GSK-7975A (10 μM) and nifedipine (1 μM). **B** Summary data showing the effects of TTA-A2 in the presence of GSK-7975A and nifedipine (n=6; Paired t-test). Double-headed arrows represents EFS frequency (Hz).

Next, I examined effects of Orai channel inhibition on PE-induced contractions at its EC_{50} concentration (1 μM) with Synta66 (10 μM) and GSK-7975A (10 μM), to compare the proportion of inhibition of PE-induced contractions (Fig. 5.15A&B). I also assessed whether subsequent LTCC blockade with nifedipine (1 μM) further attenuated PE-induced contractions after blockade of Orai channels by GSK-7975A (Fig. 5.15B&D). Synta66 inhibited PE-induced contraction AUC from 914.8 ± 293.8 to 251.5 ± 234.2 mN.s (72.5%, n=5, P=0.001; Fig 5.15A&C). Similarly, GSK-7975A decreased PE-induced contraction AUC from 506.1 ± 334.6 to 110.7 ± 100.3 mN.s (78.1%, n=5, P=0.004; Fig 5.15B&D). The inhibition of PE-induced contractions by GSK-7975A was slightly greater than that observed with Synta66 (by ~6%), and was not statistically significant (P=0.2, summary graph not shown) in male mouse USM. Nifedipine (1 μM) did not affect PE-induced contractions (n=5, P>0.99; Fig 5.15B&D) in the presence of GSK-7975A, suggesting LTCC do not provide compensatory Ca^{2+} influx during agonist-induced contraction once Orai channels are blocked, in contrast to their modest involvement during EFS-evoked responses.

In female USM, Synta66 (10 μM) decreased AVP (10 nM) induced contraction AUC from 1107 ± 153.3 to 587.4 ± 192.1 mN.s (47%, n=6, P<0.0001; Fig. 5.16A&C). GSK-7975A also attenuated AVP induced contractions from 920.8 ± 362 to 317.3 ± 251 mN.s (65.5%, n=5, P<0.0001, Fig 5.16B&D). In female USM, GSK-7975A suppressed AVP-induced contractions ~18% more in comparison to Synta66, which found to be non-significant (P=0.07, summary graph not included). Nifedipine had no additional effect after GSK-7975A on AVP-induced contraction (n=5, P>0.99; Fig 5.16B&D) in female USM. Overall, these data indicate Orai channels play a dominant role in modulating agonist / EFS-induced contractions in male and female USM. Moreover, the inhibitory effects of the Orai channel blockers, GSK-7975A and Synta66 were comparable, with no significant difference observed between them in USM.

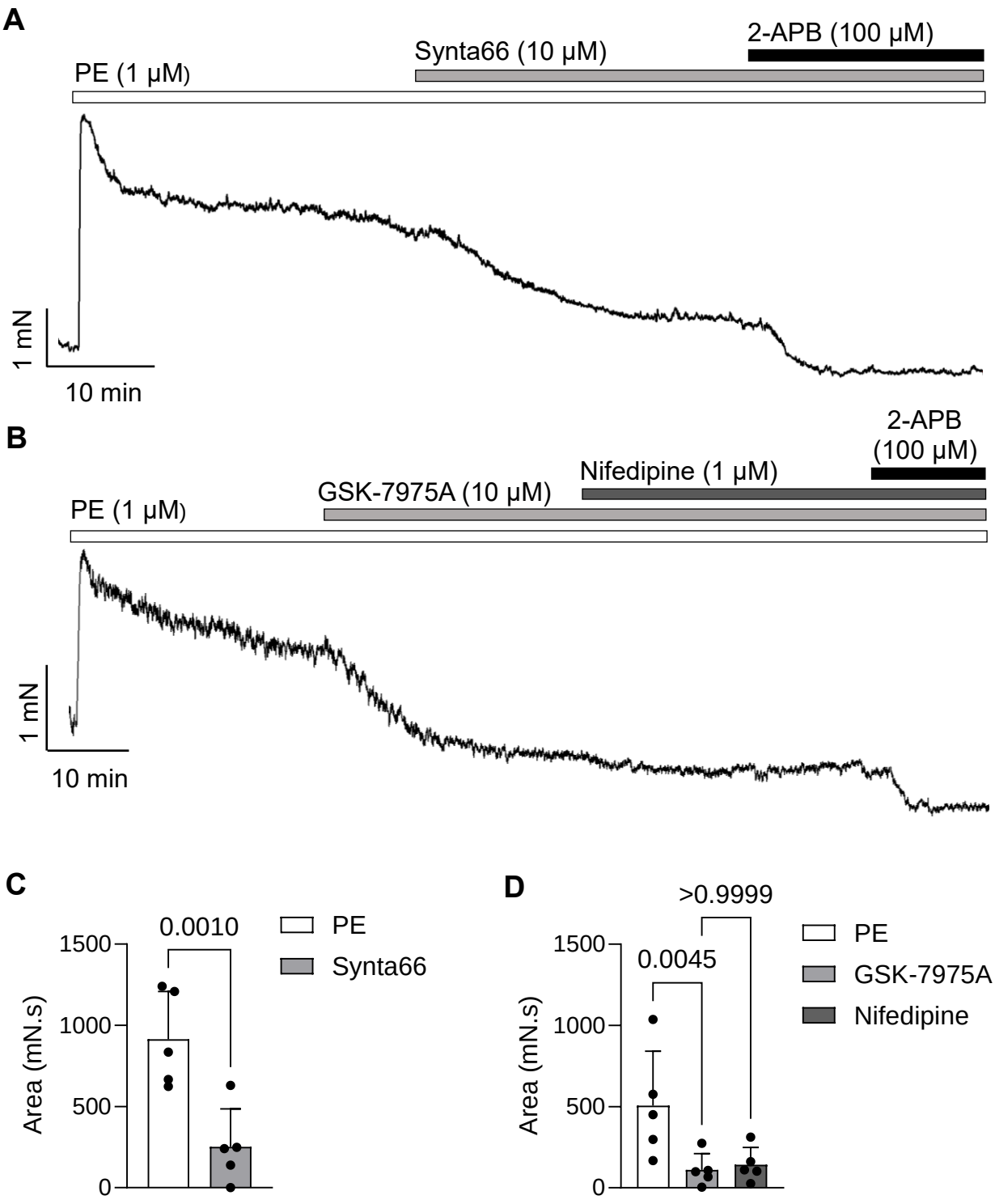

Fig 5.15: Orai channel inhibitor Synta66 and GSK-7975A reduced agonist induced contraction by more than 50% in male USM. A Representative data showing effects of Synta66 (10 μM) and 2-APB (100 μM) on PE (1 μM)-induced contraction. **B** Representative data showing effects of GSK-7975A (10 μM) and nifedipine (1 μM) on PE (1 μM)-induced contraction. Summary data showing the effects of **C** Synta66 (n=5; Paired t-test), and **D** GSK-7975A and nifedipine (n=5; One-way ANOVA, Bonferroni's test) on PE-induced contraction.

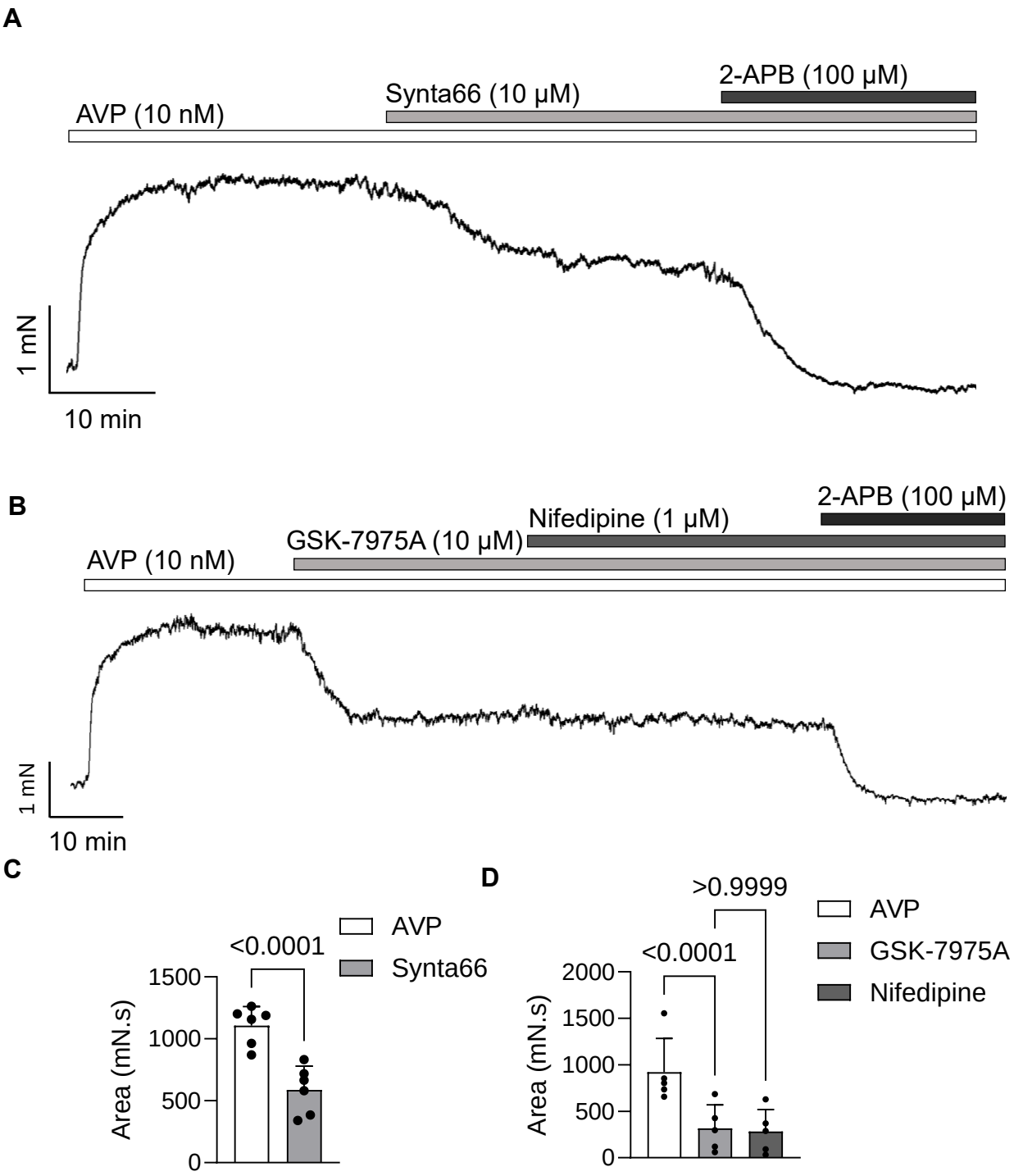

Fig. 5.16. Orai channel inhibition reduces agonist-induced contractions in female urethra. A Representative trace showing the effect of the Orai channel inhibitor Synta66 (10 μM) and 2-APB (100 μM) on AVP (10 nM)-induced contractions **B** Representative trace showing the effects of another Orai channel inhibitor, GSK-7975A (10 μM), followed by the LTCC blocker nifedipine (1 μM) on AVP-induced contractions. Summary data showing the effects of Orai channel inhibition by **C** Synta66 (n=6; Paired t-test), and **D** GSK-7975A followed by nifedipine on AVP-induced contractions (n=6; One-way ANOVA, Bonferroni's test).

Drumm *et al.,* (2018) demonstrated SOCE in male USM using Putney's protocol (Putney, 1986), and identified that Orai-mediated SOCE primarily sustains urethral contractions. However, a similar study was not performed in females. The present study addressed this gap and followed Putney's protocol in female USM, in which SOCE was activated by passive depletion of SR Ca^{2+} by blocking SERCA pumps by thapsigargin (10 μM) while USM strips were incubated in 0 mM Ca^{2+} solution followed by introduction of 2.5 mM Ca^{2+} in the continued presence of thapsigargin, which resulted in tonic contraction (Fig 5.17A). Nifedipine (1 μM) did not impact this sustained contraction (n=4, P=0.7; Fig 5.17A&B) whereas GSK-7975A (10 μM) abolished it (n=4, Fig 5.17A&B). This suggested SOCE in female mouse USM is Orai-dependent and independent of LTCC, similar to male mouse USM (Drumm *et al.,* 2018).

I also examined effects of Orai channel inhibition on spontaneous Ca^{2+} events in male and female USMC using Acta2-GCaMP8.1 mice. Basal spontaneous Ca^{2+} activity was recorded for 30 sec under control conditions, followed by incubation of USM tissue with GSK-7975A (10 μM) for 25 min, after which Ca^{2+} activity was recorded again. GSK-7975A markedly reduced spontaneous Ca^{2+} activity in both male and female USMC. In male USMC, GSK-7975A significantly attenuated Ca^{2+} activity (n=3, c=9; Fig. 5.18A&B), decreasing frequency from 42.8 ± 22.7 to 3.5 ± 5.8 events/min^{-1} (P=0.0007), amplitude from 0.14 ± 0.07 to 0.04 ± 0.06 $\Delta F/F_0$ (P=0.02), duration from 0.23 ± 0.05 to 0.07 ± 0.1 sec (P=0.08), and spatial spread from 26.2 ± 10.9 to 6.8 ± 10.8 μm (P=0.01). In female USMC, GSK-7975A abolished spontaneous Ca^{2+} events (n=4, c=7; Fig. 5.18C&D). This suggests Orai-mediated Ca^{2+} entry is crucial for generating or sustaining these basal Ca^{2+} events in both male and female USM.

A

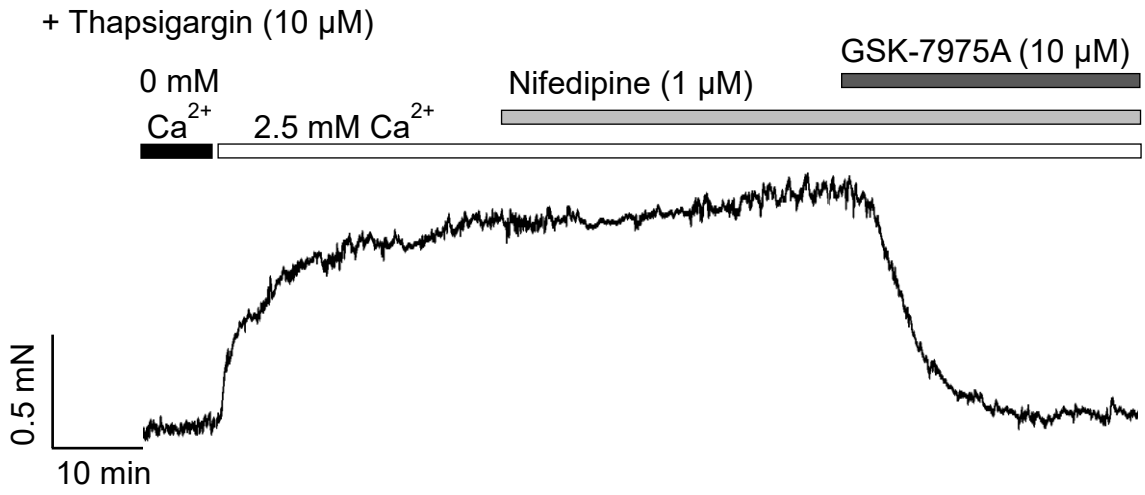

B

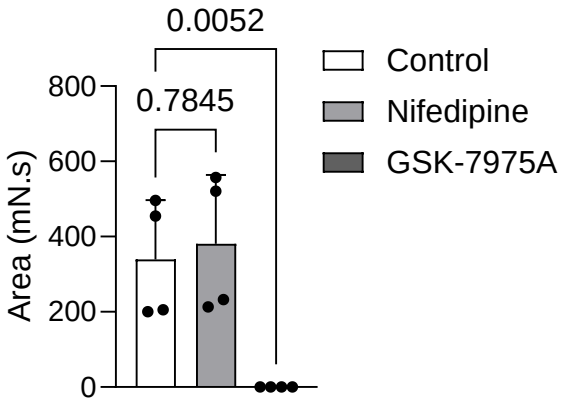

Fig. 5.17: Orai channel inhibitor GSK-7975A abolished Ca^{2+}-induced contraction but not LTCC inhibitor in female urethra. Representative data shows **A** inhibition of LTCC via nifedipine (1 μM), and Orai inhibition via GSK-7975A (10 μM) in the presence of thapsigargin (10 μM) on 2.5 mM Ca^{2+} induced contraction in female (n=4). **B** Summary data showing the effects of nifedipine and GSK-7975A on 2.5 mM Ca^{2+}-induced contraction in female USM (One way ANOVA, Dunnett's test).

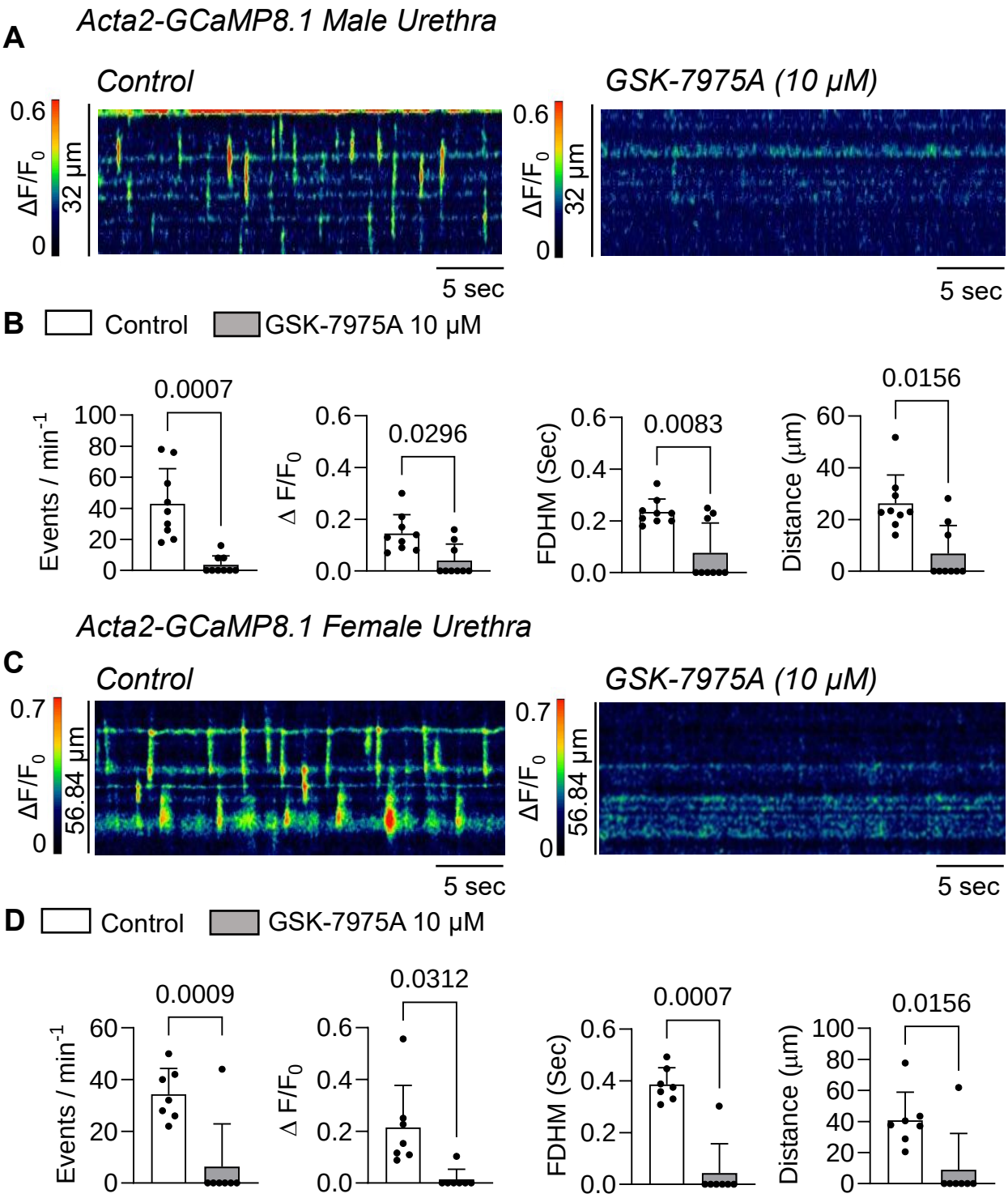

Fig. 5.18: Orai channel blockade effects on basal Ca^{2+} activity in Acta2-GCaMP8.1 USM. Representative traces of spontaneous Ca^{2+} events in control conditions and in the presence of GSK-7975A (10 μM) in **A** male, and **B** female USM. Summary data showing frequency, amplitude, duration and spread of Ca^{2+} events in the presence of control conditions vs GSK-7975A in **C** male USM (n=3, c=9; Paired t-test), and **D** female USM (n=4, c=7; Paired t-test).

5.3 Discussion

The present chapter investigated roles of LTCC, TTCC, and Orai channels in murine USM contractility. This enabled a comparison of relative roles of each channel type in regulating agonist-induced, and neurogenic contractile responses. Importantly, it allowed us to explore potential sex-specific differences in channel function, highlighting how male and female USM may differentially rely on distinct Ca^{2+} entry mechanisms to regulate contractility. Our initial investigation demonstrates the gene expression profile of *Cacna* and *Orai* subtypes in both male and female urethra. Among LTCC subunits, *Cacna1c* displayed highest expression, whereas *Cacna1f* was minimally expressed. Similarly, among *Orai* genes, *Orai1* and *Orai3* predominated. Similar finding was reported earlier in male mouse USM, where *Orai1* and *Orai3* expression was higher (Drumm *et al.,* 2018).

In murine male USMC, nifedipine, nicardipine or israpidine had no significant effect on spontaneous intracellular Ca^{2+} activity (Drumm *et al.,* 2018). Additionally, nifedipine did not affect PE (10 μM)-induced contraction in male USM (Drumm *et al.,* 2018). The present study further demonstrated that despite robust LTCC (Cav 1.2) expression, LTCC inhibition with nifedipine did not alter PE-induced contractions at any concentration tested (30 nM – 30 μM). In addition, nifedipine failed to affect resting basal tone, or EFS-evoked responses in male or agonist response in female mice USM. Taken together, these findings indicate marked species-dependent differences in the functional contribution of LTCC to USM activity. While LTCC clearly contribute to basal tone and agonist-or nerve-evoked contractions in pig urethra (Rembetski *et al.,* 2020), and to Ca^{2+} influx and intracellular Ca^{2+} dynamics in rabbit and human USMC (Bradley *et al.,* 2004; Hollywood *et al.,* 2003; Hashitani & Suzuki, 2007), the present data demonstrate that LTCC play a minimal role in regulating basal tone or contractile responses in mouse USM under the conditions tested. This divergence suggests that although LTCC are expressed in mouse USMC, their activation is either tightly constrained or overridden by alternative Ca^{2+} entry pathways.

Several earlier reports have also questioned the functional contribution of LTCC to urethral contractility. Larsson *et al.* (1984) observed nifedipine did not abolish NA-induced contractions in rabbit urethra. Similarly, oral administration of nifedipine did

not reduce urethral closure pressure in cats (Mawby *et al.,* 1991). Consistent with these findings, nifedipine had little to no effect on human urethral tone both *in vitro* and *in vivo* (Forman *et al.,* 1978). In sheep urethra, nifedipine was approximately 1000 times less effective at inhibiting NA-induced contractions than those triggered by 120 mM high K^+ induced depolarisation (Garcia-Pascual *et al.,* 1991). Similarly, in our study, 60 mM high K^+-induced depolarisation confirmed that LTCC can mediate contraction when activated, as nifedipine abolished these responses in male and female USM. However, high K^+-induced contractions in males were nearly twice as large in AUC and initial amplitude compared to females, suggesting that male USM possess greater functional LTCC than female USM.

Interestingly, LTCC activation with FPL64176 initiated phasic activity superimposed on agonist concentration-dependent contractions in male USM, representing a typical LTCC-mediated Ca^{2+} response characterized by coordinated Ca^{2+} oscillations. Such rhythmic activity is a feature of various SM tissues, including colon (see Fig. 5.4B) and bladder (Drumm *et al.,* 2024). FPL64176 also enhanced EFS-evoked contractions in male USM, and this enhancement was abolished by nifedipine, validating the specificity of the response to LTCC activation. However FPL64176 had no effect on basal urethral tone, aligning with previous studies reported that FPL 64176 had no apparent effect on basal Ca^{2+} signalling in male mice USMC (Drumm *et al.,* 2018). FPL64176 also failed to affect agonist-induced contractions in female USM. This may be attributed to lower LTCC activity in females, as indicated by the high K^+-induced depolarisation experiments, where female tissues exhibited smaller contractions in response to 60 mM K^+ as compared to males.

TTCC regulate SM excitability in several organs, including vascular and GI tissues (Ward *et al.,* 2004; Ono & Iijima, 2005; Park *et al.,* 2006; Bayguinov *et al.,* 2007; Zheng *et al.,* 2014). In rat urethra, TTCC inhibition with Ni^{2+} reduced basal tone (Shafei *et al.,* 2003). Electrophysiological studies in rabbit and human USMC identified TTCC-like currents, which were sensitive to mibefradil or Ni^{2+} (Hollywood *et al.,* 2003; Bradley *et al.,* 2004). However, mibefradil or Ni^{2+} have several off-target effects. Mibefradil inhibits not only TTCC channels but also reported to reduce release of NA from sympathetic nerves, and blocks Orai channels (Pfaffendorf *et al.,* 2000; Li *et al.,* 2019). Ni^{2+} disrupts neurotransmission and intracellular Ca^{2+} homeostasis (Brimblecombe &

Cragg, 2015). In murine male USM, a selective TTCC antagonist, TTA-A2 (Kraus *et al.,* 2010) did not affect intracellular spontaneous Ca^{2+} activity (Drumm *et al.,* 2018). In our study, TTA-A2 also failed to affect agonist-induced contractions in male and female USM. TTA-A2 also did not affect neurally-evoked contractions in male USM. This suggests TTCC do not modulate mouse USM contractions under the conditions tested.

Initially described in non-excitable cells (Putney, 1986), SOCE is now known to occur in excitable SM tissues, including airway, vascular, and GI muscles (Gibson *et al.,* 1998; Quinn *et al.,* 2004; Bradley *et al.,* 2005; Potier *et al.,* 2009; Spinelli *et al.,* 2012; Trebak *et al.,* 2013; Prakriya and Lewis, 2015). The process is mediated by Orai Ca^{2+} channels, which are activated through coupling with the ER / SR Ca^{2+} sensor STIM after store depletion (Liou *et al.,* 2005; Roos *et al.,* 2005; Feske *et al.,* 2006; Zhang *et al.,* 2006; Potier *et al.,* 2009; Soboloff *et al.,* 2012; Zheng *et al.,* 2018). Our investigation revealed a central role of Orai channels in modulating both agonist- and EFS-induced contractions in male USM and agonist contractions in female USM. Inhibition of Orai channels with GSK-7975A or Synta66 significantly reduced contractile amplitude of EFS-induced contractions by ~50%, attenuated agonist-induced contraction in both male by ~75% and female USM by ~65, and caused a rightward shift in the PE concentration-response curve in male USM. This suggests that Orai channels replenishes intracellular Ca^{2+} stores, thereby maintaining IP_3-mediated Ca^{2+} release during agonist-induced contractions in USM.

The residual EFS or agonist-induced contractions after Orai blockade were sensitive to 2-APB in both male and female, indicating that these contractions were primarily mediated by Orai channels and SR Ca^{2+} release. Similar patterns were seen in airway SM, where methacholine-induced Ca^{2+} oscillations were unaffected by nifedipine but were abolished by GSK-7975A, highlighting a predominant role of Orai-mediated Ca^{2+} influx over LTCC activity (Boie *et al.,* 2016). In contrast to mouse, pig USM relies on both LTCC and Orai channels for sustaining contractile activity as, in pig, while nifedipine produced a greater reduction in USM tone as well as agonist- and EFS-induced contractions, GSK-7975A also decreased these parameters by 40-50% (Rembetski *et al.,* 2020), highlighting a species-specific divergence in the relative contribution of LTCC and Orai channels to urethral contractility.

Interestingly, when Orai channels were already blocked, a further reduction in EFS-evoked contractions was observed with nifedipine in males, but not in agonist-induced responses in males or female. At this stage, reasons for the residual LTCC-mediated contribution during neural stimulation are not fully understood, but it may represent a compensatory Ca^{2+} entry pathway that becomes evident once Orai channels are inhibited. However, findings presented in the next chapter helps explain this observation. I also tested ANO1 inhibition following Orai channel inhibition in our EFS protocol. Ani9 had no effect on residual contractions, demonstrating two key points: first that nifedipine-sensitive residual contraction after Orai inhibition was a true LTCC-mediated effect and not a time-dependent effect of GSK-7975A incubation; and second, ANO1 channels do not modulate LTCC activity in murine USM. In addition, TTA-A2 failed to affect residual EFS-induced contractions after blockade of Orai and LTCC, suggesting no role for TTCC in modulating EFS-evoked contractions.

Previous findings in male murine USM reported a primary role of Orai in mediating SOCE and sustaining intracellular spontaneous Ca^{2+} events in USMC (Drumm *et al.,* 2018). The contribution of Orai-mediated SOCE was further confirmed in female USM in the present study, using the Putney protocol (Putney, 1986), where SR depletion-induced tonic contractions were abolished by GSK-7975A but unaffected by nifedipine. Our Ca^{2+} imaging experiments extended these observations, showing near-complete abolition of basal spontaneous Ca^{2+} events in both sexes following Orai blockade, highlighting the channel's critical role in maintaining intracellular Ca^{2+} homeostasis.

In summary, our data establish a primary role of SOCE-mediated by Orai channels and SR Ca^{2+} release in maintaining murine urethral contractions. Sustained urethral contractility requires continuous Ca^{2+} availability to support the contraction of USM bundles. We propose that sustained contraction is maintained through coordinated interactions between SOCE and SR Ca^{2+} release via IP_3Rs and RyRs, with amplification through Ca^{2+}-induced Ca^{2+} release mechanisms (Drumm & Gupta, 2025), see Fig. 5.19. There might be three possible mechanism taking place in USM: first, Orai-mediated SOCE may replenish SR Ca^{2+} stores through SERCA activity, ensuring sufficient SR Ca^{2+} loading to support continuous regenerative release via IP_3R and RyR (Potier *et al.,* 2009; Zheng *et al.,* 2018). Second, Orai-mediated SOCE may directly modulate IP_3R and RyR, amplifying Ca^{2+} release through localized CICR

(Phillips *et al.,* 2023). Third, elevated cytosolic Ca^{2+} levels generated by SOCE may indirectly increase the excitability of SR Ca^{2+} release channels, sensitizing them to spontaneous or triggered release events (Drumm *et al.,* 2015; Laver, 2007; Maxwell & Blatter, 2017). The possible crosstalk between these mechanisms could sustain the tonic urethral contractility (Drumm & Gupta, 2025).

Our findings also raise an intriguing question regarding the apparent inactivity of LTCC in murine USM. Despite their clear expression and ability to respond to pharmacological activation, they contribute minimally to basal, agonist or neurogenic-induced contractions. While LTCC can be activated by depolarisation, for example due to high K^+ solutions, these conditions are rarely achieved under normal physiological function in mouse USM. The lack of LTCC engagement may reflect the absence of sufficient depolarizing drive to activate LTCC under basal conditions. The regulation of membrane potential is primarily regulated by K^+ channels in SMC. Therefore, one plausible explanation is hyperpolarisation of murine USM membrane by K^+ channels, would indirectly inhibit LTCC opening at resting potentials. This aligns with the well-established role of K^+ channels in controlling SM excitability (Herrera *et al.,* 2000; Herrera & Nelson, 2002; Chang *et al.,* 2010; Lifshitz *et al.,* 2011; Stott, Jepps & Greenwood, 2014; Jackson, 2017; Dopico, Bukiya *et al.,* 2018; Sancho & Kyle, 2021). To test this hypothesis, pharmacological modulation of specific K^+ channels, such as BK_{Ca}, Kv7, and K_{ATP}, may reveal whether their activity indirectly suppresses LTCC function in mouse USM. The next chapter therefore investigates the role of these K^+ channels in regulating murine urethral contractility.

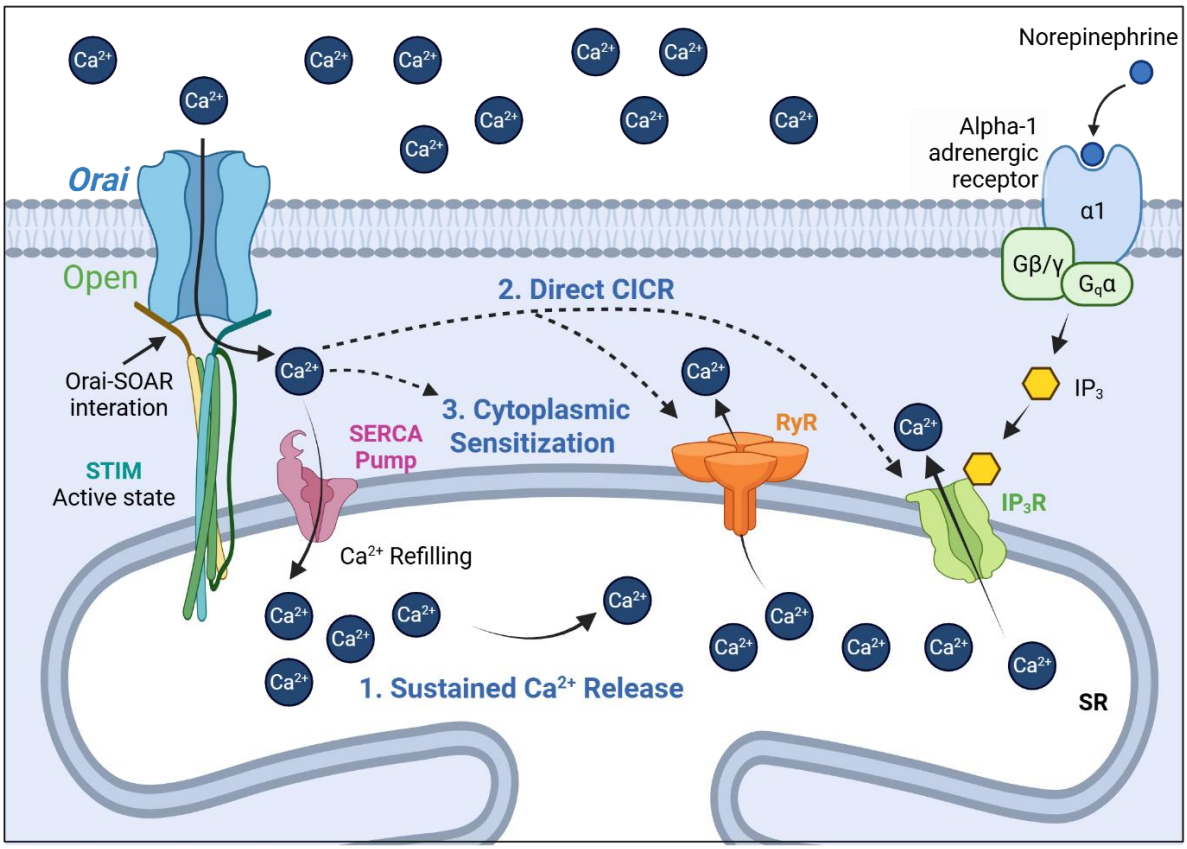

Fig 5.19: Possible mechanisms by which SOCE sustains Ca^{2+} signals and contractions in USMC. Orai-mediated SOCE may enhance USMC contractility through three possible mechanisms: **1.** Refilling SR Ca^{2+} stores via SERCA pumps, allowing sustained Ca^{2+} release through IP_3Rs and RyRs; **2.** Directly initiating or amplifying Ca^{2+} signals from IP_3Rs and RyRs via Ca^{2+}-induced Ca^{2+} release (CICR); and **3.** Elevating cytoplasmic Ca^{2+} to sensitize IP_3Rs or RyRs, promoting their opening in response to localized Ca^{2+} release.

6. Kv7 and BK_{Ca} channels opening limits L-type Ca^{2+} channels activity during G_q-coupled GPCR activation in male mouse USM

6.1 Introduction

Potassium channels (K^+ channels) are fundamental regulators of membrane potential in all cells. In excitable cells, K^+ channels counterbalance depolarizing stimuli through K^+ efflux to maintain cellular excitability and RMP (Edwards & Weston, 1995). Their interplay with LTCC creates dynamic feedback loops that govern contractility across vascular, urinary, and airways SMC (Meredith *et al.,* 2004; Liu, Freyer & Hall, 2007; Dopico *et al.,* 2018).

Voltage-gated K^+ (Kv) channels open with depolarisation, providing negative feedback to stabilize membrane potential (Grizel *et al.,* 2014). Among the Kv channel family, Kv7 channels play a pivotal role in SMC by maintaining resting membrane potential and regulating cellular excitability (Brueggemann *et al.,* 2012; Malysz & Petkov, 2020; Mccallum *et al.,* 2010; Mercer *et al.,* 2025; Stott *et al.,* 2014; Tsai *et al.,* 2020; Tykocki *et al.,* 2018). Kv7 channel inhibition by XE991 induced robust Ca^{2+} oscillations, which were significantly reduced in the presence of Kv7 channel activator, retigabine and nifedipine in rat A7r5 vascular SMC and human internal mammary artery SMC (Tsai *et al.,* 2020). In guinea pig DSMC, application of retigabine induced membrane hyperpolarisation and inhibited spontaneous action potential firing (Afeli, Malysz and Petkov, 2013). In mouse, guinea pig, rat, pig and human DSM, XE991 enhanced spontaneous contractions, whereas retagabine or flupirtine (Kv7 channel activator) suppressed it (Anderson *et al.,* 2013; Rode *et al.,* 2010; Svalø *et al.,* 2013, 2015; Tykocki *et al.,* 2018). These studies provide a mechanistic link between Kv7 channel activation and the inhibition of LTCC activity in SM organs.

Not only Kv7 channels, but also BK_{Ca} (Ca^{2+}-activated-K^+) channels, regulate LTCC activity in SM (Edwards *et al.,* 1994; Hannigan *et al.,* 2016; Hashitani & Brading, 2003; Herrera *et al.,* 2001). In BK_{Ca} knockout ($Slo^{-/-}$) mice there is increased bladder pressure and urine dripping (Meredith *et al.,* 2004). In male rabbit models of partial bladder outlet obstruction, spontaneous contractile activity was enhanced and expression of BK channel α- and β-subunits was significantly reduced in DSM (Chang *et al.,* 2010), suggesting that downregulation of BK channels contributes to the hyperexcitable phenotype observed in partial bladder outlet obstruction. In pig USMC, current-clamp

recordings reveal spontaneous transient hyperpolarisations, which were abolished by iberiotoxin, indicating functional contribution of BK_{Ca} channels (Brading, 2006).

In sheep and rabbit USMC, a large rapid transient outward current followed by multiple components of sustained current occurred under depolarizing pulses (Hollywood *et al.,* 2000; Kyle *et al.,* 2011). The large transient outward current and a component of sustained current was sensitive to BK_{Ca} antagonists such as iberiotoxin and penitrem A; however an additional Ca^{2+}-insensitive, voltage-dependent K^+ current remained (Hollywood *et al.,* 2000; Kyle *et al.,* 2011). Subsequent transcriptional expression studies with different subtypes of Kv family: *Kv1, Kv2, Kv4* and *Kv9* in rabbit urethral strips showed high expression of *Kv2.1, Kv2.2* and *Kv9.3*. Immunolabelling studies further confirmed robust expression of Kv2.1, Kv2.2 and Kv9.3 on isolated rabbit USMC membrane. Kyle *et al.,* (2011) further suggested that these voltage-dependent K^+ currents were likely be Kv2.1 in rabbit USMC, as they were ~70% sensitive to stromatoxin-1, a non-selective Kv channel blocker that inhibits Kv2.1, Kv2.2, Kv4.2, and Kv9.3 (Escoubas *et al.,* 2002; M. Chen *et al.,* 2010). However, when tested on evoked-action potentials, stromatoxin-1 alone had no effect, whereas blockade of BK_{Ca} channels with penitrem A increased action potential amplitude and duration, with subsequent stromatoxin-1 application producing further prolongation (Kyle *et al.,* 2011). Consistently, stromatoxin-1 enhanced spontaneous rabbit USM contraction amplitude only after BK_{Ca} inhibition (Kyle *et al.,* 2011), indicating that BK_{Ca} channels are the primary regulators of membrane hyperpolarisation, while voltage-dependent Kv channels provide a secondary, supportive hyperpolarising influence .

Griffin *et al.,* (2020) detected isolated murine USMC exhibited Ca^{2+} sparks activity which were abolished by ryanodine (Griffin *et al.,* 2020), indicating that these Ca^{2+} sparks events are mediated by RyR in USMC. Kyle *et al.,* (2013) showed that RyR mediated Ca^{2+} release contributes to activation of BK_{Ca} channels in rabbit USMC. They performed perforated patch clamp studies on rabbit USMC, and found that BK currents were inhibited by ryanodine (30 μM), tetracaine (100 μM), caffeine (10 mM) but were unaffected by 2-APB (Kyle *et al.,* 2013). These findings highlights possible involvement of BK_{Ca} in contraining LTCC activity in USM but direct investigation of this is lacking in USM.

Previous studies also reported the role of K_{ATP} channel activity in modulating LTCC. In guinea pig, activation of K_{ATP} channels by cromakalim suppressed the frequency and amplitude of spontaneous contractile activity of DSM in tension studies (Foster *et al.,* 1989; Andersson & Arner, 2004). Electrophysiological studies in guinea pig DSMC revealed that cromakalim and pinacidil induced dose-dependent hyperpolarisations of cell membrane and reduced spontaneous spikes activity (Foster *et al.,* 1989; Seki *et al.,* 1992). In addition, pinacidil effects were reversed with glibenclamide (K_{ATP} inhibitor) in guinea pig DSMC (Seki *et al.,* 1992). In pig urethra, levcromakalim induces relaxation and hyperpolarisation of USMC, both reversed by glibenclamide, suggesting K_{ATP} channels regulate tone (Teramoto & Brading, 1996). Consistently, in pig, pinacidil suppressed urethral myogenic tone by ~85% and EFS-induced contractions by ~65%, which was also sensitive to nifedipine (~70% inhibition), supporting the role of K_{ATP} channels in modulating LTCC activity in urethra (Rembetski *et al.,* 2020).

Although Kv7 channels have been extensively studied in bladder, their functional role in the urethra remains unexplored. While voltage-dependent K^+ currents have been described in rabbit USMC and attributed to Kv2.1 channels (Kyle *et al.,* 2011), the presence and functional role of Kv7 channels in USM remain unexplored. Similarly, roles of BK_{Ca} and K_{ATP} channels in the urethra, particularly in the mouse, have been understudied. Findings from Chapter 5 demonstrated LTCC inhibition does not affect basal or agonist- or EFS-induced responses in mouse urethra, despite LTCC being functionally expressed as they could be activated by LTCC activators or by high K^+ solution-induced membrane depolarisation. We hypothesised that the apparent lack of LTCC involvement in USMC activity reflects an insufficient depolarizing drive, potentially arising from the activity of multiple K^+ channel activity in the mouse urethra. This chapter therefore examines the contribution of BK_{Ca}, Kv7 and K_{ATP} to murine urethral contractility.

6.2 Results

6.2.1 Effect of Kv7 and BK_{Ca} inhibition in male mouse USM

To investigate if K^+ channel opening constrains LTCC-mediated activity in USM, I first investigated effects of Kv7 and BK_{Ca} inhibition on agonist-induced contractions in male USM, given that LTCC blockade had no effect in the previous chapter. XE991 (10 µM) or iberiotoxin (300 nM) were first applied on pre-contracted (PE, 1 µM) male USM (Fig 6.1A&B). Blockade of Kv7 channels with XE991 or BK_{Ca} channels with iberiotoxin produced no effect when applied individually on PE-induced contractions (n=6; Fig.6.1A&B). However, combined application of XE991 and iberiotoxin resulted in occurrence of phasic contractions superimposed on the sustained PE-induced contraction, while having minimal or no effect on PE baseline (Fig. 6.1A&B). The mean amplitude of phasic contractions that occurred after combined blockade of Kv7 and BK_{Ca} by XE991 and iberiotoxin (Fig. 6.1A&B) were 0.5 ± 0.2 mN (n=6; Fig. 6.1A&C) and 0.4 ± 0.2 mN (n=6; Fig. 6.1B&D), respectively. Mean frequency of these phasic contractions were 5.3 ± 1.3 contractions/min^{-1} (n=6; Fig. 6.1A&C) and 6.23 ± 2.21 contractions/min^{-1} (n=6; Fig. 6.1B&D), respectively. These phasic contractions induced by combined application of XE991 and iberiotoxin (Fig. 6.1A&B) were abolished by nifedipine (1 µM) (n=6, P<0.0001; Fig. 6.1A-D), indicating dependence on Ca^{2+} influx through LTCC. Application of XE991 (n=6, P=0.7; Fig. 6.2A&D) or iberiotoxin (n=7, P=0.06; Fig. 6.2B&E) individually, or in combination, produced no detectable effect on basal tone of male (n=7, P=0.6; Fig. 6.2A-F), suggesting that these channels likely influence USM contractility only under conditions of agonist stimulation.

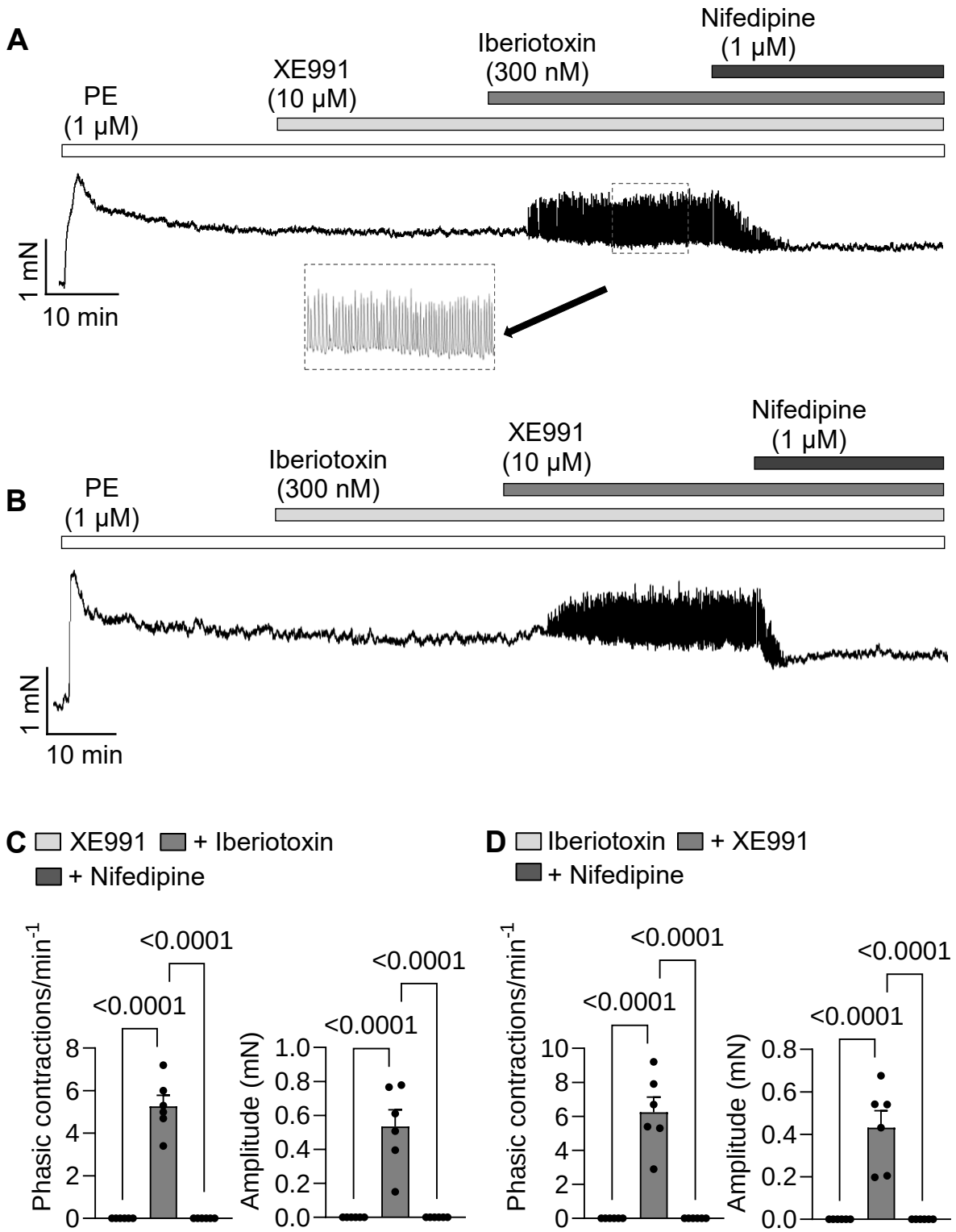

Fig 6.1: Blockade of Kv7 and BK_{Ca} channels leads to initiation of phasic contractions in pre-contracted male USM. Representative data showing the effects of **A.** XE991 (10 μM) followed by iberiotoxin (300 nM) on pre-contracted male USM with PE (1 μM). This combination led to occurrence of phasic contractions that were abolished by nifedipine (1 μM). **B** This also occurred when XE991 and iberiotoxin were applied in reverse order **C & D** Summary of amplitude and frequency of phasic contractions in the presence of combination of XE991 and iberiotoxin and subsequent effects of nifedipine (n=6; One way ANOVA, Bonferroni's test). Dotted boxes showing the enlarged view of the phasic contractions.

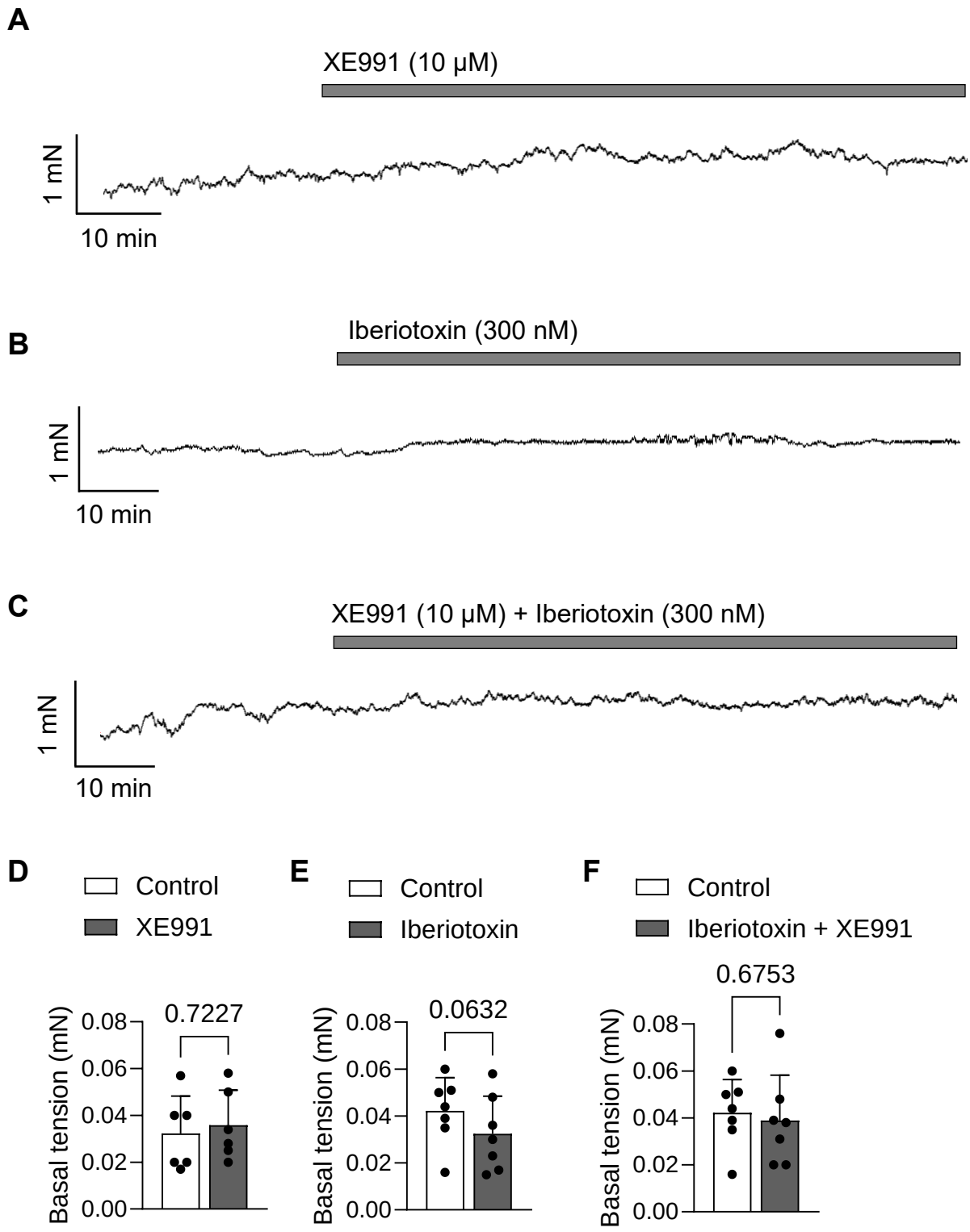

Fig 6.2: Inhibition of Kv7 and BK_{Ca} channels individually or in combination does not affect basal tone in male USM. Representative data showing the effects of **A.** XE991 (10 μM) or **B** iberiotoxin (300 nM) or **C** combination of XE991 (10 μM) and iberiotoxin (300 nM) on basal tone. Summary of basal tone under control conditions vs in the presence of **D** XE991 (n=6) or **E** iberiotoxin (n=7) or **F** combination of XE991 and iberiotoxin (n=7) in male USM (Paired t test).

Next, I investigated the role of Kv7 and BK_{Ca} channels on EFS-induced contractions. Male USM were contracted using EFS (1 - 20 Hz), followed by incubation with XE991 (10 µM) and repetition of EFS (Fig. 6.3A). XE991 alone did not affect EFS-induced contractions (n=6, P>0.3 at all frequencies, Fig. 6.3A&B). Subsequent incubation with iberiotoxin (300 nM), significantly increased amplitude of contractions at 10 Hz from 0.8 ± 0.4 to 1 ± 0.5 mN (37.1%, P= 0.02) and 20 Hz, from 1.5 ± 0.7 to 2 ± 0.9 mN (33.6%, P=0.0005) (n=6; Fig. 6.3A&B). The enhanced contractions displayed phasic occurrences superimposed on top of each EFS response, clearly seen in the enlarged panel in Fig. 6.3A. Increases in amplitude and phasic occurrences were abolished by nifedipine (1 µM) (n=6, P=0.005 at 10 Hz & P=0.0006 at 20 Hz; Fig. 6.3A&B), with amplitude of EFS-induced contractions returning to control levels (n=6, P>0.05).

I then performed the experiment in reverse order to evaluate effects of BK_{Ca} inhibition first. EFS was applied under control conditions, followed by application of iberiotoxin (300 nM), and repetition of EFS, which resulted in enhanced EFS-response amplitude at 10 Hz from 1 ± 0.1 to 1.3 ± 0.2 mN (29.4%, P= 0.01) and 20 Hz from 1.8 ± 0.3 to 2.3 ± 0.4 mN (26%, P<0.0001) in male USM (n=7; Fig. 6.4A), indicating that BK_{Ca} channels provide the primary restraint on depolarisation and contractile force. Subsequent incubation with XE991 and repetition of EFS caused a further significant increase in contraction amplitude at 20 Hz by 11.6% (P=0.004), and phasic contractions now appeared superimposed on top of all EFS-responses (Fig.6.4A&B). Nifedipine (1 µM) abolished both the enhancement and phasic activity (P<0.0001; Fig.6.4A&B). Together, this data suggests BK_{Ca} and Kv7 channels synergistically limit excitability in male USM by suppressing LTCC-mediated Ca^{2+} influx.

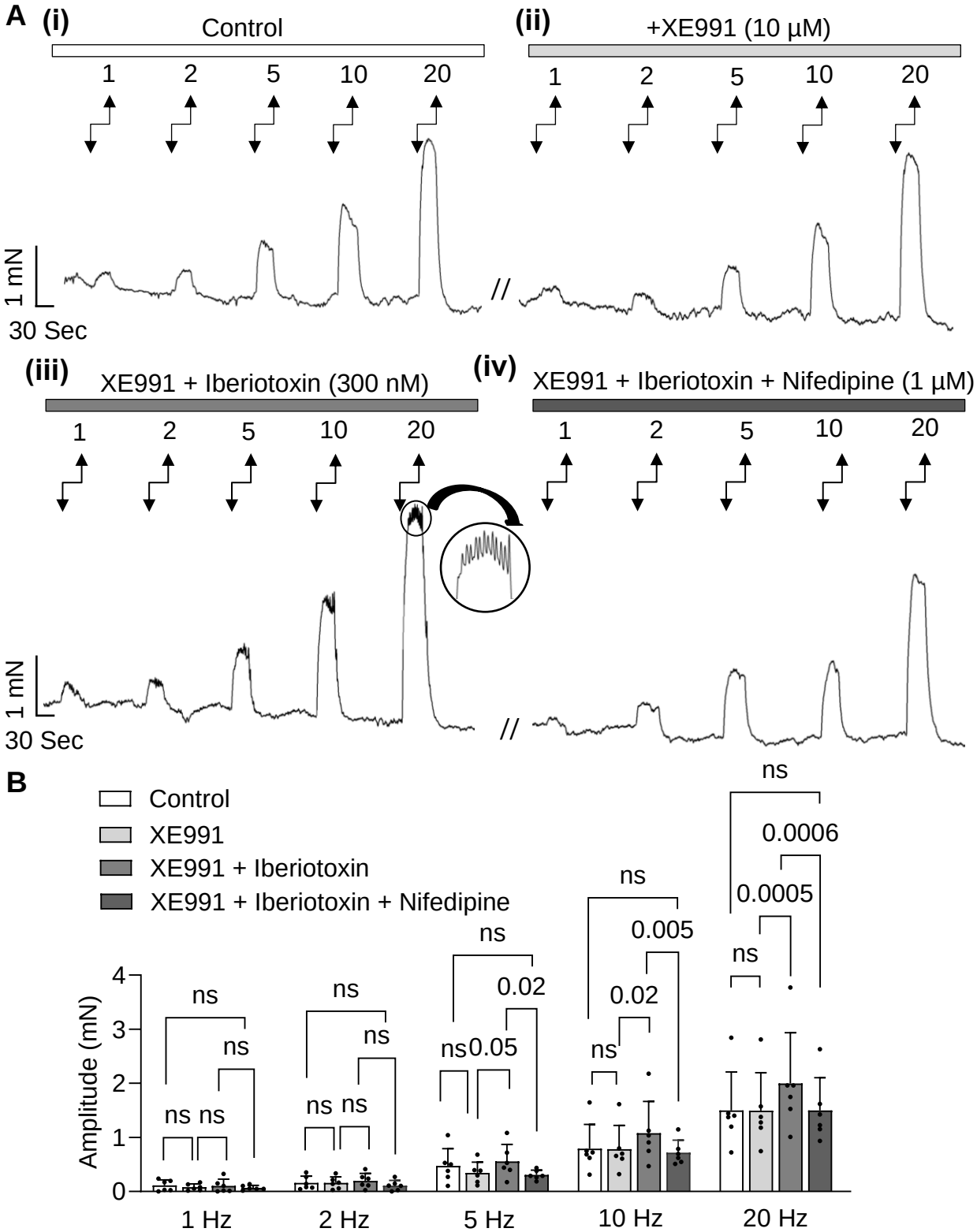

Fig. 6.3: Inhibition of Kv7 and BK_{Ca} channels increases the amplitude and initiates phasic contractions on top of EFS contractions, which are sensitive to nifedipine. Representative traces show EFS-evoked contractions **A (i)** under control conditions, **(ii)** followed by 10 µM XE991, which had shown no effects to EFS-evoked contractions, **(iii)** subsequent addition of 300 nM iberiotoxin, which increased the amplitude and initiated phasic contractions on top each EFS-induced contractions, and **(iv)** addition of 1 µM nifedipine, which reversed the effect of XE991 and iberiotoxin. **B.** Summary data showing effects of control, XE991 followed by iberiotoxin and subsequent effect of nifedipine (n=6, ns=P > 0.05, One way ANOVA, Tukey's post hoc test). ns=P > 0.05.

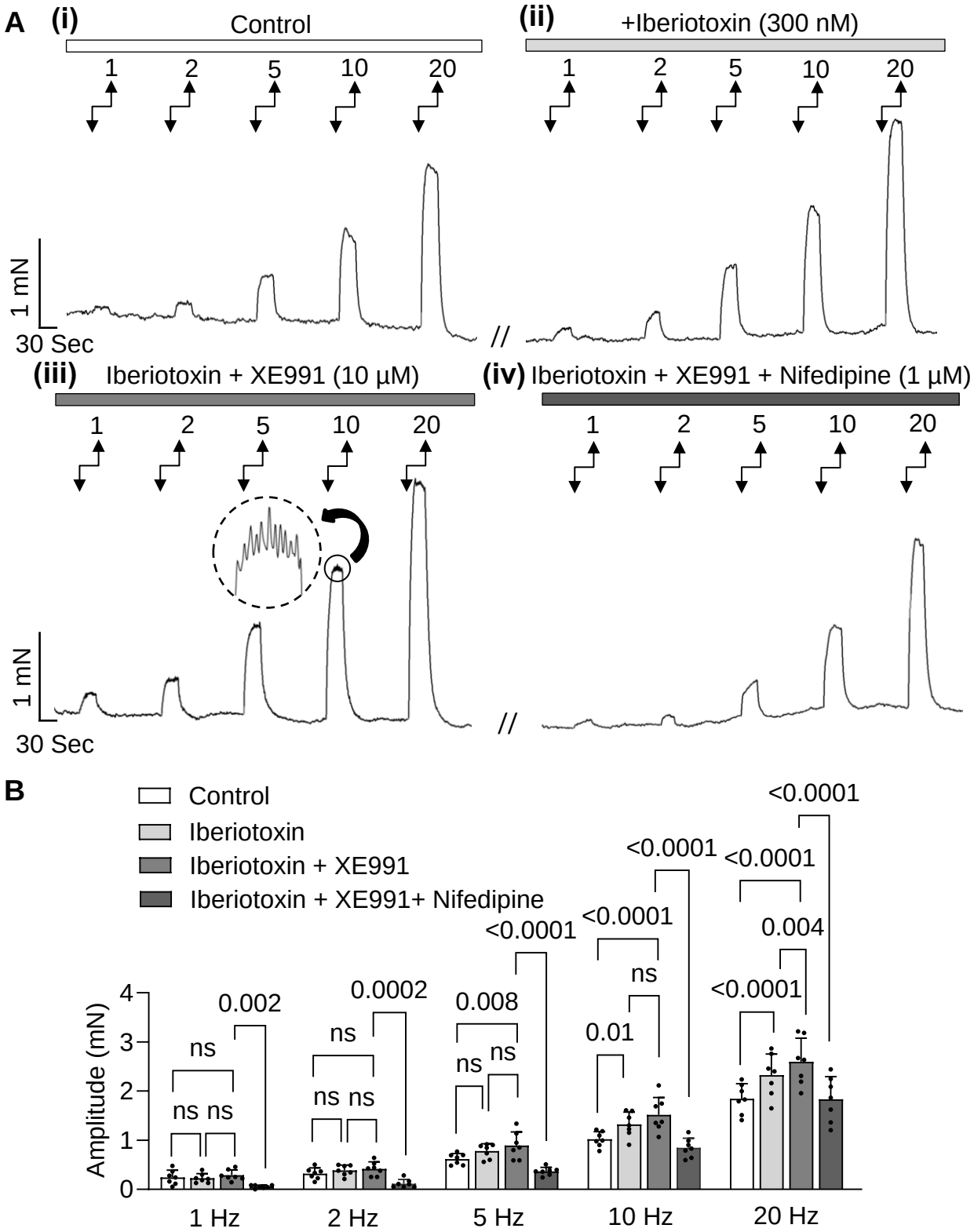

Fig. 6.4: Inhibition BK_{Ca} channels increases the amplitude and inhibition of Kv7 and BK_{Ca} together initiates phasic contractions on top of EFS contractions, which are sensitive to nifedipine. Representative traces show EFS-evoked contractions **A (i)** under control conditions, **(ii)** followed by 300 nM iberiotoxin, which enhanced the amplitude of EFS-evoked contractions, **(iii)** subsequent addition of 10 μM XE991 initiated phasic contractions on top each EFS-induced contractions, and **(iv)** addition of 1 μM nifedipine reversed the effect of iberiotoxin and XE991. **B.** Summary data showing effects of control, iberiotoxin followed by XE991 and subsequent effect of nifedipine (n=7; One way ANOVA, Tukey's test). ns=P>0.05. Dotted circle showing the enlarged view of the phasic contractions.

Next, I explored the effects of Kv7 and BK_{Ca} inhibition on Ca^{2+} activity in USMC using *in situ* Ca^{2+} imaging in male Acta2-GCaMP8.1 mice (Fig. 6.5-6.9). Ca^{2+} activity was recorded for 30 sec using a 40x objective under three conditions: 1. PE (1 µM), 2. PE with XE991 (10 µM) and iberiotoxin (300 nM), and 3. PE with XE991, iberiotoxin, and nifedipine (1 µM), each following 25-30 min of incubation (Fig. 6.5-6.9). The spontaneous intracellular Ca^{2+} activity in murine USMC was asynchronous with individual USMC firing at different time as also discussed in previous chapters 4 & 5. The summated asynchronous spontaneous intracellular Ca^{2+} activity in USMC help urethra in tone generation (Drumm *et al.,* 2018). Incubation with PE increased spontaneous intracellular Ca^{2+} activity in USMC, while the activity remained asynchronous, also previously described in Drumm *et al.,* 2018. In the present study, I observed that in the continued presence of PE, combined incubation with XE991 and iberiotoxin converted these asynchronous intracellular Ca^{2+} events into coordinated, synchronous intercellular Ca^{2+} activity that propagated across muscle bundles. During coordinated Ca^{2+} activity, the tissue exhibited vigorous rhythmic / phasic contractile pattern. In some USM preparations, coordinated contractions were associated with uniform Ca^{2+} waves originating from a focal site within the FOV and spreading to neighbouring bundles, whereas in other tissues, coordinated Ca^{2+} activity appeared as Ca^{2+} flashes occurred within individual muscle bundles. Subsequent addition of nifedipine abolished the coordinated Ca^{2+} activity, restoring asynchronous, non-coordinated intracellular Ca^{2+} events in all USM tissues.

Analysing these data was challenging, as Ca^{2+} activity shifted from asynchronous events during PE alone to coordinated Ca^{2+} activity when Kv7 and BK_{Ca} channels were blocked in the presence of PE. During coordinated activity, the tissue contracted vigorously with large Ca^{2+} waves propagating across the FOV, followed by a return to asynchronous activity upon addition of nifedipine. Therefore, I employed a different analytical approach, marking 3-4 ROIs at similar positions across all three recordings and performing plot profile analysis to compare Ca^{2+} activity under each condition. I also generated spatiotemporal maps (STM) by drawing a straight line along the direction of Ca^{2+} wave propagation within the FOV, maintaining the same line position across all three recordings for consistency.

In Fig. 6.5 to Fig. 6.9, panels A, D, and G show the FOV under PE alone, PE+XE991+iberiotoxin, and PE+XE991+iberiotoxin+nifedipine, respectively, with color-coded ROI boxes (orange, green, blue, and magenta) drawn along the direction of Ca^{2+} wave propagation. Panels B, E, and H show the corresponding STM generated by drawing a straight line across the FOV, and Panels C, F, and I show plot profiles of Ca^{2+} activity extracted from the ROI boxes and merged together in end to reveal if there is any overlap or synchronicity in the Ca^{2+} activity (Fig. 6.5-6.9).

In Fig. 6.5, for instance, in the presence of PE, the FOV showed asynchronous intracellular Ca^{2+} events of USMC (Fig. 6.5A). The STM demonstrated no sign of coordinated Ca^{2+} events across the tissue (Fig. 6.5B), horizontal streaks occasionally appearing in the STM were due to background fluorescence rather than genuine Ca^{2+} activity, as similar patterns were evident across some other STM independent of cellular events such as Fig. 6.7E&H. The plot profiles in Fig 6.5C highlight non-overlapping events firing at different times. Following incubation with PE, XE991, and iberiotoxin, the tissue contracted synchronously, with large Ca^{2+} waves propagating intercellularly across muscle bundles in FOV (Fig. 6.5D). The STM in Fig. 6.5E, and plot profiles (Fig. 6.5F) displays large rhythmic Ca^{2+} waves and temporally synchronized events across the tissues under these conditions (Fig. 6.5F). Subsequent addition of nifedipine abolished this synchronous activity, with a return to asynchronous activity similar to prior addition of XE991 and iberiotoxin (Fig. 6.5G-I).

These observations were consistent across five independent male USM preparations (Fig. 6.5-6.9). In some tissues, coordinated Ca^{2+} activity varied across different muscle bundles, as shown in Fig. 6.6F, but some coordinated events across different ROIs still temporally overlapped. In some recordings under PE (Fig. 6.7 and 6.8C), the overlap observed in the plot profiles was due to light fluctuations rather than true Ca^{2+} event overlap, as evident from the irregular traces that did not resemble typical contraction-associated activity. Overall, these findings from male USM demonstrate that combined Kv7 and BK_{Ca} inhibition promotes synchronous Ca^{2+} activity in USMC in the presence of agonist, which provides a mechanistic explanation for the phasic contractions observed in the tension experiments under the same conditions. The abolition of both synchronous Ca^{2+} activity and phasic contractions by LTCC blockade further supports a causal link.

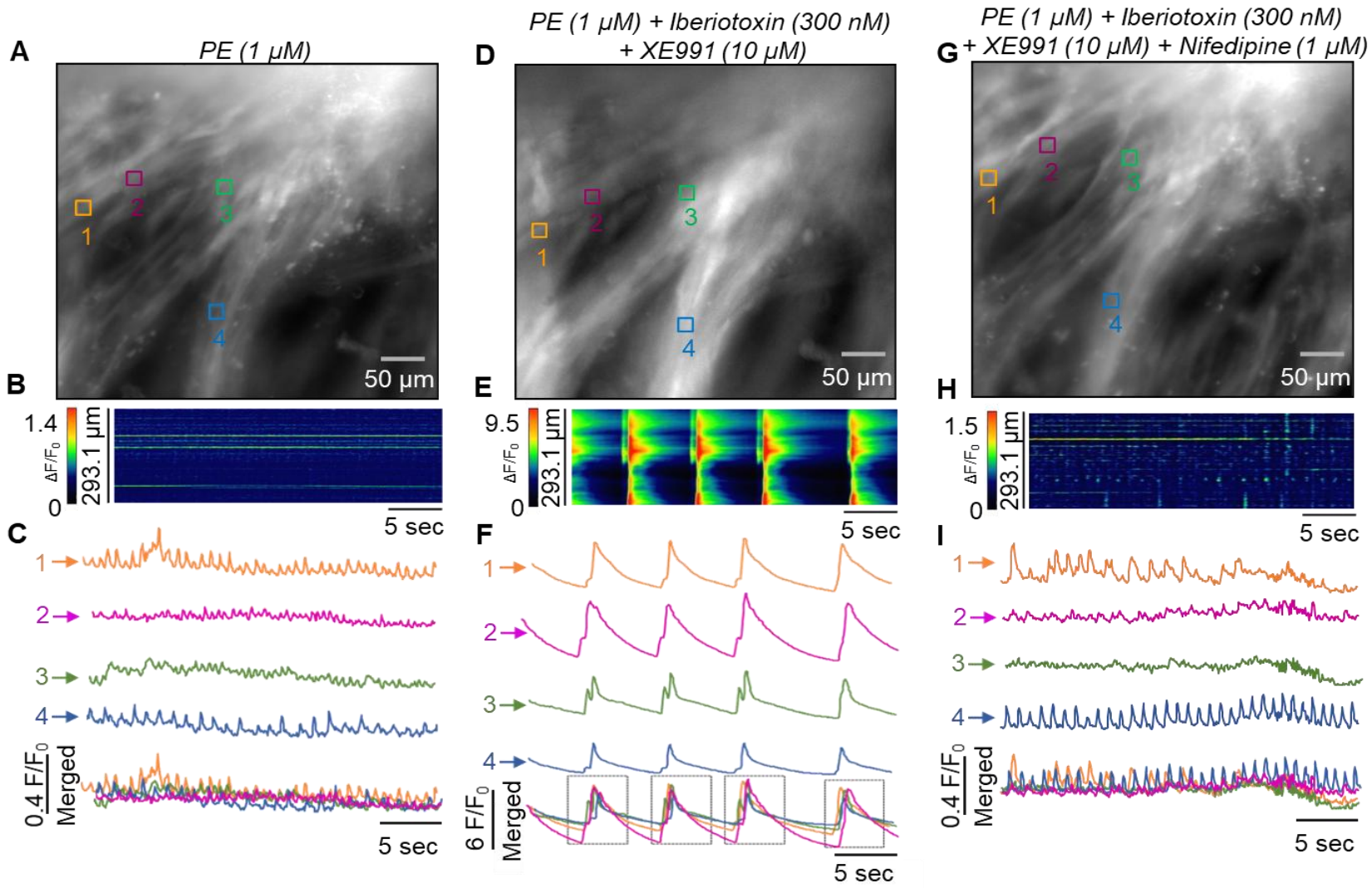

Fig. 6.5: Blockade of Kv7 and BK_{Ca} channels triggers nifedipine-sensitive coordinated Ca^{2+} events in precontracted male USM. Representative *in situ* Ca^{2+} imaging from Acta2-GCaMP8.1 mice showing FOV under **A** PE; **D** PE + XE991 + iberiotoxin; and **G** PE + XE991 + iberiotoxin + nifedipine. Selected ROIs are shown in colour coded boxes (orange, green, blue, magenta) in **A, D, G.** Corresponding spatiotemporal maps (**B, E, H**). Plot profile from ROIs (**C, F, I**).

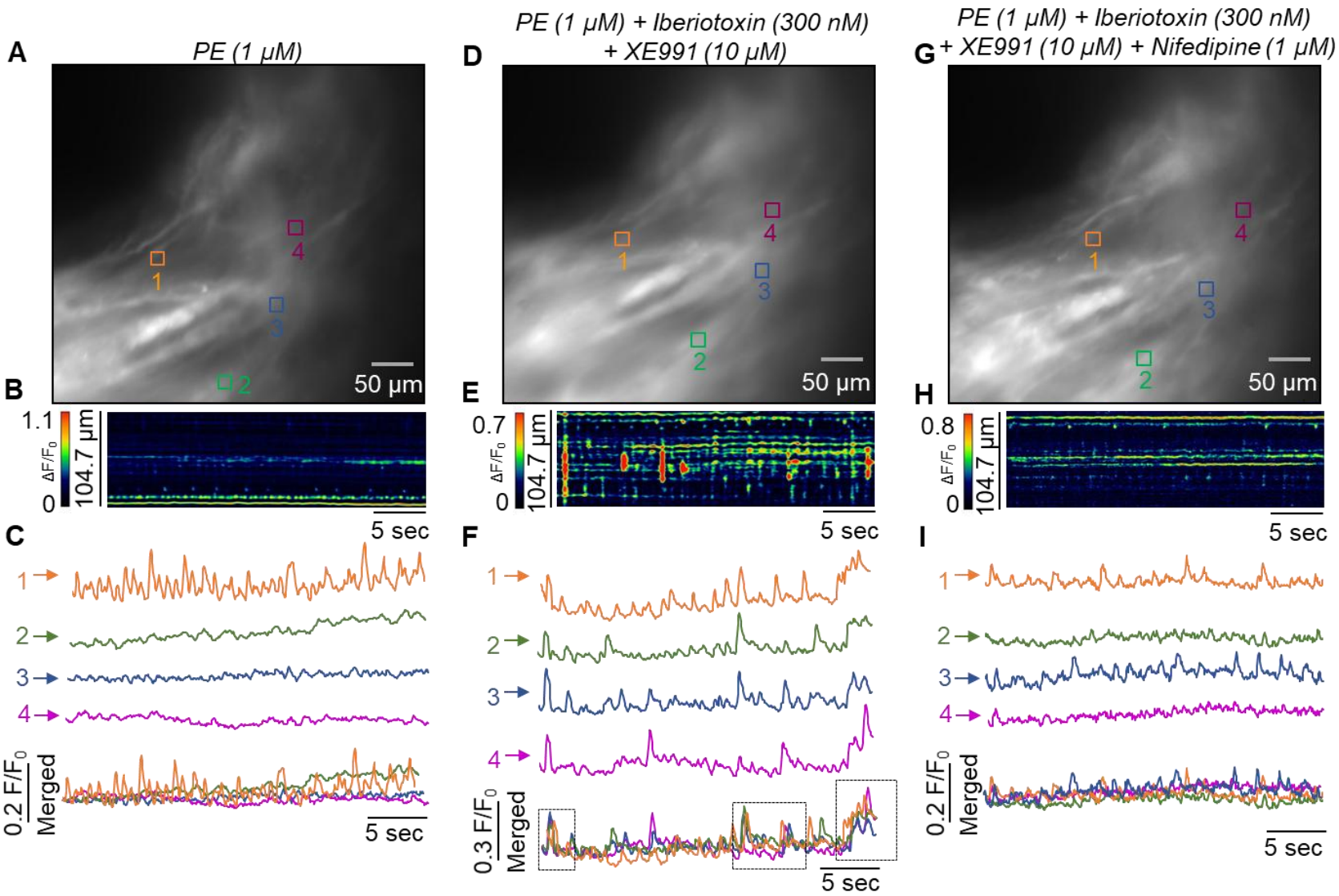

Fig. 6.6: Blockade of Kv7 and BK_{Ca} channels triggers nifedipine-sensitive coordinated Ca^{2+} events in precontracted male USM. Representative *in situ* Ca^{2+} imaging from Acta2-GCaMP8.1 mice showing FOV under **A** PE; **D** PE + XE991 + iberiotoxin; and **G** PE + XE991 + iberiotoxin + nifedipine. Selected ROIs are shown in colour coded boxes (orange, green, blue, magenta) in **A, D, G.** Corresponding spatiotemporal maps (**B, E, H**). Plot profile from ROIs (**C, F, I**).

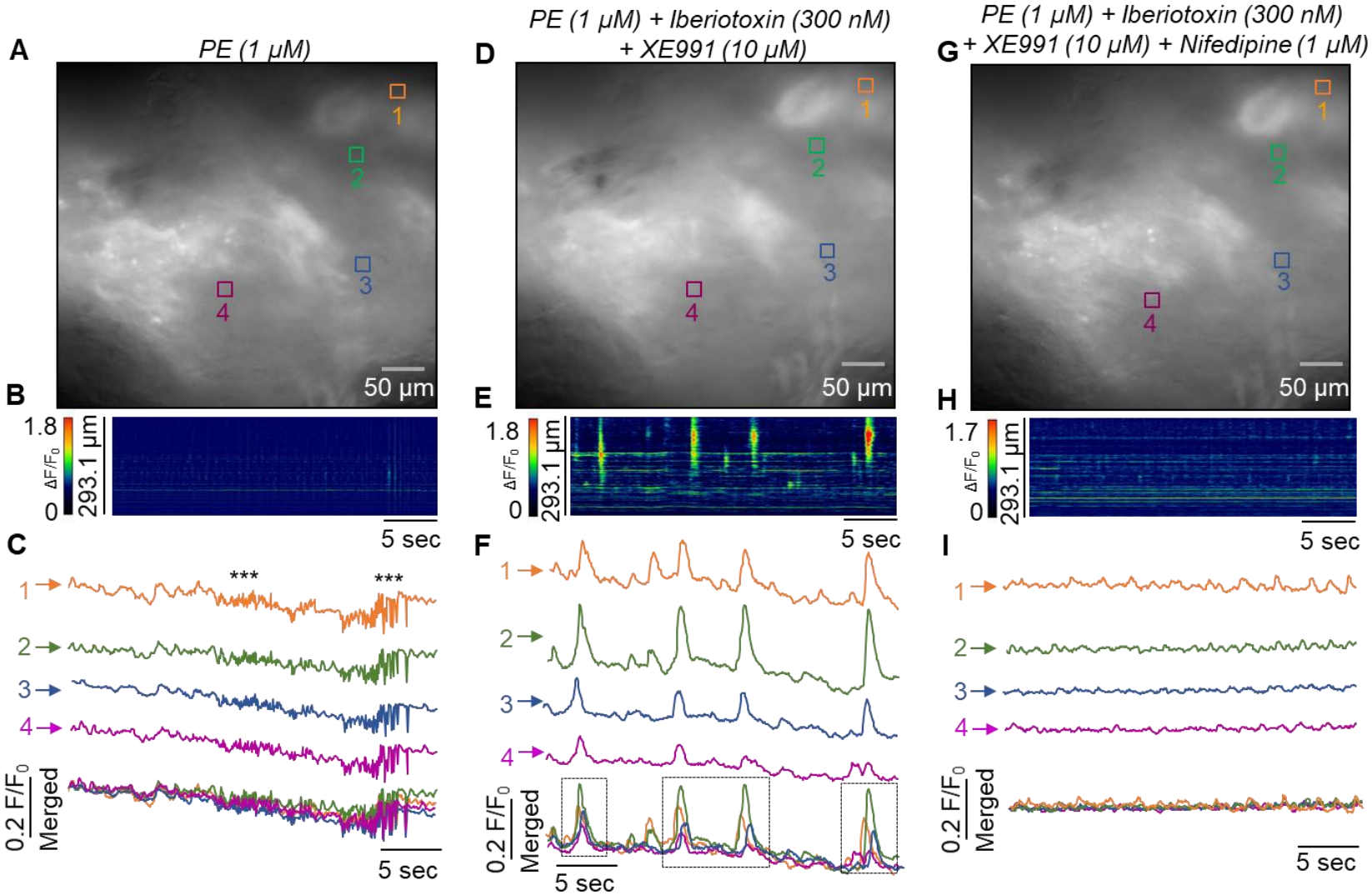

Fig. 6.7: Blockade of Kv7 and BK_{Ca} channels triggers nifedipine-sensitive coordinated Ca^{2+} events in precontracted male USM. Representative *in situ* Ca^{2+} imaging from Acta2-GCaMP8.1 mice showing FOV under **A** PE; **D** PE + XE991 + iberiotoxin; and **G** PE + XE991 + iberiotoxin + nifedipine. Selected ROIs are shown in colour coded boxes (orange, green, blue, magenta) in **A, D, G.** Corresponding spatiotemporal maps (**B, E, H**). Plot profile from ROIs (**C, F, I**). ***light flunctuation.

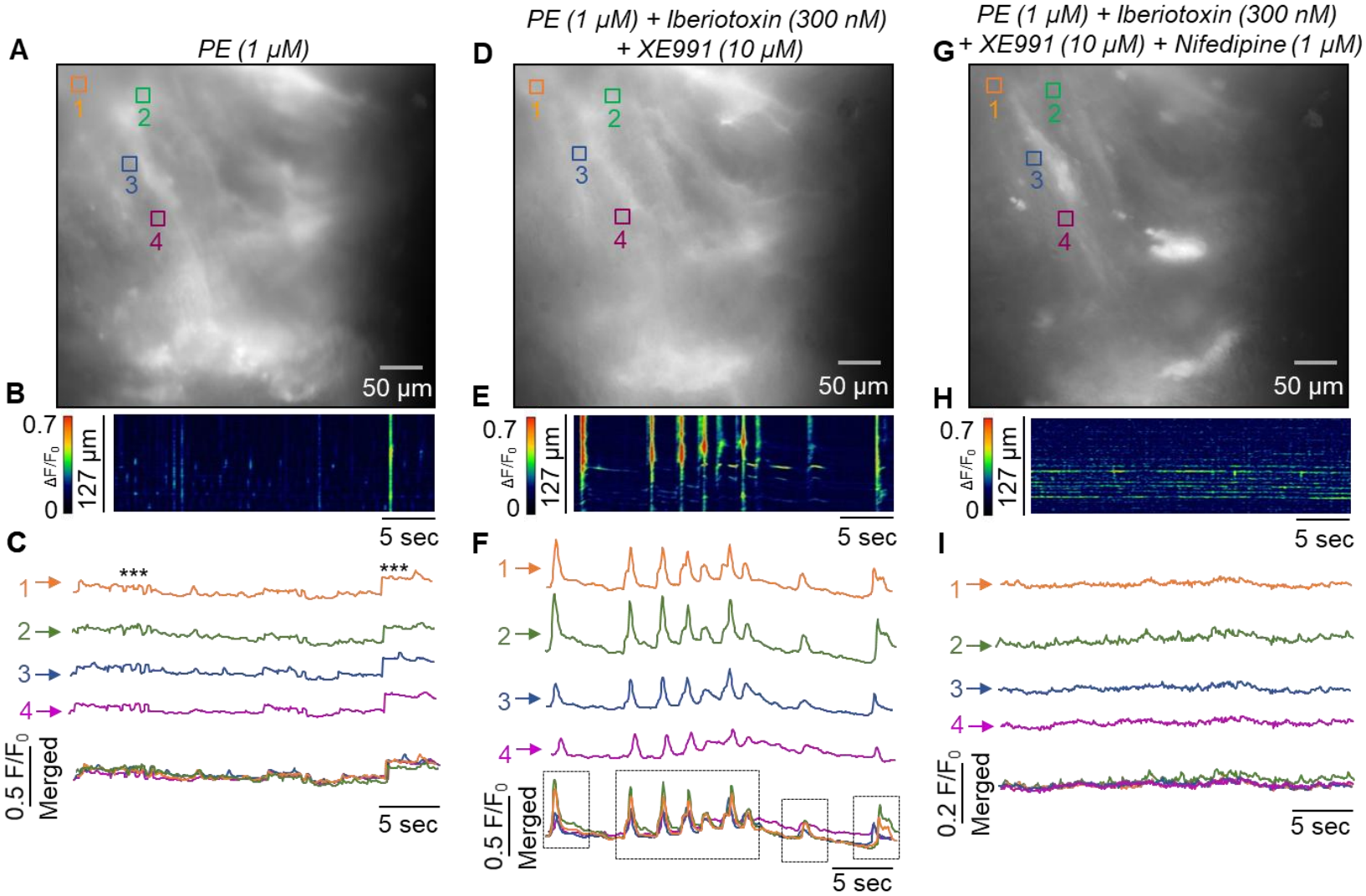

Fig. 6.8: Blockade of Kv7 and BK_{Ca} channels triggers nifedipine-sensitive coordinated Ca^{2+} events in precontracted male USM. Representative *in situ* Ca^{2+} imaging from Acta2-GCaMP8.1 mice showing FOV under **A** PE; **D** PE + XE991 + iberiotoxin; and **G** PE + XE991 + iberiotoxin + nifedipine. Selected ROIs are shown in colour coded boxes (orange, green, blue, magenta) in **A, D, G.** Corresponding spatiotemporal maps (**B, E, H**). Plot profile from ROIs (**C, F, I**). ***light flunctuation.

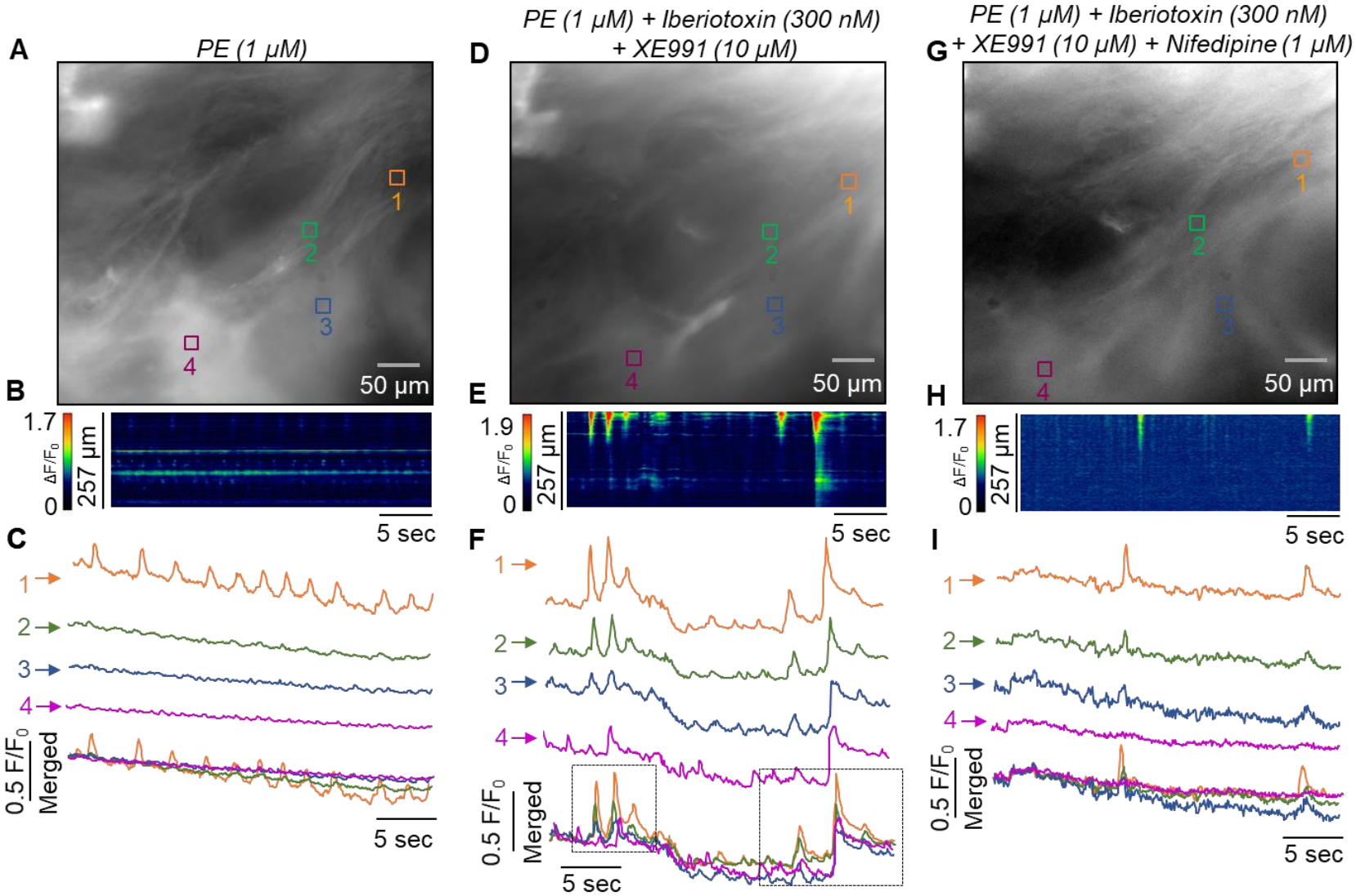

Fig. 6.9: Blockade of Kv7 and BK_{Ca} channels triggers nifedipine-sensitive coordinated Ca^{2+} events in precontracted male USM. Representative *in situ* Ca^{2+} imaging from Acta2-GCaMP8.1 mice showing FOV under **A** PE; **D** PE + XE991 + iberiotoxin; and **G** PE + XE991 + iberiotoxin + nifedipine. Selected ROIs are shown in colour coded boxes (orange, green, blue, magenta) in **A, D, G.** Corresponding spatiotemporal maps (**B, E, H**). Plot profile from ROIs (**C, F, I**).

6.2.2 Effects of Orai and Kv7 channel inhibition in precontracted male USM

Based on previous findings demonstrating that phasic activity in USM is dependent on G_q activation, and in previous chapter I observed that Orai channel inhibition attenuates but does not abolish agonist-evoked contractile responses, I next investigated whether LTCC-dependent phasic contractions could be revealed under conditions of reduced contraction or reduced Ca^{2+} entry. Male USM was precontracted with PE (1 µM), followed by application of either Synta66 (10 µM) or GSK-7975A (1 µM), and then XE991 (10 µM) (Fig. 6.10A-D). Both Synta66 (10 µM) and GSK-7975A (10 µM) reduced PE-induced contractions (Fig.6.10A&B) as described in previous chapter. Surprisingly, blockade of Kv7 channels alone with subsequent application of XE991 (10 µM) was sufficient to induce phasic contractions superimposed on the sustained PE contraction (Fig.6.10A&B). The mean amplitude and frequency of phasic contractions were 0.6 ± 0.3 mN (P=0.0003) and 3.2 ± 0.8 contractions/min^{-1} (P<0.0001) with Synta66+XE991 (n=6; Fig. 6.10C), and 0.4 ± 0.1 mN (P<0.0001) and 3.3 ± 0.4 contractions/min^{-1} (P<0.0001) with GSK-7975A+XE991 (n=6; Fig. 6.10C). These phasic contractions were abolished by nifedipine in both cases (n=6; Fig. 6.10A-D). Nifedipine eliminated phasic contractions by significantly reducing both the mean amplitude (P=0.001, Fig. 6.10C; P<0.0001, Fig. 610D) and frequency (P<0.0001, Fig. 6.10C&D).

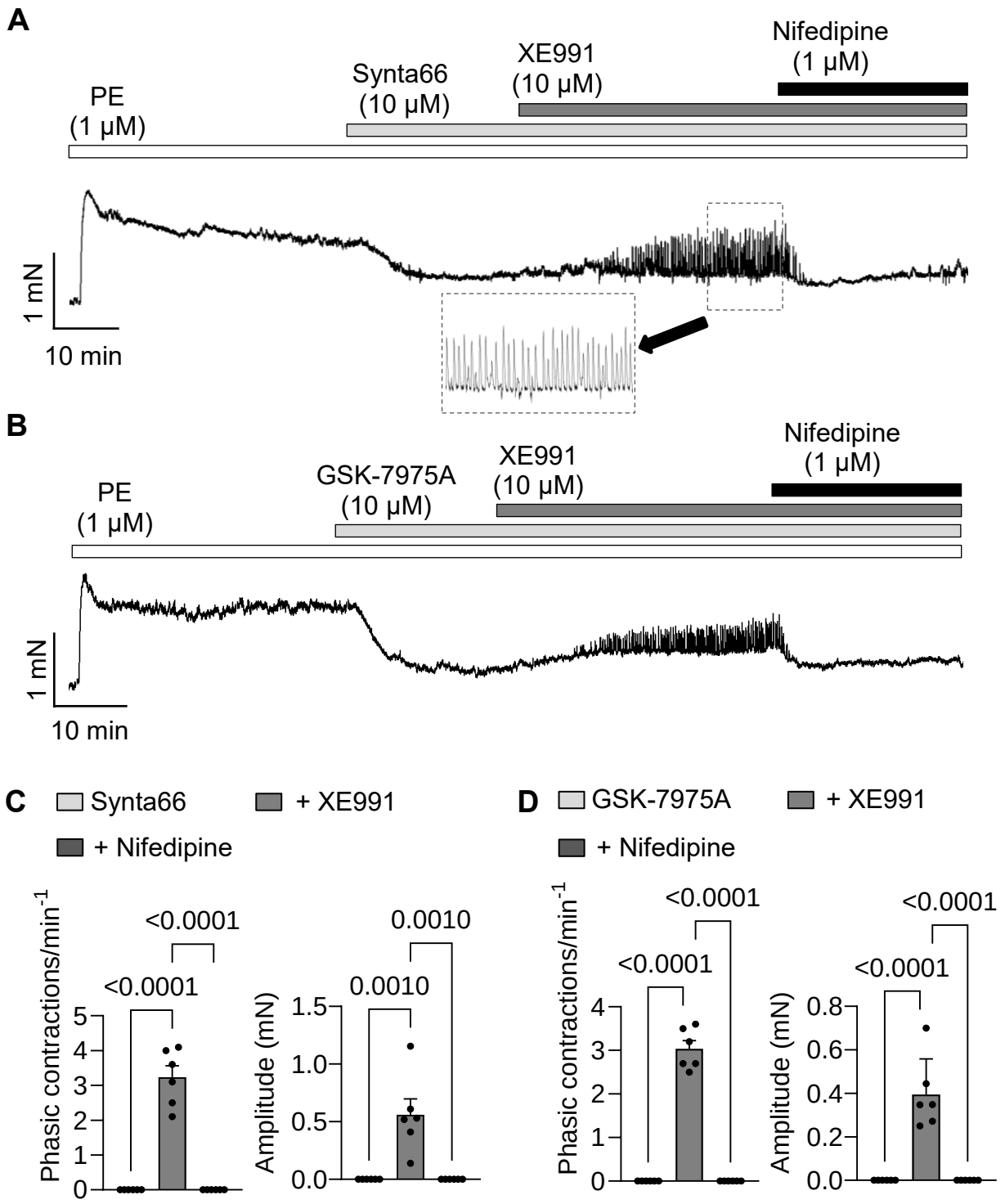

Fig. 6.10: Inhibition of Orai and Kv7 channels leads to phasic contractions in precontracted male USM. Representative data showing the effects of **A** Synta66 (10 μM) or **B** GSK-7975A (10 μM) followed by XE991 (10 μM) and nifedipine (1 μM) on precontracted male mouse urethra with PE (1 μM). Summary of amplitude and frequency of phasic contractions in the presence of **C** Synta66 (n=6) or **D** GSK-7975A (n=6) and XE991, and subsequent effect of nifedipine (One way ANOVA, Bonferroni's test). Dotted boxes showing the enlarged view of the phasic contractions.

I also examined the effects of inhibition of Orai and Kv7 channels on Ca^{2+} activity in USMC using *in situ* Ca^{2+} imaging in male Acta2-GCaMP8.1 mice. Ca^{2+} activity was recorded for 30 sec from a 40x objective under three conditions: (1) PE (1 µM) with GSK-7975A (10 µM), (2) PE with GSK-7975A and XE991 (10 µM), and (3) PE with GSK-7975A, XE991, and nifedipine (1 µM), following 20-25 minutes of incubation for each condition. Ca^{2+} imaging revealed spontaneous, asynchronous intracellular Ca^{2+} events in USMC, which were enhanced by PE without altering their asynchronous nature. In the continued presence of PE, application of the Orai inhibitor GSK-7975A reduced Ca^{2+} activity but did not abolish it, consistent with previous findings (Drumm *et al.,* 2018). Subsequent inhibition of Kv7 channels with XE991 converted the asynchronous intracellular Ca^{2+} events in USMC to synchronous Ca^{2+} activity that propagated between neighbouring muscle bundles. During coordinated Ca^{2+} activity, the USM tissue exhibited moderate rhythmic / phasic contractile pattern. In some USM preparations, coordinated Ca^{2+} waves originated from a focal site and spread across adjacent USM bundles, whereas in others, coordination was evident as simultaneous Ca^{2+} flashes within individual muscle bundles. Final subsequent incubation with nifedipine reverted the coordinated Ca^{2+} activity back to asynchronous events.

A similar analytical approach was applied to these recordings as used for the previous Ca^{2+} imaging data. In Fig. 6.11 to Fig. 6.14, panels A, D, G show the FOV under PE+GSK-7975A, PE+GSK-7975A+XE991, and PE+GSK-7975A+XE991+nifedipine, respectively, with 3 - 4 color-coded ROI boxes (orange, green, blue, and magenta) drawn along the direction of Ca^{2+} wave propagation. Panels B, E, H show corresponding STMs generated by drawing a straight line across the FOV, and Panels C, F, I show Ca^{2+} activity plot profiles extracted from the ROI and merged to determine any temporal overlap or synchronicity in Ca^{2+} activity (Fig. 6.11-6.14).

For instance, in Fig. 6.11 A-C, the FOV shows asynchronous Ca^{2+} events in the presence of PE+GSK-7975A. Overall Ca^{2+} activity was decreased with GSK-7975A, which in some recordings was reflected as downward shifts in the plot profiles (Fig. 6.11C). The STM demonstrates a lack of synchronized Ca^{2+} activity under this condition (Fig. 6.11B). However, subsequent incubation with XE991 induced coordinated Ca^{2+} activity, propagating across the muscle bundles (Fig. 6.11D-F). The STM shows synchronous Ca^{2+} events throughout (Fig. 6.11E). The plot profiles

confirm this synchrony, with Ca^{2+} activity from different ROIs temporally overlapping (Fig. 6.11F). Addition of nifedipine alongside PE, GSK-7975A and XE991 either reversed the coordinated activity back to an asynchronous pattern (Fig. 6.11G-I), or in some urethral preparations, disrupted the regular rhythmicity of coordinated patterns as illustrated in Fig. 6.13I and Fig. 6.14I. In Fig. 6.12C, under PE panel, the overlap observed in the plot profiles was due to light fluctuations during recording. Taken together, these Ca^{2+} imaging data indicate that combined blockade of Orai and Kv7 channels evokes synchronous Ca^{2+} activity, corresponding to the phasic contractions observed in tension recordings.

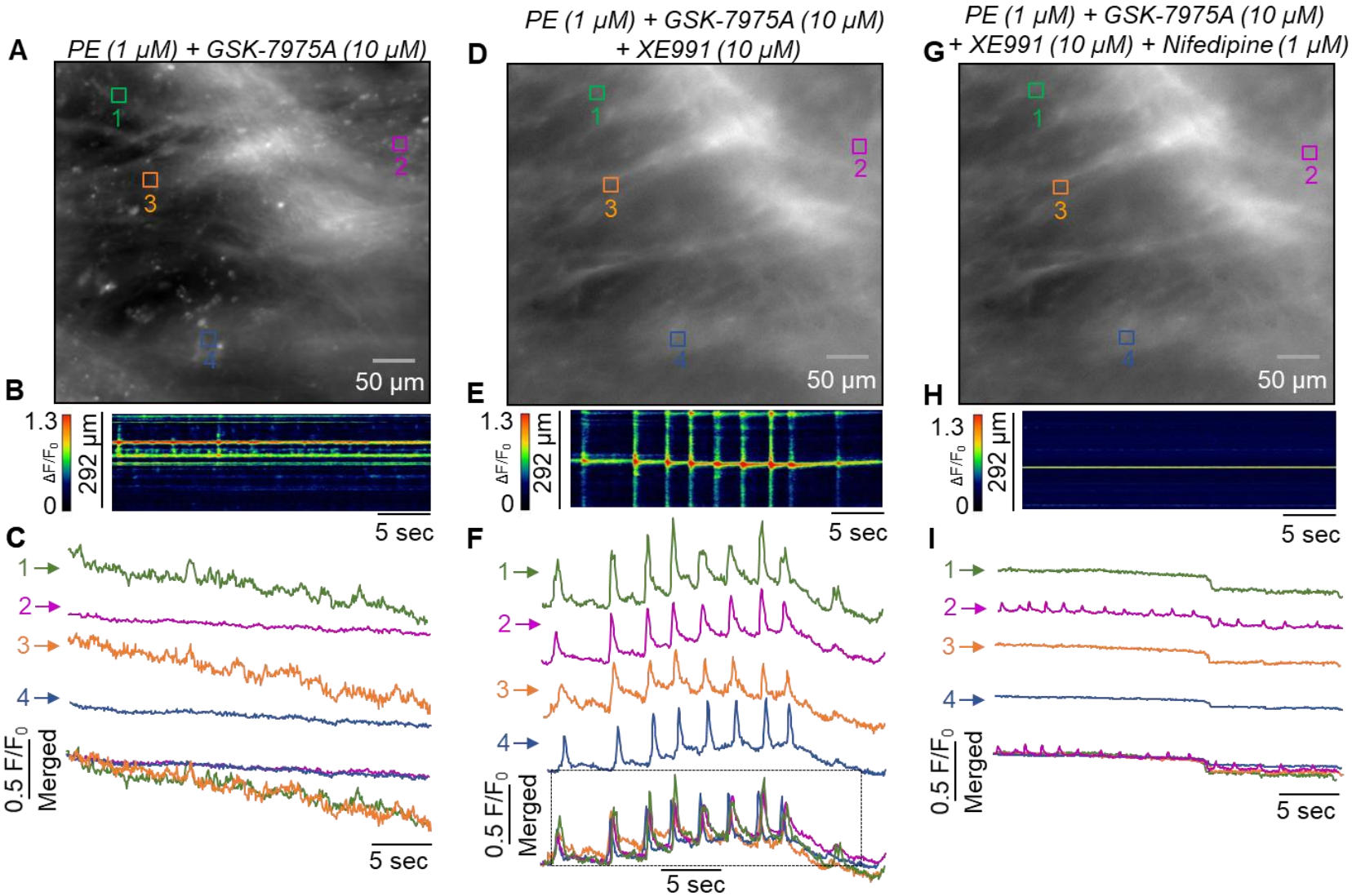

Fig. 6.11: Blockade of Orai and Kv7 channels triggers nifedipine-sensitive coordinated Ca^{2+} events in precontracted male USM. Representative *in situ* Ca^{2+} imaging from Acta2-GCaMP8.1 mice showing FOV under **A** PE + GSK-7975A; **D** PE + GSK-7975A + XE991; and **G** PE + GSK-7975A + XE991 + nifedipine. Selected ROIs are shown in colour coded boxes (orange, green, blue, magenta) in **A, D, G.** Corresponding spatiotemporal maps (**B, E, H**). Plot profile from ROIs (**C, F, I**).

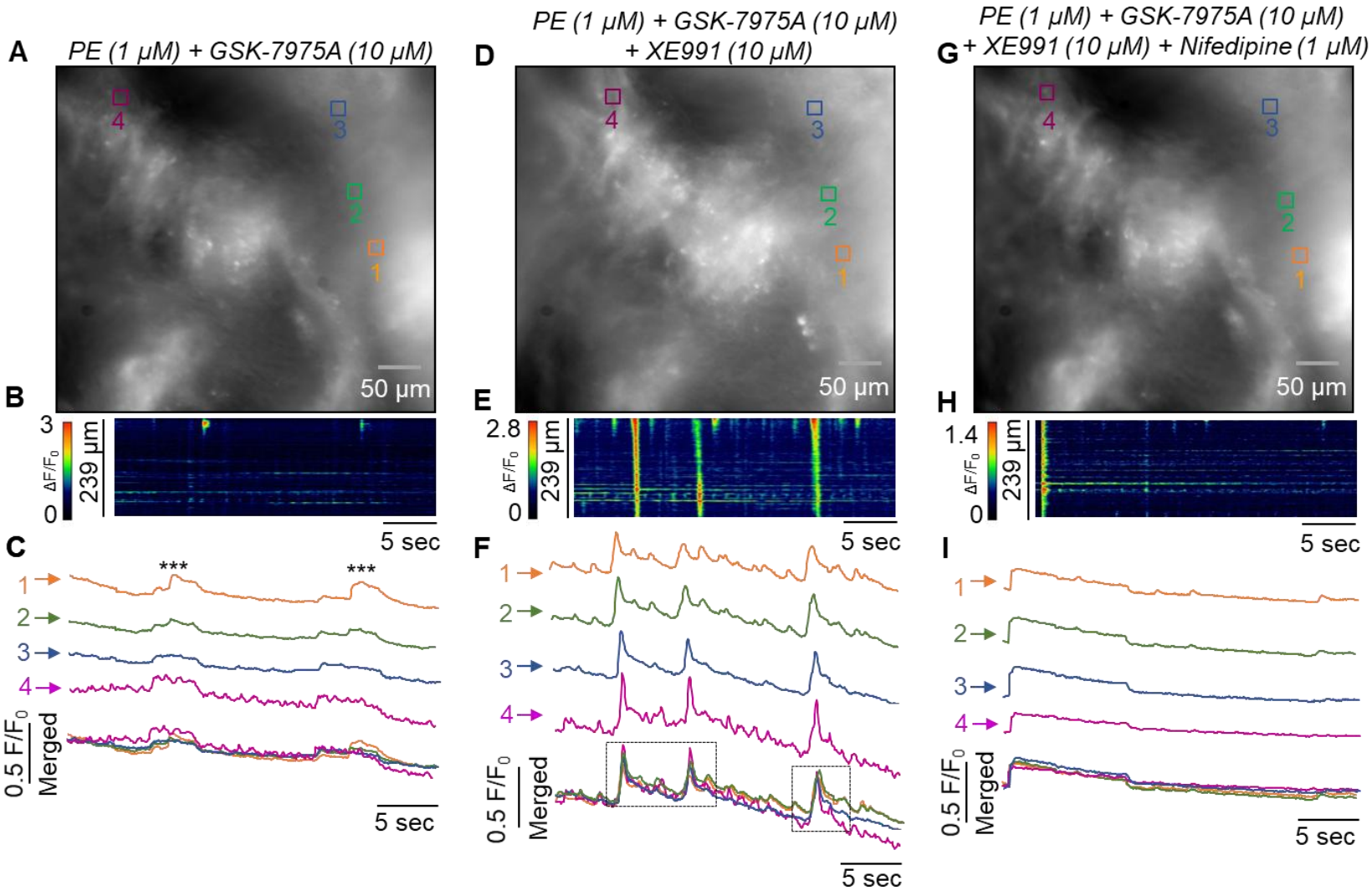

Fig. 6.12: Blockade of Orai and Kv7 channels triggers nifedipine-sensitive coordinated Ca^{2+} events in precontracted male USM. Representative *in situ* Ca^{2+} imaging from Acta2-GCaMP8.1 mice showing FOV under **A** PE + GSK-7975A; **D** PE + GSK-7975A + XE991; and **G** PE + GSK-7975A + XE991 + nifedipine. Selected ROIs are shown in colour coded boxes (orange, green, blue, magenta) in **A, D, G.** Corresponding spatiotemporal maps (**B, E, H**). Plot profile from ROIs (**C, F, I**).***light fluctuation

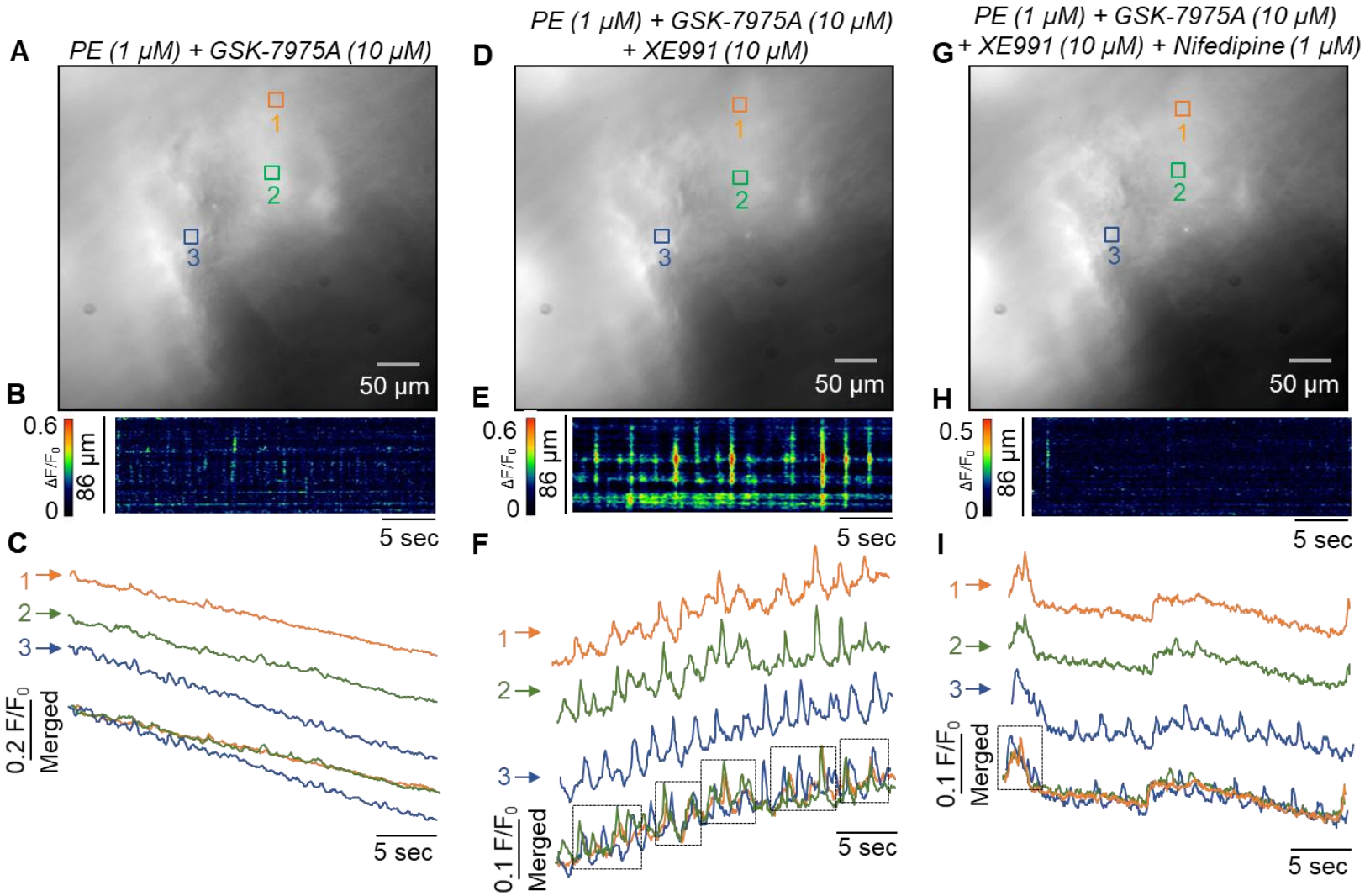

Fig. 6.13: Blockade of Orai and Kv7 channels triggers nifedipine-sensitive coordinated Ca^{2+} events in precontracted male USM. Representative *in situ* Ca^{2+} imaging from Acta2-GCaMP8.1 mice showing FOV under **A** PE + GSK-7975A; **D** PE + GSK-7975A + XE991; and **G** PE + GSK-7975A + XE991 + nifedipine. Selected ROIs are shown in colour coded boxes (orange, green, blue) in **A, D, G.** Corresponding spatiotemporal maps (**B, E, H**). Plot profile from ROIs (**C, F, I**).

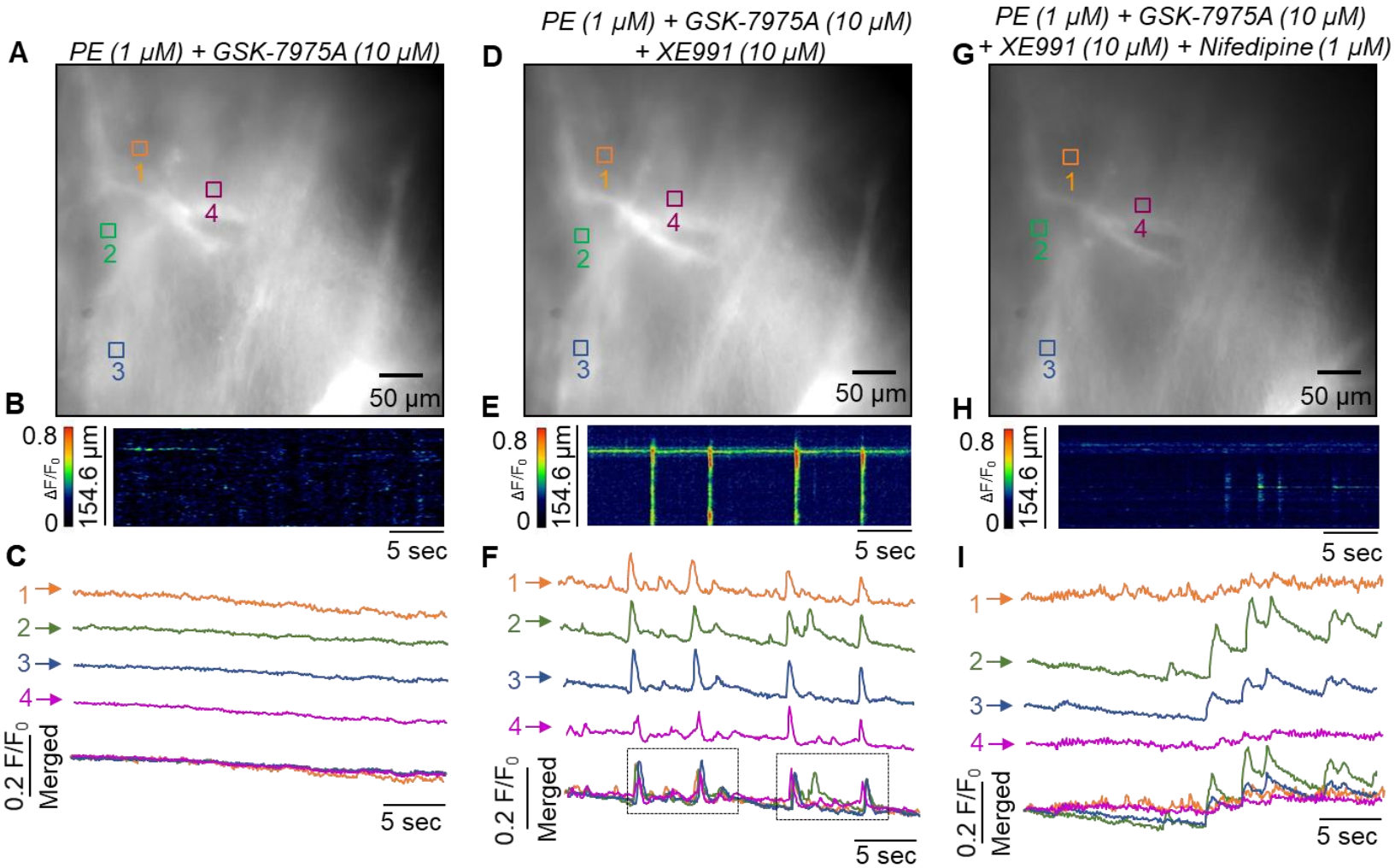

Fig. 6.14: Blockade of Orai and Kv7 channels triggers nifedipine-sensitive coordinated Ca^{2+} events in precontracted male USM. Representative *in situ* Ca^{2+} imaging from Acta2-GCaMP8.1 mice showing FOV under **A** PE + GSK-7975A; **D** PE + GSK-7975A + XE991; and **G** PE + GSK-7975A + XE991 + nifedipine. Selected ROIs are shown in colour coded boxes (orange, green, blue, magenta) in **A, D, G.** Corresponding spatiotemporal maps (**B, E, H**). Plot profile from ROIs (**C, F, I**).

Next, we compared the phasic contractions evoked by blockade of BK_{Ca} and Kv7 with those induced by inhibition of Orai and Kv7, to determine whether the phasic activity generated under these two conditions was similar or distinct in terms of frequency and amplitude. Phasic contractions in the presence of XE991 + iberiotoxin (n=21; Fig. 6.15A) occurred at a significantly higher frequency (5.6 ± 1.8 contractions/min^{-1}) compared with those induced by GSK-7975A + XE991 (2.8 ± 1.6 contractions/min^{-1}, n=11, P=0.0002; Fig. 6.15B&D) or Synta66 + XE991 (3.2 ± 0.8 contractions/min^{-1}, n=6, P=0.005; Fig. 6.15C&E). In contrast, the amplitude of phasic contractions did not differ significantly between XE991 + iberiotoxin (n=21; Fig. 6.15A) and either GSK-7975A + XE991 (n=11, P=0.19; Fig. 6.15B&D) or Synta66 + XE991 (n=6, P=0.15; Fig. 6.15C&E). This comparison reveals that phasic contractions evoked after inhibition of BK_{Ca} and Kv7 channels are greater in frequency than those induced after inhibition of Orai and Kv7 channels.

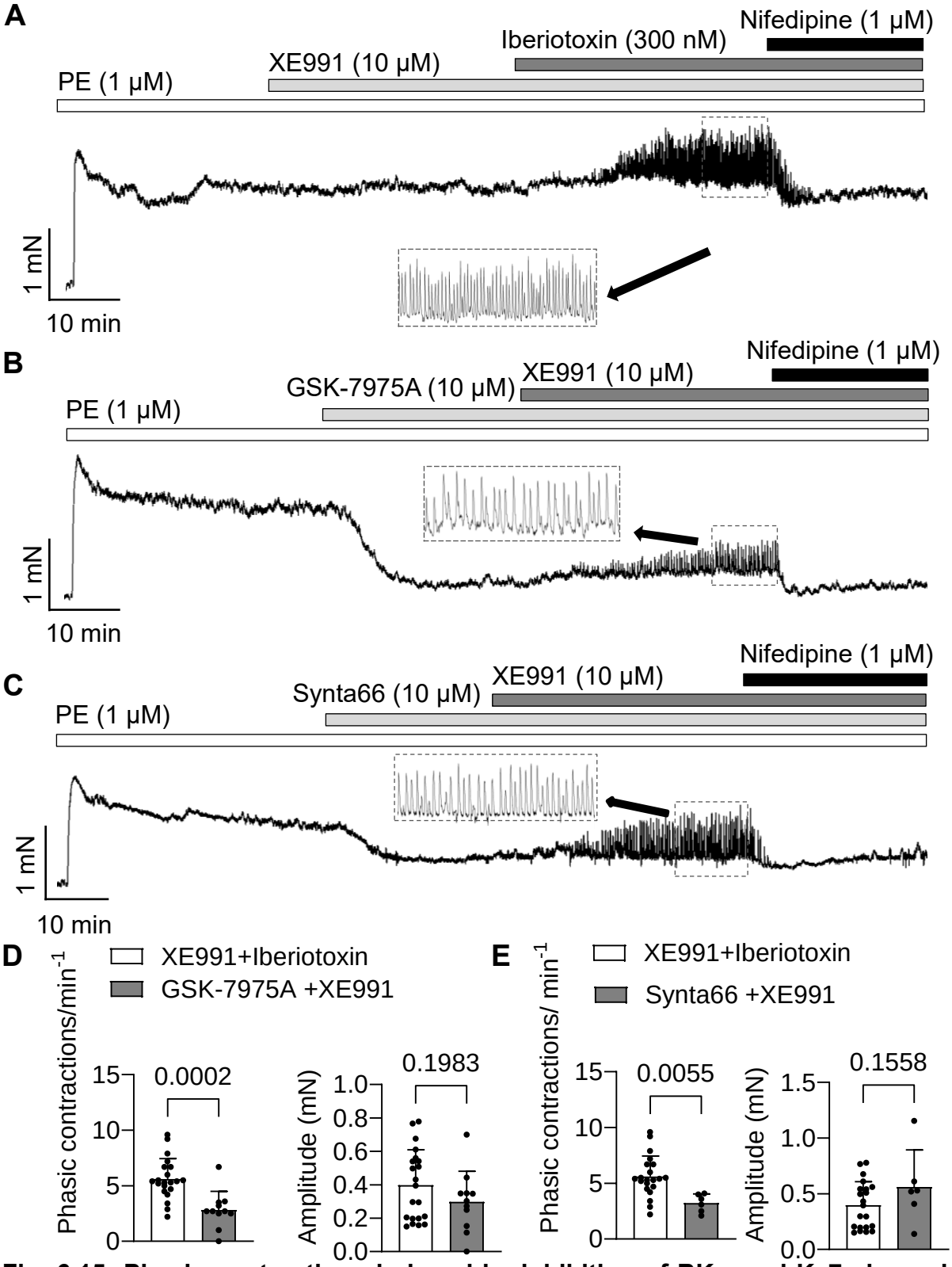

Fig. 6.15: Phasic contractions induced by inhibition of BK_{Ca} and Kv7 channels are more frequent than those induced by inhibition of Orai and Kv7 channels. Representative data showing the effects of **A** XE991 (10 μM) followed by iberiotoxin (300 nM) and then nifedipine (1 μM) and **B** GSK-7975A (10 μM) or **C** Synta66 (10 μM) followed by XE991 (10 μM) and nifedipine (1 μM) on precontracted male USM with PE (1 μM). Summary of amplitude and frequency of phasic contractions in the presence of **D** XE991 and iberiotoxin (n=21) vs GSK-7975A and XE991 (n=11) (unpaired t-test), and **E** XE991 and iberiotoxin (n=21) vs Synta66 and XE991 (n=6) (unpaired t-test).

I then investigated whether combined Orai and BK_{Ca} inhibition alone could induce phasic contractions. GSK-7975A (10 µM) was applied to precontracted male USM by 1 µM PE, followed by iberiotoxin (300 nM) (Fig. 6.16A). This combination had no effect; however, subsequent addition of XE991 initiated phasic activity, which were sensitive to nifedipine (n=6; Fig. 6.16A&C). The findings from Fig. 6.15A-E & 6.16A&C led to the hypothesis that Orai channel inhibition may partially limit BK_{Ca} activation, contributing to the emergence of phasic contractions. To test this hypothesis, I next examined the reverse order of addition of these K^+ channel blockers, I first inhibited Orai and Kv7 channels, which resulted in phasic contractions in precontracted male USM, followed by BK_{Ca} blockade to test for potential enhancement of activity (n=5; Fig. 6.16B). Under these conditions, amplitude and frequency of phasic contractions further increased upon iberiotoxin addition, from 0.18 ± 0.1 to 0.4 ± 0.1 mN (P=0.0002), and 2.6 ± 2.6 to 7 ± 2.7 contractions/min^{-1} (P=0.02, Fig. 6.16B&D). This suggests Orai inhibition combined with Kv7 blockade reduces BK_{Ca} conductance partially, and that direct BK_{Ca} inhibition further enhances phasic activity. This indicates that Ca^{2+} influx through Orai channels likely contributes to the activation of BK_{Ca} channels, either directly or indirectly via modulation of SR Ca^{2+} release. This also addresses the question raised in Chapter 5, where nifedipine alone had no effect on EFS-induced contractions, but reduced a portion of the contraction amplitude following Orai channel inhibition with GSK-7975A. This is most likely due to partial BK_{Ca} inhibition upon Orai blockade, allowing LTCC-mediated Ca^{2+} influx that becomes sensitive to nifedipine.

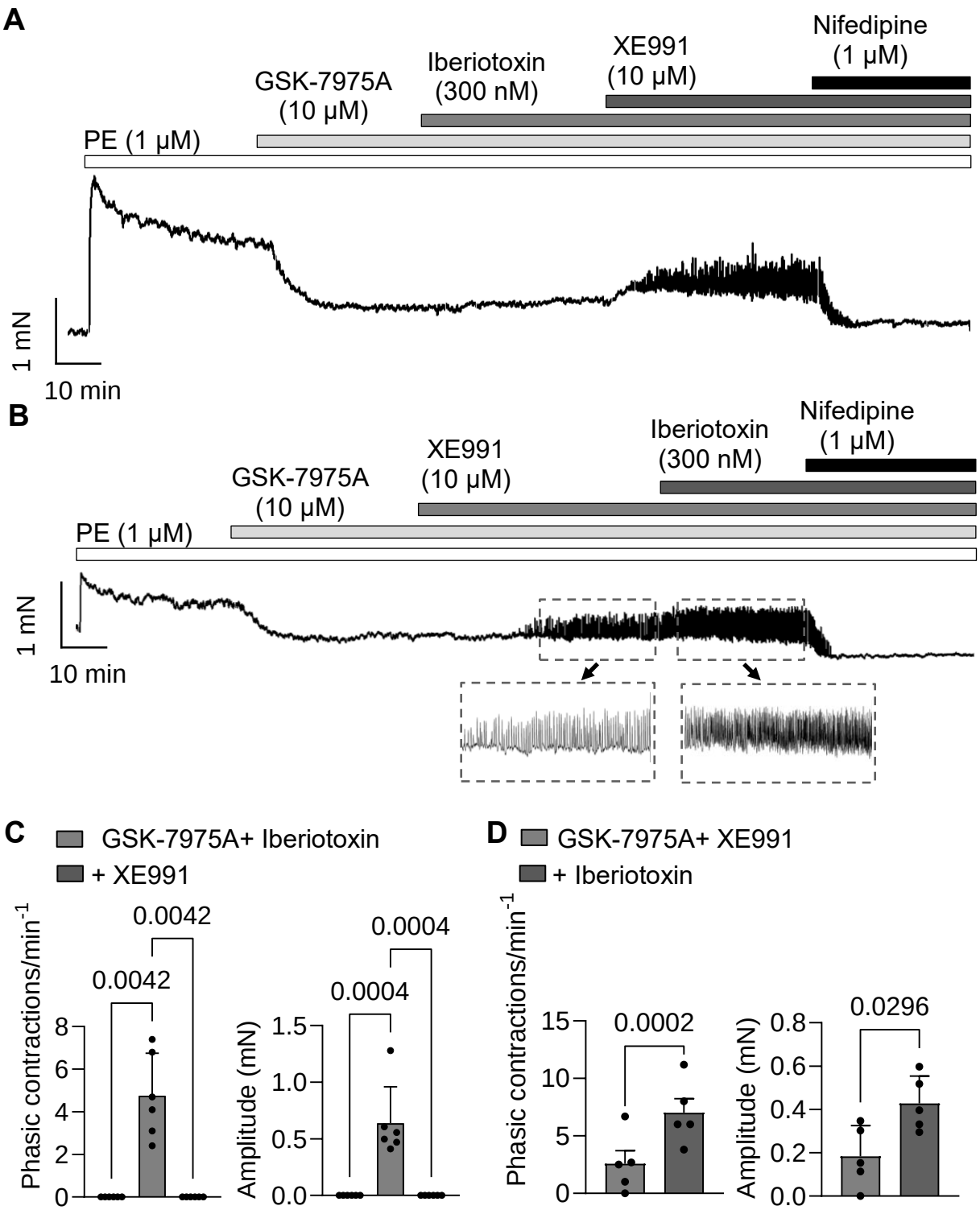

Fig. 6.16: Inhibition of Orai and Kv7 channels leads to phasic contractions which were enhanced by blocking BK_{Ca}, but blockade of Orai and BK_{Ca} shown no phasic activity on male USM. Representative data showing the effects of **A** GSK-7975A (10 μM) and iberiotoxin (300 nM) followed by XE991 (10 μM) or **B** GSK-7975A (10 μM) and XE991 (10 μM) followed by iberiotoxin (300 nM), and nifedipine (1 μM) on precontracted male USM with PE (1 μM). Summary of amplitude and frequency of phasic contractions comparing the effect of **C** GSK-7975A and iberiotoxin vs XE991 on the GSK-7975A and iberiotoxin (n=6, one way ANOVA, Bonferroni's test), **& D** GSK-7975A and XE991 vs iberiotoxin on the GSK-7975A and XE991 (n=5; Paired t test). Dotted boxes: enlarged view of the phasic contractions.

6.2.3 Effects of RyR and Kv7 inhibition on precontracted male urethra

Previous studies have shown that RyR-mediated Ca^{2+} release activates BK_{Ca} channels in DSMC (Hashitani & Brading, 2003; Herrera *et al.,* 2000; Herrera & Nelson, 2002). Similarly, studies in rabbit USMC demonstrated that BK_{Ca} currents are driven by Ca^{2+} release through RyR. In the present study, I observed that inhibition of Orai channels also reduced portion of BK_{Ca}-dependent conductance. This raised the question of whether this effect arises indirectly via reduced SR Ca^{2+} release or through a more direct contribution of Orai-mediated Ca^{2+} influx. To address this, I examined the effects of RyR inhibition in combination with Kv7 blockade to determine whether this condition could induce phasic contractions in pre-contracted male USM similar to that observed following combined Orai and Kv7 inhibition. Tissues were precontracted with PE (1 μM), followed by tetracaine (100 μM, non-selective RyR antagonist) (Fig. 6.17A). Addition of tetracaine produced a transient overshoot in contractile force that quickly returned to pre-tetracaine-induced level (Fig. 6.17A). I speculate this may result from an acute alteration in RyR behaviour, where tetracaine transiently modifies channel gating, causing a brief release of Ca^{2+} before fully inhibiting RyR-mediated Ca^{2+} release (Overend *et al.,* 1998). Subsequent application of XE991 (10 μM) induced weak phasic contractions superimposed on the sustained contraction, and further addition of iberiotoxin (300 nM) enhanced both amplitude from 0.15 ± 0.05 to 0.3 ± 0.12 mN (P=0.04) and frequency from 2.8 ± 3 to 5.6 ± 3.7 contractions/min^{-1} (P=0.01) of these phasic contractions (n=4; Fig. 6.17A&B). Phasic responses were abolished by nifedipine (1 μM) (Fig. 6.17A&B). These findings suggest that RyR-mediated SR Ca^{2+} release contributes minimally to BK_{Ca} activation.

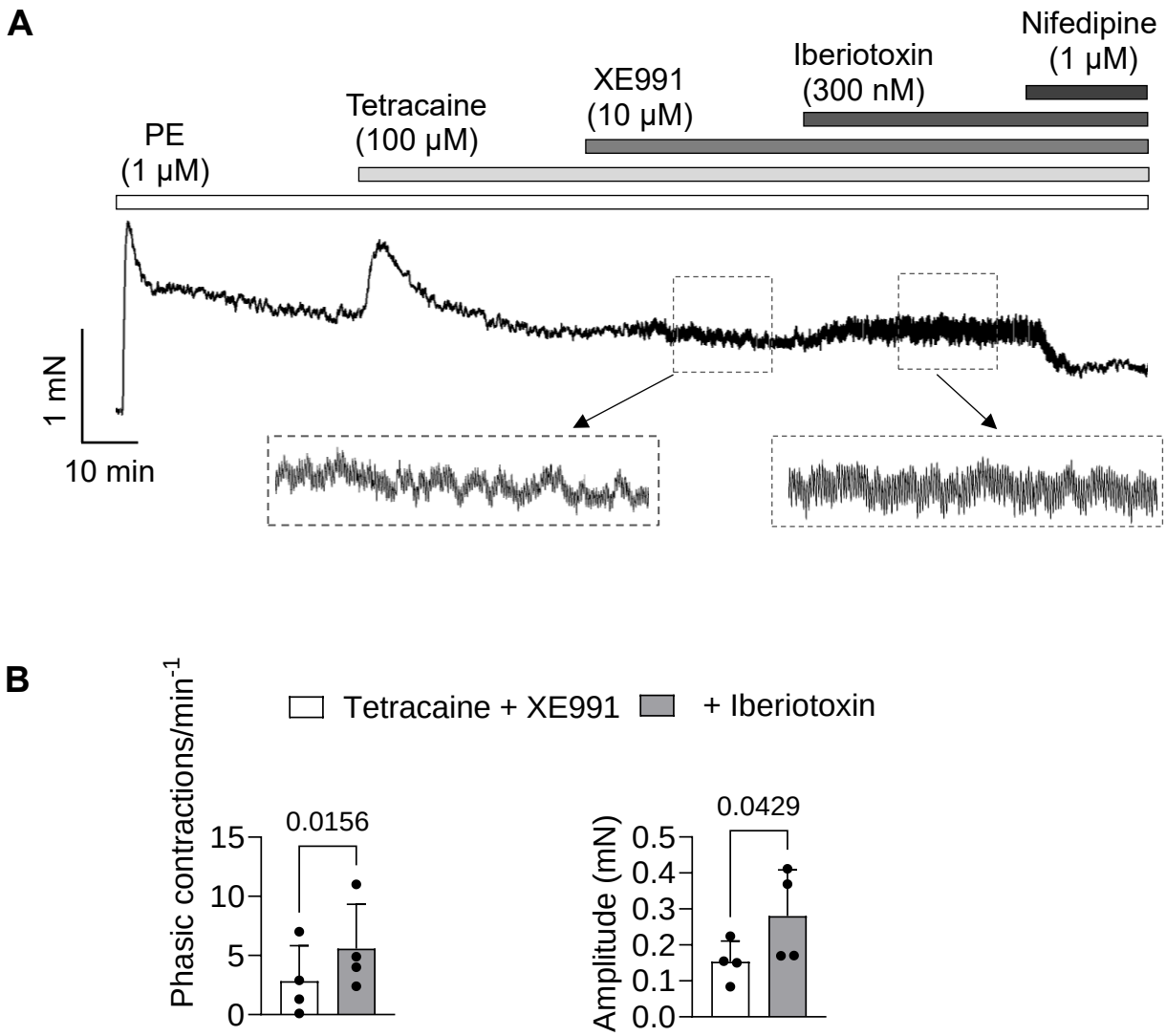

Fig. 6.17: Inhibition of RyR and Kv7 channels leads to phasic contractions which were enhanced by blocking BK_{Ca}, but blockade of Orai and BK_{Ca} shown no phasic activity on male USM. Representative data showing the effects of **A** tetracaine (100 μM) and XE991 (10 μM) followed by iberiotoxin (300 nM) and then nifedipine (1 μM) on precontracted male USM with PE (1 μM). **B** Summary of amplitude and frequency of phasic contractions comparing the effect of tetracaine+XE991 vs tetracaine+XE991+iberiotoxin (n=4, paired t-test). Dotted boxes showing the enlarged view of the phasic contractions.

6.2.4 Effects of ANO1 inhibition on phasic contractions in male USM

Next, I tested if phasic contractions induced by simultaneous blockade of Kv7 and BK_{Ca} channels were sensitive to ANO1 inhibition, to assess whether ANO1 channel activity under these conditions contributes to the maintenance of LTCC-mediated phasic contractions. I examined if blocking ANO1 with Ani9 (3 μM) would affect phasic contractions observed under Kv7+BK_{Ca} inhibition in precontracted male USM (n=6; Fig. 6.18A&B). Ani9 failed to affect phasic activity amplitude (P=0.8) or frequency (P=0.8) (n=6; Fig. 6.18A&B). Application of nifedipine later abolished phasic contractions (Fig. 6.18A&B). These findings suggest that the depolarizing drive underlying phasic contractions during Kv7 and BK_{Ca} blockade is sufficient to activate and sustain LTCC independently of ANO1, explaining the lack of effect of Ani9 under these conditions.

6.2.5 Effects of Kv7 and BK_{Ca} blockade on precontracted female USM

To determine whether Kv7 and BK_{Ca} channel inhibition induces phasic contractions in females, I examined effect of their blockade on precontracted female USM (n=6; Fig 6.19A). Female USM was precontracted with AVP (10 nM), followed by sequential application of XE991 (10 μM) and iberiotoxin (300 nM). XE991 alone had no effect on AVP-induced contractions, and combined XE991+iberiotoxin also failed to alter the contractile response (n=6; Fig 6.19A). Subsequent application of nifedipine likewise had no effect (n=6; Fig 6.19A). However, GSK-7975A reduced AVP-induced contractions (n=6; Fig 6.19A), consistent with the findings reported in Chapter 5.

To determine whether the absence of phasic contractions in female USM was due to agonist used or is a sex-specific difference, I tested the effect of Orai and Kv7 channel inhibition on AVP-induced contractions in both male and female USM. While Synta66 and XE991 failed to induce phasic contractions in female USM (n=4; Fig 6.19B&D), phasic activity was readily observed in male USM under the same conditions with mean frequency of 3.4 ± 0.7 contractions/min^{-1} and mean amplitude of 0.26 ± 0.05 mN (n=4; Fig 6.19C&D), indicating a sex-specific difference in response.

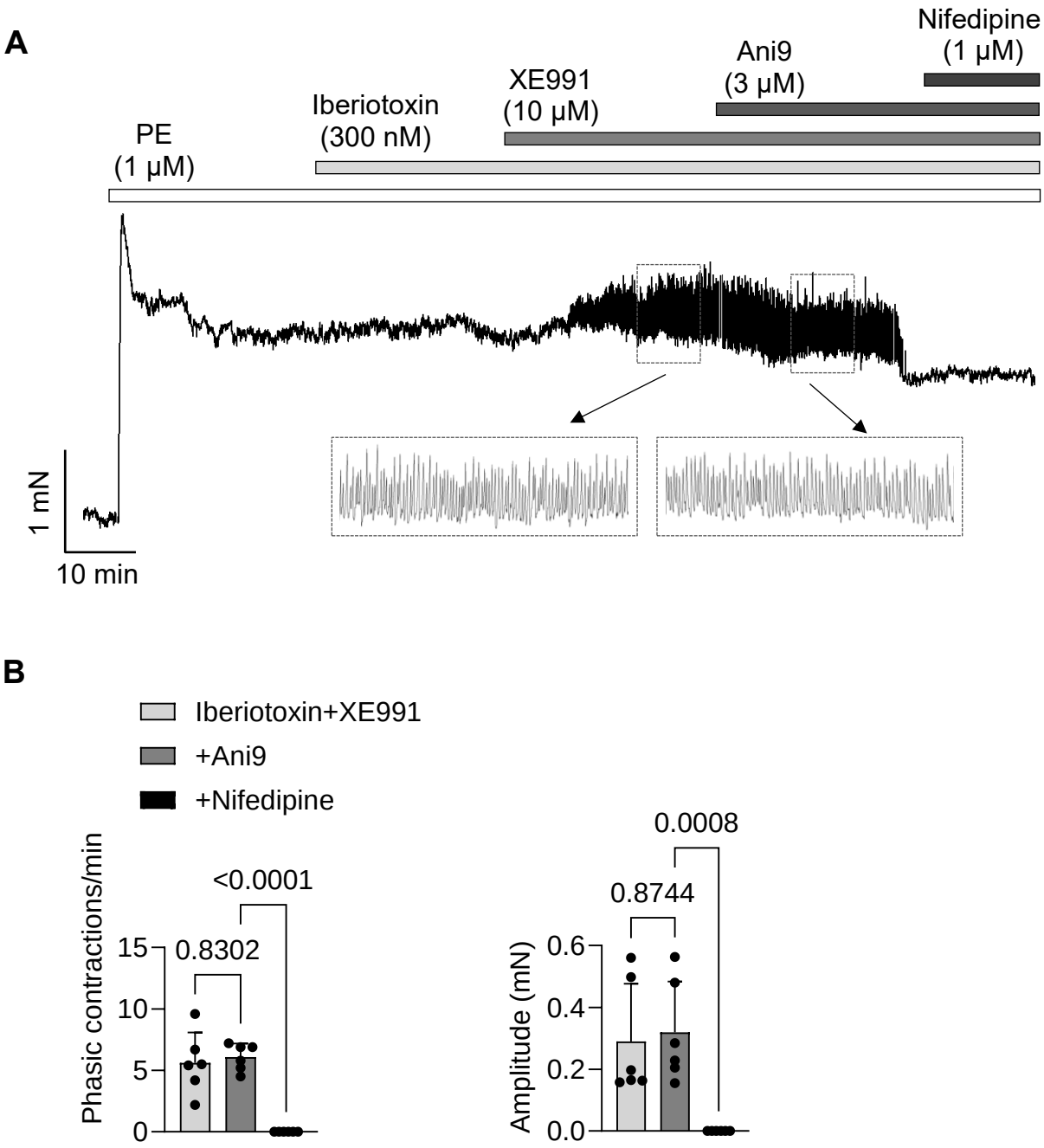

Fig 6.18: Kv7 and BK_{Ca} channels inhibition induced phasic contractions were not sensitive to ANO1 inhibition. Representative data showing the effects of **A.** XE991 (10 μM) followed by iberiotoxin (300 nM) on pre-contracted male USM with PE (1 μM). This combination led to occurrence of phasic contractions that were not sensitive to Ani9 (3 μM), but abolished by nifedipine (1 μM). **B** Summary of amplitude and frequency of phasic contractions in the presence of combination of XE991+iberiotoxin vs XE991+iberiotoxin+Ani9 vs XE991+iberiotoxin+Ani9+nifedipine (n=6; One way ANOVA, Bonferroni's test). Dotted boxes showing the enlarged view of the phasic contractions.

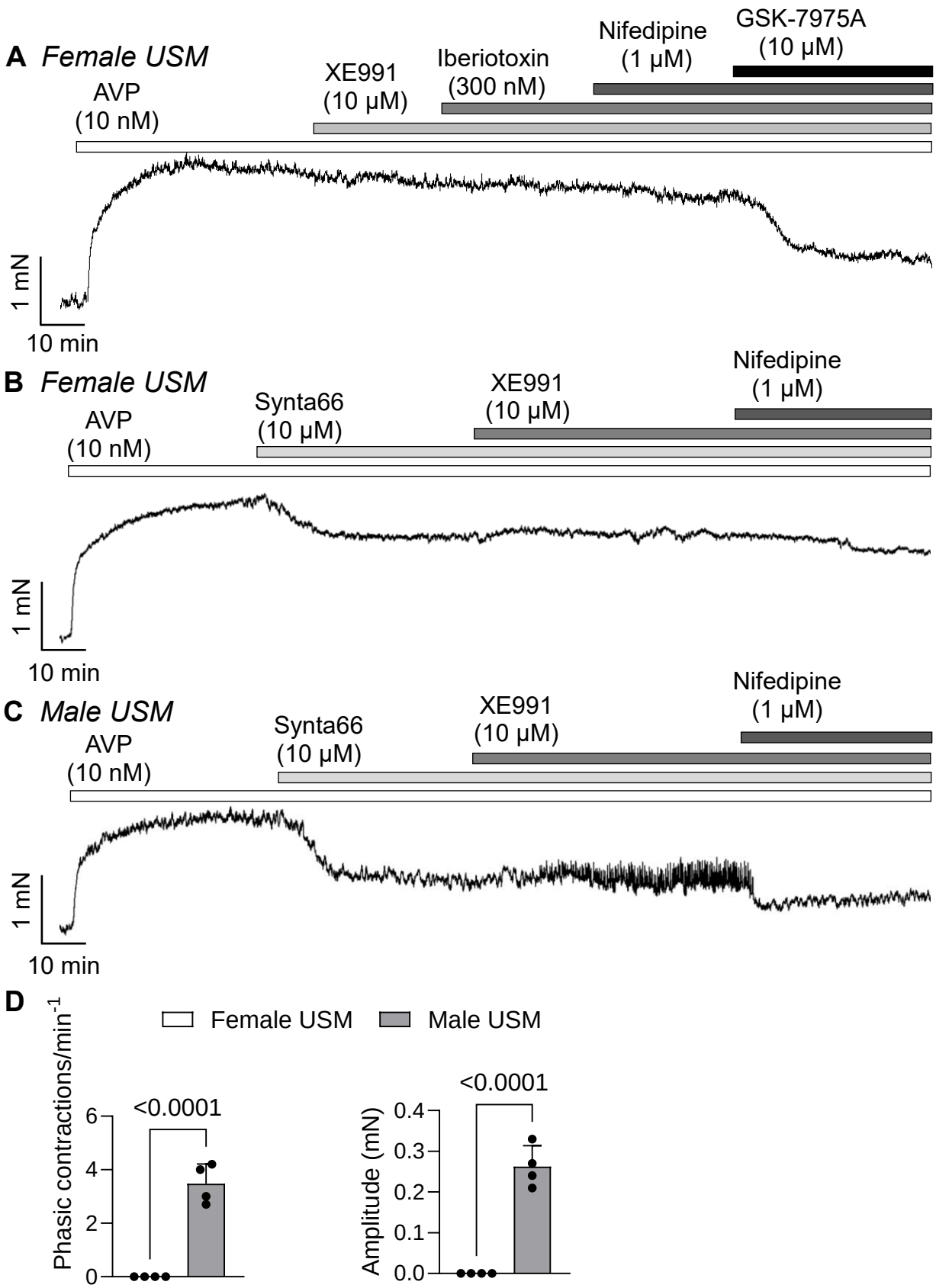

Fig 6.19: In female urethra precontracted with AVP, inhibition of Kv7 and BK_{Ca} channels or Orai and Kv7 channels did not induce phasic contractions, unlike in male urethra. Representative data showing the effects of **A** XE991 (10 μM) followed by iberiotoxin (300 nM) (n=6), **B &C** Synta66 (10 μM) followed by XE991 (10 μM) and nifedipine (1 μM) on pre-contracted female USM and male USM with AVP (10 nM), respectively. **D** Summary of amplitude and frequency of phasic contractions in the presence of Synta66 + XE991 in female vs. male USM (n = 4; Unpaired t-test).

6.2.6 Role of K_{ATP} channels in male and female USM

Previous studies suggest K_{ATP} channels modulate LTCC in pig urethra (Rembetski *et al.,* 2020; Teramoto & Brading, 1996). However, their role has never been examined in mouse USM. Therefore, I tested whether K_{ATP} inhibition, combined with BK_{Ca} and Kv7 blockade, would enhance phasic contractions in male USM. Glibenclamide (10 µM) was applied during BK_{Ca} and Kv7-induced phasic contractions on precontracted male USM (n=3; Fig. 6.20A&B). No significant changes were observed in phasic contraction frequency (P=0.3) or amplitude (P=0.3) after subsequent incubation with glibenclamide (n=3; Fig. 6.20A&B). These results suggest that K_{ATP} channel inhibition does not contribute to the LTCC-mediated phasic activity induced by combined blockade of Kv7 and BK_{Ca} channels in mouse USM.

6.2.7 Expression of Kv7 and BK_{Ca} in male USM

Given the absence of LTCC-mediated phasic activity in female USM following Kv7 and BKCa channel inhibition, I examined *Kcnq* and *Kcnma* gene expression in male and female urethra using qPCR, to determine whether differential expression relates to the observed sex differences. The gene expression levels of *Kcnq* and *Kcnma* were normalized to the housekeeping gene *β-actin*. *Kcnq1* expression was significantly higher in males (0.006 ± 0.0007) than females (0.002 ± 0.0006; n=3, P= 0.002; Fig. 6.21A). *Kcnq2* expression was also greater in males (0.00038 ± 0.00017), whereas minimal expression was observed in females (n=3, P=0.02; Fig. 6.21A). No significant sex differences were detected in the expression for *Kcnq3* (P=0.19), *Kcnq4* (P=0.76), or *Kcnq5* (P=0.85) (n=3; Fig. 6.21A). Similarly, *Kcma1* expression did not differ significantly between males and females (P=0.65; Fig. 6.21B).

Protein expression of Kv7.1, which is highly expressed at transcriptional level in the male urethra was examined. Isolated USMC were co-labelled with α-actin and Kv7.1 antibodies, confirming Kv7.1 expression in male USMC (n=3; Fig. 6.22A). Additionally, Kv7.1 was transfected into HEK293 cells for antibody validation with transfected HEK293 serving as a positive control, and untransfected HEK293 as a negative control. Kv7.1 expression was clearly detected in transfected cells (n=3; Fig. 6.22B), but absent in untransfected cells, confirming antibody specificity (n=3; Fig. 6.22C).

Similarly, I examined another Kv7 subtype, Kv7.5 in USMC. Kv7.5 was selected for analysis because recent functional studies from our and other labs in SM have implicated Kv7.5 as a key contributor to background K^+ conductance and regulation of excitability, and pharmacological inhibition with XE991 predominantly targets Kv7.5 channels (Mercer *et al.,* 2025; Tsai *et al.,* 2020). Kv7.5-transfected HEK293 cells served as a positive control, and untransfected cells served as a negative control (Fig. 6.23A-C). Kv7.5 protein colocalized with α-actin in USMC (n=3; Fig. 6.23A). Strong Kv7.5 immunoreactivity was observed in transfected HEK293 cells (n=3; Fig. 6.23B), and no detectable signal in untransfected cells (n=3; Fig. 6.23C).

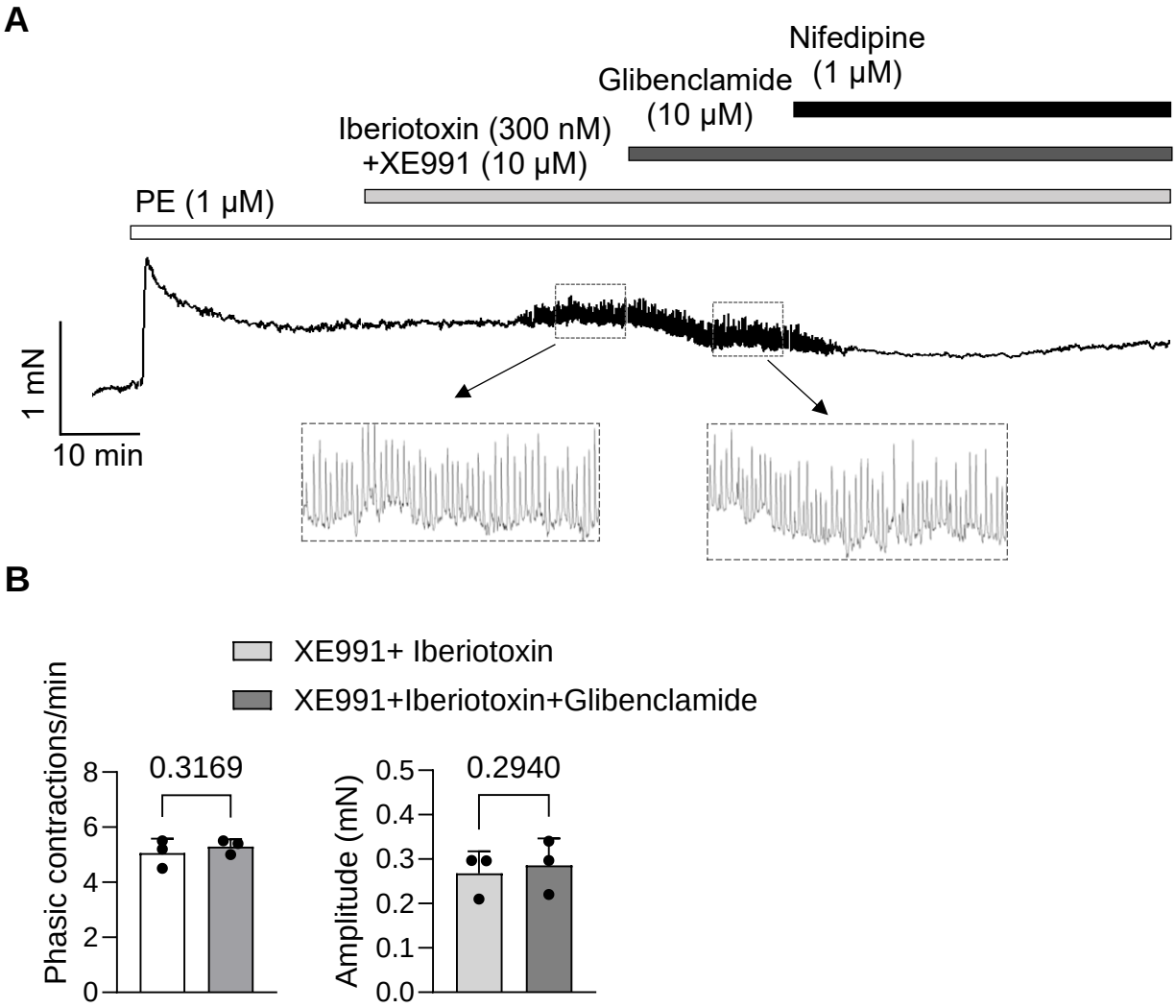

Fig 6.20: K_{ATP} inhibition had no effect on Kv7 and BK_{Ca} channels inhibition induced phasic contractions. Representative data showing the effects of **A.** XE991 (10 μM) and iberiotoxin (300 nM) followed by glibenclamide 10 μM) on pre-contracted male USM with PE (1 μM). **B** Summary of amplitude and frequency of phasic contractions in the presence of combination of XE991+iberiotoxin vs XE991+iberiotoxin+glibenclamide (n=3; Paired t-test). Dotted boxes shows the enlarged view of the phasic contractions.

A

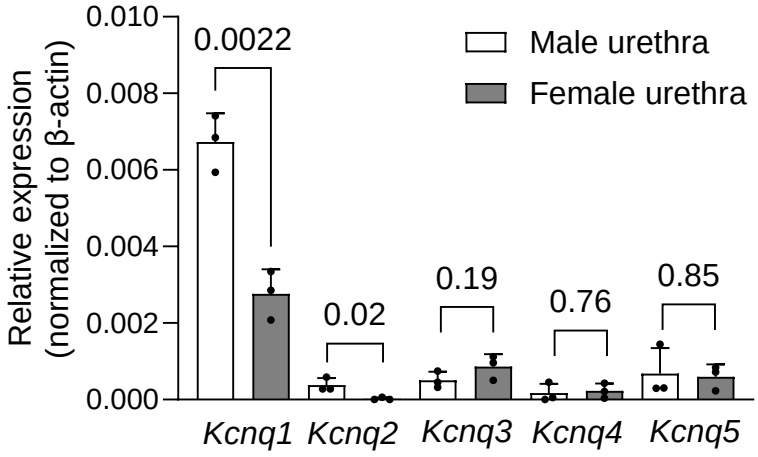

B

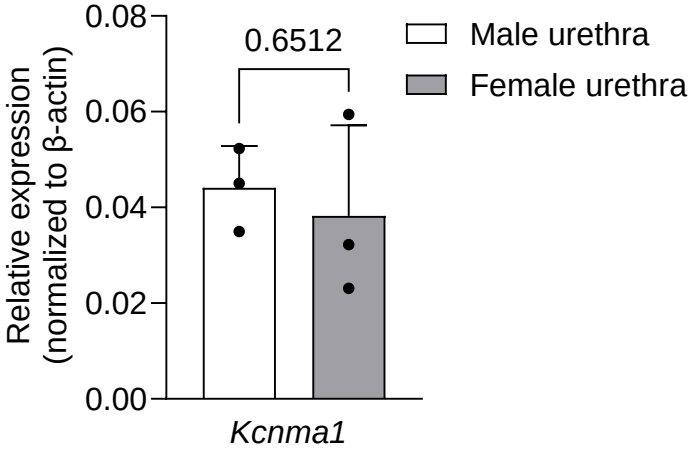

Fig 6.21: Relative expression of *Kcnq1, Kcnq2, Kcnq3, Kcnq4, Kcnq5, Kcma1* in WT male & female urethra. Real-time PCR analyses showing the gene expression of **A** *Kcnq1, Kcnq2, Kcnq3, Kcnq4, Kcnq5, and* **B** *Kcma1* normalized to β-actin gene expression (endogenous control) in male (n=3, N=18), female urethra (n=3, N=18; Unpaired t-test).

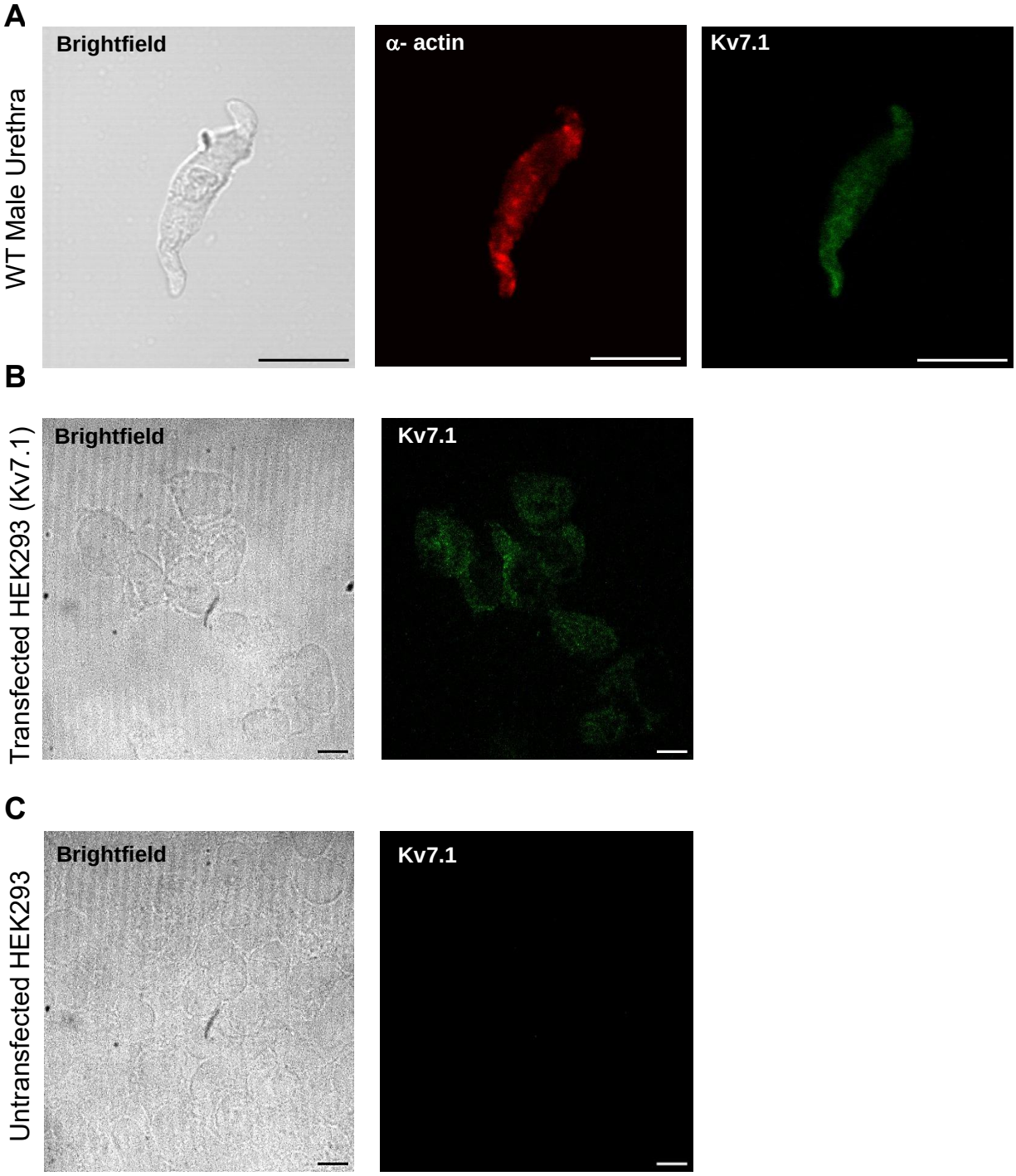

Fig 6.22: Kv7.1 is expressed in murine urethral smooth muscle cells. A Representative images of USMC captured in brightfield and at different wavelengths (488 nm and 555 nm) to show double immuno-labelling for α-actin (red) and Kv7.5 (green) from WT male urethra (n=3), and for controls, Kv7.1 antibody (green) labelling in **B** transfected HEK293 cell (n=3; Positive control) & **C** untransfected HEK293 cell (n=3; negative control). Scale bar: 20 µm in panels **A** and 50 µm in panel **B** and **C.**

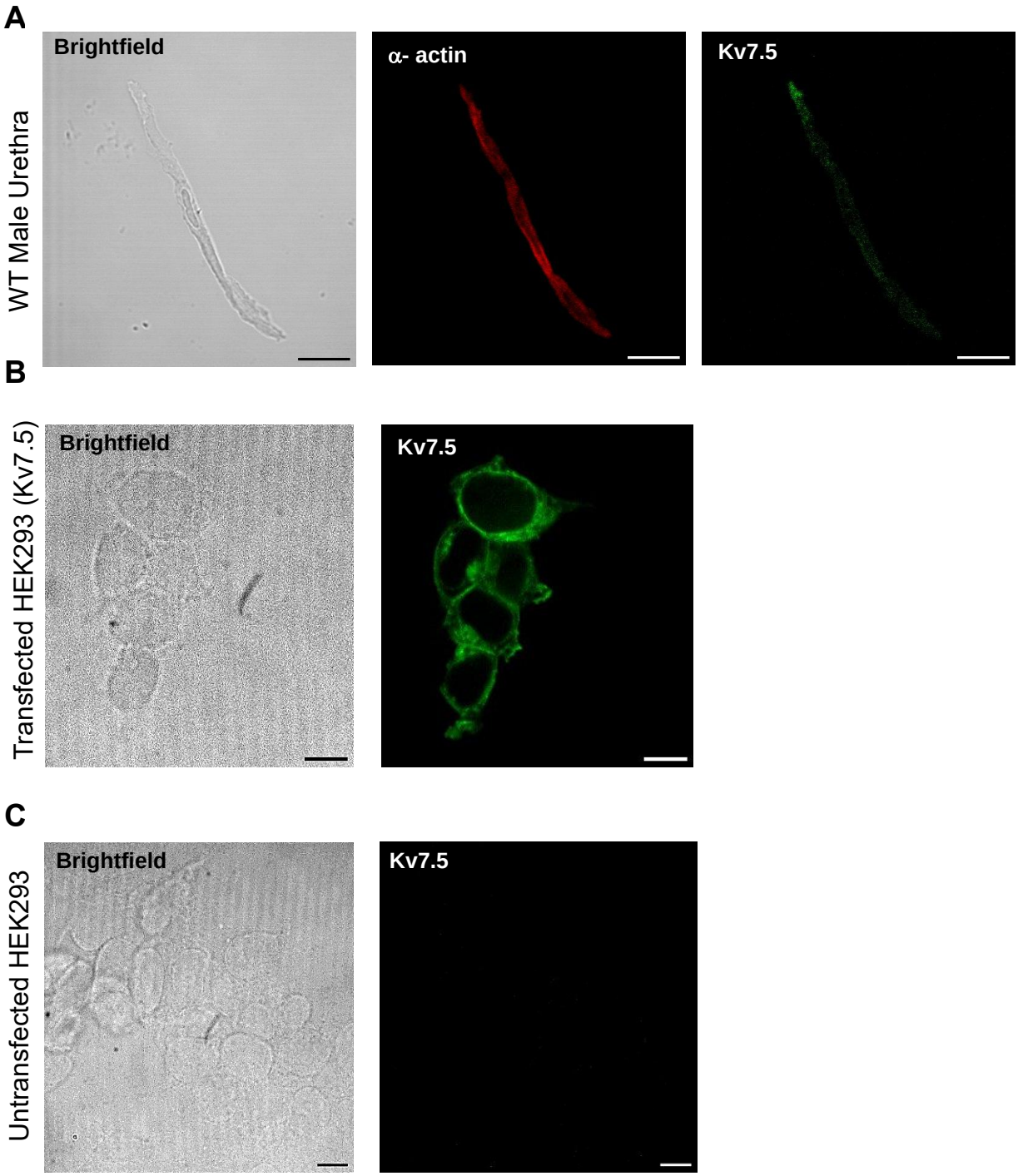

Fig 6.23: Kv7.5 is expressed in murine urethral smooth muscle cells. A Representative images of USMC captured in brightfield and at different wavelengths (488 nm and 555 nm) to show double immuno-labelling for α-actin (red) and Kv7.5 (green) from WT male urethra (n=3), and for controls, Kv7.5 antibody (green) labelling in **B** transfected HEK293 cell (n=3; Positive control) & **C** untransfected HEK293 cell (n=3; negative control). Scale bar: 20 μm in panels **A** and 50 μm in panel **B** and **C.**

6.3 Discussion

K^+ channels are well recognised for their role in stabilising membrane potential and regulating LTCC activity across a range of SM organs, including vascular, gastrointestinal, airways, reproductive and urinary tissues (Brueggemann *et al.,* 2012; Ghatta *et al.,* 2006; Jackson, 2017; Lee *et al.,* 2020; Malysz & Petkov, 2020, 2020b; Mercer *et al.,* 2025; Quayle *et al.,* 1997; Stott *et al.,* 2014; Xu *et al.,* 2011). Present study demonstrates that K^+ channels such as Kv7 and BK_{Ca} act cooperatively to regulate male mouse USM excitability. Their synergistic role becomes apparent during agonist-evoked or nerve-mediated contractions, where they work together to restrain LTCC-mediated Ca^{2+} influx to prevent rhythmic / phasic contractile activity, thereby favour a sustained tonic contraction that is essential for maintaining urethral continence.

Previous studies have reported individual role of either BK_{Ca} or Kv7 in regulating LTCC activity in bladder (Herrera *et al.,* 2000; Malysz & Petkov, 2020; Meredith *et al.,* 2004; Petkov, 2014). Previous work in pig urethral myocytes reported spontaneous transient hyperpolarisations under current-clamp conditions that were eliminated by BK_{Ca} inhibition (Brading *et al.,* 1996). In contrast, our findings in male urethra showed that inhibition of Kv7 or BK_{Ca} channels individually had no effect on PE-induced contractions, whereas combined blockade triggered phasic contractions superimposed on PE-induced contraction without altering the baseline. These phasic contractions were abolished by LTCC inhibition. Similarly, previous studies on corpus cavernosum strips from BK knockout mice ($Slo^{-/-}$) showed that baseline amplitude of agonist-induced contraction was similar between wild-type and $Slo^{-/-}$ tissues. However, $Slo^{-/-}$ mice exhibited up to a four-fold increase in phasic activity superimposed on the agonist-evoked contraction (Werner *et al.,* 2005). Another study on mouse corpus cavernosum reported that Kv7 blockade with XE991 did not alter the baseline amplitude of PE-induced contraction, but increased amplitude of phasic contractions superimposed on the PE-evoked response (Mercer *et al.,* 2025).

Previous work on DSM from BK knockout mice ($Slo^{-/-}$) showed that, in the absence of BK channels, spontaneous and nerve-evoked contractions were markedly enhanced, despite Kv channels remaining fully functional (Meredith *et al.,* 2004). In addition,

urination frequency was also elevated in $Slo^{-/-}$ mice (Meredith *et al.,* 2004), which indicated that BK channels dysfunction leads to UI. However, the effect of absence of BK channel was not assessed on urethra. In present study, combined blockade of Kv7 and BK_{Ca} channels revealed phasic activity superimposed on top of EFS-evoked contractions, along with an increase in contraction amplitude, and both effects were abolished by LTCC inhibition. Notably**,** BK_{Ca} inhibition alone increased amplitude of EFS-evoked contractions of higher frequencies (10 & 20 Hz), and subsequent addition of XE991 further enhanced the response and induced phasic contractions. This suggests that during neural stimulation, BK_{Ca} play a dominant role in limiting LTCC-mediated Ca^{2+} influx, whereas Kv7 channel activity provides an additional or secondary suppression on LTCC activity.

An important observation from the present study is that phasic contractions emerged only when Kv7 and BK_{Ca} channels were inhibited in the presence of G_q-coupled GPCR activation, and not under basal conditions. This indicates that GPCR signalling provides an essential excitatory drive required for this behaviour. Activation of α_1-adrenergic or V1a receptors engages PLC-dependent signalling pathways, leading to hydrolysis of PIP_2 into IP_3 and DAG. While IP_3 promotes Ca^{2+} release from the SR, DAG remains in the plasma membrane where, together with elevated cytosolic Ca^{2+}, it activates PKC (Huang, 1989; Takai *et al.,* 1979). In cardiomyocytes, PKC has been shown to enhance LTCC function, either by promoting channel phosphorylation or by reducing phosphatase-mediated dephosphorylation (Kirchhefer *et al.,* 2014; Pluteanu *et al.,* 2022). Similar findings were also observed in brain hippocampal neurons, where α_1-AR signalling increased LTCC activity mediated by PKC (Man *et al.,* 2023). Therefore, it could be possible that GPCR activation increases the potential for LTCC recruitment in USM, but under normal conditions this effect is functionally constrained by Kv7 and BK_{Ca} channel activity, favouring sustained tonic contraction.

Consistent with isometric tension data, *in situ* Ca^{2+} imaging data from male Acta2-GCaMP8.1USM revealed that combined Kv7 and BK_{Ca} inhibition in presence of an agonist converts asynchronous intracellular Ca^{2+} events in USMC into coordinated Ca^{2+} waves propagating across muscle bundles. After the combined blockade of Kv7 and BK_{Ca}, the USM tissue showed vigorous coordinated / phasic contractions that resembled peristaltic or rhythmic contractions observed in phasic SM organs such as

colon. This synchronized Ca^{2+} activity was reversed to asynchronous Ca^{2+} events when LTCC were blocked. These findings support the view that Kv7 and BK_{Ca} channels act together to prevent the coordinated and phasic USM contractions by restraining LTCC activity, most likely to maintain sustained urethral contraction to prevent urine leakage while bladder filling.

Previous studies in mesenteric artery SMC reported that Orai1 and BK_{Ca} were present in close proximity to each other and were functionally coupled (Chen *et al.,* 2016). The authors further proposed that the hyperpolarizing effect of Orai-BK_{Ca} coupling could contribute to reduce agonist-induced membrane depolarisation, therefore preventing excessive contraction in mesenteric artery SMC (Chen *et al.,* 2016). In gall bladder SM, Orai1 could form a signalling complex with SK3 (Small Conductance Ca^{2+}-Activated K^+ Channel 3), and Ca^{2+} entry via Orai channels activates SK3, resulting in membrane hyperpolarisation (Song *et al.,* 2015). Consistent to the previous findings, in present study, I observed that combined Orai and Kv7 inhibition was sufficient to elicit LTCC-dependent phasic contractions, and subsequent BK_{Ca} blockade further increased this activity. In addition, *in situ* Ca^{2+} imaging recordings also revealed similar results where blockade of Orai and Kv7 channels in presence of an agonist induced coordinated Ca^{2+} waves which were reversed by LTCC inhibition to asynchronous Ca^{2+} activity within USMC. One interpretation is that, under agonist stimulation, Orai-mediated Ca^{2+} entry supports a component of BK_{Ca} activation that normally provides a stabilising restraint on excitability. When Orai is inhibited, this BK_{Ca}-dependent restraint is reduced, and additional removal of BK_{Ca} further facilitates phasic activity. Although these experiments do not directly demonstrate physical coupling, they support the hypothesis that Orai-dependent Ca^{2+} signals contribute to BK_{Ca} recruitment in male USM. This mechanism aligns with Chapter 5, where nifedipine did not affect EFS-evoked contractions, but after Orai inhibition, nifedipine reduced the residual contraction by ~25%. Reduced Orai-dependent Ca^{2+} entry likely decreased BK_{Ca} activation, hence activating LTCC activity which was sensitive to nifedipine.

Previous literature have shown two major sources of Ca^{2+} in DSM through which BK_{Ca} channels are activated: 1) Ca^{2+} entry through LTCC and 2) Ca^{2+} release through RyR (Herrera *et al.,* 2000, 2001; Herrera & Nelson, 2002; Petkov, 2014). In contrast, in the present study, combined inhibition of RyR and Kv7 channels in male USM elicited only

weak and infrequent phasic activity, which was markedly smaller than that observed following combined Orai and Kv7 inhibition. This suggest that RyR-mediated Ca^{2+} release contributes minimally to BK_{Ca} activation in male USM and Orai- mediated BK_{Ca} activation may possibly happen through direct Ca^{2+} influx via Orai channels, however further investigation are needed to test the physical coupling of Orai-BK_{Ca} such as proximity ligation assay.

Similar experiments performed in female mouse USM, where Kv7 and BK_{Ca} channels were blocked in the presence of an agonist, did not induce phasic contractions. This highlights a sex-specific difference in urethral excitability. Findings from Chapter 5 support this interpretation: in males, an LTCC activator evoked phasic contractions on agonist-evoked contractions, whereas in females the same LTCC agonist did not modify AVP-induced contractions. Together, these results suggest that male USM possess a greater capacity to recruit LTCC-dependent excitability pathways, therefore it could be possible that inhibitory K^+ conductances are dominant in males in order to inhibit phasic contractions to favour sustained tonic contractions required for continence (Berridge, 2008). In contrast, female USM appears to have a reduced ability to engage LTCC or might possess less functional LTCC. This interpretation is supported by findings from previous chapter that demonstrated that high K^+ depolarisation-induced, LTCC-mediated contraction was nearly two-fold greater in males than in females. Future studies examining LTCC protein expression in male and female USM will be important to determine whether sex-specific differences exist at the protein level.

I also examined whether ANO1 contributes to the maintenance of phasic contractions unmasked by simultaneous blockade of Kv7 and BK_{Ca} channels. This was tested because ANO1-mediated Cl^- currents can depolarise SM membranes and, in other tissues, have been shown to facilitate LTCC recruitment during excitatory activity (Leblanc *et al.,* 2005; Dunford *et al.,* 2020; Drumm *et al.,* 2021; Wray *et al.,* 2021). However, inhibition of ANO1 with Ani9 had no effect on the amplitude or frequency of these phasic contractions. This indicates that ANO1 does not contribute to the depolarizing drive underlying this activity, and instead supports the conclusion that the phasic contractions observed under Kv7 and BK_{Ca} blockade are driven predominantly by LTCC activation.

In addition, inhibition of K_{ATP} channels had no effect on the phasic contractions unmasked by combined Kv7 and BK_{Ca} blockade in precontracted male mouse urethra, indicating that K_{ATP} channels do not measurably influence LTCC-dependent excitability under these conditions. This contrasts with findings in pig urethra, where K_{ATP} channels have been shown to modulate urethral tone and nerve-evoked contractions through regulation of LTCC activity (Teramoto & Brading, 1996; Brading, 2006; Kyle, 2014; Rembetski *et al.,* 2020). These differences further highlight species-specific difference in the relative contributions of K^+ channel subtypes in regulating urethral excitability and contractility.

Gene expression analysis showed higher levels of *Kcnq1* and *Kcnq2* in male urethra compared with female tissue, whereas Kcma1 expression was similar between sexes. These findings are consistent with earlier work in male guinea-pig DSM, where *Kcnq1* and *Kcnq2* were the most abundant transcripts and *Kcnq4* showed minimal expression in both whole tissue and isolated DSMC (Afeli *et al.,* 2013). Their immunolabelling studies showed robust expression of Kcnq1, Kcnq2, Kcnq3 and Kcnq5, with no detection of Kcnq4 in male guinea pig urethra (Afeli *et al.,* 2013). Anderson *et al.,* (2013) reported the expression of Kcnq1-5 transcripts in male guinea pig DSM and confirmed protein expression of all five subtypes using immunolabelling (Anderson *et al.,* 2013). Immunolabelling studies in male urethra confirmed clear expression of Kv7.1 and Kv7.5. However, other Kv7 subtypes protein expression were not examined due to time constraints. Future work comparing Kv7 protein expression in male and female urethra would help clarify the molecular basis of the sex-dependent differences in channel contribution and urethral excitability observed in this work. Moreover, future studies could employ pharmacological inhibition of specific Kv7 subtypes to elucidate their individual functional roles in male USM.

Collectively, our findings demonstrate Kv7 and BK_{Ca} channels act cooperatively to regulate male USMC excitability, primarily by limiting LTCC-mediated Ca^{2+} influx during agonist- or EFS-induced contractions, see Fig. 6.24. This coordinated K^+ channel activity likely provide a critical “brake” on membrane depolarisation, preventing phasic / coordinated contractions of USM. Such phasic contractile patterns are characteristic of organs with a propulsive function, including the colon, bladder, ureter, and uterus, where rhythmic activity is required to generate peristaltic

movements for the propulsion or expulsion of luminal contents (Berridge, 2008). In contrast, USM forms the IUS and therefore must maintain sustained tonic contraction to preserve urinary continence. Our data from previous chapters demonstrate that sustained USM contractions in both male and female USM is supported by Orai-mediated SOCE together with SR Ca^{2+} release, consistent with previous findings in male USM (Drumm *et al.,* 2018). As described previously, GPCR signalling could potentially trigger LTCC activity by PKC activation (Kirchhefer *et al.,* 2014; Pluteanu *et al.,* 2022). Therefore, to preserve the tonic contractile state, Ca^{2+} influx through Orai channels may engage BK_{Ca} channels, thereby limiting LTCC recruitment and preventing the emergence of coordinated phasic activity along with Kv7 channels (that provide additional or secondary inhibition). This interpretation is supported by the present chapter findings and aligns with evidence from other SM tissues demonstrating functional coupling between Orai-dependent Ca^{2+} entry and Ca^{2+}-activated K^+ channels (Chen *et al.,* 2016; Song *et al.,* 2015).

Recent work in airway SM has demonstrated that SR Ca^{2+} buffering via SERCA can effectively sequester Ca^{2+} entering through LTCC, thereby limiting its contribution to contraction (Ghosh *et al.,* 2025). Under nerve-evoked stimulation at 2 Hz, 10 sec interval, LTCC-dependent Ca^{2+} influx becomes functionally apparent, and inhibition of SERCA similarly unmasks LTCC-mediated Ca^{2+} entry during nerve stimulation at 2 Hz, 100 sec interval, conditions in which LTCC activity is otherwise minimal (Ghosh *et al.,* 2025). Although SERCA function was not directly examined in the present study, a comparable buffering mechanism may operate in USM. Such a mechanism could help explain why LTCC appear functionally silent under basal conditions but become recruitable during agonist- or nerve-evoked stimulation, when G_q-coupled GPCR signalling is engaged and inhibitory Kv7 and BK_{Ca} channel constraints are relieved.

Notably, this coordinated regulation is absent in females, highlighting a clear sex-specific divergence in ionic control of USMC. The minimal impact of Kv7 and BK_{Ca} inhibition, together with reduced LTCC-dependent activity in female USMC as evident in Chapter 5, suggests several possibilities: females may have lower LTCC protein expression or different subunit composition affecting channel conductance or voltage sensitivity, or employ alternative mechanisms to regulate excitability, such as enhanced reliance on Orai-mediated SOCE or IP_3-dependent Ca^{2+} release. Another

possibility could be that LTCC activity may be important in the distal urethra of males, where coordinated, phasic SM contractions are required for ejaculation (De Almeida Kiguti & Pupo, 2012). In distal region, Ca^{2+} influx through LTCC will induce coordinated contractions for effective semen expulsion, and Kv7 and BK_{Ca} channels may act as modulators to prevent premature or excessive activity when triggered by neural inputs (De Almeida Kiguti & Pupo, 2012). There is a possibility that a vestige of this regulatory mechanism may also exist in the proximal urethra of male mice, and therefore absent in females, however direct evidence for such interpretation is missing. Overall, these findings highlight fundamental differences in the ionic regulation of urethral contractility between sexes and provide a framework for future studies investigating how sex-dependent ion channel organization contributes to continence and LUT dysfunction.

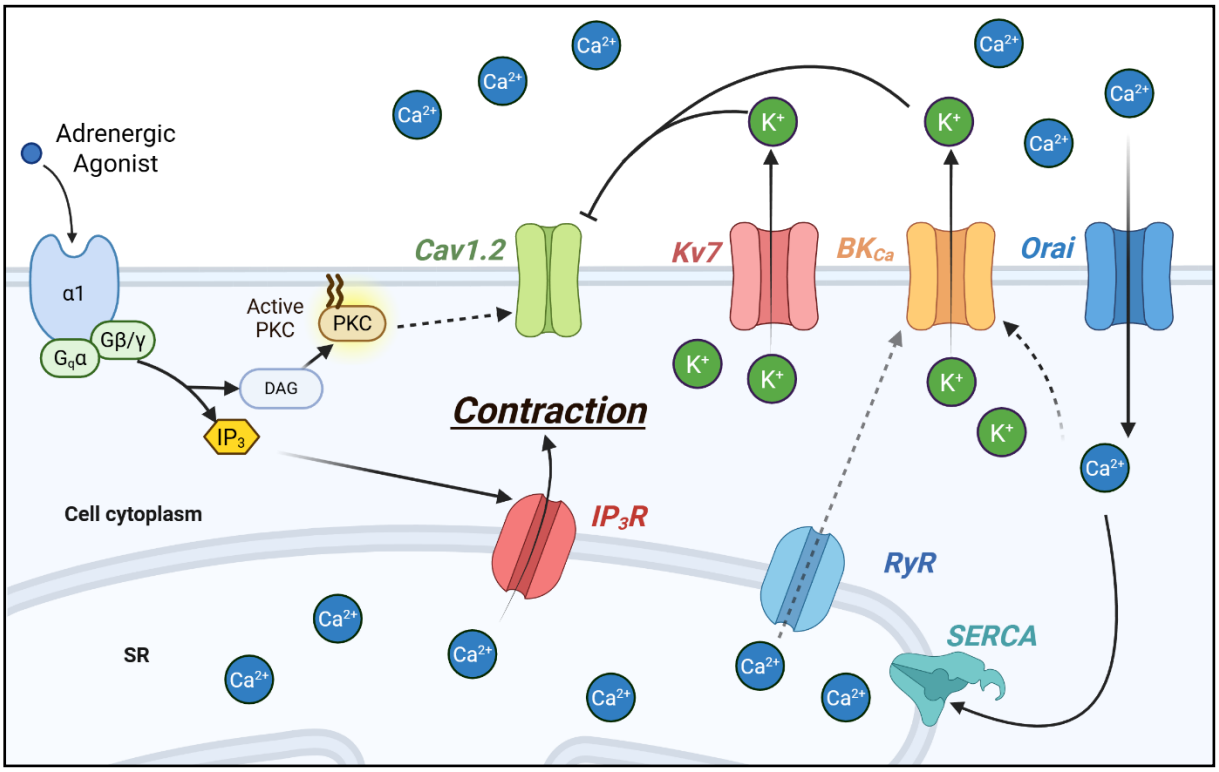

Fig 6.24: Proposed integrated model of Kv7, BK_{Ca} and Orai channel interactions sustaining tonic contractility by restraining LTCC-dependent phasic activity in male USM. Activation of G_q-coupled signalling pathways by agonists or endogenous release of NA has the potential to promote LTCC activity, likely through downstream signalling such as PKC activation. Under these conditions, the activity of Kv7 and BK_{Ca} channels acts to restrain membrane depolarisation and thereby limit LTCC recruitment. In parallel, Ca^{2+} influx through Orai channels contributes to partial activation of BK_{Ca} conductance, thereby constraining LTCC activity, whereas Ca^{2+} release mediated by RyR provides only a minimal contribution to BK_{Ca} activation.

7. General discussion & Future work

7.1 General Discussion

The central aim of this thesis was to define how different cellular and ionic mechanisms regulate USM contractility, and thereby maintain urinary continence. By employing cell-specific *in situ* Ca^{2+} imaging, transcriptional profiling, immunolabelling, pharmacological modulation, nerve stimulation, and functional contractility measurements, this work provides new insight into how excitatory and inhibitory pathways are coordinated within male and female mouse USM.

ICC-LC have long been proposed to act as pacemakers or neuromodulators in the urethra similar to ICC in gut. However, previous studies on rabbit urethral ICC-LC were largely performed on isolated cells identified as ICC-LC based on morphology and not a specific cellular marker, and intact tissue studies utilized non-selective Ca^{2+} dyes (Sergeant *et al.,* 2000; Hashitani & Suzuki, 2007). In addition, direct nerve stimulation was never attempted that more closely mimics physiological signalling. This limited the ability to distinguish ICC-LC from other cells and made it difficult to assign functional roles with certainty. By directly visualising ICC-LC *in situ* using a transgenic mouse model, KitGCaMP6f, that expressed a GCaMP Ca^{2+} sensor in Kit^{+} cells, this study demonstrates that murine ICC-LC differ fundamentally from classical gastrointestinal ICC. Murine ICC-LC lacked functional innervation as they do not respond to nerve stimulation and also lacked ANO1 expression. They display spontaneous, asynchronous Ca^{2+} activity driven predominantly by Orai-mediated Ca^{2+} entry and ER Ca^{2+} release. These observations argue strongly against a primary pacemaker or neuromodulatory role for ICC-LC in mouse USM.

Importantly, this does not imply that ICC-LC are functionally irrelevant. Rather, the data suggest a tonic role, potentially contributing to the maintenance of basal urethral tone through sustained asynchronous intracellular Ca^{2+} signalling. A comparable mechanism was also previously described in other sphincter tissues such as LES and IAS, where a subset of ICC-IM also possess asynchronous Ca^{2+} activity mediated by Orai channels and ER Ca^{2+} release, which helps in tone generation, thereby contributes to closure of sphincter. In the urethra, ICC-LC may influence USMC activity through membrane potential-independent mechanisms, such as diffusion of Ca^{2+}, IP_3, or ATP via gap junctions or paracrine signalling as shown in other tissues including

vasculature and pancreatic acinar networks (Buckley et. al., 2024; Leybaert & Sanderson, 2012; Takano & Yule, 2023; Yule & Takano, 2024). While direct evidence for this form of intercellular communication in USM remains lacking, the presence of connexins in urethral tissues and the known sensitivity of USM tone to purinergic signalling support this possibility and highlight an important avenue for future work.

A second important outcome of this thesis is the clarification of ANO1's role in mouse USM. Although ANO1 is widely regarded as a key depolarizing conductance and favours LTCC activation in various SM and has been implicated in urethral tone in previous studies, the present findings establish clear limits on its functional contribution in the mouse USM. ANO1 was detected in USMC but not in ICC-LC, excluding a gastrointestinal-type ICC-SMC coupling mechanism. Selective ANO1 inhibition (Ani9, (Seo *et al.,* 2016)) did not affect basal tone, agonist-evoked contractions, nerve-evoked responses, or *in situ* Ca^{2+}dynamics in either sex. These results help reconcile conflicting reports in the literature that relied on non-selective CaCC inhibitors that can interfere with SR Ca^{2+} handling and/or voltage-gated Ca^{2+} entry (Cruickshank *et al.,* 2003; Dwivedi, Drumm, Alkawadri, *et al.,* 2023; Genovese *et al.,* 2023; Oba, 1997), or indirect activators such as EACT, which elevate intracellular Ca^{2+} via TRP channels (TRPV1 & TRPV4) (Genovese *et al.,* 2019; Liu *et al.,* 2016). Taken together, the data indicate that ANO1 does not modulate USM tone and evoked contractions under conditions tested.

Another key contribution of this thesis is the re-evaluation of LTCC in urethral function. LTCC are traditionally viewed as central regulators of SM contraction, yet their role in the urethra has remained debated and species-dependent. This thesis work demonstrates that, despite robust gene expression of Cav1.2 transcripts, LTCC contribute minimally to basal tone, agonist-induced contractions, or nerve-evoked responses or *in situ* Ca^{2+} dynamics in mouse USM. Instead, Ca^{2+} entry via Orai channels and subsequent SR Ca^{2+} release represent the dominant pathway sustaining urethral contraction in both sexes. These finding consolidates and extends earlier observations in male mice and establishes, for the first time, that female USM shares a similar reliance on Orai-dependent Ca^{2+} signalling.

Crucially, this thesis reveal that LTCC are not absent or non-functional, particularly in males. Pharmacological activation or strong depolarisation can recruit LTCC to enhance contraction and generate phasic activity in male urethra, an effect that is largely absent in females. High-K^+ depolarisation produced significantly greater contractions in males, indicating a larger functional LTCC reserve. These findings indicate that LTCC are present but normally suppressed, rather than inactive per se.

A major mechanistic insight of this thesis is the identification of K^+ channels as central regulators of this suppression. In male USM, BK_{Ca} and Kv7 channels act together to restrain LTCC recruitment during physiological stimulation. Combined inhibition of BK_{Ca} and Kv7 unmasked coordinated Ca^{2+} waves and phasic contractions that closely resemble those seen in propulsive SM tissues such as bladder or colon. Reversal of this activity by LTCC inhibition confirmed its voltage-dependent nature. These findings demonstrate that the urethra is actively configured to suppress phasic excitability, thereby favouring sustained tonic contraction required for continence. Importantly, this phenomenon was observed only during G_q-coupled GPCR activation and not under basal conditions. This indicate that LTCC recruitment requires an excitatory signalling state generated by agonist or neural stimulation, most likely via DAG-PKC mediated LTCC activation, that is normally counterbalanced by K^+ channel restraint.

The interaction between Orai channels and K^+ channels further refines this regulatory framework. Inhibition of Orai channels reduced a component of BK_{Ca}-dependent restraint, as evidenced by the emergence of phasic contractions when Orai and Kv7 channels were blocked together, with further enhancement upon BK_{Ca} inhibition. These observations indicate that Ca^{2+} influx through Orai channels contributes to activation of BK_{Ca} channels, thereby limiting LTCC recruitment. RyR-mediated Ca^{2+} release played only a minor role in this process, as combined inhibition of RyR and Kv7 channels produced only weak phasic responses. Together, these data support a model in which Orai-mediated Ca^{2+} entry sustains tonic contraction while simultaneously engaging BK_{Ca} channels to prevent voltage-dependent excitability.

Sex-specific differences further underscore the physiological relevance of this organisation. Female urethra did not develop phasic activity following blockade of BK_{Ca} and Kv7 channels and showed minimal responsiveness to LTCC activation. This

reduced excitability likely reflects lower functional LTCC availability, as supported by smaller depolarisation-induced contractions. As a consequence, inhibitory K^+ channel restraint appears less critical in females, since the underlying voltage-dependent excitatory machinery is already limited. This sex difference may represent an adaptive mechanism reflecting distinct anatomical or functional demands on the male and female urethra.

While this thesis provides a coherent framework for understanding how USM maintains tonic contractility, several limitations and open questions remain. The proposed role of diffusible messengers in ICC-LC-USMC communication remains speculative without direct functional evidence. The molecular mechanisms linking GPCR activation to LTCC recruitment were not directly examined and may involve PKC-dependent modulation, changes in phosphatase activity, or alterations in channel microdomain organisation. Protein-level differences in LTCC expression between sexes were not assessed and represent an important avenue for future investigation. Another limitation of the present study is the reliance on pharmacological modulation to infer the functional roles of specific signalling pathways. Although these agents were carefully selected based on previously reported selectivity, pharmacological inhibitors may exhibit uncertain specificity and off-target effects. For example, the non-selective IP_3 receptor inhibitor, 2-APB is known to affect several additional pathways, including inhibition of SOCE, SERCA activity, TRPM7 channels, and mitochondrial Ca^{2+} uptake (Peppiatt *et al.,* 2003; Chokshi *et al.,* 2012). Therefore, the observed effects should be interpreted with caution. Future studies using direct electrophysiological measurements of membrane potential or channel currents, as well as genetically modified models such as targeted gene knockout approaches, would provide further mechanistic insight.

In summary, this thesis advances understanding of urethral physiology by shifting the focus from single-channel dominance to coordinated regulation of excitability. It establishes that continence in the mouse urethra is maintained not by LTCC-driven contraction, but by sustained Orai-mediated SOCE and SR Ca^{2+} release in both sexes. In males, LTCC activity is functionally greater than in females, and that is tightly constrained by K^+ channels. ICC-LC emerge not as pacemakers or neuromodulators, but as Ca^{2+} signalling elements that may contribute to tonic regulation through non-

electrical mechanisms. Together, these findings provide a refined physiological framework for urethral function and lay the groundwork for future studies targeting specific ionic pathways in LUT dysfunction.

Future prospects

- **Investigate gap-junction coupling between ICC-LC and USMC:** It is currently unknown how ICC-LC modulate USMC excitability. ICC-LC observed in our studies using Kit-GCaMP6f mouse urethra were spontaneously active yet if their activity directly influence USMC is unknown. Imunnolabelling studies of expression of gap junction, Cx43 and Cx37, which were earlier detected in rat and sheep USMC and ICC-LC (Sancho *et al.,* 2011), could be examined in mouse USMC / ICC-LC. Gap junction inhibitors such as 18α-glycyrrhetinic acid could be tested on ICC-LC and USMC intracellular Ca^{2+} activity. In addition, investigating coupling through paired electrophysiology could determine whether ICC-LC influence USMC contractility directly or act independently.

- **Determine USM resting membrane potential (RMP):** Currently RMP of mouse USM is unknown. RMP determines how close membrane potential is to the threshold for opening voltage dependent channels, therefore electrophysiological studies could be employed to determine the resting membrane potential of male and female USM under physiological conditions.

- **Investigate functional impact of ANO1 alternative splicing in USM:** The expression of ANO1 splice variants (exons a-d and exon 0) in male and female USM could examined using qPCR or RNA-sequencing. Functional characterization could involve heterologous expression of individual splice variants in HEK293 cells followed by patch-clamp studies to determine Ca^{2+} sensitivity, voltage dependence, and pharmacological responsiveness to ANO1 inhibitors. This approach may clarify whether differential splice variant expression underlies sex-specific responses and the variable sensitivity of urethral tissue to ANO1 modulation.

- **Investigate age-dependent ANO1 channel function in mouse USMC:** Based on findings in murine small intestine, where ANO1 antagonists inhibited SW in juveniles but not adults, suggesting that a conductance in addition to ANO1 may develop in small intestinal ICC with ageing and contribute to pacemaker activity (Hwang *et al.,* 2019). Future studies could examine this in urethra by investigating the ANO1 expression in juvenile vs adult mouse urethra. In addition, ANO1 inhibitors can be tested on juvenile urethral tissues in isometic tensions and also in Ca^{2+} imaging.

- **LTCC protein expression studies between sexes:** Comparative studies using western blotting and immunolabelling could be performed on male and female mouse urethra to elucidate sex-specific differences in LTCC expression, to investigate whether the lower high-K^+-induced contractility and no effect of LTCC activation observed in females is linked to differential LTCC expression.

- **Investigate STIM subtype expression in USMC:** Our preliminary qPCR data revealed high Orai1 and lower Orai2 expression in mouse USM, but STIM subtype expression remains unexplored. Future studies could examine STIM1 and STIM2 expression using qPCR and immunolabelling studies in USM.

- **Electrophysiological studies investigating Kv7 and BK_{Ca} conductance:** Patch-clamp recordings in isolated USMC could be performed to directly measure Kv7 and BK_{Ca} currents, and to determine how their inhibition affects membrane potential and could reveal LTCC currents. This would allow precise characterization of the contribution of these K^+ channels to urethral excitability.

- **Expression profile of Kv7 subtypes and functional role:** While Kv7.1 and Kv7.5 were examined in this thesis, other Kv7 subtypes could be studied in mouse USMC. Pharmacological modulation of individual subtypes with BK_{Ca} inhibition, could identify dominant Kv7 subtype regulating urethral contractility.

8. Bibliography

Adelstein, R.S. and Sellers, J.R. (1987). Effects of calcium on vascular smooth muscle contraction. *The American Journal of Cardiology*, 59(3), B4–B10.

Afeli, S.A.Y., Malysz, J. and Petkov, G.V. (2013). Molecular expression and pharmacological evidence for a functional role of Kv7 channel subtypes in guinea pig urinary bladder smooth muscle. *PLoS ONE*, 8(9), e75875.

Agarwal, P., Sharma, D., Wankhede, S., Jain, P.C. and Agrawal, N.L. (2019). Sciatic nerve to pudendal nerve transfer: Anatomical feasibility for a new proposed technique. *Indian Journal of Plastic Surgery*, 52(2), 222–225.

Ahmad, F., Boulaftali, Y., Greene, T.K., Ouellette, T.D., Poncz, M. and Feske, S. (2011). Relative contributions of stromal interaction molecule 1 and CalDAG-GEFI to calcium-dependent platelet activation and thrombosis. *Journal of Thrombosis and Haemostasis*, 9(10), 2077–2086.

Aickin, C.C. (1994). Regulation of intracellular pH in the smooth muscle of guinea-pig ureter: HCO_3^- dependence. *The Journal of Physiology*, 479(Pt 2), 317–331.

Aickin, C.C. and Vermuë, N.A. (1983). Microelectrode measurement of intracellular chloride activity in smooth muscle cells of guinea-pig ureter. *Pflügers Archiv: European Journal of Physiology*, 397(1), 25–28.

Alberts, P., Bergström, P.A.C. and Fredrickson, M.G. (1999). Characterisation of the functional α-adrenoceptor subtype in the isolated female pig urethra. *European Journal of Pharmacology*, 371(1), 31–38.

Alexandre, E.C., Leiria, L.O., Silva, F.H., Mendes, A.K., De Nucci, G. and Andersson, K.-E. (2017). How important is the α_1-adrenoceptor in primate and rodent proximal urethra? Sex differences in the contribution of α_1-adrenoceptor to urethral contractility. *American Journal of Physiology – Renal Physiology*, 312(6), F1026–F1034.

Al-Shboul, O. (2013). The importance of interstitial cells of Cajal in the gastrointestinal tract. *Saudi Journal of Gastroenterology*, 19(1), 3–8.

Ambrogi, M., Hernandez, L.L., Strand, D.W., Kumar, S., Romero, M.F., Barasch, J., Ridlon, M., Keil Stietz, K.P., and Vezina, C.M. (2025). A 5-HT-mediated urethral defense against urinary tract infections. *Proceedings of the National Academy of Sciences of the United States of America*, 122(16), e2409754122.

Andersson, K.E. (2001). Neurotransmission and drug effects in urethral smooth muscle. *Scandinavian Journal of Urology and Nephrology, Supplement*, 35(207), 26-34.

Andersson, K.E. and Arner, A. (2004). Urinary bladder contraction and relaxation: physiology and pathophysiology. *Physiological Reviews*, 84(3), 935–986.

Andersson, K.E. and McCloskey, K.D. (2014). Lamina propria: The functional center of the bladder? *Neurourology and Urodynamics*, 33(1), 9–16.

Andersson, K.E. and Persson, K. (1994). Nitric oxide synthase and nitric oxide-mediated effects in lower urinary tract smooth muscles. *World Journal of Urology*, 12(5), 274–280.

Andersson, K.E. and Uvelius, B. (2024). Urethral pharmacological mechanisms in continence and bladder emptying: An updated review. *Bladder*, 11(3), e21200015.

Ashton-Miller, J.A., Howard, D. and DeLancey, J.O.L. (2001). The functional anatomy of the female pelvic floor and stress continence control system. *Scandinavian Journal of Urology and Nephrology, Supplement*, 35(207), 1–7.

Atala, A., Lanza, R., Mikos, A.G. and Nerem, R.M. (2010). Principles of regenerative medicine. *Principles of Regenerative Medicine*, 2nd ed., 1–1182.

Bader, C.R., Bertrand, D. and Schwartz, E.A. (1982). Voltage-activated and calcium-activated currents studied in solitary rod inner segments from the salamander retina. *The Journal of Physiology*, 331(1), 253–284.

Baker, F.J. and Silverton, R.E. (1976). Renal function tests. *Introduction to Medical Laboratory Technology*, 233–282.

Baker, S.A., Drumm, B.T., Saur, D., Hennig, G.W., Ward, S.M. and Sanders, K.M. (2021). Ca^{2+} signaling driving pacemaker activity in submucosal interstitial cells of Cajal in the murine colon. *eLife*, 10, e64099.

Balderas, E., Zhang, J., Stefani, E. and Toro, L. (2012). Niflumic acid blocks native and recombinant T-type channels. *Journal of Cellular Physiology*, 227(6), 2542–2555.

Bardsley, A. (2016). An overview of urinary incontinence. *British Journal of Nursing*, 25(18), S14–S21.

Barish, M.E. (1983). A transient calcium-dependent chloride current in the immature Xenopus oocyte. *The Journal of Physiology*, 342(1), 309–325.

Bayguinov, O., Hennig, G.W., Smith, T.K. and Sanders, K.M. (2007). Voltage-gated Ca^{2+} currents are necessary for slow-wave propagation in the canine gastric antrum. *American Journal of Physiology – Cell Physiology*, 293(5), C1645–C1659.

Beckett, E.A.H., Sanders, K.M. and Ward, S.M. (2017). Inhibitory responses mediated by vagal nerve stimulation are diminished in stomachs of mice with reduced intramuscular interstitial cells of Cajal. *Scientific Reports*, 7, 44759.

Berridge M. J. (2008). Smooth muscle cell calcium activation mechanisms. *The Journal of physiology*, *586*(21), 5047–5061.

Bernstein, K., Vink, J.Y., Fu, X.W., Wakita, T., Danielsson, J., Wapner, R.J. and Gallos, G. (2014). Calcium-activated chloride channels anoctamin 1 and 2 promote murine uterine smooth muscle contractility. *American Journal of Obstetrics and Gynecology*, 211(6), 688.e1–688.e10.

Berna-Erro, A., Jardin, I., Salido, G.M. and Rosado, J.A. (2017). Role of STIM2 in cell function and physiopathology. *The Journal of Physiology*, 595(10), 3111–3128.

Birder L. A. (2014). Urinary bladder, cystitis and nerve/urothelial interactions. *Autonomic neuroscience : basic & clinical*, *182*, 89–94.

Birder, L. A. and Andersson, K.E. (2013). Urothelial signaling. *Physiological Reviews*, 93(2), 653–680.

Boedtkjer, D.M.B., Kim, S., Jensen, A.B., Matchkov, V.V. and Aalkjaer, C. (2015). New selective inhibitors of calcium-activated chloride channels – T16Ainh-A01, CaCCinh-A01 and MONNA – what do they inhibit? *British Journal of Pharmacology*, 172(16), 4158–4171.

Boie, S., Jepps, T.A., Torekov, S.S., Nyberg, M., Kroigaard, C., Orngreen, M.C. and Matchkov, V.V. (2016). The relative contributions of store-operated and voltage-gated Ca^{2+} channels to the control of Ca^{2+} oscillations in airway smooth muscle. *The Journal of Physiology*, 595(10), 3129–3145.

Boitano, S., Dirksen, E.R. and Sanderson, M.J. (1992). Intercellular propagation of calcium waves mediated by inositol trisphosphate. *Science*, 258(5080), 292–295.

Borsdorf, M., Müller, A., Hofmann, F., Hennenlotter, J., Stenzl, A. and Schwentner, C. (2019). Locational and directional dependencies of smooth muscle properties in pig urinary bladder. *Frontiers in Physiology*, 10, 63.

Brading, A.F. (1999). The physiology of the mammalian urinary outflow tract. *Experimental Physiology*, 84(1), 215–221.

Brading, A., Teramoto, N., Nakayama, S., Bramich, N., Inoue, R., Fujii, K., and Mostwin, J. (1996). Smooth muscle excitation. *Smooth Muscle Excitation*, 1–403.

Bradley, E., Hollywood, M.A., McHale, N.G., Thornbury, K.D., and Sergeant, G.P. (2005). Pacemaker activity in urethral interstitial cells is not dependent on capacitative calcium entry. *American Journal of Physiology – Cell Physiology*, 289(3), C625–C632.

Bradley, E., Hollywood, M.A., Johnston, L., Large, R.J., McHale, N.G., Thornbury, K.D., and Sergeant, G.P. (2006). Contribution of reverse Na^{+}–Ca^{2+} exchange to spontaneous activity in interstitial cells of Cajal in the rabbit urethra. *The Journal of Physiology*, 574(3), 651–661.

Bradley, E., Hollywood, M.A., Johnston, L., McHale, N.G., Thornbury, K.D., and Sergeant, G.P. (2010). Novel excitatory effects of adenosine triphosphate on contractile and pacemaker activity in rabbit urethral smooth muscle. *The Journal of Urology*, 183(2), 801–811.

Bradley, E., Fedigan, S., Webb, T.I., Hollywood, M.A., Thornbury, K.D., McHale, N.G., and Sergeant, G.P. (2014). Pharmacological characterization of TMEM16A currents. *Channels*, 8(4), 308–320.

Bradley, E., Large, R.J., Bihun, V.V., Mullins, N.D., Hollywood, M.A., Sergeant, G.P., and Thornbury, K.D. (2018). Inhibitory effects of openers of large-conductance Ca^{2+}-activated K^{+} channels on agonist-induced phasic contractions in rabbit and mouse bronchial smooth muscle. *American Journal of Physiology – Cell Physiology*, 315(6), C818–C829.

Bradley, J.E., Anderson, U.A., Woolsey, S.M., Thornbury, K.D., McHale, N.G., and Hollywood, M.A. (2004). Characterization of T-type calcium current and its contribution to electrical activity in rabbit urethra. *American Journal of Physiology – Cell Physiology*, 286(5), C1078–C1088.

Bridgewater, M., MacNeil, H.F., and Brading, A.F. (1993). Regulation of tone in pig urethral smooth muscle. *The Journal of Urology*, 150(1), 223–228.

Brommundt, G., and Kavaler, F. (1987). La^{3+}, Mn^{2+}, and Ni^{2+} effects on Ca^{2+} pump and on Na^{+}–Ca^{2+} exchange in bullfrog ventricle. *American Journal of Physiology*, 253(1 Pt 1), C45–C51.

Brueggemann, L.I., Kakad, P.P., Love, R.B., Solway, J., Dowell, M.L., Cribbs, L.L., and Byron, K.L. (2012). Kv7 potassium channels in airway smooth muscle cells: Signal transduction intermediates and pharmacological targets for bronchodilator therapy. *American Journal of Physiology – Lung Cellular and Molecular Physiology*, 302(1), L120–L132.

Buckley, C., Lee, M.D., Zhang, X., Wilson, C., and McCarron, J.G. (2024). Signalling switches maintain intercellular communication in the vascular endothelium. *British Journal of Pharmacology*, 181(16), 2810–2832.

Bulley, S., Neeb, Z.P., Burris, S.K., Bannister, J.P., Thomas-Gatewood, C.M., Jangsangthong, W., and Jaggar, J.H. (2012). TMEM16A/ANO1 channels contribute to the myogenic response in cerebral arteries. *Circulation Research*, 111(8), 1027–1036.

Bulley, S., and Jaggar, J.H. (2014). Cl^- channels in smooth muscle cells. *Pflügers Archiv – European Journal of Physiology*, 466(5), 861–872.

Burns, A.J., Lomax, A.E., Torihashi, S., Sanders, K.M., and Ward, S.M. (1996). Interstitial cells of Cajal mediate inhibitory neurotransmission in the stomach. *Proceedings of the National Academy of Sciences of the United States of America*, 93(21), 12008–12013.

Burns, A.J., Herbert, T.M., Ward, S.M., and Sanders, K.M. (1997). Interstitial cells of Cajal in the guinea-pig gastrointestinal tract as revealed by c-Kit immunohistochemistry. *Cell and Tissue Research*, 290(1), 11–20.

Burnstock, G. (2014). Purinergic signalling in the urinary tract in health and disease. *Purinergic Signalling*, 10(1), 103–155.

Bylund, D.B., Eikenberg, D.C., Hieble, J.P., Langer, S.Z., Lefkowitz, R.J., Minneman, K.P., Molinoff, P.B., Ruffolo, R.R., and Trendelenburg, U. (1994). International Union of Pharmacology nomenclature of adrenoceptors. *Pharmacological Reviews*, 46(2), 121–136.

Callahan, S.M., and Creed, K.E. (1981). Electrical and mechanical activity of the isolated lower urinary tract of the guinea-pig. *British Journal of Pharmacology*, 74(2), 353–358.

Caputo, A., Caci, E., Ferrera, L., Pedemonte, N., Barsanti, C., Sondo, E., Pfeffer, U., Ravazzolo, R., Zegarra-Moran, O., and Galietta, L.J.V. (2008). TMEM16A, a

membrane protein associated with calcium-dependent chloride channel activity. *Science*, 322(5901), 590–594.

Cass, A.S., and Hinman, F. (1968). Constant urethral flow in female dog. II. Effect of constriction of vesical neck and external meatus. *The Journal of Urology*, 99(4), 447–454.

Catterall, W.A. (2000). From ionic currents to molecular mechanisms: the structure and function of voltage-gated sodium channels. *Neuron*, 26(1), 13–25.

Catterall, W.A. (2011). Voltage-gated calcium channels. *Cold Spring Harbor Perspectives in Biology*, 3(8), a003947.

Celentano, C., Stringer, M.S., Bunke, M., Wang, Y., Zhang, Y., Pires, P.W., and Earley, S. (2024). Kv7 channel activation reduces brain endothelial cell permeability and prevents kainic acid-induced blood–brain barrier damage. *American Journal of Physiology – Cell Physiology*, 326(3), C893–C904.

Chang, S., Gomes, C.M., Hypolite, J.A., Marx, J., Alanzi, J., Zderic, S.A., Wein, A.J., Chacko, S., and DiSanto, M.E. (2010). Detrusor overactivity is associated with downregulation of large-conductance calcium- and voltage-activated potassium channel protein. *American Journal of Physiology – Renal Physiology*, 298(6), F1416–F1423.

Chen, D., Wang, Y., Zhang, J., Zhang, X., Zuo, W., Li, X., and He, Q. (2020). ANO1 in urethral smooth muscle cells contributes to sex differences in urethral spontaneous tone. *American Journal of Physiology – Renal Physiology*, 319(3), F394–F402.

Chen, D., Zhang, J., Wang, Y., Li, X., Zuo, W., Zhang, X., and He, Q. (2022). Hypertriglyceridemia impairs urethral spontaneous tone through down-regulation of ANO1 in mouse urethral smooth muscle cells. *Urology*, 165, 157–163.

Cheng, L., MacLennan, G.T., and Bostwick, D.G. (2020). *Urologic Surgical Pathology*, 4th ed., 1–965.

Chen, H., Ordög, T., Chen, J., Young, D.L., Bardsley, M.R., Redelman, D., Ward, S.M., and Sanders, K.M. (2007). Differential gene expression in functional classes of interstitial cells of Cajal in murine small intestine. *Physiological Genomics*, 31(3), 492–509.

Chen, J., and Sanderson, M.J. (2016). Store-operated calcium entry is required for sustained contraction and Ca^{2+} oscillations of airway smooth muscle. *The Journal of Physiology*, 595(10), 3203–3218.

Chen, M., Li, J., Jiang, F., Zhao, L., Wang, Y., Chen, Y., and Wang, X. (2016). Orai1 forms a signal complex with BKCa channel in mesenteric artery smooth muscle cells. *Physiological Reports*, 4(1), e12682.

Chen, S.-C., Chen, C.-H., Chen, Y.-Y., Lin, W.-Y., and Lin, C.-T. (2015). Design and evaluation of potentiometric principles for bladder volume monitoring: A preliminary study. *Sensors*, 15(6), 12802–12815.

Chen, X., Molliver, D.C., and Gebhart, G.F. (2010). The P2Y2 receptor sensitizes mouse bladder sensory neurons and facilitates purinergic currents. *The Journal of Neuroscience*, 30(6), 2365–2372.

Chen, T. W., Wardill, T. J., Sun, Y., Pulver, S. R., Renninger, S. L., Baohan, A., Schreiter, E. R., Kerr, R. A., Orger, M. B., Jayaraman, V., Looger, L. L., Svoboda, K., & Kim, D. S. (2013). Ultrasensitive fluorescent proteins for imaging neuronal activity. *Nature*, *499*(7458), 295–300.

Chess-Williams, R. (2002). Muscarinic receptors of the urinary bladder: detrusor, urothelial and prejunctional. *Autonomic and Autacoid Pharmacology*, 22(3), 133–145.

Chipperfield, A.R., and Harper, A.A. (2000). Chloride in smooth muscle. *Progress in Biophysics and Molecular Biology*, 74(3–5), 175–221.

Chokshi, R., Fruasaha, P., & Kozak, J. A. (2012). 2-aminoethyl diphenyl borinate (2-APB) inhibits TRPM7 channels through an intracellular acidification mechanism. *Channels* (Austin, Tex.), 6(5), 362–369.

Choppin, A., and Eglen, R.M. (2001). Pharmacological characterization of muscarinic receptors in mouse isolated urinary bladder smooth muscle. *British Journal of Pharmacology*, 133(7), 1035–1040.

Clemens, J.Q. (2010). Basic bladder neurophysiology. *Urologic Clinics of North America*, 37(4), 487–494.

Cobine, C.A., Hennig, G.W., Bayguinov, Y.R., Ward, S.M., and Sanders, K.M. (2017). ANO1 in intramuscular interstitial cells of Cajal plays a key role in the generation of slow waves and tone in the internal anal sphincter. *The Journal of Physiology*, 595(6), 2021–2041.

Cole, W.C., and Clément-Chomienne, O. (2003). ATP-sensitive K^+ channels of vascular smooth muscle cells. *Journal of Cardiovascular Electrophysiology*, 14(1), 94–103.

Comperat, E., Roupret, M., Chartier-Kastler, E., and Bitker, M.-O. (2007). Sensory innervation of the bladder: clinical and therapeutic implications. *Progrès en Urologie*, 17(1), 5–11.

Cooper, D.J., Robinson, D., and Cardozo, L. (1986). Internal urinary sphincter in maintenance of female continence. *British Medical Journal*, 292(6514), 166–168.

Cotton, K.D., Hollywood, M.A., McHale, N.G., and Thornbury, K.D. (1997). Ca^{2+} current and Ca^{2+}-activated chloride current in isolated smooth muscle cells of the sheep urethra. *The Journal of Physiology*, 505(1), 121–133.

Creed, K.E., Oike, M., and Ito, Y. (1997). The electrical properties and responses to nerve stimulation of the proximal urethra of the male rabbit. *British Journal of Urology*, 79(4), 543–553.

Crowe, R., Burnstock, G., and Koo, H.P. (1989). Adrenergic innervation of the striated muscle of the intrinsic external urethral sphincter from patients with lower motor spinal cord lesion. *The Journal of Urology*, 141(1), 47–49.

Cruickshank, S.F., Baxter, L.M., and Drummond, R.M. (2003). The Cl^- channel blocker niflumic acid releases Ca^{2+} from an intracellular store in rat pulmonary artery smooth muscle cells. *British Journal of Pharmacology*, 140(8), 1442–1450.

Davis, A. J., Forrest, A. S., Jepps, T. A., Valencik, M. L., Wiwchar, M., Singer, C. A., Sones, W. R., Greenwood, I. A., & Leblanc, N. (2010). Expression profile and protein translation of TMEM16A in murine smooth muscle. *American journal of physiology. Cell physiology*, *299*(5), C948–C959.

Davis, A. J., Shi, J., Pritchard, H. A., Chadha, P. S., Leblanc, N., Vasilikostas, G., Yao, Z., Verkman, A. S., Albert, A. P., & Greenwood, I. A. (2013). Potent vasorelaxant activity of the TMEM16A inhibitor T16A(inh) -A01. *British journal of pharmacology*, *168*(3), 773–784.

De Almeida Kiguti, L.R., and Pupo, A.S. (2012). Investigation of the effects of α1-adrenoceptor antagonism and L-type calcium channel blockade on ejaculation and vas deferens and seminal vesicle contractility in vitro. *The Journal of Sexual Medicine*, 9(1), 159–168.

De Groat, W. C., Fraser, M. O., Yoshiyama, M., Smerin, S., Tai, C., Chancellor, M. B., Yoshimura, N., & Roppolo, J. R. (2001). Neural control of the urethra. *Scandinavian journal of urology and nephrology. Supplementum*, (207), 35–125.

De Groat W. C. (2006). Integrative control of the lower urinary tract: preclinical perspective. *British journal of pharmacology*, *147 Suppl 2*(Suppl 2), S25–S40.

De Groat, W. C., Griffiths, D., & Yoshimura, N. (2015). Neural control of the lower urinary tract. *Comprehensive Physiology*, *5*(1), 327–396

De Groat, W. C., & Yoshimura, N. (2015). Anatomy and physiology of the lower urinary tract. *Handbook of clinical neurology*, *130*, 61–108.

Dedek, K., and Waldegger, S. (2001). Colocalization of KCNQ1/KCNE channel subunits in the mouse gastrointestinal tract. *Pflügers Archiv – European Journal of Physiology*, 442(6), 896–902.

DeLancey, J.O.L., and Ashton-Miller, J.A. (2004). Pathophysiology of adult urinary incontinence. *Gastroenterology*, 126(1 Suppl 1), S23–S32.

Dickens, E.J., Hirst, G.D.S., and Tomita, T. (1999). Identification of rhythmically active cells in guinea-pig stomach. *The Journal of Physiology*, 514(Pt 2), 515–531.

Dixon, J., and Gosling, J. (1987). Structure and innervation in the human lower urinary tract. *The Physiology of the Lower Urinary Tract*, 3–22.

Dokita, S., Morgan, W.R., Wheeler, M.A., Yoshida, M., Latifpour, J., and Weiss, R.M. (1991). NG-nitro-L-arginine inhibits non-adrenergic, non-cholinergic relaxation in rabbit urethral smooth muscle. *Life Sciences*, 48(25), 2429–2436.

Dokita, S., Smith, S.D., Nishimoto, T., Wheeler, M.A., and Weiss, R.M. (1994). Involvement of nitric oxide and cyclic GMP in rabbit urethral relaxation. *European Journal of Pharmacology: Molecular Pharmacology*, 266(3), 269–275.

Dolphin, A.C. (2012). Calcium channel auxiliary α2δ and β subunits: trafficking and one step beyond. *Nature Reviews Neuroscience*, 13(8), 542–555.

Donker, P.J., Ivanovici, F., and Noach, E.L. (1972). Analyses of the urethral pressure profile by means of electromyography and the administration of drugs. *British Journal of Urology*, 44(2), 180–193.

Dopico, A.M., Bukiya, A.N., and Jaggar, J.H. (2018). Calcium- and voltage-gated BK channels in vascular smooth muscle. *Pflügers Archiv – European Journal of Physiology*, 470(9), 1271–1289.

Drazen, J.M., Fanta, C.H., and Lacouture, P.G. (1983). Effect of nifedipine on constriction of human tracheal strips in vitro. *British Journal of Pharmacology*, 78(4), 687–691.

Drumm, B.T., Koh, S.D., Andersson, K.-E., and Ward, S.M. (2014). Calcium signalling in Cajal-like interstitial cells of the lower urinary tract. *Nature Reviews Urology*, 11(10), 555–564.

Drumm, B.T., Sergeant, G.P., Hollywood, M.A., Thornbury, K.D., and McHale, N.G. (2014). The effect of high $[K^+]o$ on spontaneous Ca^{2+} waves in freshly isolated interstitial cells of Cajal from the rabbit urethra. *Physiological Reports*, 2(1), e00203.

Drumm, B.T., Hwang, S.J., Baker, S.A., Ward, S.M., and Sanders, K.M. (2015). The role of Ca^{2+} influx in spontaneous Ca^{2+} wave propagation in interstitial cells of Cajal from the rabbit urethra. *The Journal of Physiology*, 593(15), 3333–3350.

Drumm, B.T., Hennig, G.W., Battersby, M.J., Cunningham, E.K., Sung, T.S., Ward, S.M., and Sanders, K.M. (2017). Clustering of Ca^{2+} transients in interstitial cells of Cajal defines slow wave duration. *The Journal of General Physiology*, 149(7), 703–725.

Drumm, B.T., Hennig, G.W., Baker, S.A., Sanders, K.M., and Ward, S.M. (2018). Ca^{2+} signalling in mouse urethral smooth muscle in situ: role of Ca^{2+} stores and Ca^{2+} influx mechanisms. *The Journal of Physiology*, 596(8), 1433–1466.

Drumm, B.T., Hwang, S.J., Baker, S.A., Ward, S.M., and Sanders, K.M. (2019a). Ca^{2+} signalling behaviours of intramuscular interstitial cells of Cajal in the murine colon. *The Journal of Physiology*, 597(14), 3587–3617.

Drumm, B.T., Rembetski, B.E., Baker, S.A., Hennig, G.W., Ward, S.M., and Sanders, K.M. (2019b). Tonic inhibition of murine proximal colon is due to nitrergic suppression of Ca^{2+} signalling in interstitial cells of Cajal. *Scientific Reports*, 9(1), 1–14.

Drumm, B.T., Hennig, G.W., Baker, S.A., and Sanders, K.M. (2019c). Applications of spatio-temporal mapping and particle analysis techniques to quantify intracellular Ca^{2+} signalling in situ. *Journal of Visualized Experiments*, (143), e58989.

Drumm, B.T., Hennig, G.W., Battersby, M.J., Baker, S.A., Hwang, S.J., Ward, S.M., and Sanders, K.M. (2020). Pacemaker function and neural responsiveness of subserosal interstitial cells of Cajal in the mouse colon. *The Journal of Physiology*, 598(4), 651–681.

Drumm, B.T., Gupta, N., Mircea, A., and Griffin, C.S. (2024). Cells and ionic conductances contributing to spontaneous activity in bladder and urethral smooth muscle. *The Journal of Physiology*, 602, online ahead of print.

Duckles, H., Boycott, H.E., Al-Owais, M.M., Elies, J., Johnson, E., Dallas, M.L., Porter, K.E., Giuntini, F., Boyle, J.P., and Scragg, J.L. (2015). Heme oxygenase-1 regulates cell proliferation via carbon monoxide-mediated inhibition of T-type Ca^{2+} channels. *Pflügers Archiv – European Journal of Physiology*, 467(2), 415–427.

Dudem, S., Large, R.J., Kulkarni, S., McClafferty, H., Tikhonova, I.G., Sergeant, G.P., Thornbury, K.D., Hollywood, M.A., and Shipston, M.J. (2020). LINGO1 is a regulatory subunit of large conductance, Ca^{2+}-activated potassium channels. *Proceedings of the National Academy of Sciences of the United States of America*, 117(4), 2194–2200.

Dunford, J.R., Blanks, A.M., and Gallos, G. (2020). Calcium activated chloride channels and their role in the myometrium. *Current Opinion in Physiology*, 13, 43–48.

Dwivedi, R., Drumm, B.T., Alkawadri, T., Martin, S.L., Sergeant, G.P., Hollywood, M.A. and Thornbury, K.D. (2023). The TMEM16A blockers benzbromarone and MONNA cause intracellular Ca2+-release in mouse bronchial smooth muscle cells. *European Journal of Pharmacology*, 947, 175677.

Edwards, G., Niederste-Hollenberg, A., Schneider, J., Noack, T., and Weston, A.H. (1994). Ion channel modulation by NS 1619, the putative BKCa channel opener, in vascular smooth muscle. *British Journal of Pharmacology*, 113(4), 1538–1547.

Ek, A., Alm, P., Andersson, K.-E., and Larsson, B. (1977). Adrenoceptor- and cholinoceptor-mediated responses of the isolated human urethra: A case report. *Scandinavian Journal of Urology and Nephrology*, 11(2), 97–102.

Escoubas, P., Diochot, S., Célérier, M.L., Nakajima, T., and Lazdunski, M. (2002). Novel tarantula toxins for subtypes of voltage-dependent potassium channels in the Kv2 and Kv4 subfamilies. *Molecular Pharmacology*, 62(1), 48–57.

Exintaris, B., Klemm, M.F., and Lang, R.J. (2004). Re: Spontaneous slow wave and contractile activity of the guinea-pig prostate. *The Journal of Urology*, 171(4), 1637–1638.

Exton, J.H. (1985). Mechanisms involved in alpha-adrenergic phenomena. *American Journal of Physiology – Endocrinology and Metabolism*, 248(6 Pt 1), E633–E647.

Fedigan, S., Bradley, E., Hollywood, M.A., Thornbury, K.D., McHale, N.G., and Sergeant, G.P. (2017). Effects of new-generation TMEM16A inhibitors on calcium-activated chloride currents in rabbit urethral interstitial cells of Cajal. *Pflügers Archiv – European Journal of Physiology*, 469(11), 1443–1455.

Feng, M., Wang, Z., Liu, Z., Liu, D., Zheng, K., Lu, P., Liu, C., Zhang, M., & Li, J. (2019). The RyR-Cl_{Ca} -VDCC axis contributes to spontaneous tone in urethral smooth muscle. *Journal of cellular physiology*, *234*(12), 23256–23267.

Ferrera, L., Caputo, A., Ubby, I., Bussani, E., Zegarra-Moran, O., Ravazzolo, R., Pagani, F., & Galietta, L. J. (2009). Regulation of TMEM16A chloride channel properties by alternative splicing. *The Journal of biological chemistry*, *284*(48), 33360–33368.

Ferrera, L., Scudieri, P., Sondo, E., Caputo, A., Caci, E., Zegarra-Moran, O., Ravazzolo, R., & Galietta, L. J. (2011). A minimal isoform of the TMEM16A protein associated with chloride channel activity. *Biochimica et biophysica acta*, *1808*(9), 2214–2223.

Feske, S., Gwack, Y., Prakriya, M., Srikanth, S., Puppel, S. H., Tanasa, B., Hogan, P. G., Lewis, R. S., Daly, M., & Rao, A. (2006). A mutation in Orai1 causes immune deficiency by abrogating CRAC channel function. *Nature*, *441*(7090), 179–185.

Fida, R., Lyster, D. J., Bywater, R. A., & Taylor, G. S. (1997). Colonic migrating motor complexes (CMMCs) in the isolated mouse colon. *Neurogastroenterology and motility*, *9*(2), 99–107.

Fletcher, T. F., & Bradley, W. E. (1978). Neuroanatomy of the bladder-urethra. *The Journal of urology*, *119*(2), 153–160.

Fong, Z., Griffin, C. S., Large, R. J., Hollywood, M. A., Thornbury, K. D., & Sergeant, G. P. (2021). Regulation of P2X1 receptors by modulators of the cAMP effectors PKA and EPAC. *Proceedings of the National Academy of Sciences of the United States of America*, *118*(37), e2108094118.

Forman, A., Andersson, K. E., Henriksson, L., Rud, T., & Ulmsten, U. (1978). Effects of nifedipine on the smooth muscle of the human urinary tract in vitro and in vivo. *Acta pharmacologica et toxicologica*, *43*(2), 111–118.

Fowler, C.J., Griffiths, D. and de Groat, W.C. (2008). The neural control of micturition. *Nature Reviews Neuroscience*, 9, 453–466.

Franken, J., Uvin, P., De Ridder, D., & Voets, T. (2014). TRP channels in lower urinary tract dysfunction. *British journal of pharmacology*, *171*(10), 2537–2551.

Frazier, E. P., Peters, S. L., Braverman, A. S., Ruggieri, M. R., Sr, & Michel, M. C. (2008). Signal transduction underlying the control of urinary bladder smooth muscle tone by muscarinic receptors and beta-adrenoceptors. *Naunyn-Schmiedeberg's archives of pharmacology*, *377*(4-6), 449–462.

Fröhlich, H., Boini, K.M., Seebohm, G., Strutz-Seebohm, N., Ureche, O.N., Föller, M., Eichenmüller, M., Shumilina, E., Pathare, G., Singh, A.K., *et al.* (2011). Hypothyroidism of gene-targeted mice lacking Kcnq1. *Pflügers Archiv – European Journal of Physiology*, 461(1), 45–52.

Fry, C.H., Meng, E. and Young, J.S. (2010). The physiological function of lower urinary tract smooth muscle. *Autonomic Neuroscience: Basic and Clinical*, 154(1–2), 3–13.

Fujimura, T., Tamura, K., Tsutsumi, T., Yamamoto, T., Nakamura, K., Koibuchi, Y., Kobayashi, M. and Yamaguchi, O. (1999). Expression and possible functional role of the beta 3-adrenoceptor in human and rat detrusor muscle. *The Journal of Urology*, 161(2), 680–685.

Garcia-Pascual, A., Costa, G., Garcia-Sanchez, O., Triguero, D., and Martinez-Cuesta, M.A. (1991). Relaxation of sheep urethral muscle induced by electrical stimulation of nerves: Involvement of nitric oxide. *Acta Physiologica Scandinavica*, 141(4), 531–539.

Garcia-Pascual, A., Costa, G., Garcia-Sacristan, A., & Andersson, K. E. (1991). Relaxation of sheep urethral muscle induced by electrical stimulation of nerves: involvement of nitric oxide. *Acta physiologica Scandinavica*, *141*(4), 531–539.

García-Pascual, Á., Sancho, M., Triguero, D., and Costa, G. (2008). Interstitial cells of Cajal in the urethra are cGMP-mediated targets of nitrergic neurotransmission. *American Journal of Physiology – Renal Physiology*, 295(4), F971–F983.

Genovese, M., Borrelli, A., Venturini, A., Guidone, D., Caci, E., Viscido, G., Gambardella, G., di Bernardo, D., Scudieri, P., and Galietta, L.J.V. (2019). TRPV4 and purinergic receptor signalling pathways are separately linked in airway epithelia to CFTR and TMEM16A chloride channels. *The Journal of Physiology*, 597(24), 5859–5878.

Genovese, M., Scudieri, P., Venturini, A., Guidone, D., Caci, E., Viscido, G., Gambardella, G., di Bernardo, D., and Galietta, L.J.V. (2023). Analysis of inhibitors of the anoctamin-1 chloride channel (TMEM16A) reveals indirect mechanisms involving alterations in calcium signalling. *British Journal of Pharmacology*, 180(6), 775–785.

Ghatta, S., Nimmagadda, D., Xu, X., & O'Rourke, S. T. (2006). Large-conductance, calcium-activated potassium channels: structural and functional implications. *Pharmacology & therapeutics*, *110*(1), 103–116.

Ghosh, S., Alkawadri, T., McGarvey, L. P., Hollywood, M. A., Thornbury, K. D., & Sergeant, G. P. (2025). Role of voltage-gated Ca^{2+} channels and Ano1 Ca^{2+}-activated Cl^- channels in M2 muscarinic receptor-dependent contractions of murine airway smooth muscle. *American journal of physiology. Lung cellular and molecular physiology*, *328*(2), L301–L312.

Gibson, A., McFadzean, I., Wallace, P., & Wayman, C. P. (1998). Capacitative Ca2+ entry and the regulation of smooth muscle tone. *Trends in pharmacological sciences*, *19*(7), 266–269.

Gomez-Pinilla, P. J., Gibbons, S. J., Bardsley, M. R., Lorincz, A., Pozo, M. J., Pasricha, P. J., Van de Rijn, M., West, R. B., Sarr, M. G., Kendrick, M. L., Cima, R. R., Dozois, E. J., Larson, D. W., Ordog, T., & Farrugia, G. (2009). Ano1 is a selective marker of interstitial cells of Cajal in the human and mouse gastrointestinal tract. *American journal of physiology. Gastrointestinal and liver physiology*, *296*(6), G1370–G1381.

Gonzalez-Perez, V., Zhou, Y., Ciorba, M. A., & Lingle, C. J. (2022). The LRRC family of BK channel regulatory subunits: potential roles in health and disease. *The Journal of physiology*, *600*(6), 1357–1371.

Gonzalez-Perez, V., & Lingle, C. J. (2019). Regulation of BK Channels by Beta and Gamma Subunits. *Annual review of physiology*, *81*, 113–137.

Gosling, J. A., & Dixon, J. S. (1975). The structure and innervation of smooth muscle in the wall of the bladder neck and proximal urethra. *British journal of urology*, *47*(5), 549–558.

Goto, K., & Kitazono, T. (2022). Chloride Ions, Vascular Function and Hypertension. *Biomedicines*, *10*(9), 2316.

Grainger, N., Freeman, R. S., Shonnard, C. C., Drumm, B. T., Koh, S. D., Ward, S. M., & Sanders, K. M. (2020). Identification and classification of interstitial cells in the mouse renal pelvis. *The Journal of physiology*, *598*(15), 3283–3307.

Grainger, N., Shonnard, C. C., Quiggle, S. K., Fox, E. B., Presley, H., Daugherty, R., Shonnard, M. C., Drumm, B. T., & Sanders, K. M. (2022). Propagation of Pacemaker Activity and Peristaltic Contractions in the Mouse Renal Pelvis Rely on Ca^{2+}-activated Cl^{-} Channels and T-Type Ca^{2+} Channels. *Function (Oxford, England)*, *3*(6), zqac041.

Greenland, J. E., Dass, N., & Brading, A. F. (1996). Intrinsic urethral closure mechanisms in the female pig. *Scandinavian journal of urology and nephrology. Supplementum*, *179*, 75–80.

Greenwood, I. A., & Leblanc, N. (2007). Overlapping pharmacology of Ca2+-activated Cl- and K+ channels. *Trends in pharmacological sciences*, *28*(1), 1–5.

Griffin, C. S., Alvarado, M. G., Yamasaki, E., Drumm, B. T., Krishnan, V., Ali, S., Nagle, E. M., Sanders, K. M., & Earley, S. (2020). The intracellular Ca^{2+} release channel TRPML1 regulates lower urinary tract smooth muscle contractility. *Proceedings of the National Academy of Sciences of the United States of America*, *117*(48), 30775–30786.

Grosse, J., Braun, A., Varga-Szabo, D., Beyersdorf, N., Schneider, B., Zeitlmann, L., Hanke, P., Schropp, P., Mühlstedt, S., Zorn, C., *et al.,* (2007). An EF hand mutation in Stim1 causes premature platelet activation and bleeding in mice. *The Journal of clinical investigation*, *117*(11), 3540–3550.

Gudlur, A., Zeraik, A.E., Hirve, N., *et al.,* (2020). “STIM calcium sensing and conformational change”. *The Journal of Physiology*, 598(9), pp.1695–1705.

Gutman, G. A., Chandy, K. G., Adelman, J. P., Aiyar, J., Bayliss, D. A., Clapham, D. E., Covarriubias, M., Desir, G. V., Furuichi, K., Ganetzky, B., *et al.,* International Union of Pharmacology (2003). International Union of Pharmacology. XLI. Compendium of voltage-gated ion channels: potassium channels. *Pharmacological reviews*, *55*(4), 583–586.

Hannigan, K. I., Large, R. J., Bradley, E., Hollywood, M. A., Sergeant, G. P., McHale, N. G., & Thornbury, K. D. (2016). Effect of a novel BKCa opener on BKCa currents and contractility of the rabbit corpus cavernosum. *American journal of physiology. Cell physiology*, *310*(4), C284–C292.

Hannigan, K. I., Griffin, C. S., Large, R. J., Sergeant, G. P., Hollywood, M. A., McHale, N. G., & Thornbury, K. D. (2017). The role of Ca^{2+}-activated Cl^{-} current in tone

generation in the rabbit corpus cavernosum. *American journal of physiology. Cell physiology*, *313*(5), C475–C486

Hannigan, K. I., Bossey, A. P., Foulkes, H. J. L., Drumm, B. T., Baker, S. A., Ward, S. M., Sanders, K. M., Keef, K. D., & Cobine, C. A. (2020). A novel intramuscular Interstitial Cell of Cajal is a candidate for generating pacemaker activity in the mouse internal anal sphincter. *Scientific reports*, *10*(1), 10378.

Hannigan, K. I., Ni Bhraonain, E. P., Gould, T. W., Keef, K. D., & Cobine, C. A. (2024). Modulation of intracellular calcium activity in interstitial cells of Cajal by inhibitory neural pathways within the internal anal sphincter. *American journal of physiology. Gastrointestinal and liver physiology*, *327*(3), G382–G404.

Hashimoto, S., Kigoshi, S., & Muramatsu, I. (1993). Nitric oxide-dependent and -independent neurogenic relaxation of isolated dog urethra. *European journal of pharmacology*, *231*(2), 209–214.

Hashitani, H., Fukuta, H., Takano, H., Klemm, M. F., & Suzuki, H. (2001). Origin and propagation of spontaneous excitation in smooth muscle of the guinea-pig urinary bladder. *The Journal of physiology*, *530*(Pt 2), 273–286.

Hashitani, H., Mitsui, R., Hirai, Y., Tanaka, H., & Miwa-Nishimura, K. (2024). Nitrergic inhibition of sympathetic arteriolar constrictions in the female rodent urethra. *The Journal of physiology*, *602*(10), 2199–2226.

Hashitani, H., & Edwards, F. R. (1999). Spontaneous and neurally activated depolarisations in smooth muscle cells of the guinea-pig urethra. *The Journal of physiology*, *514 (Pt 2)*(Pt 2), 459–470.

Hashitani, H., Van Helden, D. F., & Suzuki, H. (1996). Properties of spontaneous depolarisations in circular smooth muscle cells of rabbit urethra. *British journal of pharmacology*, *118*(7), 1627–1632.

Hashitani, H., & Suzuki, H. (2007). Properties of spontaneous Ca2+ transients recorded from interstitial cells of Cajal-like cells of the rabbit urethra in situ. *The Journal of physiology*, *583*(Pt 2), 505–519.

Hawn, M. B., Akin, E., Hartzell, H. C., Greenwood, I. A., & Leblanc, N. (2021). Molecular mechanisms of activation and regulation of ANO1-Encoded Ca^{2+}-Activated Cl^{-} channels. *Channels (Austin, Tex.)*, *15*(1), 569–603.

Hegde, S. S., & Eglen, R. M. (1999). Muscarinic receptor subtypes modulating smooth muscle contractility in the urinary bladder. *Life sciences*, *64*(6-7), 419–428.

Hennig, G. W., Spencer, N. J., Jokela-Willis, S., Bayguinov, P. O., Lee, H. T., Ritchie, L. A., Ward, S. M., Smith, T. K., & Sanders, K. M. (2010). ICC-MY coordinate smooth muscle electrical and mechanical activity in the murine small intestine. *Neurogastroenterology and motility*, *22*(5), e138–e151.

Heppner, T. J., Bonev, A. D., & Nelson, M. T. (1997). Ca(2+)-activated K+ channels regulate action potential repolarization in urinary bladder smooth muscle. *The American journal of physiology*, *273*(1 Pt 1), C110–C117.

Herrera, G. M., Heppner, T. J., & Nelson, M. T. (2000). Regulation of urinary bladder smooth muscle contractions by ryanodine receptors and BK and SK channels. *American journal of physiology. Regulatory, integrative and comparative physiology*, *279*(1), R60–R68

Herrera, G. M., Heppner, T. J., & Nelson, M. T. (2001). Voltage dependence of the coupling of Ca(2+) sparks to BK(Ca) channels in urinary bladder smooth muscle. *American journal of physiology. Cell physiology*, *280*(3), C481–C490.

Herrera, G. M., & Nelson, M. T. (2002). Differential regulation of SK and BK channels by Ca(2+) signals from Ca(2+) channels and ryanodine receptors in guinea-pig urinary bladder myocytes. *The Journal of physiology*, *541*(Pt 2), 483–492.

Hickling, D. R., Sun, T. T., & Wu, X. R. (2015). Anatomy and Physiology of the Urinary Tract: Relation to Host Defense and Microbial Infection. *Microbiology spectrum*, *3*(4), 10.1128/microbiolspec.UTI-0016-2012.

Hill-Eubanks, D. C., Werner, M. E., Heppner, T. J., & Nelson, M. T. (2011). Calcium signaling in smooth muscle. *Cold Spring Harbor perspectives in biology*, *3*(9), a004549.

Hirota, S., & Janssen, L. J. (2007). Store-refilling involves both L-type calcium channels and reverse-mode sodium-calcium exchange in airway smooth muscle. *The European respiratory journal*, *30*(2), 269–278.

Hirst, G. D., Bramich, N. J., Teramoto, N., Suzuki, H., & Edwards, F. R. (2002). Regenerative component of slow waves in the guinea-pig gastric antrum involves a delayed increase in [Ca(2+)](i) and Cl(-) channels. *The Journal of physiology*, *540*(Pt 3), 907–919.

Hobai, I.A., Bates, J.A., Howarth, F.C. and Levi, A.J., (1997). “Inhibition by external Cd2+ of Na^+/Ca^{2+} exchange and L-type Ca^{2+} channel in rabbit ventricular myocytes”. *American Journal of Physiology*, 272(5 Pt 2), pp.H2164–H2172.

Hollywood, M. A., McCloskey, K. D., McHale, N. G., & Thornbury, K. D. (2000). Characterization of outward K(+) currents in isolated smooth muscle cells from sheep urethra. *American journal of physiology. Cell physiology*, *279*(2), C420–C428.

Hollywood, M. A., Woolsey, S., Walsh, I. K., Keane, P. F., McHale, N. G., & Thornbury, K. D. (2003). T- and L-type Ca2+ currents in freshly dispersed smooth muscle cells from the human proximal urethra. *The Journal of physiology*, *550*(Pt 3), 753–764.

Hongo, M., Traube, M., McAllister, R. G., Jr, & McCallum, R. W. (1984). Effects of nifedipine on esophageal motor function in humans: correlation with plasma nifedipine concentration. *Gastroenterology*, *86*(1), 8–12.

Hoth, M., & Penner, R. (1992). Depletion of intracellular calcium stores activates a calcium current in mast cells. *Nature*, *355*(6358), 353–356.

Hsieh, P. C., Chang, S. J., Chang, H. H., & Yang, S. S. (2023). The differences in the adrenergic receptors of proximal urethra between sexes. *Tzu chi medical journal*, *35*(3), 253–259.

Huang, F., Rock, J. R., Harfe, B. D., Cheng, T., Huang, X., Jan, Y. N., & Jan, L. Y. (2009). Studies on expression and function of the TMEM16A calcium-activated chloride channel. *Proceedings of the National Academy of Sciences of the United States of America*, *106*(50), 21413–21418.

Huang, F., Zhang, H., Wu, M., Yang, H., Kudo, M., Peters, C. J., Woodruff, P. G., Solberg, O. D., Donne, M. L., Huang, X., *et al.,* (2012). Calcium-activated chloride channel TMEM16A modulates mucin secretion and airway smooth muscle contraction. *Proceedings of the National Academy of Sciences of the United States of America*, *109*(40), 16354–16359.

Huang K. P. (1989). The mechanism of protein kinase C activation. *Trends in neurosciences*, *12*(11), 425–432.

Huizinga, J. D., Zhu, Y., Ye, J., & Molleman, A. (2002). High-conductance chloride channels generate pacemaker currents in interstitial cells of Cajal. *Gastroenterology*, *123*(5), 1627–1636.

Huizinga, J. D., Thuneberg, L., Klüppel, M., Malysz, J., Mikkelsen, H. B., & Bernstein, A. (1995). W/kit gene required for interstitial cells of Cajal and for intestinal pacemaker activity. *Nature*, *373*(6512), 347–349.

Hwang, S. J., Blair, P. J., Britton, F. C., O'Driscoll, K. E., Hennig, G., Bayguinov, Y. R., Rock, J. R., Harfe, B. D., Sanders, K. M., & Ward, S. M. (2009). Expression of anoctamin 1/TMEM16A by interstitial cells of Cajal is fundamental for slow wave activity in gastrointestinal muscles. *The Journal of physiology*, *587*(Pt 20), 4887–4904.

Hwang, S. J., Basma, N., Sanders, K. M., & Ward, S. M. (2016). Effects of new-generation inhibitors of the calcium-activated chloride channel anoctamin 1 on slow

waves in the gastrointestinal tract. *British journal of pharmacology*, *173*(8), 1339–1349.

Hwang, S. J., Pardo, D. M., Zheng, H., Bayguinov, Y., Blair, P. J., Fortune-Grant, R., Cook, R. S., Hennig, G. W., Shonnard, M. C., Grainger, N., Peri, L. E., Verma, S. D., Rock, J., Sanders, K. M., & Ward, S. M. (2019). Differential sensitivity of gastric and small intestinal muscles to inducible knockdown of anoctamin 1 and the effects on gastrointestinal motility. *The Journal of physiology*, *597*(9), 2337–2360.

Hwang, S. J., Drumm, B. T., Kim, M. K., Lyu, J. H., Baker, S., Sanders, K. M., & Ward, S. M. (2022). Calcium transients in intramuscular interstitial cells of Cajal of the murine gastric fundus and their regulation by neuroeffector transmission. *The Journal of physiology*, *600*(20), 4439–4463.

Iftinca M. C. (2011). Neuronal T-type calcium channels: what's new? Iftinca: T-type channel regulation. *Journal of medicine and life*, *4*(2), 126–138.

Igawa, Y. (2023) “Peripheral Neural Control of the Lower Urinary Tract,” *Handbook of Neurourology*, pp. 35–45.

Igawa, Y., Aizawa, N., & Michel, M. C. (2019). β_3 -Adrenoceptors in the normal and diseased urinary bladder-What are the open questions?. *British journal of pharmacology*, *176*(14), 2525–2538.

Ishida, H., Saito, S. Y., Hishinuma, E., & Ishikawa, T. (2017). Differential Contribution of Nerve-Derived Noradrenaline to High K^+-Induced Contraction Depending on Type of Artery. *Biological & pharmaceutical bulletin*, *40*(1), 56–60.

Ito, Y., & Kimoto, Y. (1985). The neural and non-neural mechanisms involved in urethral activity in rabbits. *The Journal of physiology*, *367*, 57–72.

Jackson W. F. (2017). Potassium Channels in Regulation of Vascular Smooth Muscle Contraction and Growth. *Advances in pharmacology (San Diego, Calif.)*, *78*, 89–144.

Jepps, T. A., Olesen, S. P., & Greenwood, I. A. (2013). One man's side effect is another man's therapeutic opportunity: targeting Kv7 channels in smooth muscle disorders. *British journal of pharmacology*, *168*(1), 19–27.

Jiang, X., Luttrell, I., Chitaley, K., & Yang, C. C. (2014). T- and L-type voltage-gated calcium channels: their role in diabetic bladder dysfunction. *Neurourology and urodynamics*, *33*(1), 147–152.

Jin, X., Shah, S., Du, X., Zhang, H., & Gamper, N. (2016). Activation of Ca(2+) -activated Cl(-) channel ANO1 by localized Ca(2+) signals. *The Journal of physiology*, *594*(1), 19–30.

Johnston, L., Sergeant, G. P., Hollywood, M. A., Thornbury, K. D., & McHale, N. G. (2005). Calcium oscillations in interstitial cells of the rabbit urethra. *The Journal of physiology*, *565*(Pt 2), 449–461.

Jung, J., Ahn, H. K., & Huh, Y. (2012). Clinical and functional anatomy of the urethral sphincter. *International neurourology journal*, *16*(3), 102–106.

Keane, D. P., & O'Sullivan, S. (2000). Urinary incontinence: anatomy, physiology and pathophysiology. *Bailliere's best practice & research. Clinical obstetrics & gynaecology*, *14*(2), 207–226.

Keyser, A. J., Montgomerie, J. Z., & Howard, E. B. (1992). Nonmucinous nature of the surface material of the bladder mucosa. *The American journal of the medical sciences*, *304*(5), 285–288.

Khandelwal, P., Abraham, S. N., & Apodaca, G. (2009). Cell biology and physiology of the uroepithelium. *American journal of physiology. Renal physiology*, *297*(6), F1477–F1501.

King, C. H., & Scherer, S. S. (2012). Kv7.5 is the primary Kv7 subunit expressed in C-fibers. *The Journal of comparative neurology*, *520*(9), 1940–1950.

Kirchhefer, U., Heinick, A., König, S., Kristensen, T., Müller, F. U., Seidl, M. D., & Boknik, P. (2014). Protein phosphatase 2A is regulated by protein kinase Cα (PKCα)-dependent phosphorylation of its targeting subunit B56α at Ser41. *The Journal of biological chemistry*, *289*(1), 163–176.

Kito Y. (2011). The functional role of intramuscular interstitial cells of Cajal in the stomach. *Journal of smooth muscle research = Nihon Heikatsukin Gakkai kikanshi*, *47*(2), 47–53.

Kito, Y., Fukuta, H., & Suzuki, H. (2002). Components of pacemaker potentials recorded from the guinea pig stomach antrum. *Pflugers Archiv : European journal of physiology*, *445*(2), 202–217.

Koesling, D., Friebe, A. (2000). Enzymology of Soluble Guanylyl Cyclase. In: Mayer, B. (eds) Nitric Oxide*. Handbook of Experimental Pharmacology, vol 143. Springer,* Berlin, Heidelberg.

Kohrogi, H., Horio, S., Ando, M., Sugimoto, M., Honda, I., & Araki, S. (1985). Nifedipine inhibits human bronchial smooth muscle contractions induced by leukotrienes C4 and D4, prostaglandin F2 alpha, and potassium. *The American review of respiratory disease*, *132*(2), 299–304.

Koh, S. D., Drumm, B. T., Lu, H., Kim, H. J., Ryoo, S. B., Kim, H. U., Lee, J. Y., Rhee, P. L., Wang, Q., Gould, T. W., *et al,.* (2022). Propulsive colonic contractions are mediated by inhibition-driven poststimulus responses that originate in interstitial cells of Cajal. *Proceedings of the National Academy of Sciences of the United States of America*, *119*(18), e2123020119.

Koh, S. D., Lee, J. Y., Ryoo, S. B., Drumm, B. T., Kim, H. J., Baker, S. A., & Sanders, K. M. (2024). Integrated responses of the SIP syncytium generate a major motility pattern in the colon. *The Journal of physiology*, *602*(24), 6659–6682.

Kopecky, B. J., Liang, R., & Bao, J. (2014). T-type calcium channel blockers as neuroprotective agents. *Pflugers Archiv : European journal of physiology*, *466*(4), 757–765.

Kraus, R. L., Li, Y., Gregan, Y., Gotter, A. L., Uebele, V. N., Fox, S. V., Doran, S. M., Barrow, J. C., Yang, Z. Q., Reger, T. S., Koblan, K. S., & Renger, J. J. (2010). In vitro characterization of T-type calcium channel antagonist TTA-A2 and in vivo effects on arousal in mice. *The Journal of pharmacology and experimental therapeutics*, *335*(2), 409–417.

Krhut, J., Skugarevská, B., Míka, D., Lund, L., & Zvara, P. (2022). Clinical Utility of β_3-Adrenoreceptor Agonists for the Treatment of Overactive Bladder: A Review of the Evidence and Current Recommendations. *Research and reports in urology*, *14*, 167–175.

Kudo, W., Mitsui, R., & Hashitani, H. (2024). Involvement of ANO1 currents in pacemaking of PDGFRα-positive specialised smooth muscle cells in rat caudal epididymis. *Cell and tissue research*, *397*(1), 1–12.

Kuntz, A. (1965). Physiology of urinary bladder and urethra, normal and pathological. In: Physiologie und Pathologische Physiologie / Physiology and Pathological Physiology / Physiologie Normale et Pathologique. Handbuch der Urologie / Encyclopedia of Urology / Encyclopédie D'urologie, vol 2. Springer, Berlin, Heidelberg.

Kyle, B., Bradley, E., Ohya, S., Sergeant, G. P., McHale, N. G., Thornbury, K. D., & Hollywood, M. A. (2011). Contribution of Kv2.1 channels to the delayed rectifier current in freshly dispersed smooth muscle cells from rabbit urethra. *American journal of physiology. Cell physiology*, *301*(5), C1186–C1200.

Kyle, B. D., Bradley, E., Large, R., Sergeant, G. P., McHale, N. G., Thornbury, K. D., & Hollywood, M. A. (2013). Mechanisms underlying activation of transient BK current in rabbit urethral smooth muscle cells and its modulation by IP3-generating agonists. *American journal of physiology. Cell physiology*, *305*(6), C609–C622.

Kyle, B. D. (2014). Ion channels of the mammalian urethra. *Channels*, *8*(5), 393–401.

Lacampagne, A., Gannier, F., Argibay, J., Garnier, D. and Le Guennec, J.-Y. (1994). The stretch-activated ion channel blocker gadolinium also blocks L-type calcium channels in isolated ventricular myocytes of the guinea-pig. *Biochimica et Biophysica Acta*, 1191(1), 205–208.

Lang, R.J., Hashitani, H., Tonta, M.A., Parkington, H.C. and Suzuki, H. (2007). Spontaneous electrical and Ca2+ signals in typical and atypical smooth muscle cells and interstitial cell of Cajal-like cells of mouse renal pelvis. *The Journal of Physiology*, 583(3), 1049–1068.

Larsson, B., Högestätt, E.D., Mattiasson, A. and Andersson, K.-E. (1984). Differential effects of nifedipine, verapamil, and diltiazem on noradrenaline-induced contractions, adrenergic transmitter release, and alpha-adrenoceptor binding in the female rabbit urethra. *Naunyn-Schmiedeberg's Archives of Pharmacology*, 326(1), 14–21.

Latifpour, J., Morita, T. and O'Hollaren, B. (1989). Characterization of autonomic receptors in neonatal urinary tract smooth muscle. *Developmental Pharmacology and Therapeutics*, 13(1), 1–10.

Latorre, R. and Brauchi, S. (2006). Large conductance Ca^{2+}-activated K^{+} (BK) channel: Activation by Ca^{2+} and voltage. *Biological Research*, 39(3), 385–401.

Laver, D.R. (2007). Ca^{2+} stores regulate ryanodine receptor Ca^{2+} release channels via luminal and cytosolic Ca^{2+} sites. *Biophysical Journal*, 92(10), 3541–3555.

Lazarowski, E.R. and Boucher, R.C. (2001). UTP as an extracellular signaling molecule. *News in Physiological Sciences*, 16(1), 1–5.

Leblanc, N., Greenwood, I.A., and Jaggar, J.H. (2005). Regulation of calcium-activated chloride channels in smooth muscle cells: a complex picture is emerging. *Canadian Journal of Physiology and Pharmacology*, 83(7), 541–556.

Lee, H.T., Hennig, G.W., Fleming, N.W., Keef, K.D., Spencer, N.J., Ward, S.M., Sanders, K.M., and Smith, T.K. (2007). Septal interstitial cells of Cajal conduct pacemaker activity to excite muscle bundles in human jejunum. *Gastroenterology*, 133(3), 907–917.

Lee, H., Koh, S.D., Hennig, G.W., Sanders, K.M., and Ward, S.M. (2014). Purinergic inhibitory regulation of murine detrusor muscles mediated by PDGFRα^{+} interstitial cells. *The Journal of Physiology*, 592(6), 1283–1299.

Lee, J.H., Kim, J.S., Kim, H.J., Kim, J.H., Park, S.H., Kim, S.Y., and Choi, B.H. (2020). Characterization and functional roles of KCNQ-encoded voltage-gated potassium (Kv7) channels in human corpus cavernosum smooth muscle. *Pflügers Archiv – European Journal of Physiology*, 472(1), 89–102.

Lee, M.P., Ravenel, J.D., Hu, R.J., Lustig, L.R., Tomaselli, G., Berger, R.D., Brandenburg, S.A., Litzi, T.J., Bunton, T.E., and Limb, C. (2000). Targeted disruption of the Kvlqt1 gene causes deafness and gastric hyperplasia in mice. *The Journal of Clinical Investigation*, 106(12), 1447–1455.

Leybaert, L. and Sanderson, M.J. (2012). Intercellular Ca^{2+} waves: mechanisms and function. *Physiological Reviews*, 92(3), 1359–1392.

Liebhold, M., Brenner, W., Meissner, C., and Schaefer, H.E. (1995). Light- and electron-microscopic studies of the structure of normal bladder epithelium in female swine. *Anatomia, Histologia, Embryologia*, 24(1), 17–24.

Lies, B., Groneberg, D. and Friebe, A. (2013). Correlation of cellular expression with function of NO-sensitive guanylyl cyclase in the murine lower urinary tract. *The Journal of Physiology*, 591(21), 5365–5375.

Lifshitz, L.M., Carmichael, J.D., Zilberter, Y., Sorrentino, V., and Lederer, W.J. (2011). Spatial organization of ryanodine receptors and BK channels underlying the activation of STOCs by Ca^{2+} sparks in airway myocytes. *The Journal of General Physiology*, 138(2), 195–209.

Li, M., Hansen, J.B., Huang, L., Keyser, B.M., Taylor, J.T., and Zhuang, H. (2005). Towards selective antagonists of T-type calcium channels: design, characterization and potential applications of NNC 55-0396. *Cardiovascular Drug Reviews*, 23(2), 173–196.

Lim, X.R., Drumm, B.T., Sergeant, G.P., Hollywood, M.A., Thornbury, K.D., and Sanders, K.M. (2022). Ca^{2+}-activated Cl^{-} channels (TMEM16A) underlie spontaneous electrical activity in isolated mouse corpus cavernosum smooth muscle cells. *Physiological Reports*, 10(22), e15504.

Lincoln, J., Crowe, R., Burnstock, G., and Griffiths, D. (1986). Adrenergic and cholinergic innervation of the smooth and striated muscle components of the urethra from patients with spinal cord injury. *The Journal of Urology*, 135(2), 402–408.

Liou, J., Kim, M.L., Heo, W.D., Jones, J.T., Myers, J.W., Ferrell, J.E., and Meyer, T. (2005). STIM is a Ca^{2+} sensor essential for Ca^{2+} store-depletion-triggered Ca^{2+} influx. *Current Biology*, 15(13), 1235–1241.

Liou, J., Fivaz, M., Inoue, T. and Meyer, T. (2007). Live-cell imaging reveals sequential oligomerization and local plasma membrane targeting of stromal interaction molecule 1 after Ca^{2+} store depletion. *Proceedings of the National Academy of Sciences of the United States of America*, 104(22), 9301–9306.

Li, P., Chen, Y., Dong, X., Li, J., Wang, H., and Yang, J. (2019). Mibefradil, a T-type Ca^{2+} channel blocker also blocks Orai channels by action at the extracellular surface. *British Journal of Pharmacology*, 176(19), 3845–3857.

Li, Q. and Yan, J. (2016). Modulation of BK channel function by auxiliary beta and gamma subunits. *International Review of Neurobiology*, 128, 51–90.

Liu, B., Freyer, A.M. and Hall, I.P. (2007). Bradykinin activates calcium-dependent potassium channels in cultured human airway smooth muscle cells. *American Journal of Physiology – Lung Cellular and Molecular Physiology*, 292(4), L898–L907.

Liu, S., Feng, J., Luo, J., Yang, P., Brett, T.J., and Hu, H. (2016). Eact, a small molecule activator of TMEM16A, activates TRPV1 and elicits pain- and itch-related behaviours. *British Journal of Pharmacology*, 173(7), 1208–1218.

Liu, Z., Wang, Y., Zhang, X., Chen, Y., Li, J., and Yang, J. (2024). The T-type calcium channel CACNA1H is required for smooth muscle cytoskeletal organization during tracheal tubulogenesis. *Advanced Science*, 11(44), 2308622.

Li, Y., Sparks, R.L., and Little, J.B. (2001). Vasopressin-stimulated Ca^{2+} spiking in vascular smooth muscle cells involves phospholipase D. *American Journal of Physiology – Heart and Circulatory Physiology*, 280(6), H2658–H2664.

Lubberding, A.F., Schuilenburg, M.J., van der Heyden, M.A.G., and Verkerk, A.O. (2022). Celebrities in the heart, strangers in the pancreatic beta cell: voltage-gated potassium channels Kv7.1 and Kv11.1 bridge long QT syndrome with hyperinsulinaemia as well as type 2 diabetes. *Acta Physiologica*, 234(3), e13781.

Lyons, A.D., Gardiner, T.A. and McCloskey, K.D. (2007). Kit-positive interstitial cells in the rabbit urethra: structural relationships with nerves and smooth muscle. *BJU International*, 99(3), 687–694.

Mahadevan, V. (2016). Anatomy of the lower urinary tract. *Surgery (Oxford)*, 34(7), 318–325.

Malysz, J., Gibbons, S. J., Saravanaperumal, S. A., Du, P., Eisenman, S. T., Cao, C., Oh, U., Saur, D., Klein, S., Ordog, T., & Farrugia, G. (2017). Conditional genetic deletion of Ano1 in interstitial cells of Cajal impairs Ca^{2+} transients and slow waves in adult mouse small intestine. *American journal of physiology. Gastrointestinal and liver physiology*, *312*(3), G228–G245.

Malysz, J., & Petkov, G. V. (2020). Detrusor Smooth Muscle K_V7 Channels: Emerging New Regulators of Urinary Bladder Function. *Frontiers in physiology*, *11*, 1004.

Man, K. N. M., Bartels, P., Henderson, P. B., Kim, K., Shi, M., Zhang, M., Ho, S. Y., Nieves-Cintron, M., Navedo, M. F., Horne, M. C., & Hell, J. W. (2023). α_1-Adrenergic

receptor-PKC-Pyk2-Src signaling boosts L-type Ca^{2+} channel $Ca_V1.2$ activity and long-term potentiation in rodents. *eLife*, *12*, e79648.

Mangera, A., Patel, A.K. and Chapple, C.R. (2010) “Anatomy of the lower urinary tract,” *Surgery (United Kingdom)*. Elsevier Ltd, pp. 307–313.

Masson, B., Le Ribeuz, H., Sabourin, J., Laubry, L., Woodhouse, E., Foster, R., Ruchon, Y., Dutheil, M., Boët, A., Ghigna, M. R., *et al.* (2022). Orai1 Inhibitors as Potential Treatments for Pulmonary Arterial Hypertension. *Circulation research*, *131*(9), e102–e119.

Mawby, D. I., Meric, S. M., Crichlow, E. C., & Papich, M. G. (1991). Pharmacological relaxation of the urethra in male cats: a study of the effects of phenoxybenzamine, diazepam, nifedipine and xylazine. *Canadian journal of veterinary research = Revue canadienne de recherche veterinaire*, *55*(1), 28–32.

Maxwell, J. T., & Blatter, L. A. (2017). A novel mechanism of tandem activation of ryanodine receptors by cytosolic and SR luminal Ca^{2+} during excitation-contraction coupling in atrial myocytes. *The Journal of physiology*, *595*(12), 3835–3845.

Mazzone, A., Bernard, C. E., Strege, P. R., Beyder, A., Galietta, L. J., Pasricha, P. J., Rae, J. L., Parkman, H. P., Linden, D. R., Szurszewski, J. H., Ördög, T., Gibbons, S. J., & Farrugia, G. (2011). Altered expression of Ano1 variants in human diabetic gastroparesis. *The Journal of biological chemistry*, *286*(15), 13393–13403.

Mazzone, A., Gibbons, S. J., Bernard, C. E., Nowsheen, S., Middha, S., Almada, L. L., Ordog, T., Kendrick, M. L., Reid Lombardo, K. M., Shen, K. R., *et al.* (2015). Identification and characterization of a novel promoter for the human ANO1 gene regulated by the transcription factor signal transducer and activator of transcription 6 (STAT6). *FASEB journal: official publication of the Federation of American Societies for Experimental Biology*, *29*(1), 152–163.

Mazzucato, M., Pradella, P., Cozzi, M. R., De Marco, L., & Ruggeri, Z. M. (2002). Sequential cytoplasmic calcium signals in a 2-stage platelet activation process induced by the glycoprotein Ibalpha mechanoreceptor. *Blood*, *100*(8), 2793–2800.

McCallum, L. A., Pierce, S. L., England, S. K., Greenwood, I. A., & Tribe, R. M. (2011). The contribution of Kv7 channels to pregnant mouse and human myometrial contractility. *Journal of cellular and molecular medicine*, *15*(3), 577–586.

McCloskey, K. D., & Gurney, A. M. (2002). Kit positive cells in the guinea pig bladder. *The Journal of urology*, *168*(2), 832–836.

McHale, N. G., Hollywood, M. A., Sergeant, G. P., Shafei, M., Thornbury, K. T., & Ward, S. M. (2006). Organization and function of ICC in the urinary tract. *The Journal of physiology*, *576*(Pt 3), 689–694.

McRory, J. E., Santi, C. M., Hamming, K. S., Mezeyova, J., Sutton, K. G., Baillie, D. L., Stea, A., & Snutch, T. P. (2001). Molecular and functional characterization of a family of rat brain T-type calcium channels. *The Journal of biological chemistry*, *276*(6), 3999–4011.

Meir, A., Ginsburg, S., Butkevich, A., Kachalsky, S. G., Kaiserman, I., Ahdut, R., Demirgoren, S., & Rahamimoff, R. (1999). Ion channels in presynaptic nerve terminals and control of transmitter release. *Physiological reviews*, *79*(3), 1019–1088.

Mercer, J. C., Dehaven, W. I., Smyth, J. T., Wedel, B., Boyles, R. R., Bird, G. S., & Putney, J. W., Jr (2006). Large store-operated calcium selective currents due to co-expression of Orai1 or Orai2 with the intracellular calcium sensor, Stim1. *The Journal of biological chemistry*, *281*(34), 24979–24990.

Mercer, M., Hollywood, M. A., Sergeant, G. P., & Thornbury, K. D. (2025). K_V7 channels modulate tension and calcium signaling in mouse corpus cavernosum. *American journal of physiology. Cell physiology*, *328*(3), C729–C742.

Meredith, A. L., Thorneloe, K. S., Werner, M. E., Nelson, M. T., & Aldrich, R. W. (2004). Overactive bladder and incontinence in the absence of the BK large conductance

Ca2+-activated K+ channel. *The Journal of biological chemistry*, *279*(35), 36746–36752.

Metzger, R., Rolle, U., Fiegel, H. C., Franke, F. E., Muenstedt, K., & Till, H. (2008). C-kit receptor in the human vas deferens: distinction of mast cells, interstitial cells and interepithelial cells. *Reproduction (Cambridge, England)*, *135*(3), 377–384.

Miceli, F., Soldovieri, M. V., Iannotti, F. A., Barrese, V., Ambrosino, P., Martire, M., Cilio, M. R., & Taglialatela, M. (2011). The Voltage-Sensing Domain of K(v)7.2 Channels as a Molecular Target for Epilepsy-Causing Mutations and Anticonvulsants. *Frontiers in pharmacology*, *2*, 2.

Michel, M. C., & Vrydag, W. (2006). Alpha1-, alpha2- and beta-adrenoceptors in the urinary bladder, urethra and prostate. *British journal of pharmacology*, *147 Suppl 2*(Suppl 2), S88–S119.

Mistry, M. A., Klarskov, N., DeLancey, J. O., & Lose, G. (2020). A structured review on the female urethral anatomy and innervation with an emphasis on the role of the urethral longitudinal smooth muscle. *International urogynecology journal*, *31*(1), 63–71.

Moosmang, S., Schulla, V., Welling, A., Feil, R., Feil, S., Wegener, J. W., Hofmann, F., & Klugbauer, N. (2003). Dominant role of smooth muscle L-type calcium channel Cav1.2 for blood pressure regulation. *The EMBO journal*, *22*(22), 6027–6034.

Morita, T., Latifpour, J., O'Hollaren, B., Wheeler, M. A., & Weiss, R. M. (1987). Sex differences in function and distribution of alpha 1- and alpha 2-adrenoceptors in rabbit urethra. *The American journal of physiology*, *252*(6 Pt 2), F1124–F1128.

Mueller, M., Drumm, B. T., Hannan, J. L., & Ruetten, H. (2025). Advancing our Understanding of the Urothelium and Lamina Propria, Hormone Receptors, Vascular Supply, and Sensory Aspects of the Female Human Urethra.

Murtazina, D. A., Chung, D., Ulloa, A., Bryan, E., Galan, H. L., & Sanborn, B. M. (2011). TRPC1, STIM1, and ORAI influence signal-regulated intracellular and

endoplasmic reticulum calcium dynamics in human myometrial cells. *Biology of reproduction*, *85*(2), 315–326.

Nagahama, K., Tsujii, T., Morita, T., Azuma, H., & Oshima, H. (1998). Differences between proximal and distal portions of the male rabbit posterior urethra in the physiological role of muscarinic cholinergic receptors. *British journal of pharmacology*, *124*(6), 1175–1180.

Nakai, J., Ohkura, M., & Imoto, K. (2001). A high signal-to-noise Ca(2+) probe composed of a single green fluorescent protein. *Nature biotechnology*, *19*(2), 137–141.

Nasu, K., Moriyama, N., Fukasawa, R., Tsujimoto, G., Tanaka, T., Yano, J., & Kawabe, K. (1998). Quantification and distribution of alpha1-adrenoceptor subtype mRNAs in human proximal urethra. *British journal of pharmacology*, *123*(7), 1289–1293.

Ng, F. L., Davis, A. J., Jepps, T. A., Harhun, M. I., Yeung, S. Y., Wan, A., Reddy, M., Melville, D., Nardi, A., Khong, T. K., & Greenwood, I. A. (2011). Expression and function of the K+ channel KCNQ genes in human arteries. *British journal of pharmacology*, *162*(1), 42–53.

Ni Bhraonain, E.P., Turner, J.A., Hannigan, K.I., Sanders, K.M. & Cobine, C.A., (2025a). “Immunohistochemical characterization of interstitial cells and their spatial relationship to motor neurons within the mouse esophagus”. *Cell and Tissue Research*, 399(1), pp.61–84.

Ni Bhraonain, E.P., Hannigan, K.I., Turner, J.A., Wildbore, G.A., Sanders, K.M. & Cobine, C.A., (2025b). “A specialized population of intramuscular interstitial cells of Cajal regulates motility within the mouse oesophagogastric junction”. *The Journal of Physiology.*

Nishikawa, M., Sellers, J. R., Adelstein, R. S., & Hidaka, H. (1984). Protein kinase C modulates in vitro phosphorylation of the smooth muscle heavy meromyosin by myosin light chain kinase. *The Journal of biological chemistry*, *259*(14), 8808–8814.

Noma A. (1983). ATP-regulated K+ channels in cardiac muscle. *Nature*, *305*(5930), 147–148.

Oba T. (1997). Niflumic acid differentially modulates two types of skeletal ryanodine-sensitive Ca(2+)-release channels. *The American journal of physiology*, *273*(5), C1588–C1595..

O'Driscoll, K. E., Pipe, R. A., & Britton, F. C. (2011). Increased complexity of Tmem16a/Anoctamin 1 transcript alternative splicing. *BMC molecular biology*, *12*, 35.

Ono, K., & Iijima, T. (2005). Pathophysiological significance of T-type Ca2+ channels: properties and functional roles of T-type Ca2+ channels in cardiac pacemaking. *Journal of pharmacological sciences*, *99*(3), 197–204.

Overend, C. L., Eisner, D. A., & O'Neill, S. C. (1997). The effect of tetracaine on spontaneous Ca2+ release and sarcoplasmic reticulum calcium content in rat ventricular myocytes. *The Journal of physiology*, *502 (Pt 3)*(Pt 3), 471–479.

Ordög, T., Ward, S. M., & Sanders, K. M. (1999). Interstitial cells of cajal generate electrical slow waves in the murine stomach. *The Journal of physiology*, *518*(Pt 1), 257–269.

Ottolia, M., & Toro, L. (1994). Potentiation of large conductance KCa channels by niflumic, flufenamic, and mefenamic acids. *Biophysical journal*, *67*(6), 2272–2279.

Owen N. E. (1984). Regulation of Na/K/Cl cotransport in vascular smooth muscle cells. *Biochemical and biophysical research communications*, *125*(2), 500–508.

Ozaki, H., Stevens, R. J., Blondfield, D. P., Publicover, N. G., & Sanders, K. M. (1991). Simultaneous measurement of membrane potential, cytosolic Ca2+, and tension in intact smooth muscles. *The American journal of physiology*, *260*(5 Pt 1), C917–C925.

Pan, C.G. (2018). Urinary Incontinence and Polyuria. *Nelson Pediatric Symptom-Based Diagnosis*, pp. 824-830.e1.

Parekh, A.B., (2003). Store-operated Ca2+ entry: dynamic interplay between endoplasmic reticulum, mitochondria and plasma membrane. *The Journal of Physiology*, 547(Pt 2), pp.333–348.

Parekh, A.B. (2010). Store-operated CRAC channels: function in health and disease. *Nature Reviews Drug Discovery 2010 9:5*, 9(5), pp. 399–410.

Park, K. J., Hennig, G. W., Lee, H. T., Spencer, N. J., Ward, S. M., Smith, T. K., & Sanders, K. M. (2006). Spatial and temporal mapping of pacemaker activity in interstitial cells of Cajal in mouse ileum in situ. *American journal of physiology. Cell physiology*, *290*(5), C1411–C1427.

Pedemonte, N., & Galietta, L. J. (2014). Structure and function of TMEM16 proteins (anoctamins). *Physiological reviews*, *94*(2), 419–459.

Peppiatt, C. M., Collins, T. J., Mackenzie, L., Conway, S. J., Holmes, A. B., Bootman, M. D., Berridge, M. J., Seo, J. T., & Roderick, H. L. (2003). 2-Aminoethoxydiphenyl borate (2-APB) antagonises inositol 1,4,5-trisphosphate-induced calcium release, inhibits calcium pumps and has a use-dependent and slowly reversible action on store-operated calcium entry channels. *Cell calcium*, 34(1), 97–108.

Perez-Reyes E. (2003). Molecular physiology of low-voltage-activated t-type calcium channels. *Physiological reviews*, *83*(1), 117–161.

Persson, K., Pandita, R. K., Aszòdi, A., Ahmad, M., Pfeifer, A., Fässler, R., & Andersson, K. E. (2000). Functional characteristics of urinary tract smooth muscles in mice lacking cGMP protein kinase type I. *American journal of physiology. Regulatory, integrative and comparative physiology*, *279*(3), R1112–R1120.

Persson, K., & Andersson, K. E. (1992). Nitric oxide and relaxation of pig lower urinary tract. *British journal of pharmacology*, *106*(2), 416–422.

Pezzone, M. A., Watkins, S. C., Alber, S. M., King, W. E., de Groat, W. C., Chancellor, M. B., & Fraser, M. O. (2003). Identification of c-kit-positive cells in the mouse ureter:

the interstitial cells of Cajal of the urinary tract. *American journal of physiology. Renal physiology*, *284*(5), F925–F929.

Pfaffendorf, M., Mathy, M. J., van der Lee, R., & van Zwieten, P. A. (2000). Evidence for a sympatholytic effect of mibefradil in the pithed rat preparation. *Journal of hypertension*, *18*(2), 203–207.

Phillips, B., Clark, J., Martineau, É., & Rungta, R. L. (2023). Orai, RyR, and IP_3R channels cooperatively regulate calcium signaling in brain mid-capillary pericytes. *Communications biology*, *6*(1), 493.

Pirpiris, A., Shek, K. L., & Dietz, H. P. (2010). Urethral mobility and urinary incontinence. *Ultrasound in obstetrics & gynecology: the official journal of the International Society of Ultrasound in Obstetrics and Gynecology*, *36*(4), 507–511.

Pluteanu, F., Boknik, P., Heinick, A., König, C., Müller, F. U., Weidlich, A., & Kirchhefer, U. (2022). Activation of PKC results in improved contractile effects and Ca^{2+} cycling by inhibition of PP2A-B56α. *American journal of physiology. Heart and circulatory physiology*, *322*(3), H427–H441.

Popescu, L. M., Ciontea, S. M., Cretoiu, D., Hinescu, M. E., Radu, E., Ionescu, N., Ceausu, M., Gherghiceanu, M., Braga, R. I., Vasilescu, F., Zagrean, L., & Ardeleanu, C. (2005). Novel type of interstitial cell (Cajal-like) in human fallopian tube. *Journal of cellular and molecular medicine*, *9*(2), 479–523.

Potier, M., Gonzalez, J. C., Motiani, R. K., Abdullaev, I. F., Bisaillon, J. M., Singer, H. A., & Trebak, M. (2009). Evidence for STIM1- and Orai1-dependent store-operated calcium influx through ICRAC in vascular smooth muscle cells: role in proliferation and migration. *FASEB journal : official publication of the Federation of American Societies for Experimental Biology*, *23*(8), 2425–2437.

Pradidarcheep, W., Wallner, C., Dabhoiwala, N. F., & Lamers, W. H. (2011). Anatomy and histology of the lower urinary tract. *Handbook of experimental pharmacology*, (202), 117–148.

Prakriya, M., & Lewis, R. S. (2015). Store-Operated Calcium Channels. *Physiological reviews*, *95*(4), 1383–1436.

Purtell, K., Paroder-Belenitsky, M., Reyna-Neyra, A., Nicola, J. P., Koba, W., Fine, E., Carrasco, N., & Abbott, G. W. (2012). The KCNQ1-KCNE2 K^+ channel is required for adequate thyroid I^- uptake. *FASEB journal : official publication of the Federation of American Societies for Experimental Biology*, *26*(8), 3252–3259.

Putney J. W., Jr (1986). A model for receptor-regulated calcium entry. *Cell calcium*, *7*(1), 1–12.

Putney J. W., Jr (1990). Capacitative calcium entry revisited. *Cell calcium*, *11*(10), 611–624.

Putney, J. W., Jr, Poggioli, J., & Weiss, S. J. (1981). Receptor regulation of calcium release and calcium permeability in parotid gland cells. *Philosophical transactions of the Royal Society of London. Series B, Biological sciences*, *296*(1080), 37–45.

Quayle, J. M., Nelson, M. T., & Standen, N. B. (1997). ATP-sensitive and inwardly rectifying potassium channels in smooth muscle. *Physiological reviews*, *77*(4), 1165–1232.

Quinn, T., Molloy, M., Smyth, A., & Baird, A. W. (2004). Capacitative calcium entry in guinea pig gallbladder smooth muscle in vitro. *Life sciences*, *74*(13), 1659–1669.

Ralevic V. (2021). Purinergic signalling in the cardiovascular system-a tribute to Geoffrey Burnstock. *Purinergic signalling*, *17*(1), 63–69.

Reis, L. O., Sopena, J. M., Fávaro, W. J., Martin, M. C., Simão, A. F., Reis, R. B., Andrade, M. F., Domenech, J. D., & Cardo, C. C. (2011). Anatomical features of the urethra and urinary bladder catheterization in female mice and rats. An essential translational tool. *Acta cirurgica brasileira*, *26 Suppl 2*, 106–110.

M. Shafei, K.D. Thornbury, N.G. McHale and M.A. Hollywood. (2003). *Relative contributions of calcium influx and calcium stores to myogenic tone in the rat urethra - The Physiological Society* (2003).

Rembetski, B. E., Cobine, C. A., & Drumm, B. T. (2018). Laboratory practical to study the differential innervation pathways of urinary tract smooth muscle. *Advances in physiology education*, *42*(2), 295–304.

Rembetski, B. E., Sanders, K. M., & Drumm, B. T. (2020). Contribution of $Ca_V1.2$ Ca^{2+} channels and store-operated Ca^{2+} entry to pig urethral smooth muscle contraction. *American journal of physiology. Renal physiology*, *318*(2), F496–F505.

Reyes-García, J., Flores-Soto, E., Carbajal-García, A., Sommer, B., & Montaño, L. M. (2018). Maintenance of intracellular Ca2+ basal concentration in airway smooth muscle (Review). *International journal of molecular medicine*, *42*(6), 2998–3008.

Rodman, D. M., Reese, K., Harral, J., Fouty, B., Wu, S., West, J., Hoedt-Miller, M., Tada, Y., Li, K. X., Cool, C., Fagan, K., & Cribbs, L. (2005). Low-voltage-activated (T-type) calcium channels control proliferation of human pulmonary artery myocytes. *Circulation research*, *96*(8), 864–872.

Rodriguez-Tapia, E., Perez-Medina, A., Bian, X., & Galligan, J. J. (2016). Upregulation of L-type calcium channels in colonic inhibitory motoneurons of P/Q-type calcium channel-deficient mice. *American journal of physiology. Gastrointestinal and liver physiology*, *311*(4), G763–G774.

Roehrborn C. G. (2005). Benign prostatic hyperplasia: an overview. *Reviews in urology*, *7 Suppl 9*(Suppl 9), S3–S14.

Rogers, D. C., & Burnstock, G. (1966). The interstitial cell and its place in the concept of the autonomic ground plexus. *The Journal of comparative neurology*, *126*(2), 255–284.

Roos, J., DiGregorio, P. J., Yeromin, A. V., Ohlsen, K., Lioudyno, M., Zhang, S., Safrina, O., Kozak, J. A., Wagner, S. L., Cahalan, M. D., Veliçelebi, G., & Stauderman,

K. A. (2005). STIM1, an essential and conserved component of store-operated Ca2+ channel function. *The Journal of cell biology*, *169*(3), 435–445.

Ruiz Rubio, J. L., Hernández, M., Rivera de los Arcos, L., Benedito, S., Recio, P., García, P., García-Sacristán, A., & Prieto, D. (2004). Role of ATP-sensitive K+ channels in relaxation of penile resistance arteries. *Urology*, *63*(4), 800–805.

Rumessen, J. J., Mikkelsen, H. B., Qvortrup, K., & Thuneberg, L. (1993). Ultrastructure of interstitial cells of Cajal in circular muscle of human small intestine. *Gastroenterology*, *104*(2), 343–350.

Sallinger, M., Grabmayr, H., Humer, C., Bonhenry, D., Romanin, C., Schindl, R., & Derler, I. (2024). Activation mechanisms and structural dynamics of STIM proteins. *The Journal of physiology*, *602*(8), 1475–1507.

Sam P, Nassereddin A, LaGrange CA. Anatomy, Abdomen and Pelvis: Bladder Detrusor Muscle. [Updated 2023 Aug 8]. In: StatPearls [Internet]. Treasure Island (FL): StatPearls Publishing; 2025 Jan-.

Sancho, M., Bradley, E., Garcia-Pascual, A., Triguero, D., Thornbury, K. D., Hollywood, M. A., & Sergeant, G. P. (2017). Involvement of cyclic nucleotide-gated channels in spontaneous activity generated in isolated interstitial cells of Cajal from the rabbit urethra. *European journal of pharmacology*, *814*, 216–225.

Sancho, M., García-Pascual, A., & Triguero, D. (2012). Presence of the Ca2+-activated chloride channel anoctamin 1 in the urethra and its role in excitatory neurotransmission. *American journal of physiology. Renal physiology*, *302*(3), F390–F400.

Sancho, M., & Kyle, B. D. (2021). The Large-Conductance, Calcium-Activated Potassium Channel: A Big Key Regulator of Cell Physiology. *Frontiers in physiology*, *12*, 750615.

Sancho, M., Triguero, D., & Garcia-Pascual, A. (2011). Direct coupling through gap junctions is not involved in urethral neurotransmission. *American journal of physiology. Renal physiology*, *300*(4), F864–F872.

Sanders, K.M. (1996). A case for interstitial cells of Cajal as pacemakers and mediators of neurotransmission in the gastrointestinal tract. *Gastroenterology*, 111(2), pp. 492–515.

Sanders K. M. (2019). Spontaneous Electrical Activity and Rhythmicity in Gastrointestinal Smooth Muscles. *Advances in experimental medicine and biology*, *1124*, 3–46.

Sanders, K. M., Baker, S. A., Drumm, B. T., & Kurahashi, M. (2022). Ca^{2+} Signaling Is the Basis for Pacemaker Activity and Neurotransduction in Interstitial Cells of the GI Tract. *Advances in experimental medicine and biology*, *1383*, 229–241.

Sanders, K. M., Drumm, B. T., Cobine, C. A., & Baker, S. A. (2024). Ca^{2+} dynamics in interstitial cells: foundational mechanisms for the motor patterns in the gastrointestinal tract. *Physiological reviews*, *104*(1), 329–398.

Sanders, K. M., Koh, S. D., & Ward, S. M. (2006). Interstitial cells of cajal as pacemakers in the gastrointestinal tract. *Annual review of physiology*, *68*, 307–343.

Sanders, K. M., Santana, L. F., & Baker, S. A. (2023). Interstitial cells of Cajal - pacemakers of the gastrointestinal tract. *The Journal of physiology*, 10.1113/JP284745.

Sanders, K. M., Ward, S. M., & Koh, S. D. (2014). Interstitial cells: regulators of smooth muscle function. *Physiological reviews*, *94*(3), 859–907.

Sangsawang, B., & Sangsawang, N. (2013). Stress urinary incontinence in pregnant women: a review of prevalence, pathophysiology, and treatment. *International urogynecology journal*, *24*(6), 901–912.

Saravanaperumal, S. A., Gibbons, S. J., Malysz, J., Sha, L., Linden, D. R., Szurszewski, J. H., & Farrugia, G. (2018). Extracellular Cl^- regulates electrical slow waves and setting of smooth muscle membrane potential by interstitial cells of Cajal in mouse jejunum. *Experimental physiology*, *103*(1), 40–57.

Sausbier, M., Arntz, C., Bucurenciu, I., Zhao, H., Zhou, X. B., Sausbier, U., Feil, S., Kamm, S., Essin, K., Sailer, C. A., *et al.* (2005). Elevated blood pressure linked to primary hyperaldosteronism and impaired vasodilation in BK channel-deficient mice. *Circulation*, *112*(1), 60–68.

Schmidt, M., Sand, C., Jakobs, K. H., Michel, M. C., & Weernink, P. A. (2007). Epac and the cardiovascular system. *Current opinion in pharmacology*, *7*(2), 193–200.

Schroeder, B. C., Cheng, T., Jan, Y. N., & Jan, L. Y. (2008). Expression cloning of TMEM16A as a calcium-activated chloride channel subunit. *Cell*, *134*(6), 1019–1029.

Seo, Y., Lee, H. K., Park, J., Jeon, D. K., Jo, S., Jo, M., & Namkung, W. (2016). Ani9, A Novel Potent Small-Molecule ANO1 Inhibitor with Negligible Effect on ANO2. *PloS one*, *11*(5), e0155771.

Sergeant, G. P., Hollywood, M. A., McCloskey, K. D., Thornbury, K. D., & McHale, N. G. (2000). Specialised pacemaking cells in the rabbit urethra. *The Journal of physiology*, *526 Pt 2*(Pt 2), 359–366.

Sergeant, G. P., Hollywood, M. A., McCloskey, K. D., McHale, N. G., & Thornbury, K. D. (2001a). Role of IP(3) in modulation of spontaneous activity in pacemaker cells of rabbit urethra. *American journal of physiology. Cell physiology*, *280*(5), C1349–C1356.

Sergeant, G. P., Hollywood, M. A., McHale, N. G., & Thornbury, K. D. (2001b). Spontaneous Ca2+ activated Cl- currents in isolated urethral smooth muscle cells. *The Journal of urology*, *166*(3), 1161–1166.

Sergeant, G. P., Thornbury, K. D., McHale, N. G., & Hollywood, M. A. (2002). Characterization of norepinephrine-evoked inward currents in interstitial cells isolated

from the rabbit urethra. *American journal of physiology. Cell physiology*, *283*(3), C885–C894.

Sergeant, G. P., Johnston, L., McHale, N. G., Thornbury, K. D., & Hollywood, M. A. (2006a). Activation of the cGMP/PKG pathway inhibits electrical activity in rabbit urethral interstitial cells of Cajal by reducing the spatial spread of Ca2+ waves. *The Journal of physiology*, *574*(Pt 1), 167–181.

Sergeant, G. P., Hollywood, M. A., McHale, N. G., & Thornbury, K. D. (2006b). Ca2+ signalling in urethral interstitial cells of Cajal. *The Journal of physiology*, *576*(Pt 3), 715–720.

Sergeant, G. P., Thornbury, K. D., McHale, N. G., & Hollywood, M. A. (2006c). Interstitial cells of Cajal in the urethra. *Journal of cellular and molecular medicine*, *10*(2), 280–291.

Sergeant, G. P., Hollywood, M. A., & Thornbury, K. D. (2019). Spontaneous Activity in Urethral Smooth Muscle. *Advances in experimental medicine and biology*, *1124*, 149–167.

Serrano-Novillo, C., Oliveras, A., Ferreres, J. C., Condom, E., & Felipe, A. (2020). Remodeling of Kv7.1 and Kv7.5 Expression in Vascular Tumors. *International journal of molecular sciences*, *21*(17), 6019.

Sigala, S., Mirabella, G., Peroni, A., Pezzotti, G., Simeone, C., Spano, P., & Cunico, S. C. (2002). Differential gene expression of cholinergic muscarinic receptor subtypes in male and female normal human urinary bladder. *Urology*, *60*(4), 719–725.

Silva, I., Magalhães-Cardoso, M. T., Ferreirinha, F., Moreira, S., Costa, A. F., Silva, D., Vieira, C., Silva-Ramos, M., & Correia-de-Sá, P. (2020). β_3 Adrenoceptor-induced cholinergic inhibition in human and rat urinary bladders involves the exchange protein directly activated by cyclic AMP 1 favoring adenosine release. *British journal of pharmacology*, *177*(7), 1589–1608.

Singh, A., Hildebrand, M.E., Garcia, E. and Snutch, T.P., (2010). “The transient receptor potential channel antagonist SKF96365 is a potent blocker of low-voltage-activated T-type calcium channels”. *British Journal of Pharmacology*, 160(6), pp.1464–1475.

Smet, P. J., Jonavicius, J., Marshall, V. R., & de Vente, J. (1996). Distribution of nitric oxide synthase-immunoreactive nerves and identification of the cellular targets of nitric oxide in guinea-pig and human urinary bladder by cGMP immunohistochemistry. *Neuroscience*, *71*(2), 337–348.

Soboloff, J., Rothberg, B. S., Madesh, M., & Gill, D. L. (2012). STIM proteins: dynamic calcium signal transducers. *Nature reviews. Molecular cell biology*, *13*(9), 549–565.

Soldovieri, M. V., Miceli, F., & Taglialatela, M. (2011). Driving with no brakes: molecular pathophysiology of Kv7 potassium channels. *Physiology (Bethesda, Md.)*, *26*(5), 365–376.

Somlyo, A. P., & Himpens, B. (1989). Cell calcium and its regulation in smooth muscle. *FASEB journal : official publication of the Federation of American Societies for Experimental Biology*, *3*(11), 2266–2276.

Sommer, B., Flores-Soto, E., Reyes-García, J., Díaz-Hernández, V., Carbajal, V., & Montaño, L. M. (2016). Na(+) permeates through L-type Ca(2+) channel in bovine airway smooth muscle. *European journal of pharmacology*, *782*, 77–88.

Song, K., Zhong, X. G., Xia, X. M., Huang, J. H., Fan, Y. F., Yuan, R. X., Xue, N. R., Du, J., Han, W. X., Xu, A. M., & Shen, B. (2015). Orai1 forms a signal complex with SK3 channel in gallbladder smooth muscle. *Biochemical and biophysical research communications*, *466*(3), 456–462.

Spinelli, A. M., González-Cobos, J. C., Zhang, X., Motiani, R. K., Rowan, S., Zhang, W., Garrett, J., Vincent, P. A., Matrougui, K., Singer, H. A., & Trebak, M. (2012). Airway smooth muscle STIM1 and Orai1 are upregulated in asthmatic mice and mediate

PDGF-activated SOCE, CRAC currents, proliferation, and migration. *Pflugers Archiv : European journal of physiology*, *464*(5), 481–492.

Stathopulos, P.B., Zheng, L., Li, G.Y., Plevin, M.J. and Ikura, M., (2008). “Structural and mechanistic insights into STIM1-mediated initiation of store-operated calcium entry”. *Cell*, 135(1), pp.110–122.

Stott, J. B., Jepps, T. A., & Greenwood, I. A. (2014). K(V)7 potassium channels: a new therapeutic target in smooth muscle disorders. *Drug discovery today*, *19*(4), 413–424.

Strasser, H., Ninkovic, M., Hess, M., Bartsch, G., & Stenzl, A. (2000). Anatomic and functional studies of the male and female urethral sphincter. *World journal of urology*, *18*(5), 324–329.

Striessnig, J., Pinggera, A., Kaur, G., Bock, G., & Tuluc, P. (2014). L-type Ca^{2+} channels in heart and brain. *Wiley interdisciplinary reviews. Membrane transport and signaling*, *3*(2), 15–38.

Stull, J. T., Tansey, M. G., Tang, D. C., Word, R. A., & Kamm, K. E. (1993). Phosphorylation of myosin light chain kinase: a cellular mechanism for Ca2+ desensitization. *Molecular and cellular biochemistry*, *127-128*, 229–237.

Sung, T. S., O'Driscoll, K., Zheng, H., Yapp, N. J., Leblanc, N., Koh, S. D., & Sanders, K. M. (2016). Influence of intracellular Ca2+ and alternative splicing on the pharmacological profile of ANO1 channels. *American journal of physiology. Cell physiology*, *311*(3), C437–C451.

Sung, T. S., Hwang, S. J., Koh, S. D., Bayguinov, Y., Peri, L. E., Blair, P. J., Webb, T. I., Pardo, D. M., Rock, J. R., Sanders, K. M., & Ward, S. M. (2018). The cells and conductance mediating cholinergic neurotransmission in the murine proximal stomach. *The Journal of physiology*, *596*(9), 1549–1574.

Suskind, A.M. (2017) “Frailty and Lower Urinary Tract Symptoms,” *Current Urology Reports*. Current Medicine Group LLC 1. Available at: https://doi.org/10.1007/s11934-017-0720-9.

Suzuki, H., Ward, S. M., Bayguinov, Y. R., Edwards, F. R., & Hirst, G. D. (2003). Involvement of intramuscular interstitial cells in nitrergic inhibition in the mouse gastric antrum. *The Journal of physiology*, *546*(Pt 3), 751–763.

Szeto, V., Chen, N. H., Sun, H. S., & Feng, Z. P. (2018). The role of K_{ATP} channels in cerebral ischemic stroke and diabetes. *Acta pharmacologica Sinica*, *39*(5), 683–694.

Takano, T., & Yule, D. I. (2023). Ca^{2+} signals in pancreatic acinar cells in response to physiological stimulation in vivo. *The Journal of physiology*, *601*(12), 2391–2405.

Takai, Y., Kishimoto, A., Kikkawa, U., Mori, T., & Nishizuka, Y. (1979). Unsaturated diacylglycerol as a possible messenger for the activation of calcium-activated, phospholipid-dependent protein kinase system. *Biochemical and biophysical research communications*, *91*(4), 1218–1224.

Takeda, H., Yoshiki, A., Nishikawa, S., Nishikawa, S., Kunisada, T., Sakakura, T., Amanuma, H., & Kusakabe, M. (1992). Expression of c-kit, a proto-oncogene of the murine W locus, in cerebella of normal and neurological mutant mice: immunohistochemical and in situ hybridization analysis. *Differentiation; research in biological diversity*, *51*(2), 121–127.

Tanwar, J., Trebak, M., & Motiani, R. K. (2017). Cardiovascular and Hemostatic Disorders: Role of STIM and Orai Proteins in Vascular Disorders. *Advances in experimental medicine and biology*, *993*, 425–452.

Teramoto, N., Aishima, M., Zhu, H. L., Tomoda, T., Yunoki, T., Takahashi-Yanaga, F., Brading, A. F., & Ito, Y. (2004). Effects of U-37883A on intracellular Ca2+ -activated large-conductance K+ channels in pig proximal urethral myocytes. *European journal of pharmacology*, *506*(1), 1–7.

Teramoto, N., & Brading, A. F. (1996). Activation by levcromakalim and metabolic inhibition of glibenclamide-sensitive K channels in smooth muscle cells of pig proximal urethra. *British journal of pharmacology*, *118*(3), 635–642.

Thornbury, K. D., Hollywood, M. A., & McHale, N. G. (1992). Mediation by nitric oxide of neurogenic relaxation of the urinary bladder neck muscle in sheep. *The Journal of physiology*, *451*, 133–144.

Thuneberg L. (1982). Interstitial cells of Cajal: intestinal pacemaker cells?. Advances in anatomy, embryology, and cell biology, 71, 1–130.

Tica, A. A., Dun, E. C., Tica, O. S., Gao, X., Arterburn, J. B., Brailoiu, G. C., Oprea, T. I., & Brailoiu, E. (2011). G protein-coupled estrogen receptor 1-mediated effects in the rat myometrium. *American journal of physiology. Cell physiology*, *301*(5), C1262–C1269.

Tokutomi, N., Maeda, H., Tokutomi, Y., Sato, D., Sugita, M., Nishikawa, S., Nishikawa, S., Nakao, J., Imamura, T. & Nishi, K., (1995). “Rhythmic chloride current and physiological roles of intestinal c-kit–positive cells”. *Pflüger’s Archiv: European Journal of Physiology*, 431(2), pp.169–177.

Torihashi, S., Ward, S. M., Nishikawa, S., Nishi, K., Kobayashi, S., & Sanders, K. M. (1995). c-kit-dependent development of interstitial cells and electrical activity in the murine gastrointestinal tract. *Cell and tissue research*, *280*(1), 97–111.

Trebak, M., Zhang, W., Ruhle, B., Henkel, M. M., González-Cobos, J. C., Motiani, R. K., Stolwijk, J. A., Newton, R. L., & Zhang, X. (2013). What role for store-operated Ca^{2+} entry in muscle?. *Microcirculation (New York, N.Y. : 1994)*, *20*(4), 330–336.

Triggle D. J. (1985). Calcium ions and respiratory smooth muscle function. *British journal of clinical pharmacology*, *20 Suppl 2*(Suppl 2), 213S–219S.

Tsai, Y. M., Jones, F., Mullen, P., Porter, K. E., Steele, D., Peers, C., & Gamper, N. (2020). Vascular Kv7 channels control intracellular Ca^{2+} dynamics in smooth muscle. *Cell calcium*, *92*, 102283.

Tykocki, N. R., Heppner, T. J., Dalsgaard, T., Bonev, A. D., & Nelson, M. T. (2019). The K_V 7 channel activator retigabine suppresses mouse urinary bladder afferent

nerve activity without affecting detrusor smooth muscle K^+ channel currents. *The Journal of physiology*, *597*(3), 935–950.

Tykocki, N. R., Jackson, W. F., & Watts, S. W. (2012). Reverse-mode Na+/Ca2+ exchange is an important mediator of venous contraction. *Pharmacological research*, *66*(6), 544–554.

Tzeng, B. H., Chen, Y. H., Huang, C. H., Lin, S. S., Lee, K. R., & Chen, C. C. (2012). The Ca(v)3.1 T-type calcium channel is required for neointimal formation in response to vascular injury in mice. *Cardiovascular research*, *96*(3), 533–542.

Van der Werf, B. A., & Creed, K. E. (2002). Mechanical properties and innervation of the smooth muscle layers of the urethra of greyhounds. *BJU international*, *90*(6), 588–595.

Venema, P. L., Kramer, G., van Koeveringe, G. A., & Heesakkers, J. P. F. A. (2023). The Maximal Urethral Pressure at Rest and during Normal Bladder Filling Is Only Determined by the Activity of the Urethral Smooth Musculature in the Female. *Journal of clinical medicine*, *12*(7), 2575.

Venema, P. L., Elzevier, H. W., van Koeveringe, G. A., Kramer, A. E., & Kummeling, M. T. M. (2025). Pathophysiology of Urethral Instability: Dysfunction of Smooth Urethral Musculature. *Neurourology and urodynamics*, *44*(4), 931–934.

Waldeck, K., Ny, L., Persson, K., & Andersson, K. E. (1998). Mediators and mechanisms of relaxation in rabbit urethral smooth muscle. *British journal of pharmacology*, *123*(4), 617–624.

Wang, H., Zou, L., Ma, K., Yu, J., Wu, H., Wei, M., & Xiao, Q. (2017). Cell-specific mechanisms of TMEM16A Ca^{2+}-activated chloride channel in cancer. *Molecular cancer*, *16*(1), 152.

Wang, H. S., Dixon, J. E., & McKinnon, D. (1997). Unexpected and differential effects of Cl- channel blockers on the Kv4.3 and Kv4.2 K+ channels. Implications for the study of the I(to2) current. *Circulation research*, *81*(5), 711–718.

Ward, S.M. & Sanders, K.M., (1990). “Pacemaker activity in septal structures of canine colonic circular muscle”. *The American Journal of Physiology*, 259(2 Pt 1), pp.G264–G273.

Ward, S. M., Burns, A. J., Torihashi, S., & Sanders, K. M. (1994). Mutation of the proto-oncogene c-kit blocks development of interstitial cells and electrical rhythmicity in murine intestine. *The Journal of physiology*, *480 (Pt 1)*(Pt 1), 91–97.

Ward, S. M., Morris, G., Reese, L., Wang, X. Y., & Sanders, K. M. (1998). Interstitial cells of Cajal mediate enteric inhibitory neurotransmission in the lower esophageal and pyloric sphincters. *Gastroenterology*, *115*(2), 314–329.

Ward, S. M., Beckett, E. A., Wang, X., Baker, F., Khoyi, M., & Sanders, K. M. (2000). Interstitial cells of Cajal mediate cholinergic neurotransmission from enteric motor neurons. *The Journal of neuroscience: the official journal of the Society for Neuroscience*, *20*(4), 1393–1403.

Ward, S. M., Dixon, R. E., de Faoite, A., & Sanders, K. M. (2004). Voltage-dependent calcium entry underlies propagation of slow waves in canine gastric antrum. *The Journal of physiology*, *561*(Pt 3), 793–810.

Ward, S. M., & Sanders, K. M. (2006). Involvement of intramuscular interstitial cells of Cajal in neuroeffector transmission in the gastrointestinal tract. *The Journal of physiology*, *576*(Pt 3), 675–682.

Ward, S. M., McLaren, G. J., & Sanders, K. M. (2006). Interstitial cells of Cajal in the deep muscular plexus mediate enteric motor neurotransmission in the mouse small intestine. *The Journal of physiology*, *573*(Pt 1), 147–159.

Watanabe, H., & Yamamoto, T. Y. (1979). Autonomic innervation of the muscles in the wall of the bladder and proximal urethra of male rats. *Journal of anatomy*, *128*(Pt 4), 873–886.

Woll, K. A., & Van Petegem, F. (2022). Calcium-release channels: structure and function of IP_3 receptors and ryanodine receptors. *Physiological reviews*, *102*(1), 209–268.

Wray, S., Prendergast, C., & Arrowsmith, S. (2021). Calcium-Activated Chloride Channels in Myometrial and Vascular Smooth Muscle. *Frontiers in physiology*, *12*, 751008.

Wu, C., Sui, G., & Fry, C. H. (2002). The role of the L-type Ca(2+) channel in refilling functional intracellular Ca(2+) stores in guinea-pig detrusor smooth muscle. *The Journal of physiology*, *538*(Pt 2), 357–369.

Wu, R. S., & Marx, S. O. (2010). The BK potassium channel in the vascular smooth muscle and kidney: α- and β-subunits. *Kidney international*, *78*(10), 963–974.

Xiao, Q., Yu, K., Perez-Cornejo, P., Cui, Y., Arreola, J., & Hartzell, H. C. (2011). Voltage- and calcium-dependent gating of TMEM16A/Ano1 chloride channels are physically coupled by the first intracellular loop. *Proceedings of the National Academy of Sciences of the United States of America*, *108*(21), 8891–8896.

Xin, W., Li, N., Cheng, Q., Fernandes, V. S., & Petkov, G. V. (2014). Constitutive PKA activity is essential for maintaining the excitability and contractility in guinea pig urinary bladder smooth muscle: role of the BK channel. *American journal of physiology. Cell physiology*, *307*(12), C1142–C1150.

Xu, C., You, X., Gao, L., Zhang, L., Hu, R., Hui, N., Olson, D. M., & Ni, X. (2011). Expression of ATP-sensitive potassium channels in human pregnant myometrium. *Reproductive biology and endocrinology : RB&E*, *9*, 35.

Yamada, S., & Ito, Y. (2011). α(1)-Adrenoceptors in the urinary tract. *Handbook of experimental pharmacology*, (202), 283–306.

Yamaguchi, O., Shishido, K., Tamura, K., Ogawa, T., Fujimura, T., & Ohtsuka, M. (1996). Evaluation of mRNAs encoding muscarinic receptor subtypes in human detrusor muscle. *The Journal of urology*, *156*(3), 1208–1213.

Yamaguchi, O., & Chapple, C. R. (2007). Beta3-adrenoceptors in urinary bladder. *Neurourology and urodynamics*, *26*(6), 752–756.

Yang, Y. D., Cho, H., Koo, J. Y., Tak, M. H., Cho, Y., Shim, W. S., Park, S. P., Lee, J., Lee, B., Kim, B. M., Raouf, R., Shin, Y. K., & Oh, U. (2008). TMEM16A confers receptor-activated calcium-dependent chloride conductance. *Nature*, *455*(7217), 1210–1215.

Yan, J., & Aldrich, R. W. (2012). BK potassium channel modulation by leucine-rich repeat-containing proteins. *Proceedings of the National Academy of Sciences of the United States of America*, *109*(20), 7917–7922.

Yoast, R. E., Emrich, S. M., Zhang, X., Xin, P., Johnson, M. T., Fike, A. J., Walter, V., Hempel, N., Yule, D. I., Sneyd, J., Gill, D. L., & Trebak, M. (2020). The native ORAI channel trio underlies the diversity of Ca^{2+} signaling events. *Nature communications*, *11*(1), 2444.

Yoshimura, N., & Chancellor, M. B. (2003). Neurophysiology of lower urinary tract function and dysfunction. *Reviews in urology*, *5 Suppl 8*(Suppl 8), S3–S10.

Young, H. H. & D. I. Macht (1923): A contribution to the physiology and pharmacology of the trigonum vesicae. *J. Pharmacol. Exp. Ther.* 22, 329–354.

Yule, D. I., & Takano, T. (2024). Pacing intracellular Ca^{2+} signals in exocrine acinar cells. *The Journal of physiology*, 10.1113/JP284755.

Yuan, J. P., Zeng, W., Dorwart, M. R., Choi, Y. J., Worley, P. F., & Muallem, S. (2009). SOAR and the polybasic STIM1 domains gate and regulate Orai channels. *Nature cell biology*, *11*(3), 337–343.

Yunoki, T., Teramoto, N., & Ito, Y. (2003). Functional involvement of sulphonylurea receptor (SUR) type 1 and 2B in the activity of pig urethral ATP-sensitive K+ channels. *British journal of pharmacology*, *139*(3), 652–660.

Yu W. (2022). Reviving Cav1.2 as an attractive drug target to treat bladder dysfunction. *FASEB journal: official publication of the Federation of American Societies for Experimental Biology*, *36*(1), e22118.

Zawieja, S. D., Castorena, J. A., Gui, P., Li, M., Bulley, S. A., Jaggar, J. H., Rock, J. R., & Davis, M. J. (2019). Ano1 mediates pressure-sensitive contraction frequency changes in mouse lymphatic collecting vessels. *The Journal of general physiology*, *151*(4), 532–554.

Zhang, S. L., Yeromin, A. V., Zhang, X. H., Yu, Y., Safrina, O., Penna, A., Roos, J., Stauderman, K. A., & Cahalan, M. D. (2006). Genome-wide RNAi screen of Ca(2+) influx identifies genes that regulate Ca(2+) release-activated Ca(2+) channel activity. *Proceedings of the National Academy of Sciences of the United States of America*, *103*(24), 9357–9362.

Zheng, H., Park, K. S., Koh, S. D., & Sanders, K. M. (2014). Expression and function of a T-type Ca2+ conductance in interstitial cells of Cajal of the murine small intestine. *American journal of physiology. Cell physiology*, *306*(7), C705–C713.

Zheng, H., Drumm, B. T., Earley, S., Sung, T. S., Koh, S. D., & Sanders, K. M. (2018). SOCE mediated by STIM and Orai is essential for pacemaker activity in the interstitial cells of Cajal in the gastrointestinal tract. *Science signaling*, *11*(534), eaaq0918.

Zhu, M. H., Kim, T. W., Ro, S., Yan, W., Ward, S. M., Koh, S. D., & Sanders, K. M. (2009). A Ca(2+)-activated Cl(-) conductance in interstitial cells of Cajal linked to slow wave currents and pacemaker activity. *The Journal of physiology*, *587*(Pt 20), 4905–4918.

Zimmern, P., Litman, H. J., Nager, C. W., Lemack, G. E., Richter, H. E., Sirls, L., Kraus, S. R., Sutkin, G., & Mueller, E. R. (2014). Effect of aging on storage and voiding function in women with stress predominant urinary incontinence. *The Journal of urology*, *192*(2), 464–468.

Zygmunt, P. K., Zygmunt, P. M., Högestätt, E. D., & Andersson, K. E. (1995). NANC neurotransmission in lamina propria of the rabbit urethra: regulation by different subsets of calcium channels. *British journal of pharmacology*, *115*(6), 1020–1026.